

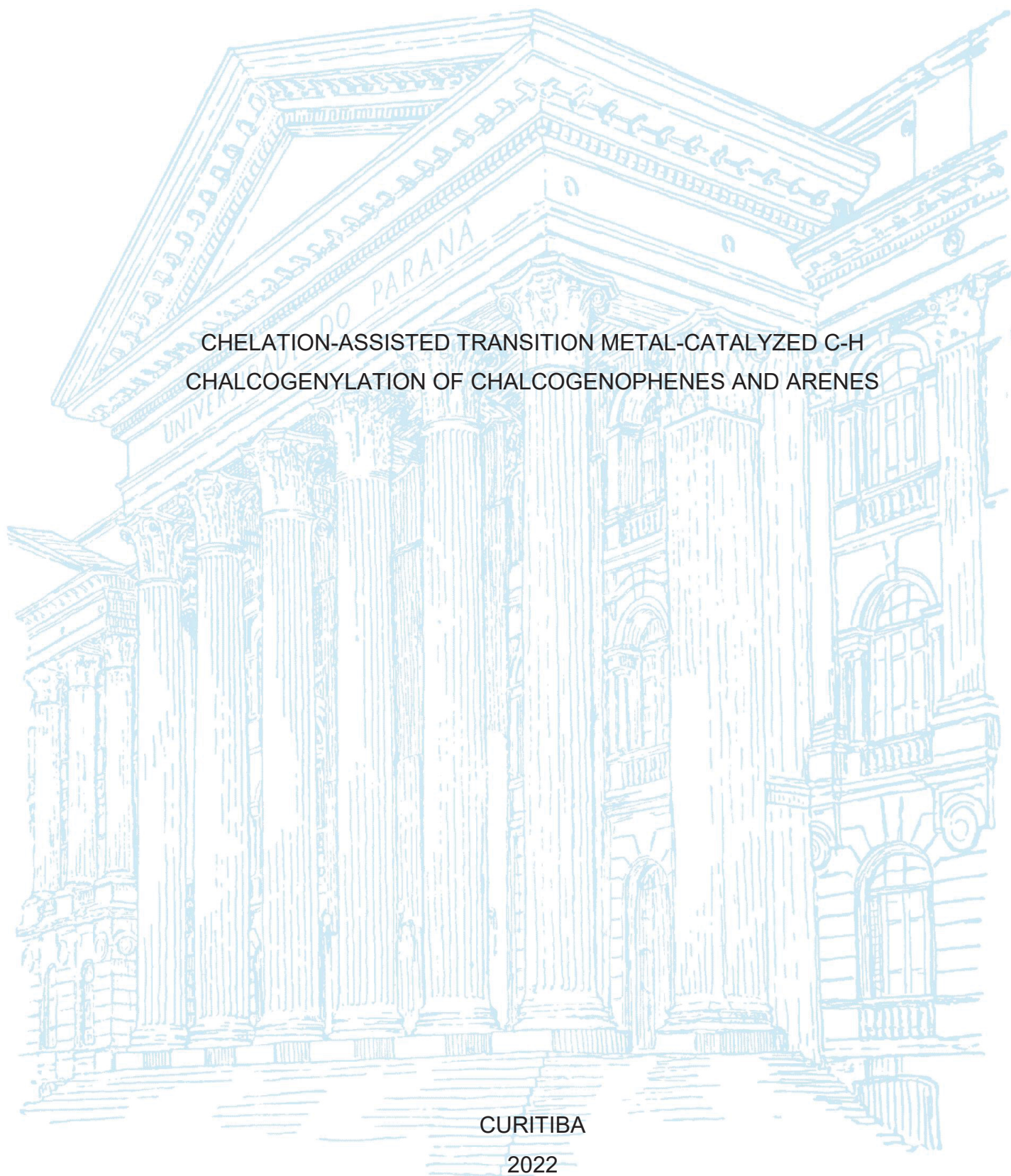
UNIVERSIDADE FEDERAL DO PARANÁ

GUL BADSHAH

CHELATION-ASSISTED TRANSITION METAL-CATALYZED C-H
CHALCOGENYLATION OF CHALCOGENOPHENES AND ARENES

CURITIBA

2022



GUL BADSHAH

CHELATION-ASSISTED TRANSITION METAL-CATALYZED C-H
CHALCOGENYLATION OF CHALCOGENOPHENES AND ARENES

Tese apresentada ao curso de Pós-Graduação em Química, Departamento de Química, Setor de Ciências Exatas, Universidade Federal do Paraná, como requisito parcial à obtenção do título de Doutor em Química, área de concentração Química Orgânica.

Orientador: Prof. Dr. Daniel da Silveira Rampon

CURITIBA 2022

DADOS INTERNACIONAIS DE CATALOGAÇÃO NA PUBLICAÇÃO (CIP)
UNIVERSIDADE FEDERAL DO PARANÁ
SISTEMA DE BIBLIOTECAS – BIBLIOTECA DE CIÊNCIA E TECNOLOGIA

Badshah, Gul

Chelation-assisted transition metal catalyzed c-h chalcogenylation of chalcogenophenes and arenes / Gul Badshah. – Curitiba, 2022.

1 recurso on-line : PDF.

Tese (Doutorado) - Universidade Federal do Paraná, Setor de Ciências Exatas, Programa de Pós-Graduação em Química.

Orientador: Daniel da Silveira Rampon

1. Calcogênios. 2. Calcogenofenos. 3. Arenos. 4. Paládio. 5. Cobre. I. Universidade Federal do Paraná. II. Programa de Pós-Graduação em Química. III. Rampon, Daniel da Silveira. IV. Título.

Bibliotecário: Elias Barbosa da Silva CRB-9/1894



MINISTÉRIO DA EDUCAÇÃO
SETOR DE CIÊNCIAS EXATAS
UNIVERSIDADE FEDERAL DO PARANÁ
PRÓ-REITORIA DE PESQUISA E PÓS-GRADUAÇÃO
PROGRAMA DE PÓS-GRADUAÇÃO QUÍMICA -
40001016026P2

TERMO DE APROVAÇÃO

Os membros da Banca Examinadora designada pelo Colegiado do Programa de Pós-Graduação QUÍMICA da Universidade Federal do Paraná foram convocados para realizar a arguição da tese de Doutorado de GUL BADSHAH intitulada: CHELATION-ASSISTED TRANSITION METAL CATALYZED C-H CHALCOGENYLATION OF CHALCOGENOPHENES AND ARENES, sob orientação do Prof. Dr. DANIEL DA SILVEIRA RAMPON, que após terem inquirido o aluno e realizada a avaliação do trabalho, são de parecer pela sua APROVAÇÃO no rito de defesa.

A outorga do título de doutor está sujeita à homologação pelo colegiado, ao atendimento de todas as indicações e correções solicitadas pela banca e ao pleno atendimento das demandas regimentais do Programa de Pós-Graduação.

CURITIBA, 23 de Dezembro de 2022.

Assinatura Eletrônica
03/01/2023 11:54:35.0

DANIEL DA SILVEIRA RAMPON
Presidente da Banca Examinadora

Assinatura Eletrônica
04/01/2023 12:03:25.0
ANTONIO LUIZ BRAGA

Avallador Externo (UNIVERSIDADE FEDERAL DE SANTA CATARINA)

Assinatura Eletrônica
04/01/2023 10:50:17.0
RICARDO SAMUEL SCHWAB

Avallador Externo (UNIVERSIDADE FEDERAL DE SÃO CARLOS)

Assinatura Eletrônica
05/01/2023 10:11:01.0
MARCELO GONÇALVES MONTES D'OCA

Avallador Interno (UNIVERSIDADE FEDERAL DO PARANÁ)

Assinatura Eletrônica
17/01/2023 13:10:01.0
FILIPE VINICIUS PENTEADO SCARANARO

Avallador Externo (UNIVERSIDADE FEDERAL DE SANTA MARIA)

I dedicate this work to my dearest father Said Bacha and mother, as well as my brothers Fazal Karim, Amir Sohail and sisters for their unconditional love, encouragement and support from the very beginning until today.

Acknowledgements

First and foremost, I would like to thank God for his never-ending grace, mercy, and provision during what ended up being one of the toughest times of my life.

Special and incomparable thanksgivings to my respectable mentor, Prof. Dr. Daniel da Silveira Rampon for accepting me as doctoral student, who always encouraged, supported me like a friend in scientific accomplishments, knowledge and enabled me how to be a researcher. Without your support this would not be possible, thank you very much professor.

I sincerely very much thankful to both CNPq (National Council for Scientific and Technological Development) and TWAS (The World Academy of Sciences) for the undistinguished financial support under TWAS-CNPq Fellowship 2017 program.

The Post-Graduate Program in Chemistry (PPGQ), UFPR is highly acknowledged for providing me the facilities with open and creative working environment for my research. I thank all my colleagues and whole teaching and non-teaching staff for support.

I feel great pleasure to express my deep and sincere gratitude to Prof. Dr. Ronilson V. Barbosa for friendly support, advice, knowledge, ethical support and contribute a lot to my education.

I would like to thank Prof. Dr. Caroline Da Ros Montes D'Oca, for friendly support, knowledge, ethical support and as a committee member in my doctoral thesis evaluation.

I convey my distinct thanks to Prof. Dr. Marcelo Gonçalves Montes D'Oca for the valuable teachings transmitted and as a committee member in my doctoral thesis evaluation.

I also thank to professors Leandro Piovan, Claudiney, Paulo Zarbin, Andersson Barison and prof. Beatriz H.L.N.S. Maia for their teachings transmitted and various contributions to work and my training.

I feel great pleasure to express my deep and honest gratitude to Prof. Dr. Antonio Luiz Braga, Prof. Dr. Ricardo Frederico Schumacher, prof. Dr Ricardo Samuel Schwab and Prof. Dr. Filipe Vinicius Penteado Scaranaro, for participation and evaluation of my PhD thesis.

Special thanks to my friends and colleagues of LaPoCa! David, Fedro, Eduardo, Diego, Gabriel Silvério, Gabriel Bueno, Evaldir, Emerson and Eron Rafael for the friendship, lots of support, conversation, collaboration, and for everything's which I learn from them during my PhD.

I am also very much thankful to my female friends and colleagues! Elise, Carla, Giuliana, Amanda, Camila, Joelma, Priscila Fiori, Priscila Dário for friendship, daily conversation, collaboration and your contribution.

I am very much thankful to my brother and friend Dr. Sher Ali for their immense support, collaboration and lots of contribution in my PhD. And also, to Dr. Muhammad Siddique Afridi and Kelly Mara Seronato, for their friendship and collaboration.

I immensely appreciate to the people very close to me whom always accompanied, appreciated, and fully supported me, Farman Ullah Shah, Ijaz Ahmad Rehan Ullah, Muhammad Riaz, Latif Ullah, Niaz Muhammad, Umar Ali, Ajmal Khan, Nasir Ali, and Abdul Tahir.

To Marwa Gul, my life partner. Thank you very much for being part of my life, in both good and bad times, immense support and huge contribution. This achievement is also yours.

Last but not least, I deeply wish my undistinguishable thanks to my family members specifically my dearest father, mother, brother and sisters for supporting me spiritually, morally and financially in throughout educational career and my life in general.

"I walk slowly, but I never walk backward"

(Abraham Lincoln, 1809-1865)

RESUMO

Esta tese descreve o desenvolvimento de um novo método para a calcogenilação direta regioseletiva de calcogenofenos e arenos usando dois sistemas catalíticos diferentes. O primeiro sistema envolve uma reação catalisada por paládio com 2-(metiltio)amida, enquanto o segundo sistema envolve uma reação catalisada por cobre com 2-(4,5-diidrooxazol-2-il)anilina como grupo direcionador. Desta forma, caminhos sintéticos com melhor economia de passos e átomos podem ser alcançados para a preparação de novos compostos organocalcogenados. O estudo começou testando diferentes condições de reação para a calcogenilação direta na posição C3 da *N*-(2-(metiltio)fenil)furan-2-carboxamida (**3a**) usando Pd(II). Os estudos de otimização foram iniciados com o composto (**3a**) e disseleneto de difenila (**9a**), sendo avaliados vários parâmetros, como fonte de catalisador de paládio, quantidade de catalisador, estequiometria da reação, solvente, tempo, aditivos e atmosfera do sistema. As condições de reação otimizadas forneceram 98% de rendimento isolado da *N*-(2-(metiltio)fenil)-3-(fenilselanil)furan-2-carboxamida (**10a**) usando Pd(OAc)₂ (2,5 mol%) como catalisador e CuBr₂ (0,33 Equivalentes) como aditivo em *N,N*-dimetilformamida (DMF) como solvente, sob temperatura de 100 °C por 24 h. Por outro lado, os resultados relativos à calcogenilação direta C3 regioseletiva da 2-(4,5-diidrooxazol-2-il)amida como grupo orientador foram apresentados no segundo projeto. Este protocolo desenvolve a calcogenilação direta C3 regioseletiva de *N*-(2-(4,5-diidrooxazol-2-il)fenil)furan-2-carboxamida (**5a**) com Cu(II). Da mesma forma, a otimização da reação começa a partir dos reagentes de partida (**5a**) e disseleneto de difenila (**9a**), e vários parâmetros desta reação foram analisados, incluindo estequiometria da reação, quantidade de catalisador, diferentes bases, ligantes, atmosfera do sistema, tempo e temperatura. A condição de reação aprimorada proporcionou 73% de produto *N*-(2-(4,5-dihidrooxazol-2-il)fenil)-3-(fenilselanil)furan-2-carboxamida (**11a**) empregando Cu(OAc)₂ (1,0 Equivalente) como catalisador, TMEDA (*N,N,N',N'*-Tetrametiletilenodiamina) (1,0 Equivalente) como ligante e base Na₂CO₃ (2,0 Equivalentes) em sulfóxido de dimetila (DMSO) a 80 °C de temperatura por 8 h sob atmosfera inerte de argônio. As estruturas de **10a** e **11a** foram investigadas por Espectrometria de Massas acoplada à Cromatografia Gasosa (GC-MS), Ressonância Magnética Nuclear (RMN) de ¹H e de ¹³C, como também experimentos de RMN bidimensional, como correlação heteronuclear (¹H-¹³C) de ligação direta (HSQC) e correlação heteronuclear (¹H-¹³C) à longa distância (HMBC). Os dados espectroscópicos confirmaram a regioseletividade da reação na posição C3 da *N*-(2-(metiltio)fenil)furan-2-carboxamida (**3a**) e da *N*-(2-(4,5-dihidrooxazol-2-il)fenil) furan-2-carboxamida (**5a**), como também regioseletividade C2 em diferentes arenos substituídos. A regioseletividade C3 das reações foi adicionalmente confirmada por difração de raios X de monocristal de **10a** e **11a**. O escopo da reação usando 2-(metiltio)amidas foi investigado, sendo preparados 23 novos organoselenetos, derivados de furanos, benzo[*b*]furanos, tiofenos, benzo[*b*]tiofenos e arenos (C2-selanilados) com bons a excelentes rendimentos.

Palavras-chave: Grupos Orientadores. Calcogenilação Direta. 2-(Metiltio)amida. 2-(4,5-diidrooxazol-2-il)amida. Calcogenofenos. Arenos. Paládio. Cobre.

ABSTRACT

This thesis describes the development of a novel method for the regioselective direct chalcogenylation of chalcogenophenes and arenes using two different catalyst systems. The first system involves a palladium-catalyzed reaction with 2-(methylthio)amide, while the second system involves a copper-catalyzed reaction with 2-(4,5-dihydrooxazol-2-yl)aniline as a directing group. In this way, synthetic "shortcuts" with improved step and atom economy can be achieved for the preparation of new organochalcogen compounds. The study started by testing different reaction conditions for the envisioned regioselective C3 direct chalcogenylation of *N*-(2-(methylthio)phenyl)furan-2-carboxamide (**3a**) with Pd(II). The optimization studies were started with compound (**3a**) and diphenyl diselenide (**9a**) evaluating several parameters such as the palladium catalyst source, catalyst amount, reaction stoichiometry, solvent, time, additives, and system atmosphere. The optimized reaction conditions gave 98% isolated yield of *N*-(2-(methylthio)phenyl)-3-(phenylselanyl)furan-2-carboxamide (**10a**) using Pd(OAc)₂ (2.5 mol%) as catalyst and CuBr₂ (0.33 Equivalents) as additive in *N,N*-dimethylformamide (DMF) as solvent at temperature of 100 °C for 24 h. On the other hand, the results related to the regioselective C3 direct chalcogenylation of chalcogenophenes by copper catalyst using the 2-(4,5-dihydrooxazol-2-yl)aniline as a directing group were presented in the second project. This protocol begins the regioselective C3 direct chalcogenylation of *N*-(2-(4,5-dihydrooxazol-2-yl)phenyl)furan-2-carboxamide (**5a**) with Cu(II). Similarly, the reaction optimization begins from the starting reagents (**5a**) and diphenyl diselenide (**9a**), and several parameters of this protocol were analyzed including reaction stoichiometry, amount of catalyst, different bases, ligand sources, system atmosphere, time and temperature of the reaction. The reaction condition afforded 73% product of *N*-(2-(4,5-dihydrooxazol-2-yl)phenyl)-3-(phenylselanyl)furan-2-carboxamide (**11a**) employing Cu(OAc)₂ (1.0 Equivalent) as catalyst, TMEDA (*N,N,N',N'*-Tetramethylethylenediamine) (1.0 Equivalent) as ligand and Na₂CO₃ (2.0 Equivalent) base in Dimethyl sulfoxide (DMSO) solvent at 80 °C of temperature for 8 h under inert atmosphere of argon. The structures of **10a** and **11a** were investigated by Mass Spectrometry coupled with gas chromatography (GC-MS), ¹H and ¹³C Nuclear Magnetic Resonance (NMR), Heteronuclear (¹H-¹³C) Single Quantum Correlation (HSQC), and Heteronuclear (¹H-¹³C) Multiple Quantum Correlation (HMBC) experiments. Spectroscopic data confirmed the regioselectivity of the reaction at the C3 position of *N*-(2-(methylthio)phenyl)furan-2-carboxamide (**3a**), *N*-(2-(4,5-dihydrooxazol-2-yl)phenyl)furan-2-carboxamide (**5a**), and C2 position of different substituted arenes. The reaction scope led to the regioselective preparation of several C3-selanylated furans, benzo[*b*]furan, thiophene, benzo[*b*]thiophene, and C2-selanylated arenes in good to excellent yields. Similarly, the structural characterization of the scope compound 3-((4-chlorophenyl)selanyl)-*N*-(2-(methylthio)phenyl)furan-2-carboxamide (**10b**) and *N*-(2-(4,5-dihydrooxazol-2-yl)phenyl)-3-(phenylselanyl)furan-2-carboxamide (**11a**) were also confirmed by single crystal X-ray diffraction (XRD), the reaction regioselectivity established at the C3 position of furans, benzo[*b*]furan, thiophene, benzo[*b*]thiophene.

Keywords: Directing Groups. Direct Chalcogenylation. 2-(Methylthio)amide. 2-(4,5-dihydrooxazol-2-yl)amide. Chalcogenophenes. Arenes. Palladium. Copper.

LIST OF TABLES

Table 1: Synthesis of starting materials through Steglich conditions.	43
Table 2: Optimization of the reaction conditions for C3 regioselective direct selanylation of (3a).....	60
Table 3: Optimization of the reaction conditions for C3 regioselective direct selanylation of (3a).....	62
Table 4: Scope of the C3-selective direct chalcogenylation of chalcogenophenes and benzo[<i>b</i>]chalcogenophenes.	65
Table 5: Scope of <i>ortho</i> direct selanylation of benzamides.....	67
Table 6: Optimization of the reaction conditions for C3 regioselective direct selanylation of (5a).....	77
Table 7: Optimization of the reaction conditions for C3 regioselective direct. selanylation of (5a).....	78
Table 8: Optimization of the reaction conditions for C3 regioselective direct selanylation of (5a).....	81
Table 9: Crystal data and structure refinement for 10b (C ₁₈ H ₁₄ ClNO ₂ SSe).....	86
Table 10: Crystal data and structure refinement for 11a (C ₂₀ H ₁₆ N ₂ O ₃ Se).....	87

LIST OF FIGURES

Figure 1: Molecular structure of chalcogenophenes.	17
Figure 2: Molecular structure of some relevant marketed drugs based on five-membered aromatic rings.	18
Figure 3: a) Comparison between the energies of HOMO orbitals in tetracene and compound A ; ^{21g} b) Fused chalcogenophenes with high charge mobility (μh).	19
Figure 4: Dewar aromaticity scale (DRE) and unified aromaticity index (IA) of chalcogenophenes compared to benzene. ^{23,12}	20
Figure 5: Low-resolution mass spectrum (EI, 70 eV) of <i>N</i> -(2-(methylthio)phenyl)furan-2-carboxamide (3a).	46
Figure 6: ¹ H NMR spectrum (400 MHz, CDCl ₃) of <i>N</i> -(2-(methylthio)phenyl)furan-2-carboxamide (3a).	47
Figure 7: ¹³ C NMR spectrum (100 MHz, CDCl ₃) of <i>N</i> -(2-(methylthio)phenyl)furan-2-carboxamide (3a).	48
Figure 8: ¹ H- ¹³ C HSQC correlation map (¹ H, 400 MHz; ¹³ C, 100 MHz) of <i>N</i> -(2-(methylthio)phenyl)furan-2-carboxamide (3a).	49
Figure 9: ¹ H- ¹³ C HMBC correlation map (¹ H, 400 MHz; ¹³ C, 100 MHz) of <i>N</i> -(2-(methylthio)phenyl)furan-2-carboxamide (3a).	50
Figure 10: ¹ H NMR spectrum (400 MHz, CDCl ₃) of <i>N</i> -2-(4,5-phenyl)furan-2-carboxamide (5a).	51
Figure 11: ¹³ C NMR spectrum (100 MHz, CDCl ₃) of <i>N</i> -2-(4,5-phenyl)furan-2-carboxamide (5a).	52
Figure 12: Low-resolution mass spectrum (EI, 70 eV) of <i>N</i> -(2-methylthio)phenyl-3-(phenylselanyl)furan-2-carboxamide (10a).	54
Figure 13: ¹ H NMR spectrum (400 MHz, CDCl ₃) of <i>N</i> -(2-methylthio)phenyl-3-(phenylselanyl)furan-2-carboxamide (10a).	55
Figure 14: ¹³ C NMR spectrum (100 MHz: CDCl ₃) of <i>N</i> -(2-methylthio)phenyl-3-(phenylselanyl)furan-2-carboxamide (10a).	56
Figure 15: ¹ H- ¹³ C direct correlation HSQC map (400 vs. 100 MHz, CDCl ₃) of <i>N</i> -(2-methylthio)phenyl-3-(phenylselanyl)furan-2-carboxamide (10a).	57
Figure 16: ¹ H- ¹³ C HMBC correlation map (400 MHz and 100 MHz, CDCl ₃) of <i>N</i> -(2-methylthio)phenyl-3-(phenylselanyl)furan-2-carboxamide (10a).	58

Figure 17: ORTEP diagram of compound (10b).	58
Figure 18: Packing of molecules of (C ₁₈ H ₁₄ ClNO ₂ SSe) (10b), viewed along b axis showing the intra-molecular hydrogen bonds (double-dotted lines). Thermal ellipsoids are drawn at the 50% probability level.	59
Figure 19: Reactional follow-up via Gas Chromatography coupled to Mass Spectrometry.	71
Figure 20: ¹ H NMR spectrum (400 MHz, CDCl ₃) of <i>N</i> -(2-(4,5-dihydrooxazol-2-yl)phenyl)-3-(phenylselanyl)furan-2-carboxamide (11a).	75
Figure 21: ¹³ C NMR spectrum (100 MHz: CDCl ₃) of <i>N</i> -(2-(4,5-dihydrooxazol-2-yl)phenyl)-3-(phenylselanyl)furan-2-carboxamide (11a).	76
Figure 22: ORTEP diagram of compound 11a .	76
Figure 23: Mass spectrum (EI, 70 eV) of compound <i>N</i> -(2-(methylthio)phenyl)thiophene-2-carboxamide (3b).	105
Figure 24: ¹ H NMR spectrum (400 MHz, CDCl ₃ :) of compound <i>N</i> -(2-(methylthio)phenyl)thiophene-2-carboxamide (3b).	105
Figure 25: ¹³ C NMR spectrum (100 MHz, CDCl ₃ :) of compound <i>N</i> -(2-(methylthio)phenyl)thiophene-2-carboxamide (3b).	106
Figure 26: Mass spectrum (EI, 70 eV) of 5-methyl- <i>N</i> -(2-(methylthio)phenyl)furan-2-carboxamide (3c).	106
Figure 27: ¹ H NMR Spectrum (400 MHz, CDCl ₃) of 5-methyl- <i>N</i> -(2-(methylthio)phenyl)furan-2-carboxamide (3c).	107
Figure 28: ¹³ C NMR Spectrum (100 MHz, CDCl ₃) of 5-methyl- <i>N</i> -(2-(methylthio)phenyl)furan-2-carboxamide (3c).	107
Figure 29: Mass spectrum (EI, 70 eV) of <i>N</i> -(2-(methylthio)phenyl)benzofuran-2-carboxamide (3d).	108
Figure 30: ¹ H NMR Spectrum (400 MHz, CDCl ₃) of <i>N</i> -(2-(methylthio)phenyl)benzofuran-2-carboxamide (3d).	108
Figure 31: ¹³ C NMR Spectrum (100 MHz, CDCl ₃) of <i>N</i> -(2-(methylthio)phenyl)benzofuran-2-carboxamide (3d).	109
Figure 32: Mass spectrum (EI, 70 eV) of <i>N</i> -(2-(methylthio)phenyl)benzo[b]thiophene-2-carboxamide (3e).	109
Figure 33: ¹ H NMR Spectrum (400 MHz, CDCl ₃) of <i>N</i> -(2-(methylthio)phenyl)benzo[b]thiophene-2-carboxamide (3e).	110

Figure 34: ^{13}C NMR Spectrum (100 MHz, CDCl_3) <i>N</i> -(2-(methylthio)phenyl)benzo[<i>b</i>]thiophene-2-carboxamide (3e).....	110
Figure 35: Mass spectrum (EI, 70 eV) of <i>N</i> -(2-(methylthio)phenyl)benzamide (7a).	111
Figure 36: ^1H NMR spectrum (400 MHz, CDCl_3) of <i>N</i> -(2-(methylthio)phenyl)benzamide (7a).....	111
Figure 37: ^{13}C NMR spectrum (100 MHz, CDCl_3) of <i>N</i> -(2-(methylthio)phenyl)benzamide (7a).....	112
Figure 38: ^1H NMR spectrum (400 MHz, CDCl_3) of 4-bromo- <i>N</i> -(2-(methylthio)phenyl)benzamide (7b).....	112
Figure 39: ^{13}C NMR spectrum (100 MHz, CDCl_3) of 4-bromo- <i>N</i> -(2-(methylthio)phenyl)benzamide (7b).....	113
Figure 40: ^1H NMR spectrum (400 MHz, CDCl_3) of <i>N</i> -(2-(methylthio)phenyl)-4-nitrobenzamide (7c).	113
Figure 41: ^{13}C NMR spectrum (100 MHz, CDCl_3) of <i>N</i> -(2-(methylthio)phenyl)-4-nitrobenzamide (7c).	114
Figure 42: Mass spectrum (EI, 70 eV) of 3-fluoro- <i>N</i> -(2-(methylthio)phenyl)benzamide (7d).	114
Figure 43: ^1H NMR spectrum (400 MHz, CDCl_3) of 3-fluoro- <i>N</i> -(2-(methylthio)phenyl)benzamide (7d).....	115
Figure 44: ^{13}C NMR spectrum (100 MHz, CDCl_3) of 3-fluoro- <i>N</i> -(2-(methylthio)phenyl)benzamide (7d).....	115
Figure 45: Mass spectrum (EI, 70 eV) of 3-chloro- <i>N</i> -(2-(methylthio)phenyl)benzamide (7e).....	116
Figure 46: ^1H NMR spectrum (400 MHz, CDCl_3) of 3-chloro- <i>N</i> -(2-(methylthio)phenyl)benzamide (7e).....	116
Figure 47: ^{13}C NMR spectrum (100 MHz, CDCl_3) of 3-chloro- <i>N</i> -(2-(methylthio)phenyl)benzamide (7e).....	117
Figure 48: Mass spectrum (EI, 70 eV) of <i>N</i> -(2-(methylthio)phenyl)-2-(trifluoromethyl)benzamide (7f).	117
Figure 49: ^1H NMR spectrum (400 MHz, CDCl_3) <i>N</i> -(2-(methylthio)phenyl)-3-(trifluoromethyl)benzamide (7f).	118
Figure 50: ^{13}C NMR spectrum (100 MHz, CDCl_3) <i>N</i> -(2-(methylthio)phenyl)-3-(trifluoromethyl)benzamide (7f).	118

Figure 51: Mass spectrum (EI, 70 eV) 2-bromo-5-methoxy- <i>N</i> -(2-(methylthio)phenyl)benzamide (7g).....	119
Figure 52: ¹ H NMR spectrum (400 MHz, CDCl ₃) 2-bromo-5-methoxy- <i>N</i> -(2-(methylthio)phenyl)benzamide (7g).....	119
Figure 53: ¹³ C NMR spectrum (100 MHz, CDCl ₃) 2-bromo-5-methoxy- <i>N</i> -(2-(methylthio)phenyl)benzamide (7g).....	120
Figure 54: Mass spectrum (EI, 70 eV) of 2-methyl- <i>N</i> -(2-(methylthio)phenyl)benzamide (7h).....	120
Figure 55: ¹ H NMR (400 MHz, CDCl ₃) of 2-methyl- <i>N</i> -(2-(methylthio)phenyl)benzamide (7h).....	121
Figure 56: ¹³ C NMR (100 MHz, CDCl ₃) of 2-methyl- <i>N</i> -(2-(methylthio)phenyl)benzamide (7h).....	121
Figure 57: Mass spectrum (EI, 70 eV) of 2-chloro- <i>N</i> -(2-(methylthio)phenyl)benzamide (7i).....	122
Figure 58: ¹ H NMR (400 MHz, CDCl ₃) of 2-chloro- <i>N</i> -(2-(methylthio)phenyl)benzamide (7i).....	122
Figure 59: ¹³ C NMR (100 MHz, CDCl ₃) of 2-chloro- <i>N</i> -(2-(methylthio)phenyl)benzamide (7i).....	123
Figure 60: Mass spectrum (EI, 70 eV) of 2-bromo- <i>N</i> -(2-(methylthio)phenyl)benzamide (7j).....	123
Figure 61: ¹ H NMR (400 MHz, CDCl ₃) of 2-bromo- <i>N</i> -(2-(methylthio)phenyl)benzamide (7j).....	124
Figure 62: ¹³ C NMR (100 MHz, CDCl ₃) of 2-bromo- <i>N</i> -(2-(methylthio)phenyl)benzamide (7j).....	124
Figure 63: Mass spectrum (EI, 70 eV) of 3-((4-chlorophenyl)selanyl)- <i>N</i> -(2-(methylthio)phenyl)furan-2-carboxamide (10b).....	125
Figure 64: ¹ H NMR spectrum (400 MHz, CDCl ₃) of 3-((4-chlorophenyl)selanyl)- <i>N</i> -(2-(methylthio)phenyl)furan-2-carboxamide (10b).....	125
Figure 65: ¹³ C NMR spectrum (100 MHz: CDCl ₃) of 3-((4-chlorophenyl)selanyl)- <i>N</i> -(2-(methylthio)phenyl)furan-2-carboxamide (10b).....	126
Figure 66: Mass spectrum (EI, 70 eV) of <i>N</i> -(2-(methylthio)phenyl)-3-((3-(trifluoromethyl)phenyl)selanyl)furan-2-carboxamide (10c).....	126
Figure 67: ¹ H NMR spectrum (400 MHz, CDCl ₃) of <i>N</i> -(2-(methylthio)phenyl)-3-((3-(trifluoromethyl)phenyl)selanyl)furan-2-carboxamide (10c).....	127

Figure 68: ^{13}C NMR spectrum (100 MHz: CDCl_3) of <i>N</i> -(2-(methylthio)phenyl)-3-((3-(trifluoromethyl)phenyl)selanyl)furan-2-carboxamide (10c).....	127
Figure 69: Mass spectrum (EI, 70 eV) of <i>N</i> -(2-(methylthio)phenyl)-3-(p-tolylselanyl)furan-2-carboxamide (10d).....	128
Figure 70: ^1H NMR spectrum (400 MHz, CDCl_3) of <i>N</i> -(2-(methylthio)phenyl)-3-(p-tolylselanyl)furan-2-carboxamide (10d).....	128
Figure 71: ^{13}C NMR spectrum (100 MHz: CDCl_3) of <i>N</i> -(2-(methylthio)phenyl)-3-(p-tolylselanyl)furan-2-carboxamide (10d).....	129
Figure 72: Mass spectrum (EI, 70 eV) of 3-((4-methoxyphenyl)selanyl)- <i>N</i> -(2-(methylthio)phenyl)furan-2-carboxamide (10e).....	129
Figure 73: ^1H NMR spectrum (400 MHz, CDCl_3) of 3-((4-methoxyphenyl)selanyl)- <i>N</i> -(2-(methylthio)phenyl)furan-2-carboxamide (10e).....	130
Figure 74: ^{13}C NMR spectrum (100 MHz: CDCl_3) of 3-((4-methoxyphenyl)selanyl)- <i>N</i> -(2-(methylthio)phenyl)furan-2-carboxamide (10e).....	130
Figure 75: Mass spectrum (EI, 70 eV) of 3-(butylselanyl)- <i>N</i> -(2-(methylthio)phenyl)furan-2-carboxamide (10f).....	131
Figure 76: ^1H NMR spectrum (400 MHz, CDCl_3) of 3-(butylselanyl)- <i>N</i> -(2-(methylthio)phenyl)furan-2-carboxamide (10f).....	131
Figure 77: ^{13}C NMR spectrum (100 MHz: CDCl_3) of 3-(butylselanyl)- <i>N</i> -(2-(methylthio)phenyl)furan-2-carboxamide (10f).....	132
Figure 78: Mass spectrum (EI, 70 eV) of 3-(mesitylseyanyl)- <i>N</i> -(2-(methylthio)phenyl)furan-2-carboxamide (10g).....	132
Figure 79: ^1H NMR spectrum (400 MHz, CDCl_3) of 3-(mesitylseyanyl)- <i>N</i> -(2-(methylthio)phenyl)furan-2-carboxamide (10g).....	133
Figure 80: ^{13}C NMR spectrum (100 MHz: CDCl_3) of 3-(mesitylseyanyl)- <i>N</i> -(2-(methylthio)phenyl)furan-2-carboxamide (10g).....	133
Figure 81: Mass spectrum (EI, 70 eV) of <i>N</i> -(2-(methylthio)phenyl)-3-(naphthalen-1-ylselanyl)furan-2-carboxamide (10h).....	134
Figure 82: ^1H NMR spectrum (400 MHz, CDCl_3) of <i>N</i> -(2-(methylthio)phenyl)-3-(naphthalen-1-ylselanyl)furan-2-carboxamide (10h).....	134
Figure 83: ^{13}C NMR spectrum (100 MHz: CDCl_3) of <i>N</i> -(2-(methylthio)phenyl)-3-(naphthalen-1-ylselanyl)furan-2-carboxamide (10h).....	135
Figure 84: Mass spectrum (EI, 70 eV) of <i>N</i> -(2-(methylthio)phenyl)-3-(phenylselanyl)thiophene-2-carboxamide (10i).....	135

Figure 85: ^1H NMR spectrum (400 MHz, CDCl_3) of <i>N</i> -(2-(methylthio)phenyl)-3-(phenylselanyl)thiophene-2-carboxamide (10i).	136
Figure 86: ^{13}C NMR spectrum (100 MHz, CDCl_3) of <i>N</i> -(2-(methylthio)phenyl)-3-(phenylselanyl)thiophene-2-carboxamide (10i).	136
Figure 87: Mass spectrum (EI, 70 eV) of 5-methyl- <i>N</i> -(2-(methylthio)phenyl)-3-(phenylselanyl)furan-2-carboxamide (10j).	137
Figure 88: ^1H NMR Spectrum (400 MHz, CDCl_3) of 5-methyl- <i>N</i> -(2-(methylthio)phenyl)-3-(phenylselanyl)furan-2-carboxamide (10j).	137
Figure 89: ^{13}C NMR Spectrum (100 MHz, CDCl_3) of 5-methyl- <i>N</i> -(2-(methylthio)phenyl)-3-(phenylselanyl)furan-2-carboxamide (10j).	138
Figure 90: Mass spectrum (EI, 70 eV) of <i>N</i> -(2-(methylthio)phenyl)-3-(phenylselanyl)benzofuran-2-carboxamide (10k).	138
Figure 91: ^1H NMR Spectrum (400 MHz, CDCl_3) of <i>N</i> -(2-(methylthio)phenyl)-3-(phenylselanyl)benzofuran-2-carboxamide (10k).	139
Figure 92: ^{13}C NMR Spectrum (100 MHz, CDCl_3) <i>N</i> -(2-(methylthio)phenyl)-3-(phenylselanyl)benzofuran-2-carboxamide (10k).	139
Figure 93: ^1H NMR Spectrum (400 MHz, CDCl_3) of <i>N</i> -(2-(methylthio)phenyl)-3-(phenylselanyl)benzo[b]thiophene-2-carboxamide (10l).	140
Figure 94: ^{13}C NMR Spectrum (100 MHz, CDCl_3) of <i>N</i> -(2-(methylthio)phenyl)-3-(phenylselanyl)benzo[b]thiophene-2-carboxamide (10l).	140
Figure 95: ^1H NMR spectrum (400 MHz, CDCl_3) of <i>N</i> -(2-(methylthio)phenyl)-2,6-bis(phenylselanyl)benzamide (12a).	141
Figure 96: ^{13}C NMR spectrum (100 MHz, CDCl_3) of <i>N</i> -(2-(methylthio)phenyl)-2,6-bis(phenylselanyl)benzamide (12a).	141
Figure 97: ^1H NMR spectrum (400 MHz, CDCl_3) of 4-bromo- <i>N</i> -(2-(methylthio)phenyl)-2,6-bis(phenylselanyl)benzamide (12b).	142
Figure 98: ^{13}C NMR spectrum (100 MHz, CDCl_3) of 4-bromo- <i>N</i> -(2-(methylthio)phenyl)-2,6-bis(phenylselanyl)benzamide (12b).	142
Figure 99: ^1H NMR spectrum (400 MHz, CDCl_3) of <i>N</i> -(2-(methylthio)phenyl)-4-nitro-2,6-bis(phenylselanyl)benzamide (12c).	143
Figure 100: ^{13}C NMR spectrum (100 MHz, CDCl_3) of <i>N</i> -(2-(methylthio)phenyl)-4-nitro-2,6-bis(phenylselanyl)benzamide (12c).	143
Figure 101: ^1H NMR spectrum (400 MHz, CDCl_3) 3-fluoro- <i>N</i> -(2-(methylthio)phenyl)-2,6-bis(phenylselanyl)benzamide (12d).	144

Figure 102: ^{13}C NMR spectrum (100 MHz, CDCl_3) 3-fluoro- <i>N</i> -(2-(methylthio)phenyl)-2,6-bis(phenylselanyl)benzamide (12d).	144
Figure 103: ^1H NMR spectrum (400 MHz, CDCl_3) 3-chloro- <i>N</i> -(2-(methylthio)phenyl)-2,6-bis(phenylselanyl)benzamide (12e).	145
Figure 104: ^{13}C NMR spectrum (100 MHz, CDCl_3) 3-chloro- <i>N</i> -(2-(methylthio)phenyl)-2,6-bis(phenylselanyl)benzamide (12e).	145
Figure 105: Mass spectrum (EI, 70 eV) of 2-methyl- <i>N</i> -(2-(methylthio)phenyl)-6-(phenylselanyl)benzamide (12f).	146
Figure 106: ^1H NMR (400 MHz, CDCl_3) of 2-methyl- <i>N</i> -(2-(methylthio)phenyl)-6-(phenylselanyl)benzamide (12f).	146
Figure 107: ^{13}C NMR (100 MHz, CDCl_3) of 2-methyl- <i>N</i> -(2-(methylthio)phenyl)-6-(phenylselanyl)benzamide (12f).	147
Figure 108: Mass spectrum (EI, 70 eV) of 2-chloro- <i>N</i> -(2-(methylthio)phenyl)-6-(phenylselanyl)benzamide (12g).	147
Figure 109: ^1H NMR (400 MHz, CDCl_3) of 2-chloro- <i>N</i> -(2-(methylthio)phenyl)-6-(phenylselanyl)benzamide (12g).	148
Figure 110: ^{13}C NMR (100 MHz, CDCl_3) of 2-chloro- <i>N</i> -(2-(methylthio)phenyl)-6-(phenylselanyl)benzamide (12g).	148
Figure 111: Mass spectrum (EI, 70 eV) of 2-bromo- <i>N</i> -(2-(methylthio)phenyl)-6-(phenylselanyl)benzamide (12h).	149
Figure 112: ^1H NMR (400 MHz, CDCl_3) of 2-bromo- <i>N</i> -(2-(methylthio)phenyl)-6-(phenylselanyl)benzamide (12h).	149
Figure 113: ^{13}C NMR (100 MHz, CDCl_3) of 2-bromo- <i>N</i> -(2-(methylthio)phenyl)-6-(phenylselanyl)benzamide (12h).	150
Figure 114: Mass spectrum (EI, 70 eV) of <i>N</i> -(2-(methylthio)phenyl)-2-(phenylselanyl)-3-(trifluoromethyl)benzamide (12i).	150
Figure 115: ^1H NMR spectrum (400 MHz, CDCl_3) <i>N</i> -(2-(methylthio)phenyl)-2-(phenylselanyl)-3-(trifluoromethyl)benzamide (12i).	151
Figure 116: ^{13}C NMR spectrum (100 MHz, CDCl_3) <i>N</i> -(2-(methylthio)phenyl)-2-(phenylselanyl)-3-(trifluoromethyl)benzamide (12i).	151
Figure 117: ^1H NMR spectrum (400 MHz, CDCl_3) 6-bromo-3-methoxy- <i>N</i> -(2-(methylthio)phenyl)-2-(phenylselanyl)benzamide (12j).	152
Figure 118: ^{13}C NMR spectrum (100 MHz, CDCl_3) 6-bromo-3-methoxy- <i>N</i> -(2-(methylthio)phenyl)-2-(phenylselanyl)benzamide (12j).	152

Figure 119: ^1H NMR spectrum (400 MHz, CDCl_3) of 2-(4,5-dihydrooxazol-2-yl)aniline (4).....	153
Figure 120: ^{13}C NMR spectrum (100 MHz: CDCl_3) of 2-(4,5-dihydrooxazol-2-yl)aniline (4).....	153
Figure 121: Mass spectrum (EI, 70 eV) of <i>N</i> -(2-(4,5-dihydrooxazol-2-yl)phenyl)furan-2-carboxamide (5a).....	154
Figure 122: ^1H NMR spectrum (400 MHz, CDCl_3) of <i>N</i> -(2-(4,5-dihydrooxazol-2-yl)phenyl)furan-2-carboxamide (5a).	154
Figure 123: ^{13}C NMR spectrum (100 MHz: CDCl_3) of <i>N</i> -(2-(4,5-dihydrooxazol-2-yl)phenyl)furan-2-carboxamide (5a).	155

LIST OF SYMBOLS AND ACRONYMS

BHT– 2,6-di-tert-butyl-4-methylphenol
TLC– Thin Layer Chromatography
DMF– *N,N'*-Dimethylformamide
DMSO– Dimethyl Sulfoxide
MeCN– Acetonitrile
DCM– Dichloromethane
DCC– *N,N'*-Dicyclohexylcarbodiimide
DMAP– 4-Dimethylaminopyridine
HRMS– Low Resolution Mass Spectrometry
NMP– *N*-methylpyrrolidone
TEMPO– *N*-oxyl-2,2,6,6-tetramethylpiperidine
¹³C NMR– Nuclear Magnetic Resonance of Carbon 13
¹H NMR– ¹H Nuclear Magnetic Resonance Spectroscopy
r.t.– Room temperature
THF– Tetrahydrofuran
δ = chemical shift
ppm = part per million
HSQC = Heteronuclear Single Quantum Coherence
HMBC = Heteronuclear Multiple Bond Correlation
GC-MS = Gas Chromatography–Mass Spectrometry
XRD = X-ray Diffraction
DRE = Dewar Resonance Energy
HOMO = Highest Occupied Molecular Orbital
LUMO = Lowest Unoccupied Molecular Orbital
OFETs = Organic Field-Effect Transistors
EAS = Electrophilic Aromatic Substitution
DOM = Directed Ortho Metalation
CMD = Concerted Metalation-Deprotonation
DGs = Directing Groups

SUMMARY

1 INTRODUCTION	16
1.1 CHALCOGENOPHENES	17
1.2 TRANSITION METAL CATALYSED DIRECT CHALCOGENYLATION OF ARENES AND HETEROARENES	25
2 OBJECTIVES	40
2.1 GENERAL OBJECTIVES	40
2.2 SPECIFIC OBJECTIVES	40
2.3 SYNTHESIS OF STARTING MATERIALS	42
2.4 REGIOSELECTIVE C3 DIRECT CHALCOGENYLATION OF CHALCOGENOPHENES USING 2-(METHYLTHIO)AMIDES AS DIRECTING GROUP	52
2.5 REGIOSELECTIVE C3 DIRECT CHALCOGENYLATION OF CHALCOGENOPHENES USING 2-(4,5-DIHYDROOXAZOL-2-YL)AMIDES AS DIRECTING GROUP	73
3 CONCLUSIONS	83
4 EXPERIMENTAL SECTION	85
4.1 GENERAL INFORMATION	85
4.1.1 Single-crystal X-ray diffraction analysis	85
4.1.2 Nuclear Magnetic Resonance (NMR) Spectroscopy	88
4.2 EXPERIMENTAL PROCEDURES	89
4.2.1 General procedure A for the synthesis of 2-(methylthio)amide (3a, 3b, 3d, 3e, 3f, 8a, 8b, 8c, 8d, 8e, 8f, 8g, 8h, 8i,8j, 8k)	89
4.2.2 General procedure A for the synthesis of 2-(4,5-dihydrooxazol-2-yl)aniline	89
4.2.3 General procedure B for the synthesis of compounds 10:.....	94
4.2.4 General procedure C for the synthesis of compounds 11:.....	95
4.2.5 Charecterized data of scope compounds:	95
5.2.2 Selected spectra.....	105
REFERENCES	156

1 INTRODUCTION

Reactions catalyzed by transition metals have reached an exciting level of sophistication and have been enhanced by C-H functionalization reactions that represent a paradigm shift in the standard logic of organic synthesis.¹ A considerable number of catalytic systems have been developed for C-C bond formation,² providing opportunities for stereo-, regio-, and chemoselective transformations for almost all classes of organic compounds.³ In parallel with the significant advances in organometallic chemistry, fascinating discoveries have been made in the formation of C-heteroatom (C-Het) bonds, although the development of direct conversion of usually unreactive C-H bonds to C-heteroatoms remains a critical challenge in organic chemistry.⁴ Initial approaches usually focus on developing methods for forming C-N, C-O, C-B, C-Si, C-P, and C-X bonds (where X is a halide or triflate) because the backbone of several natural products contains C-N and C-O bonds, and useful synthetic intermediates often contain C-X, C-B, or C-Si bonds that are later converted to C-C, C-O, or C-N bonds in the final products.⁵

However, in general organic synthesis, as well as in the pharmaceutical and materials science industry, there is a great pursuit for the development of straightforward C-S, C-Se, and C-Te bond formation to meet the industrial synthesis requirements for such compounds.⁶ Thus, the direct conversion of an inert C-H bond to a C-S, C-Se or C-Te bond catalyzed by transition metals, known as direct chalcogenylation, is groundbreaking technology in synthetic organic chemistry, considering the atom- economy and step-economy principles required for these purposes.⁷ Nevertheless, the development of such methods is highly challenging, primarily because of the catalytic poisoning of the transition metal catalysts by heavier chalcogen species.⁸

Organic molecular materials have been studied intensively in recent years and important contributions have made to the development of organic light-emitting diodes (OLEDs),⁹ organic field-effect transistors (OFETs),¹⁰ and organic photovoltaics (OPVs).¹¹ Among them, π -electron cores based on chalcogenophenes have arisen with outstanding properties, which are close to meeting the various requirements for electronic industrial applications. In the way to get these new and improved compounds commercialized, the active compounds will be required in larger quantities. Therefore, the efficient synthesis of these compounds is of paramount

importance, and the direct chalcogenylations could fulfill the requirements for these purposes. In addition, several organochalcogen compounds exhibit relevant biological properties, and the direct chalcogenylations could also open the way for new exotic molecular structures with potential pharmaceutical applications.

1.1 CHALCOGENOPHENES

Furan, thiophene, selenophene, and tellurophene, known collectively as chalcogenophenes, are considered a class of fully aromatic five-membered rings containing a heteroatom (Figure 1),¹² which are widely used in the field of biologically active molecules¹³ and organic semiconductor materials.¹⁴ Compared to furan and thiophenes, which have been ubiquitously used as building blocks to comprise enormous fascinating conjugated molecules and bioactive compounds, selenophene-containing compounds are relatively underdeveloped.¹⁵ In contrast, tellurophene-containing compounds are reported only sporadically because they are even more synthetically challenging.¹⁶

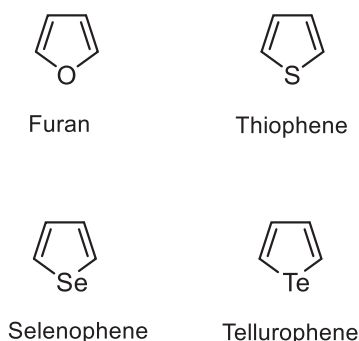


Figure 1: Molecular structure of chalcogenophenes.

Five-membered aromatic rings are the building blocks of many drugs. They are used as bioisosteres for structures such as phenyl, which can lead to improved pharmacokinetic and pharmacodynamic properties of a drug.¹⁷ Among them, thiophene, a five-membered aromatic sulphur-containing heterocycle, has been shown to be an attractive isosteres leading to improved efficacy of a drug.¹⁷ For instance, duloxetine (Figure 2) is commonly used as an antidepressant,¹⁸ and olanzapine (Figure 2) is an atypical antipsychotic widely used for the treatment of schizophrenia and bipolar disorder.¹⁹ Among furan compounds, furazolidone is a

synthetic nitrofuran derivative with a broad spectrum of antiprotozoal and antibacterial activity that also acts as a MAO (monoamine oxidase) inhibitor.²⁰

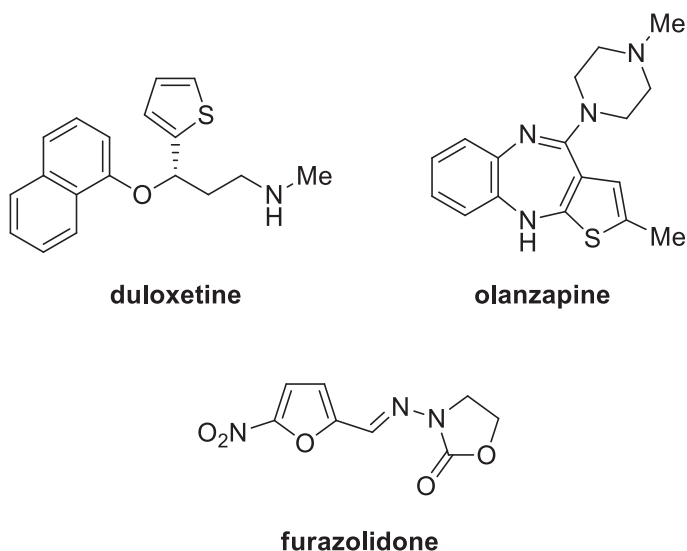


Figure 2: Molecular structure of some relevant marketed drugs based on five-membered aromatic rings.

From an organic materials perspective, highly extended polyacenes, of which tetracene²¹ is a representative example, are prototypical organic semiconductors that have advanced the field of organic electronics in the past three decades. The carrier mobility of such polyacene-based organic field-effect transistors (OFETs) is generally high, however, their low chemical stability is a drawback. Therefore, stabilization of tetracene and related compounds by chemical modification is one of the promising approaches to develop better organic semiconductors.^{14a} On the other hand, many other material classes of compounds with extended π -conjugation frameworks have also been examined as the active material in OFETs to achieve high charge mobility and stability. Mobility enhancement and environmental robustness to oxidation at room atmosphere are the two major requirements of organic semiconductors for OFETs. For the development of air-stable p-channel organic semiconductors, lowering the HOMO (Highest Occupied Molecular Orbital) energy level (E_{HOMO}) while keeping it suitable to hole injection from an electrode is a feasible strategy.²² Among the many organic structures examined, π -extended heteroaromatics seem to be promising because carrier transport in the molecular solid is also governed by intermolecular orbital overlap, and heteroatoms such as sulfur and selenium that have a larger atomic radius and higher polarizability than carbon, are expected to facilitate intermolecular nonbonded interactions (Figure 3).^{14a} In fact, many

thiophene, selenophene and tellurophene-based organic semiconductors, including π -extended oligochalcogenophenes and fused-chalcogenophenes, have been developed and examined as the active material for OFETs since the late 1990s.^{14a, 22}

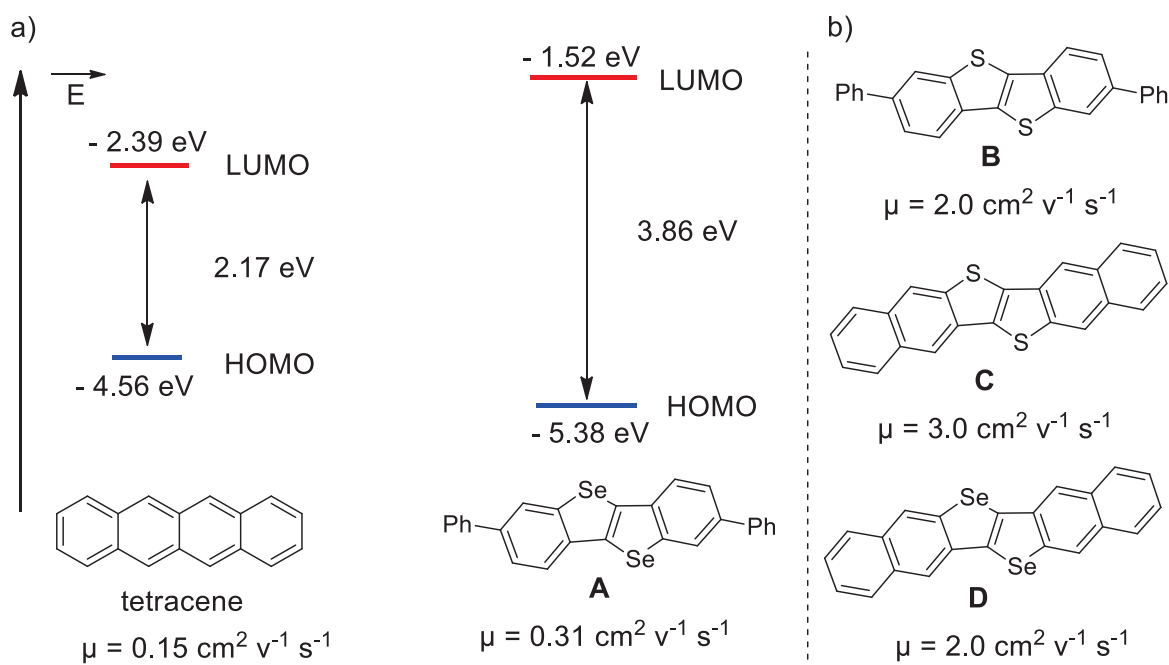


Figure 3: a) Comparison between the energies of HOMO orbitals in tetracene and compound **A**;^{21g} b) Fused chalcogenophenes with high charge mobility (μ h).

A great majority of the organic semiconductors are derived from thiophene-based π -conjugated systems, oligothiophenes, and C-S fused rings. In this sense, within the context of aromaticity, and following the Hückel rule, the replacement of oxygen by sulfur heteroatoms at an aromatic heterocycle gives rise to a larger covalent radius that reduces the ring strain.²³ Also, d-orbital participation in thiophene is not significant in the ground state, and thiophene exhibits a pronounced aromatic character that is substantiated by its physical and chemical properties.^{23,12} Despite several studies suggesting the greater aromaticity of thiophene when compared to furan²³ recently this trend has been questioned.²⁴

Regarding the propensity towards oxidation of simple chalcogenophenes, the introduction of higher chalcogen atoms as selenium and tellurium introduces a destabilizing effect due to their larger covalent radius and higher energy of valence electrons, which means a higher propensity towards oxidation.²⁵ As observed in the DRE (Dewar Resonance Energy) values, referenced to benzene as a prototype with greater aromaticity and the unified aromaticity index (I_A)^{23,26,12} selenophene and tellurophene lie in-between furan and thiophene on the aromaticity scale (Figure 4).

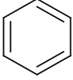
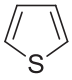
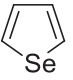
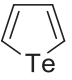
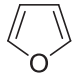
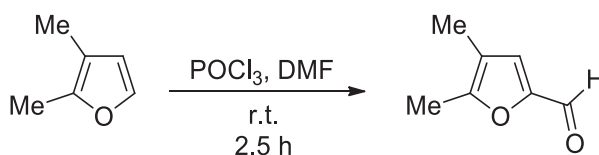
		>		>		>		>	
DRE (kcal mol ⁻¹)	22.6		6.5		-		-		4.3
I _A	100		82		73		59		53

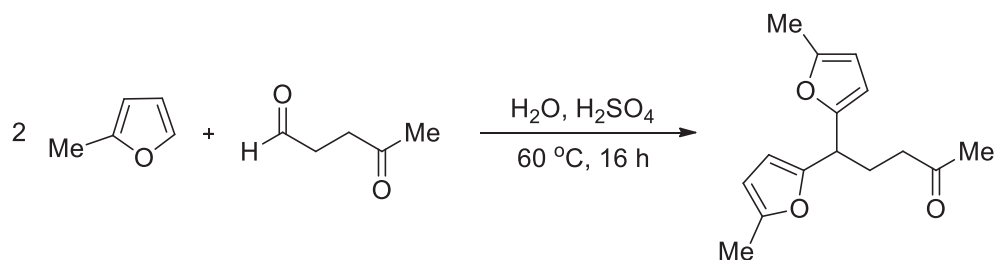
Figure 4: Dewar aromaticity scale (DRE) and unified aromaticity index (IA) of chalcogenophenes compared to benzene.^{23,12}

Since chalcogenophenes are electron-rich π systems, the reaction of these heterocycles with electrophilic reagents is still extremely useful in many cases.¹² For instance, the Vilsmeier-Haack formylation of chalcogenophenes derivatives is a useful method for functionalization of these compounds in high yields. In this sense, the formylation of 2,3-dimethylfuran was developed with POCl_3 and DMF with high regioselectivity at C5 position (Scheme 1).²⁷ Because of the high intrinsic selectivity for the C2-position of the furan ring, the direct formylation at the C3-position is only possible if the C2- and C5-positions are blocked, and harsh conditions are often required.²⁸



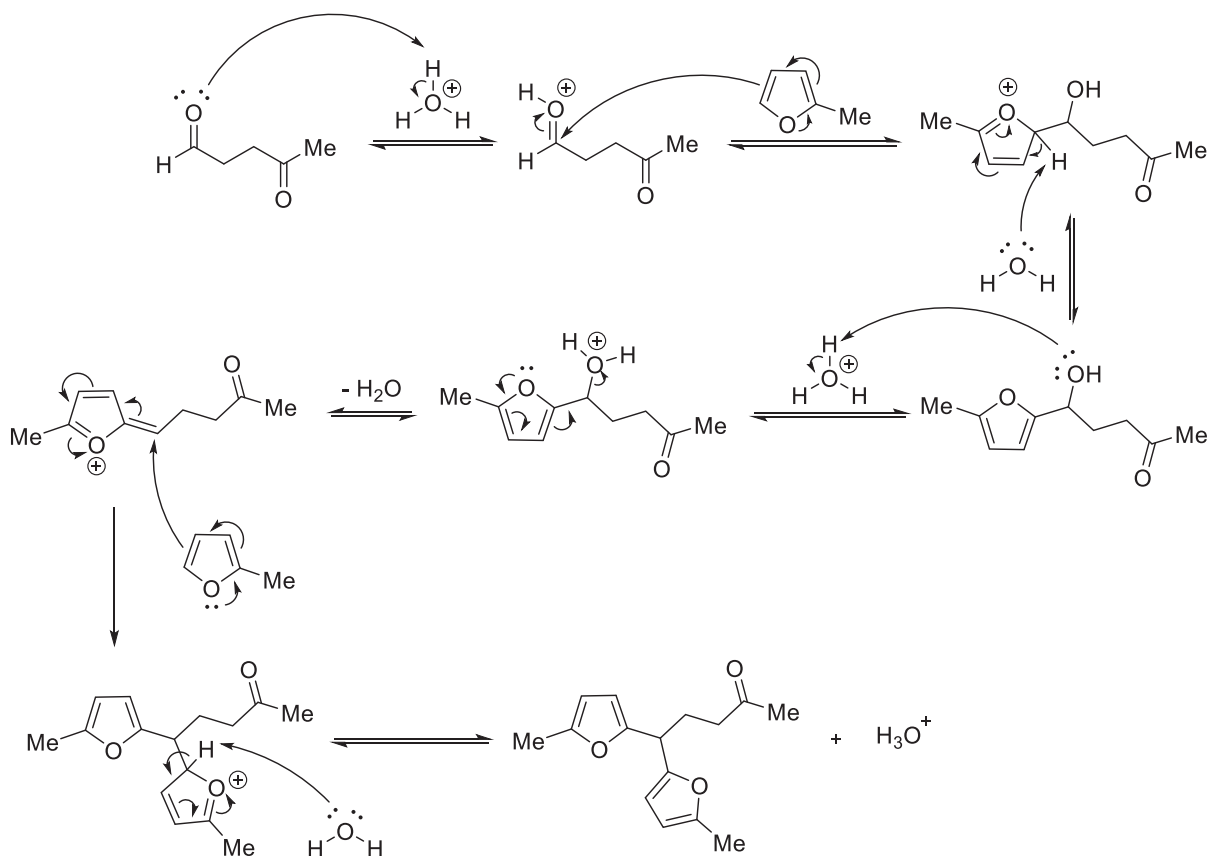
Scheme 1: Vilsmeier-Haack formylation of 2,3-dimethylfuran.²⁷

Similarly, the reaction of 2 equivalents of 2-methylfuran with 4-oxopentanal showed the regioselectivity at C5-position of 2-methylfuran (Scheme 2). The reaction of 2-methylfuran takes place in Brønsted acid medium affording the product by electrophilic aromatic substitution (EAS).²⁹ As an electron-donating group, the methyl at C2-position of 2-methylfuran accelerates the EAS and also protects the reagents and products from oligomerization and polymerization under the reaction conditions. The authors further subjected the product to a hydrodeoxygenation step in order to obtain a high-quality diesel.



Scheme 2: Electrophilic aromatic substitution at C5-position of 2-methylfuran using 4-oxopentanal.

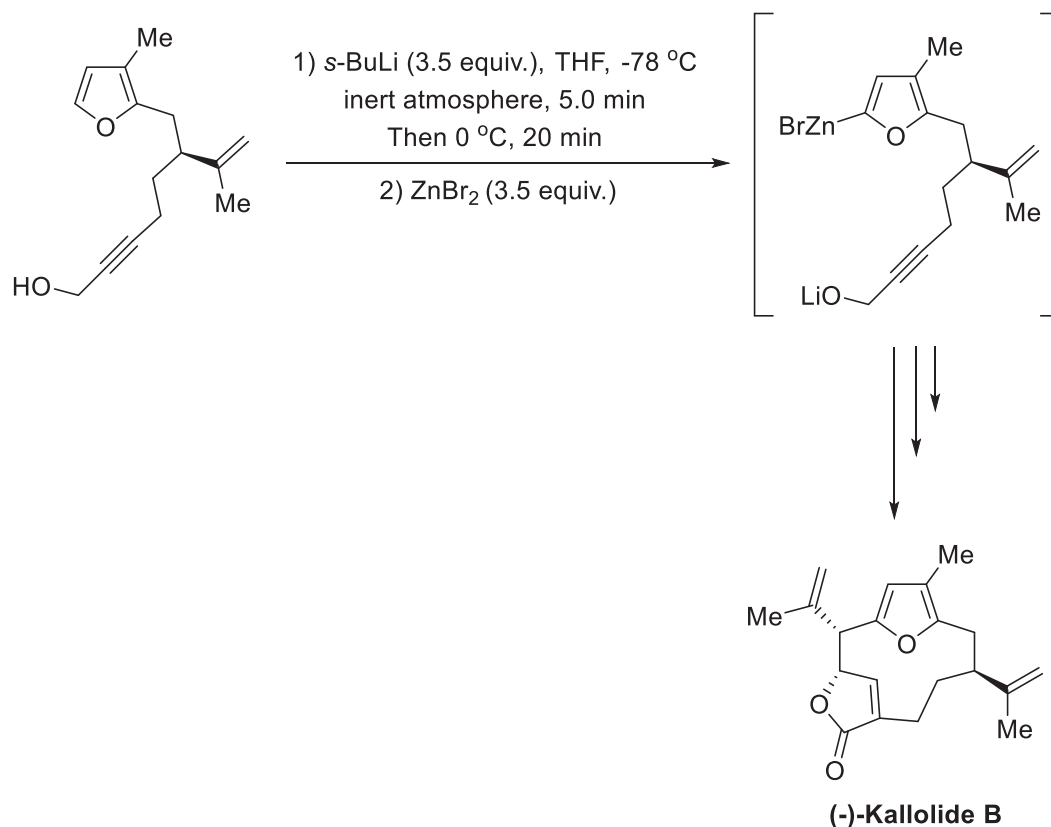
In the first step, the reaction mechanism follows the protonation of the aldehyde group on the 4-oxopentanal (Scheme 3). After this, an EAS at C5-position of the 2-methylfuran takes place to produce the respective alcohol. Then, the rearomatization via deprotonation by water and dehydration of alcohol in the acid medium furnish an oxonium intermediate that follows again an EAS with another 2-methylfuran molecule, providing the expected product.



Scheme 3: Mechanism of acid catalyzed electrophilic aromatic substitution between 2-methylfuran and 4-oxopentanal.²⁹

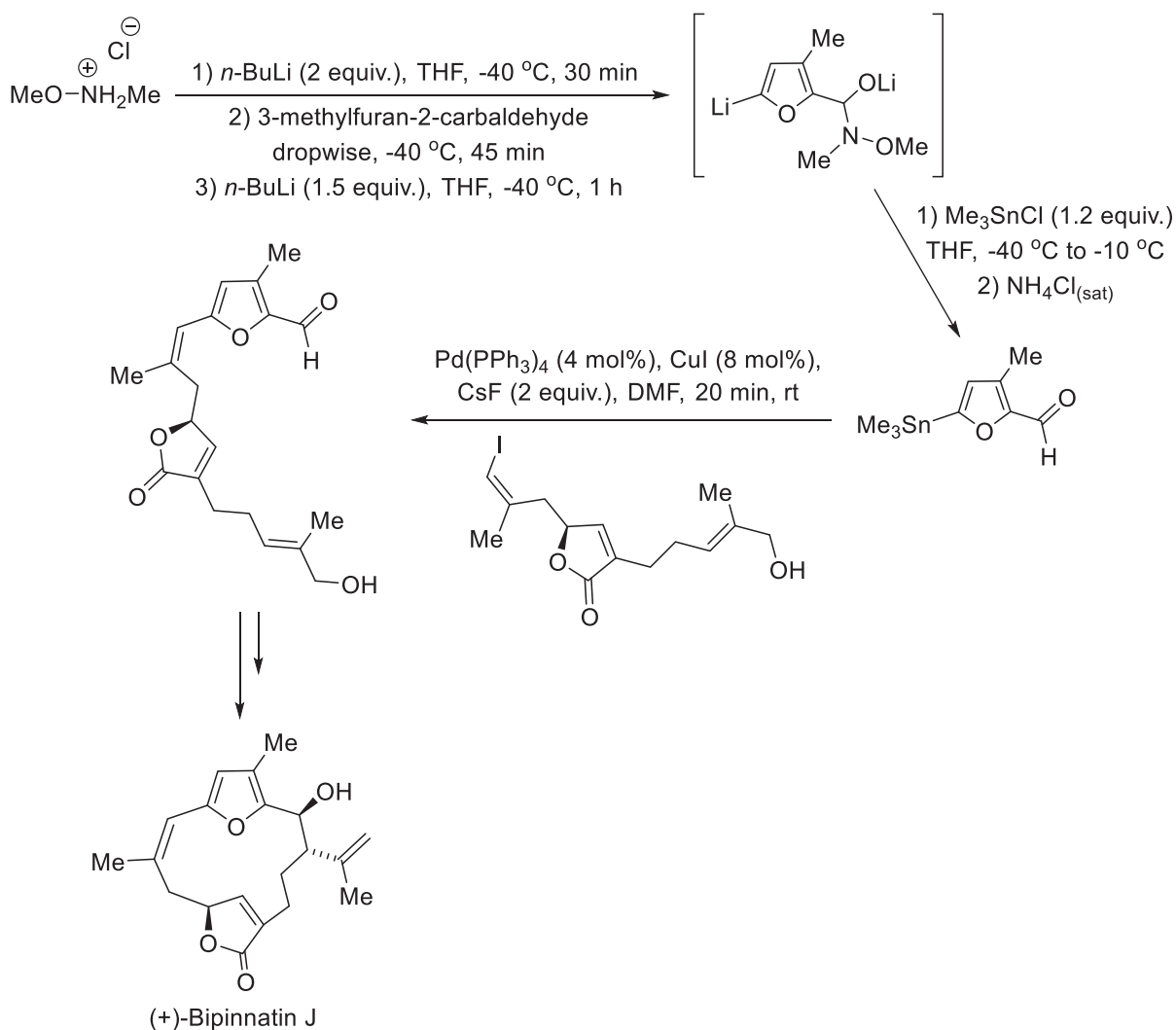
In many ways, the electron-rich five-membered aromatic heterocycles behave much like electron-deficient aromatic compounds when it comes to lithiation. The lithiation at C-2-position of furans and thiophenes derivatives is straightforward

considering the higher acidity of the hydrogen α -heteroatom in these compounds.³⁰ The furan lithiation with *s*-BuLi was explored for the synthesis of (-)-Kallolide B, the enantiomer of natural (+)-Kallolide B.³¹ The (+)-Kallolide B is a pseudopterane diterpenoid isolated from a Caribbegorgonian *Pseudopterogorgia bipinnata*.



Scheme 4: C2 regioselective lithiation of furan derivatives for the synthesis of (-)-Kallolide B, the natural enantiomer (+)-Kallolide B.

Similarly, the total synthesis of the diterpene (\pm)-Bipinnatin J was initiated by the deprotonation at the C-5-position of the 3-methyl-furan-2-carbaldehyde with *n*-BuLi under low temperature and an inert atmosphere (Scheme 5).³² In order to avoid the addition of *n*-BuLi to the aldehyde group, the protection strategy employing *in situ* preparation of the stable tetrahedral intermediate with *N,O*-dimethylhydroxylamine was successfully applied. After this, the addition of Me₃SnCl on the same reaction vessel of C2-lithiated furan afforded the respective stannane in 85% yield. Then, the stannane was subjected to a Stille cross-coupling reaction to produce an advanced synthetic intermediate on the synthesis of this natural product. It is worth mentioning that this was the first total synthesis of (\pm)-Bipinnatin J, which was isolated from the gorgonian octocoral *Pseudopterogorgia bipinnata*.

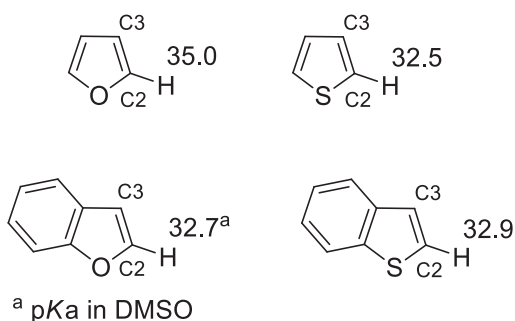


Scheme 5: C5-position regioselective lithiation of furan derivatives for the synthesis of diterpene (+)-Bipinnatin J.³²

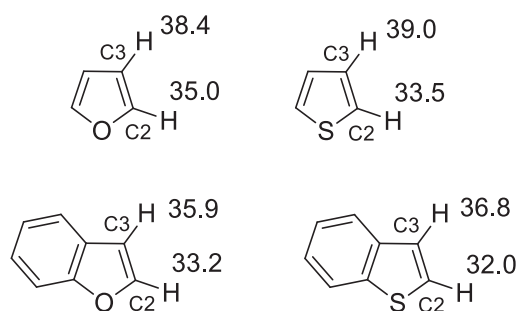
The regioselectivity on lithiation with strong bases can be explained by the relative acidity of the C-H bonds of the chalcogenophenes and benzo[*b*]chalcogenophenes, and therefore the stability of the conjugated bases from these compounds.³⁰ Generally, the acidity of chalcogenophenes and other five-member aromatic heterocycles lies in between 25 to 45 p*K*_a units (Scheme 6).³³ The proton α-heteroatom (bonded to C-2-position) in chalcogenophenes and benzo[*b*]chalcogenophenes shows about 3-5 p*K*_a units lower than the proton bonded to the C-3-position, so the C2-carbon is easily deprotonated with a strong base as, for instance, organolithiums or Grignard reagents. The proton α-heteroatom has stronger acidity since its respective conjugated base reach more stability arising from the inductive effect of the more electronegative heteroatom bonded to C2-carbon. On the other hand, the repulsion between the lone electron pairs of α-heteroatom and

the high-energy electrons at the C2-Li bond destabilize the conjugated base. Although, this lone electrons pairs repulsion is slightly reduced when the α -heteroatom is sulfur since the increase in bond length (Csp²-S) lowers the overlap of the vicinal lone electrons pairs, decreasing this unfavorable effect. The higher polarizability of the α -heteroatom is of critical importance since the high electron density at the lithiated C2-carbon is well accommodated for a high polarizable atom as sulfur, allowing higher stability for the conjugated base and then higher acidity to thiophene and benzo[*b*]thiophene. The C2-carbon is also deprotonated under kinetically-controlled conditions, since the Lewis acid-base reaction between the heteroatom and the lithium cation affords a point of coordination, increasing reactivity specifically in the locality close to the coordination site.

Experimental pKa values in THF



Theoretical pKa values in DMSO



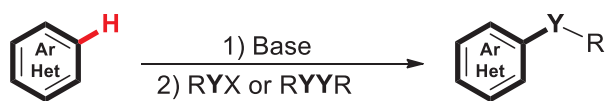
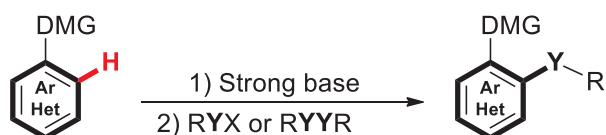
Scheme 6: Experimental and theoretical pKa values of furan, thiophene, benzo[*b*]furan and benzo[*b*]thiophene.

Over the last decades, organoselenium has moved from an unusual, bad-smelling chemistry, to an eco-friendly tool for organic synthesis. Despite not being an easy journey and there is no foreseeable shortcut to change this paradigm - some recent efforts by the selenium chemists community have brought up remarkable behavior of selenium-containing small molecules.^{34,35} For example, several studies have been conducted on the functionalization of chalcogenophenes with organoselenium fragments, but they are still limited to the innate C-2/C-5 regioselectivity of these heteroarenes on electrophilic aromatic substitutions and C-2/C-5 regioselectivity by metallations with strong bases. Given the interest in the introduction of selenium, sulfur, and tellurium containing functionalities as tools for selective chemical transformations and modification of materials or biological

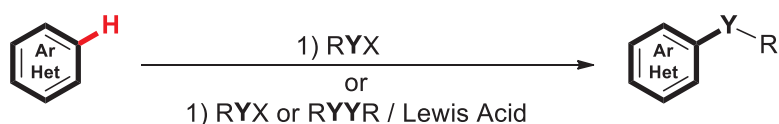
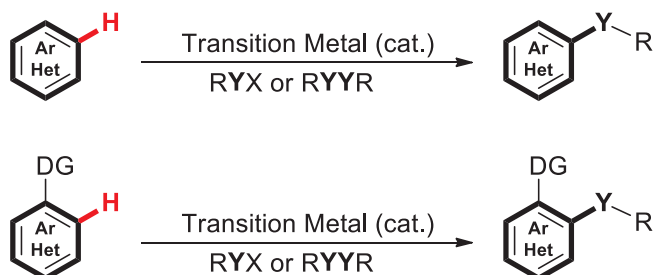
properties, the development of new synthetic methodologies for C-3/C-4 functionalization are required, and the transition metal-catalyzed direct chalcogenylations could allow the access to these outstanding regioselective control.⁷

1.2 TRANSITION METAL CATALYSED DIRECT CHALCOGENYLATION OF ARENES AND HETEROARENES

Conventional direct chalcogenylations of arenes and heteroarenes have been carried out with strong bases by simple deprotonation (Scheme 7a), directed *ortho* metallation (DoM) (Scheme 7b),³⁶ or by a combination of electrophilic organochalcogen reagents/electron rich arenes (Scheme 7c).³⁷ These methods have their importance but usually they show a limited substrate scope, involve multiple synthetic steps to prepare the starting materials, and often require difficult reaction conditions.

(a) Direct chalcogenylation with bases**(b) Direct chalcogenylation via DoM with strong bases**

Y = S, Se, Te
X = Leaving group
R = Aryl or alkyl

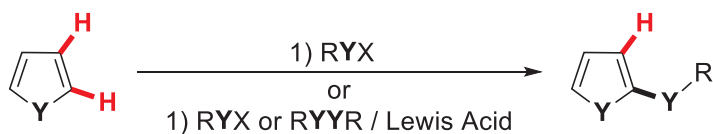
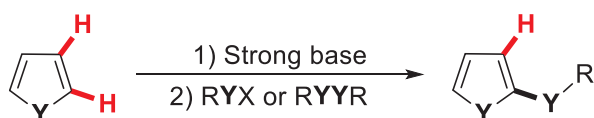
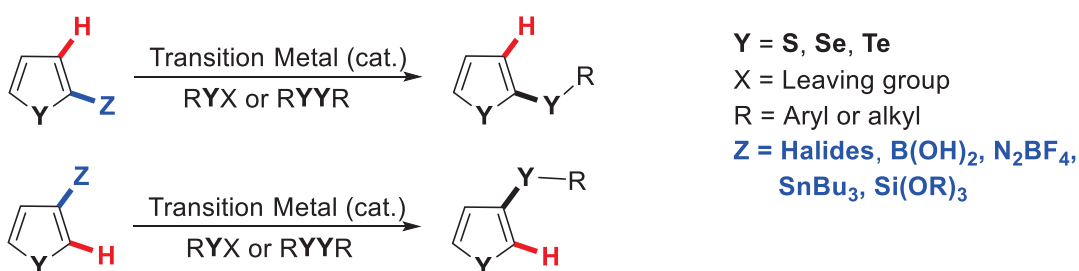
(c) Direct chalcogenylation with electron rich arenes/electrophilic organochalcogen reagents**(d) Transition metal catalyzed direct chalcogenylation**

Y = S, Se, Te
X = Leaving group
R = Aryl or alkyl

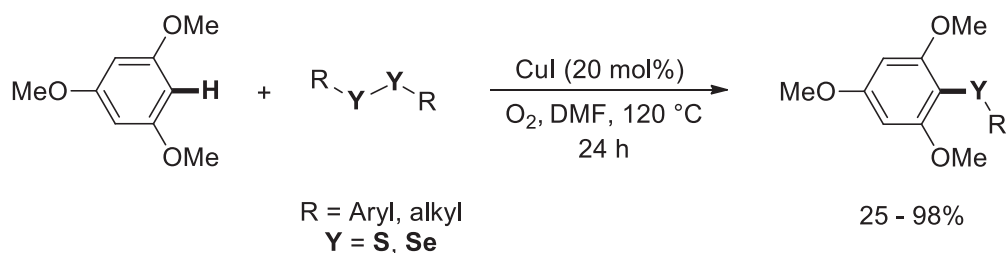
Scheme 7: Conventional and new approaches for direct chalcogenylation of (hetero)arenes.

In the perspective of synthetic analysis, transition metal-catalyzed direct chalcogenylation offers several opportunities (Scheme 7d), for the synthesis of a broad range of organochalcogen compounds, therefore, providing unprecedented disconnections for efficient C–Y (Y = S, Se, Te) bond formation. There are a large number of other conventional transition metal-based methods described for the regioselective formation of C–S, C–Se and C–Te bonds in hetero(arenes),³⁸ however, more recently much attention has been focused on the development of transition metals based C–H bond activation protocols considering the advantages of atom-economy and step-economy.^{7,39} Thus, numerous publications have appeared describing the transition metal-catalyzed direct chalcogenylation of unreactive C–H bonds.

Since chalcogenophenes are electron rich π systems, the reactions of these heterocycles with electrophilic organochalcogen reagents are extremely useful; however, they are limited to the innate C-2/C-5 regioselectivity through electrophilic aromatic substitutions (Scheme 8a).⁴⁰ When it comes to metallation with strong bases, the deprotonation of C-2 or C-5 carbon is straightforward considering the higher acidity of the hydrogen α -heteroatom in these heteroarenes, therefore the C-2/C-5 regioselectivity with organochalcogen electrophiles is retained (Scheme 8b).^{30,41} More recently, the direct cross-coupling reactions between the functionalized chalcogenophenes and a suitable organochalcogen coupling partners also have emerged as mild and efficient methods for C-Y (Y = S, Se, Te) bond formation (Scheme 8c),⁴² but the reaction regioselectivity was still limited to the pre-functionalization reactivity of these substrates. Major challenges in developing the chalcogenylations of chalcogenophenes involve the control of the C-3 regioselectivity, and only a few examples through chelation-assisted transition metal-catalyzed direct chalcogenylation were developed (Scheme 8d).⁴³

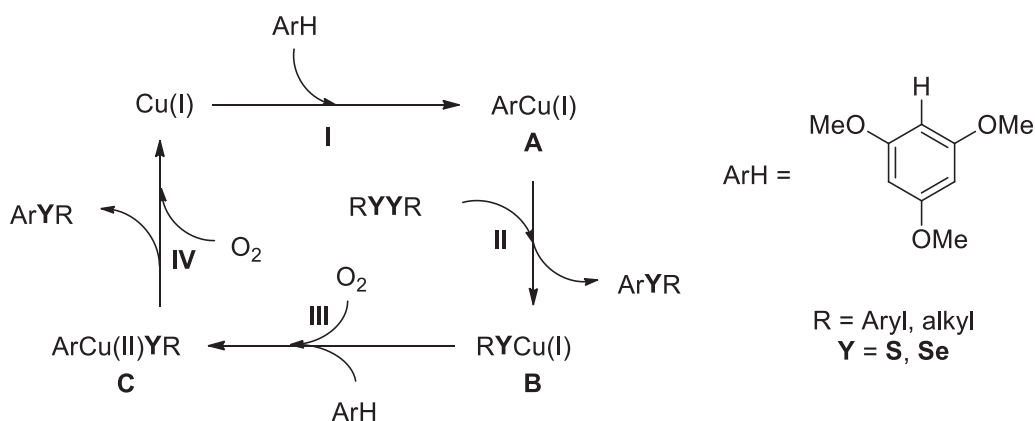
(a) Chalcogenylation with electrophilic selenium reagents (C-2 or C-5)**(b) Chalcogenylation with strong bases (C-2 or C-5)****(c) Chalcogenylation through cross-coupling reactions (C-2 or C-3)****(d) Chelation-assisted transition metal catalyzed direct selanylation (C-3)****Scheme 8:** Strategies for the C2/C5 and C3 chalcogenylation of chalcogenophenes.

Several studies have appeared describing the direct chalcogenylation of arenes and heteroarenes using various Cu complexes as catalysts, especially due to their low cost, abundance, and relatively low toxicity. For instance, in a seminal paper using this metal for these reactions, Cheng and co-workers have shown the Cu-catalysed selanylation of electron rich arenes (1,3,5-trimethoxybenzene) via C–H activation and using with diorganoyl dichalcogenide (Scheme 9).⁴⁴ The use of CuI as cheap catalyst and O₂ as an oxidant improved the practicality of this C–H functionalization reaction. By the use of these conditions only the mono-chalcogenylation product was obtained with good yield.



Scheme 9: Cu(I)-catalyzed direct chalcogenylation of 1,3,5-trimethoxybenzene through C-H bond activation.⁴⁴

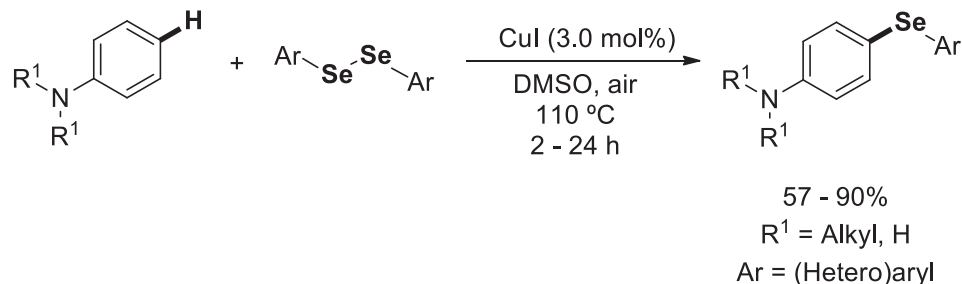
Based on the various experimental results, a plausible pathway for the chalcogenylation reaction was outlined by the authors (Scheme 10). Step I involve the formation of an cuprate from trimethoxybenzene via an unspecified C-H bond activation mechanism to afford the intermediate **A**. In step II, the ArCu(I) species (**A**) reacts with diphenyl dichalcogenide via an oxidative addition followed by a reductive elimination to afford the expected product and RYCu(I) (**B**). Then, in step III, oxidation and C-H activation of intermediate (**B**) occurs under O₂ to form the ArCu(II)YR intermediate (**C**). Finally, reductive elimination of the Cu(II) complex **C** leads to the product and Cu(0), which is oxidized by O₂ to Cu(I).



Scheme 10: Proposed reaction steps for the Cu(I)-catalyzed direct chalcogenylation of 1,3,5-trimethoxybenzene with diorganoyl dichalcogenides.⁴⁴

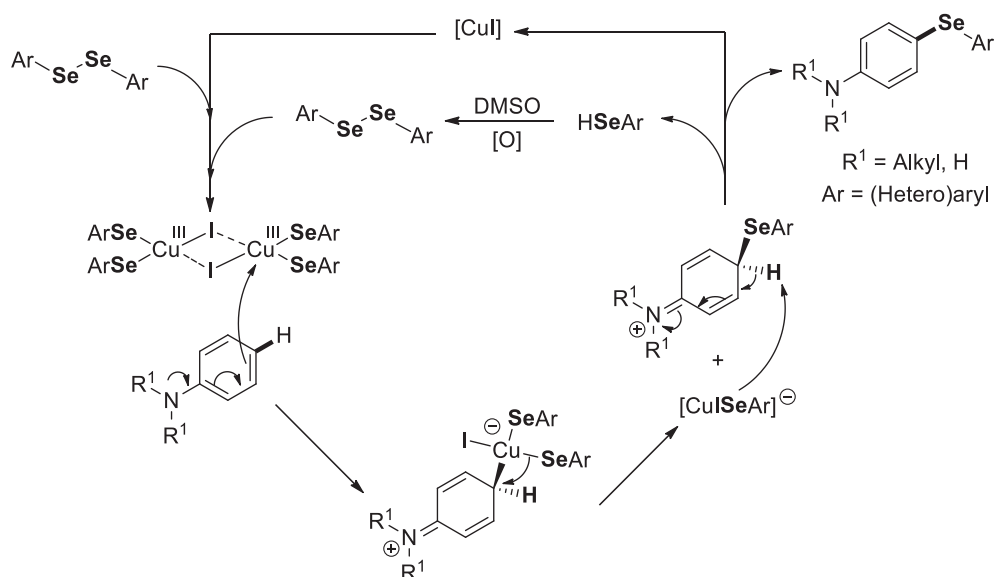
In 2015, Alves and co-workers reported an efficient and regioselective approach for the direct arylselanylation of anilines (Scheme 11).⁴⁵ In this methodology, a series of anilines and diaryl diselenides were employed. A catalytic amount of CuI was used and DMSO was the solvent to afford arylselanyl anilines in good to excellent yields. Both acyclic and cyclic tertiary amines were used at the optimum reaction conditions and the direct selanylation occurred regioselectively at the *para* position. When primary amines were tested, good results were also

obtained. The observed regioselectivity at *para* position also suggested an electrophilic aromatic substitution mechanism, considering the higher electron density at this site in anilines.



Scheme 11: Cu(I)-catalyzed direct selenylation of anilines.⁴⁵

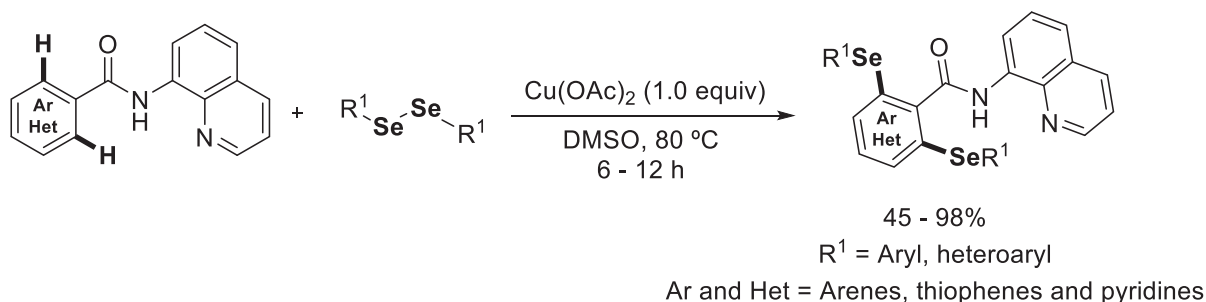
The proposed catalytic cycle (Scheme 12) involves an initial oxidative addition of CuI into Se-Se bond of the diaryl diselenide, leading to a dimeric Cu(III) arylselenolate intermediate. Next, the aniline performed a nucleophilic attack to Cu(III), furnishing the arenium intermediate, and then the C-Se bond was formed by reductive elimination. After the deprotonation of the cationic species produced in the reductive elimination by the anionic complex $[\text{ArSeCu}]^-$ formed in the previous step, the desired product was obtained.



Scheme 12: Proposed catalytic cycle for the Cu(I)-catalyzed direct selanylation of anilines.⁴⁵

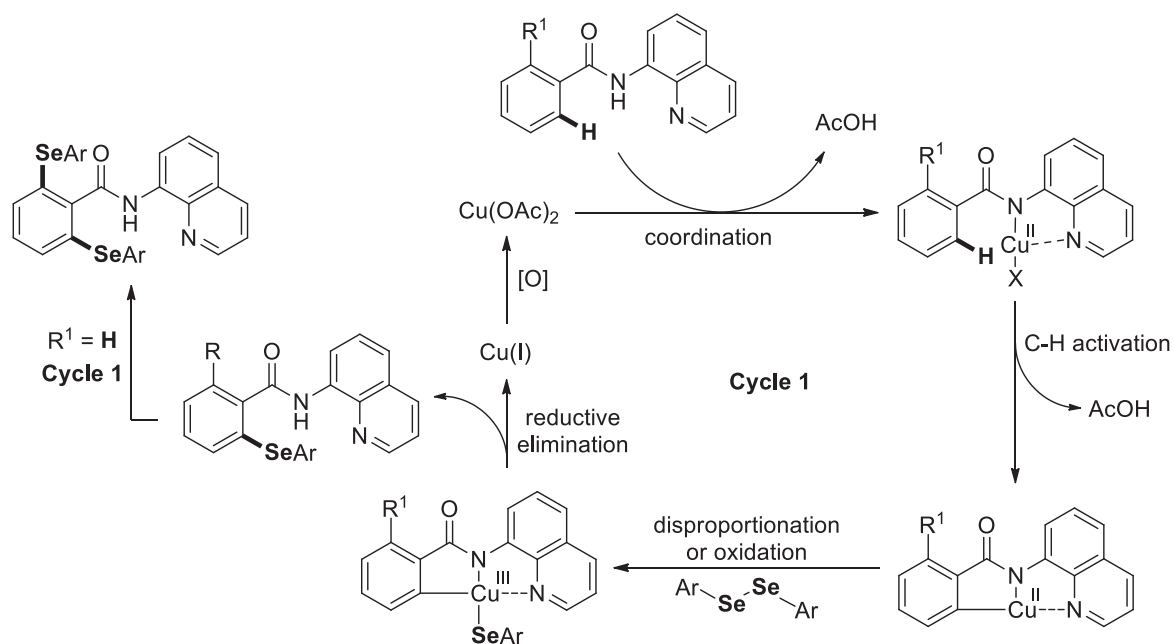
Regioselective control of direct chalcogenylations was also achieved with copper catalysts using the 8-amidoquinoline directing group. In 2016, Mandal and co-workers reported the chelation assisted direct selanylation of arenes and heteroarenes using Cu(II) and 8-amidoquinoline as the directing group.⁴⁶ The scope

also comprised thiophenes. Initially, this methodology focused on the synthesis of selanylated *N*-(quinolin-8-yl)benzamide derivatives by Cu(II)-mediated *ortho*-selanylation of arenes and heteroarenes with diaryl diselenides using 8-amidoquinoline as a directing group (Scheme 13). The reaction scope was broad and interestingly the mono-selanylation was achieved with a *meta*-disubstituted amide. After that, the authors investigated the catalytic version of this protocol. For this purpose, Cu(OAc)₂ (20 mol%), 1.0 equivalent of Ag₂CO₃ and KF were successfully employed to afford the desired products in good to excellent yields.



Scheme 13: Cu(II)-mediated 8-aminoquinoline directed selanylation of (hetero)arenes.⁴⁶

Several tests were conducted to clarify the mechanism, where it was observed that Csp²-H bond cleavage was irreversible, and that the involvement of radical species was unlikely in the reaction pathway. In this way, the authors suggested that the mechanism occurs via coordination of the Cu(II) catalyst with the amide, producing the chelated Cu(II)-aryl species, which by a CMD mechanism (concerted metalation-deprotonation mechanism) produces another Cu(II)-aryl specie. The C,N,N-pincer type Cu(III)-aryl intermediate is formed by disproportionation/oxidation and transfer of the arylselanyl moiety. After that, a reductive elimination produces the mono-selanylated product and Cu(I), which is oxidized to Cu(II) catalyst to enter again in the catalytic cycle. The mono-selanylated product (R¹ = H) enter again into the catalytic cycle to produce the di-selanylated product (Scheme 14).



Scheme 14: Proposed catalytic cycle for Cu(II)-catalyzed 8-aminoquinoline oriented directed selenylation of (hetero)arenes.⁴⁶

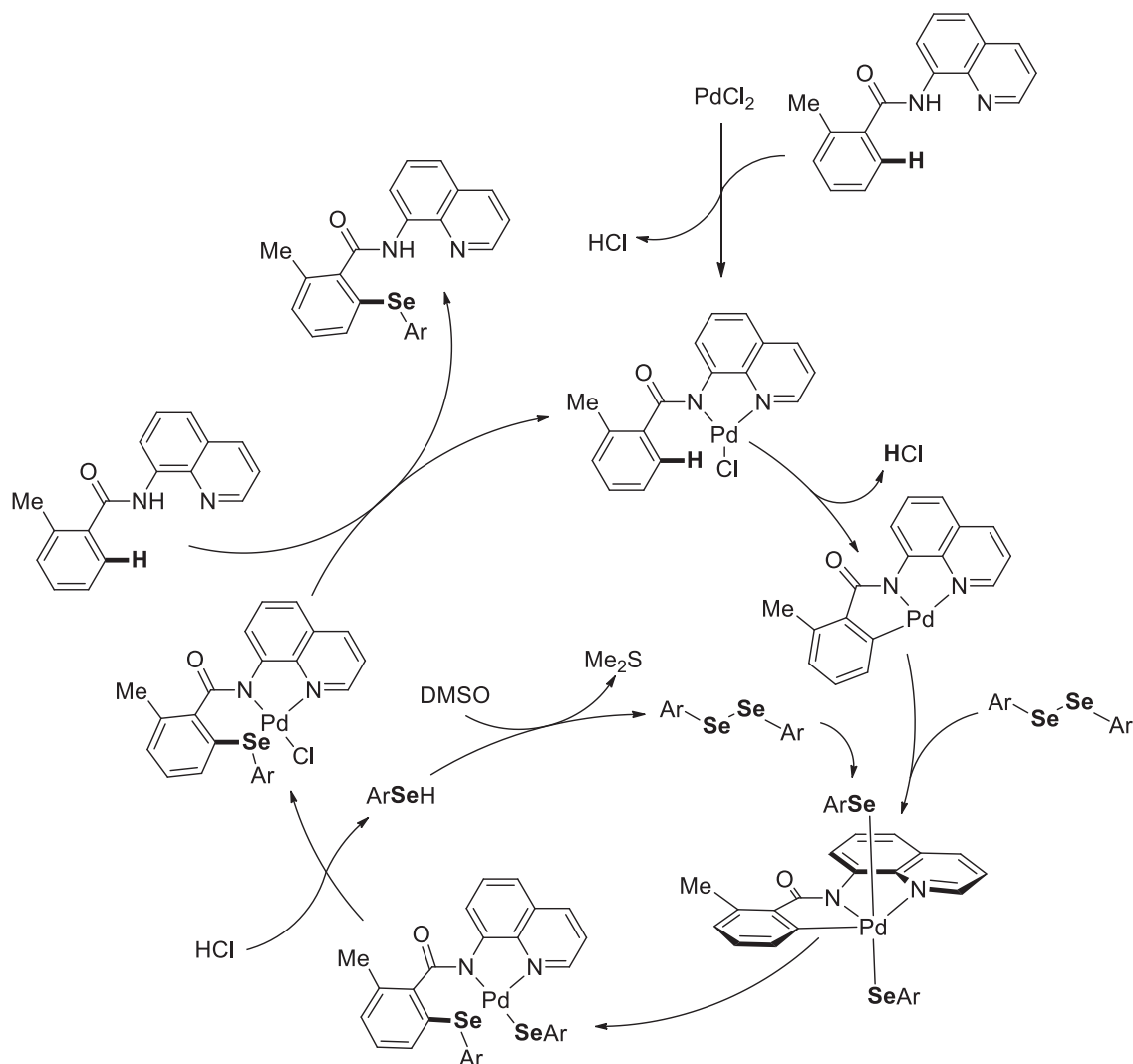
The outstanding advances in Pd-catalyzed direct C-H bond functionalization also paved the way for the development of direct chalcogenylations. An interesting case was described by Iwasaki and co-workers for the chelation-assisted Pd(II)-catalyzed direct selanylation of Csp²-H bonds with diphenyl dichalcogenides.⁴⁷ This was a straightforward method for the synthesis of diaryl selenides through chelation-assisted Csp²-H bond activation. 8-amidoquinoline and 2-phenylpyridine derivatives were used as directing groups, providing selanylated products in good to excellent yields (Scheme 15). PdCl₂(PhCN)₂ (5 mol%) was the best catalyst in the presence of 0.5 equivalents of diaryl diselenides and DMSO as solvent.



Scheme 15: Chelate-assisted Pd(II)-direct selanylation of aryl Csp²-H bonds.⁴⁷

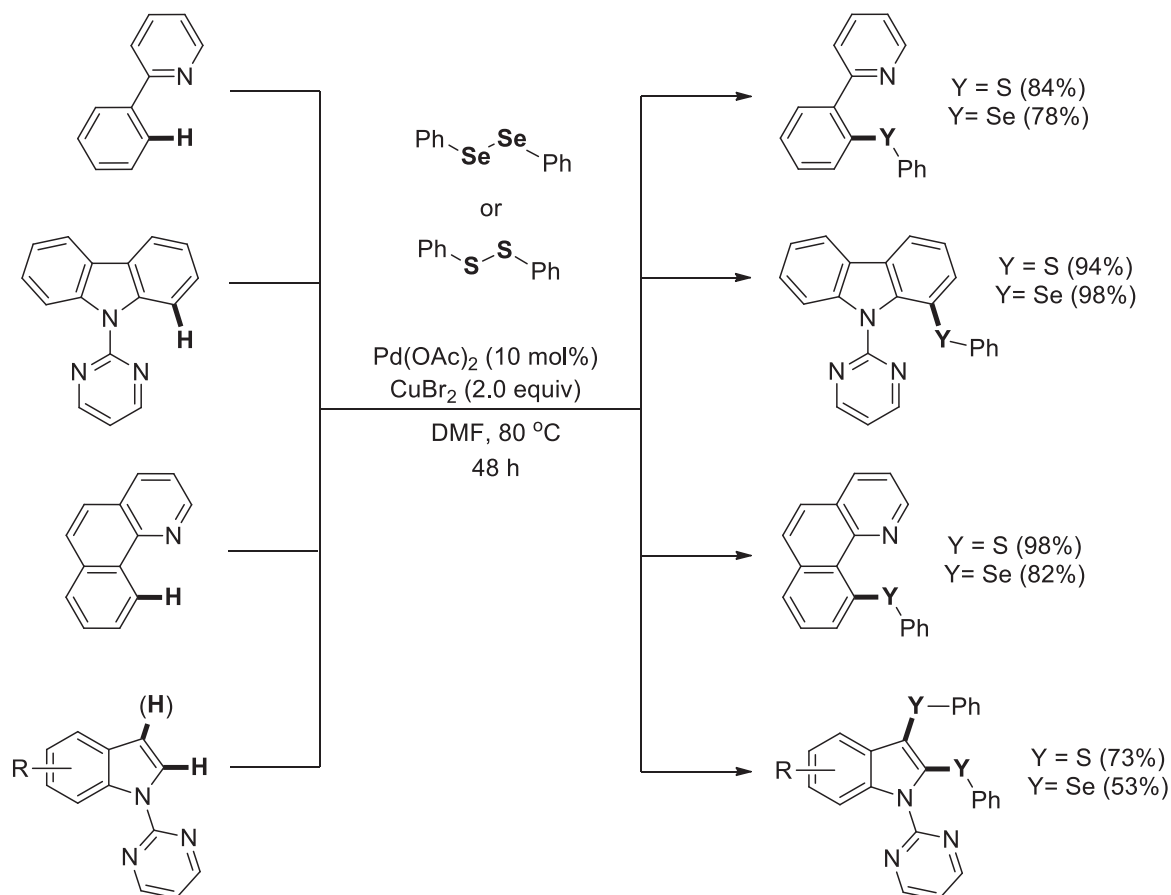
The authors performed several control experiments and gained insights about this catalytic cycle (Scheme 16). Initial coordination of the 8-amidoquinoline derivative with Pd(II) occurred. Subsequently, the activation of the Csp²-H by and

undefined mechanism gave a palladacycle, that undergoes oxidative addition in the presence of diaryl diselenide to form high-valent palladium Pd(IV) or Pd(III). Reductive elimination in the subsequent step leads to the formation of the Csp²-Se bond. After neutralization of palladium aryl selenide with HCl, the chloropalladium chelate and benzeneselenol can be produced. This last step is fundamental for the catalytic reaction. The role of HCl was not clear, but in the absence of the HCl produced in situ the reaction yield is low. The authors suggested that due the strong affinity of the Pd–Se bond, HCl is required to release again the Pd(II) catalyst and the arylselenols, which could be oxidized by DMSO to regenerate diaryl diselenides, that goes back into the catalytic cycle. At the end, the ligand exchange of chloro palladacycle with the substrate provides the product and produces again the initial palladacycle.



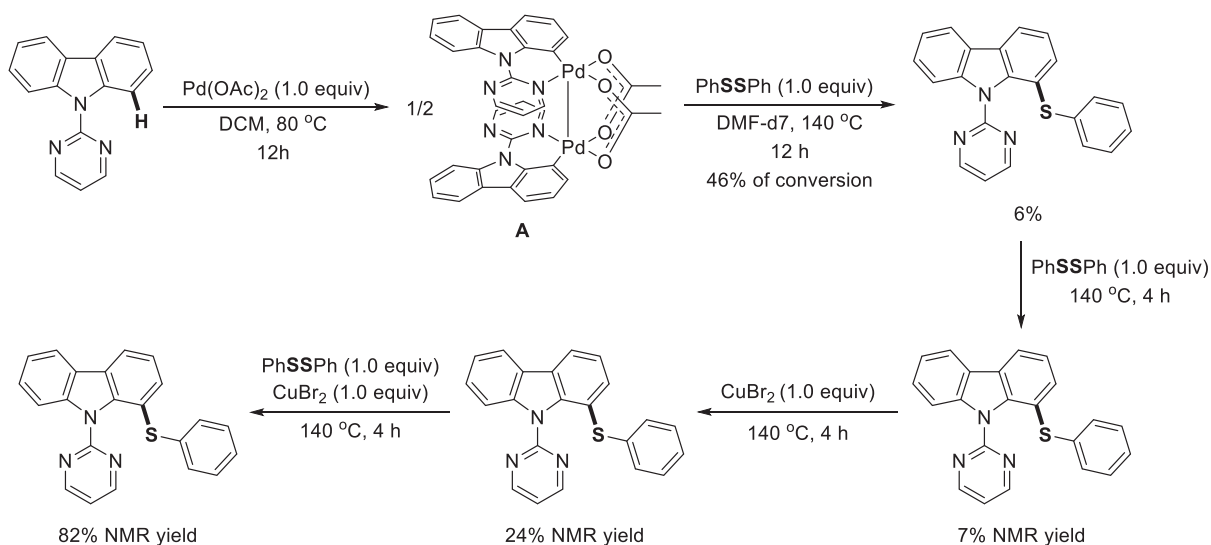
Scheme 16: Proposed catalytic cycle for chelate-assisted Pd(II)-direct selenylation of benzamides and 2-phenylpyridine.

The direct chalcogenylation of 2-phenylpyridine, carbazole, benzo[*h*]quinoline, and indole derivatives was described by Kambe and co-workers using Pd(II) and Cu(II) (Scheme 17).⁴⁸ The reaction was suitable with pyridine and pyrimidine directing groups, which are well tolerated by various synthetically useful functionalized arenes and heteroarenes. The authors observed that 2.0 equivalents of CuBr₂ as an oxidant significantly improved the product yield compared to other Cu(II) or Ag(I) salts. The optimized reaction conditions lead to the expected products in good reaction yields.

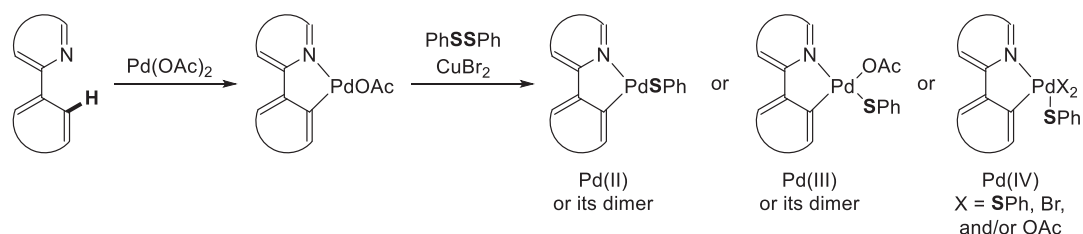


Scheme 17: Pd(II)-catalyzed chelate-assisted direct chalcogenylation of carbazole, 2-phenylpyridine, benzo[*h*]quinoline, and indole derivatives.

In order to clarify the reaction mechanism, the dimer **A** was synthesized and subjected to reaction conditions with 1.0 equivalent of diphenyl disulfide as model reaction (Scheme 18). The complex **A** and diaryl disulfide were partially consumed, but the product was formed in only 6% yield. In contrast, when both the disulfide and 1.0 equivalent of CuBr_2 were added, the sulfenylation did proceed efficiently to the formation of the coupling product in 82% yield, suggesting that Cu(II) mediates the transfer of the PhS group to Pd to form a thiolate complexes, however, Pd thiolate complexes at higher oxidation states (dinuclear Pd(III) or mononuclear Pd(IV) complexes) cannot be ruled out (Scheme 18). The formed Pd complexes containing the PhS group would then undergo reductive elimination to form the expected product. Unfortunately, the detailed mechanism is still unclear.

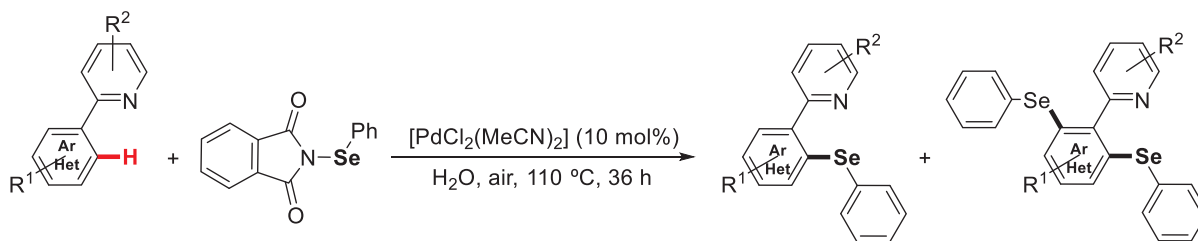


Proposed reaction steps:



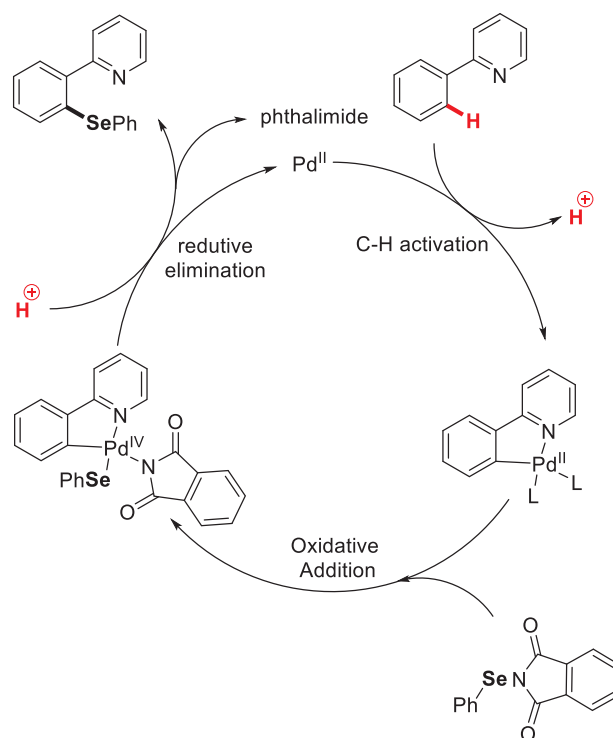
Scheme 18: Control experiments of Pd(II)-catalyzed direct chalcogenylation of carbazole, 2-phenylpyridine, benzo[*h*]quinoline, and indole derivatives and proposed reaction steps.

The direct selenylation of arenes and heteroarenes with *N*-(phenylselenyl)phthalimide in water was described by Law and co-workers using oxidant-free Pd(II) (Scheme 19).⁴⁹ The protocol provided chelate-assisted aryl and heteroaryl selenide in good yields via $\text{Csp}^2\text{-H}$ activation of 2-phenylpyridines derivatives. The scope also comprised furan. The reaction under optimal condition afforded 70% yield by using $\text{PdCl}_2(\text{MeCN})_2$ (10 mol%) after 36 h at $110\text{ }^\circ\text{C}$. On the other hand, the influence of different electron-donating groups bonded to 2-phenylpyridine derivatives was examined, as a result good yields was observed. While the 2-phenylpyridine derivatives functionalized with electron-withdrawing groups, comparatively lower yields were detected. Similarly, due to steric hinderance, the methyl group in relation to the directing group at ortho position provided 47% yield. In contrast, when the methyl group changed from ortho to meta position, the yield was significantly increased.



Scheme 19: Chelate-assisted Pd(II)-direct selenylation of arenes and heteroarenes with *N*-(phenylselenenyl)phthalimide in water.

The mechanism of the reaction was described after a series of control experiments. Initially the radical scavengers such as 2,2,6,6-tetramethyl-1-piperidinyloxy (TEMPO) and 2,6-di-*tert*-butyl-4-methylphenol (BHT) were evaluated, as a result no modification occurred in reaction, which proved that the reaction do not proceeds through radical pathway. Similarly, the intermolecular kinetic isotopic effect ($k_H/k_D = 1.4$) indicates that the arene C^{sp2}-H bond activation may not be involved in rate determining step in the second test. In addition, the equimolar meta and para-substituted 2-phenylpyridines and 2-phenylpyridines reaction was compared in optimal reaction condition and with a base, as a result a Hammett plot was obtained. The results indicated that electron-donating groups enable the formation of electrophilic metal complex intermediate in the reaction. according to these observations a proposed mechanism was presented. At the beginning, a cyclopalladation intermediate was formed from the combination of 2-phenylpyridine and PdCl₂(MeCN)₂. In the next step, *N*-(phenylselenenyl)phthalimide leads Pd(IV) intermediate through oxidative addition, which produced the desired product and regenerate the Pd(II) species after reductive elimination in the final step. (Scheme 20).



Scheme 20: Proposed mechanism for chelate-assisted Pd(II)-direct selenylation of arenes and heteroarenes with *N*-(phenylselenenyl)phthalimide.⁴⁹

The C-H functionalization reactions are attractive alternatives to cross-coupling reactions and has a great impact on the C-C and C-Het bond formations. Thus, several efforts were focused on the development of transition metal catalytic systems for the selective C-Y (Y = S, Se, Te) bond formation based in C-H functionalization reactions.^{7, 40b,c} The direct conversion of an inert C-H bond to C-Y bond catalyzed by transition metals has offered an innovative technology in synthetic methodology considering the atom and step-economy principles, opening novel possibilities in the synthesis of functionalized organochalcogen compounds. The use of suitable directing groups has been successfully applied to control the regioselectivity of direct chalcogenylations., and the investigation in this area could afford several new organic transformations by the study of structural straightforward and easily to add and remove directing groups.

The development of transition metal-catalyzed direct chalcogenylations through C-H activation has seen rapid recent advances. The most versatile transition metal-based systems for synthetically useful C-H functionalization have emerged from an early focus on Pd, Rh, Ru and Ir based catalysts for direct arylations and dehydrogenative cross-couplings. In aromatic heterocycles, the heteroatoms usually guide the regioselectivity of C-H functionalization reactions due to their influence on

the electron density of the different C-H positions. One way to achieve a new regioselectivity involves the assistance of directing groups (DGs), consisting of a coordinating moiety (an “internal ligand”), which directs a transition metal catalyst into the proximity of a certain C-H bond in the molecule, leading to its selective cleavage and subsequent functionalization. This strategy enables overruling innate reactivity in (hetero)arenes.

2 OBJECTIVES

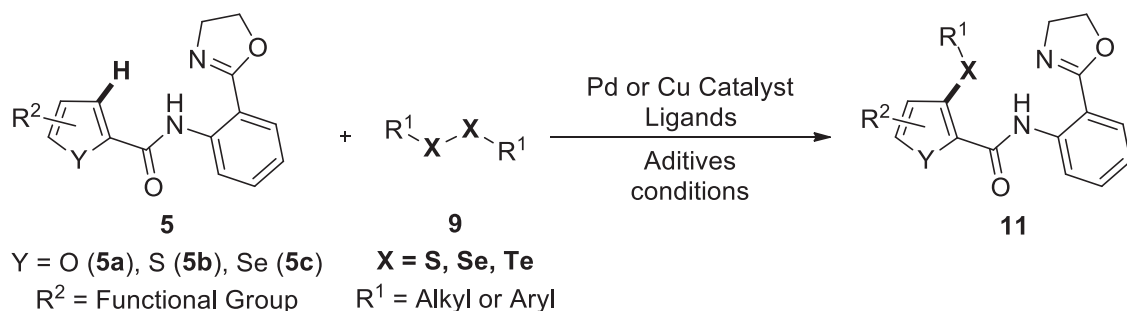
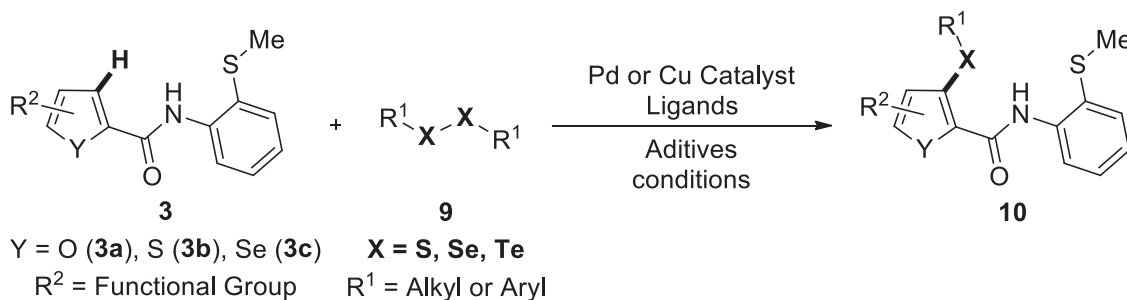
2.1 GENERAL OBJECTIVES

This PhD thesis aims the development of a new regioselective C3 direct chalcogenylation of chalcogenophenes catalyzed by transition metals using the 2-(methylthio)amide or 2-(4,5-dihydrooxazol-2-yl)amides as directing groups.

2.2 SPECIFIC OBJECTIVES

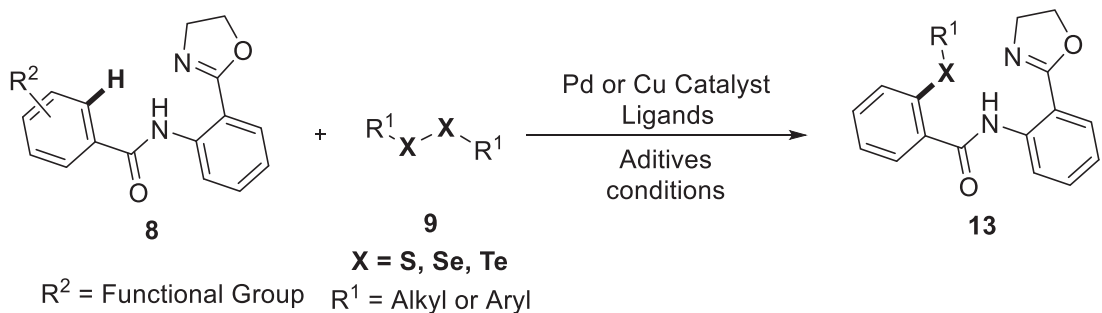
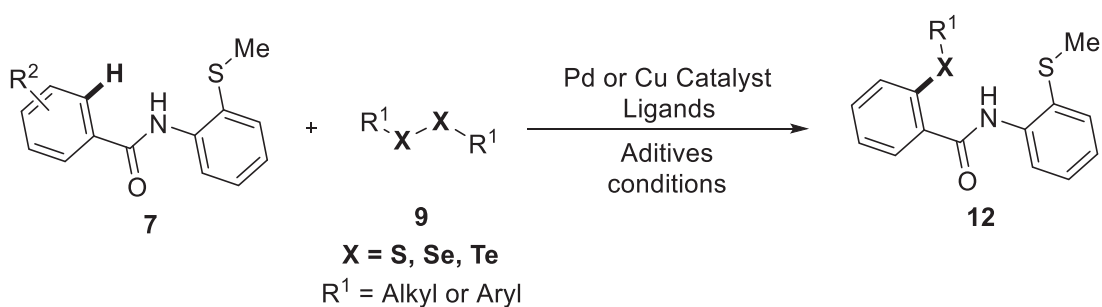
- Synthesis of starting materials with the general structures **3**, **5**, **7**, **8**, (Scheme 23). The amide synthesis will be developed using the Steglich conditions with DCC (*N,N'*-dicyclohexylcarbodiimide) and DMAP (4-dimethylaminopyridine) in dichloromethane.
- Subsequently, the compounds with general structure **3**, **5**, **7**, **8**, will be evaluated through transition metal-catalyzed direct chalcogenylations with palladium or copper catalysts, in order to identify the optimal conditions for the regiocontrolled functionalization at C3 position in chalcogenophenes and at C2 position in benzamides (Scheme 21 and 22).

(a) Regioselective C3 Direct Chalcogenylation of Chalcogenophenes using Directing Groups



Scheme 21: Regioselective C3 transition metal (Pd or Cu) direct chalcogenylation of chalcogenophenes using directing groups.

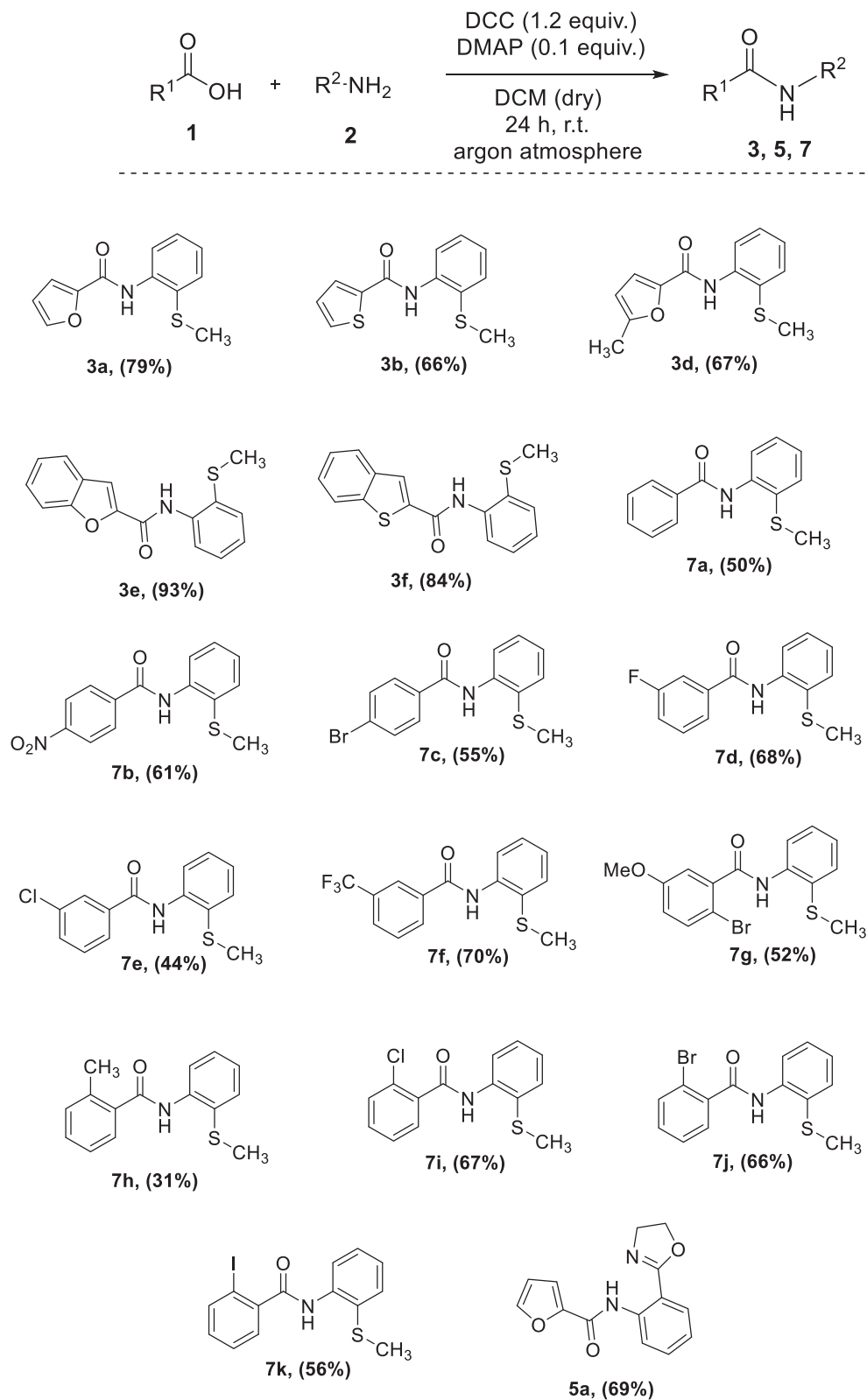
(b) Regioselective C2 Direct Chalcogenylation of Arenes using Directing Groups



Scheme 22: Regioselective C2 transition metal (Pd or Cu) direct chalcogenylation of arenes using directing groups.

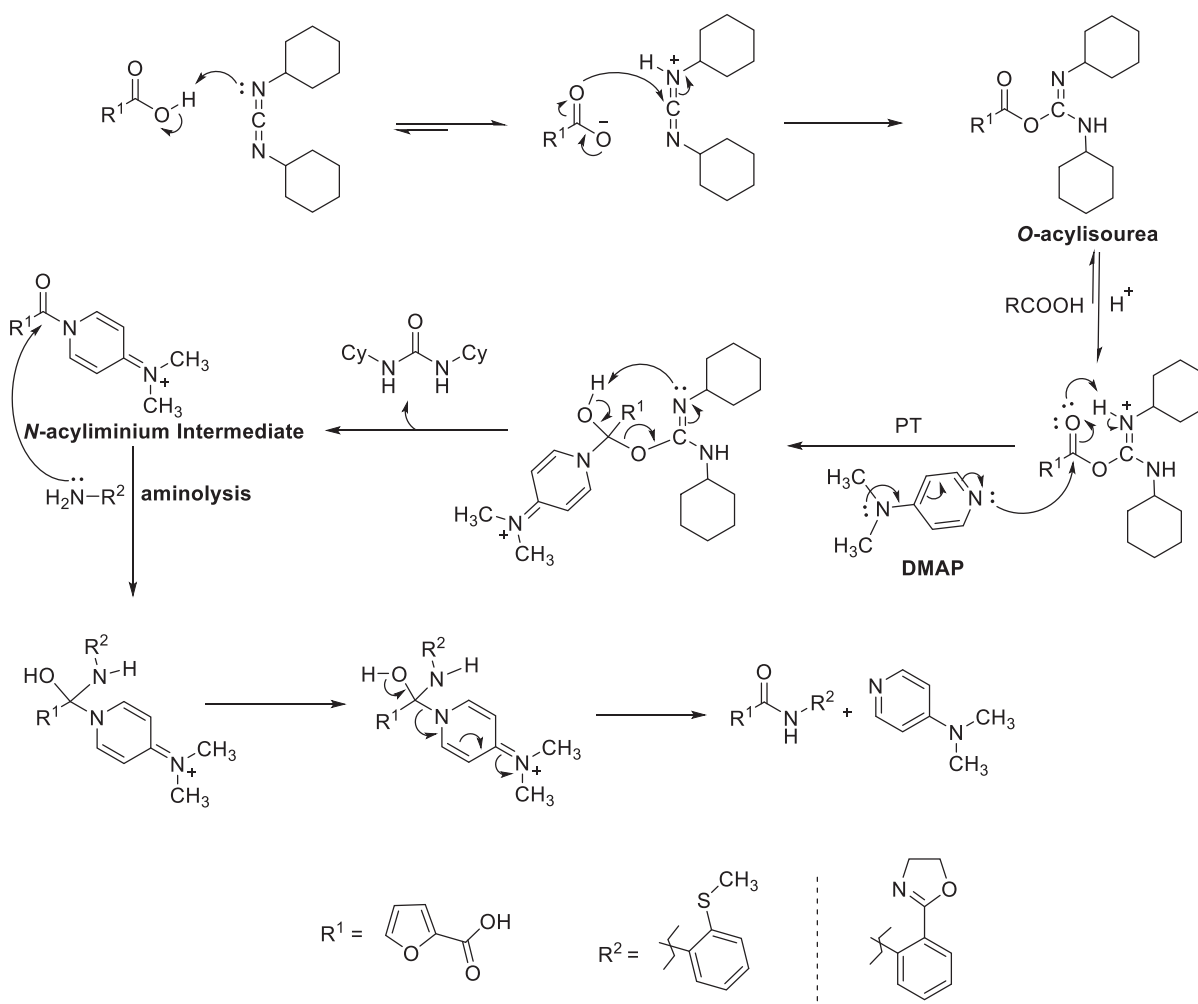
2.3 SYNTHESIS OF STARTING MATERIALS

The starting materials containing the amide functional group were synthesized at the first step of this project. One of the traditional approaches used to produce amide groups from simple carboxylic acids and amines is the carbodiimide method, using *N,N'*-dicyclohexylcarbodiimide (DCC).⁵⁰ Carbodiimides contain two nitrogen atoms attached to the same carbon atom (C-sp), which makes it electronically deficient enough to trigger a reaction between the carbodiimide and the carboxylic acid to generate the *O*-acylisourea intermediate.⁵¹ This intermediate is the reactive specie toward nucleophiles as alcohols or amines, although these reactions can be accelerated with a catalytic amount of pyridine or *N,N'*-dimethylaminopyridine (DMAP), as reported in 1978 by Neises and Steglich.⁵² As a good nucleophile, DMAP reacts with the *O*-acylisourea leading to an acyliminium intermediate.⁵³ This reactive specie rapidly undergoes aminolysis in the presence of amine to yield the amide.⁵⁴ In order to synthesize the 2-(methylthio)amides (**3**) and *N*-2-(4,5-phenyl)furan-2-amide (**5**), the DCC/DMAP method was employed using experimental conditions in according to the seminal method.⁵² On the basis of the results of the reaction, the compounds which contain heteroatom at alpha position such as furan, thiophene, benzo[*b*]furan and benzo[*b*]thiophene afforded good yields of expected product. On the other hand, the aryl group bonded to carboxyl group provided the yield around 50-60% while the methyl group on the ortho position of aryl group gave lower yield by employing this methodology (Table 1).^{50,54}

Table 1: Synthesis of starting materials through Steglich conditions.

Reaction conditions: Acid (2 mmol), amine (2 mmol), DCC (2.4) and DMAP (0.2 mmol) in dry CH_2Cl_2 solvent (10 mL) at room temperature under argon atmosphere for 24 h (Table 1). Isolated yields

The mechanism of the above reactions begins with the proton transfer from carboxylic acid to the basic nitrogen on carbodiimide to give an ion pair. After that, the addition of the carboxylate group to the carbodiimide provides the *O*-acylisourea, a reactive acylating agent. Although, the *O*-acylisourea could follow an intramolecular rearrangement to produce an unreactive *N*-acylurea. In order to prevent this side reaction of *O*-acylisourea, catalytic amounts of *N,N*'-dimethylaminopyridine (DMAP) is added to reaction, which quickly react with *O*-acylisourea in the second step to generate a reactive *N*-acyliminium intermediate and *N,N*'-dicyclohexylurea as byproduct. The intermediate *N*-acyliminium undergoes aminolysis in the last step to produce the expected amide and regeneration of DMAP nucleophilic catalyst (Scheme 23).⁵⁰⁻⁵⁴



Scheme 23: Mechanism of DCC/DMAP mediated synthesis of starting materials.

The starting materials were characterized by means of low resolution Mass Spectrometry (MS), ^1H and ^{13}C Nuclear Magnetic Resonance (NMR) Spectroscopy,

Heteronuclear (^1H - ^{13}C) Single Quantum Correlation (HSQC) and Heteronuclear (^1H - ^{13}C) Multiple Bond Correlation (HMBC) experiments. All data are included in the supplementary materials. In order to illustrate the spectrometric and spectroscopic characterization, the compound **3a** was used to demonstrate the methodology employed. The compound **3a** was isolated by column chromatography with silica gel (grade 60, 0-63 μm , 70-230 mesh) as stationary phase and a mixture of hexane and ethyl acetate as eluent [hexane (95%):ethyl acetate (5%)(v:v)]. It was observed by low-resolution Mass Spectrometry (MS) under electron impact (EI, 70 eV) the molecular ion with m/z 233, as expected for molecular structure of compound **3a** (Figure 5). The fragment ion peak with m/z 186 arises from the heterolytic $\text{Csp}^2\text{-S}$ cleavage, related to the loss of CH_3S radical, and the ion peak with m/z 95 arises from the conventional homolytic $\text{Csp}^2\text{-N}$ cleavage of amides.

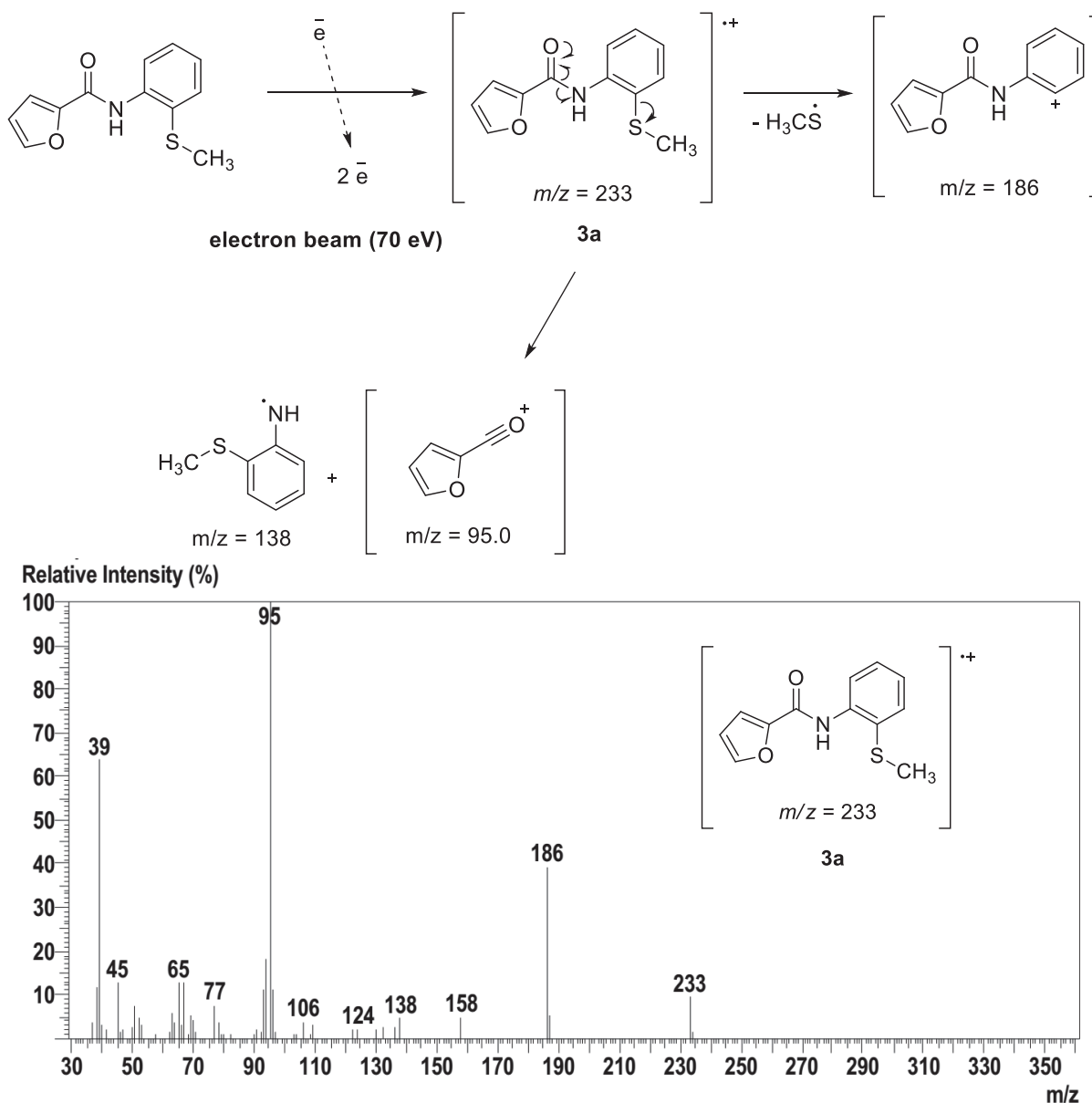


Figure 5: Low-resolution mass spectrum (EI, 70 eV) of *N*-(2-(methylthio)phenyl)furan-2-carboxamide (**3a**).

The ^1H NMR spectrum of compound **3a** (Figure 6) shows that most of the signals were observed in the characteristic region of aromatic hydrogens and only one signal of the methyl group in lower frequencies. The ^1H NMR spectrum of product **3a** also shows the relative integrals of 11 hydrogen atoms, in accordance with the molecular structure of *N*-(2-(methylthio)phenyl)furan-2-carboxamide (**3a**). In order to identify the specific signals a careful analysis of the ^1H NMR spectrum was done. It was observed a broad singlet at 9.37 ppm (br. s; 1H) relative to the H atom attached to nitrogen atom (H-4) of the amide group. Additionally, the doublet of doublets at 8.48 ppm (dd, $J = 8.2, 1.2$ Hz, 1H) is related to the H-10 hydrogen atom, and the doublet of doublets at 7.53 ppm (dd, $J = 7.8, 1.4$ Hz, 1H) to the H-7 hydrogen

atom. Also, the triplet of doublets at 7.34 ppm (td, $J = 7.9, 1.4$ Hz, 1H) is related to H-9 hydrogen atom and the triplet of doublets at 7.09 ppm (td, $J = 7.6, 1.3$ Hz, 1H) to the H-8 hydrogen atom. Considering the coupling constants values, chemical shifts and multiplicities, we can suggest that the remaining signals are related to the hydrogens bonded to the furan ring. In this way, the doublet of doublet at 7.56 ppm (dd, $J = 1.6, 0.8$ Hz, 1H) belongs to the H-15 hydrogen atom, and the doublet of doublets at 7.25 ppm (dd, $J = 3.6, 0.8$ Hz, 1H) to the H-13 hydrogen atom. Finally, the doublet of doublets at 6.57 ppm (dd, $J = 3.5, 1.8$ Hz, 1H) is related to the H-14 hydrogen atom and the singlet at 2.41 ppm (s, 3H) to H-12 hydrogen atoms of the methyl group.

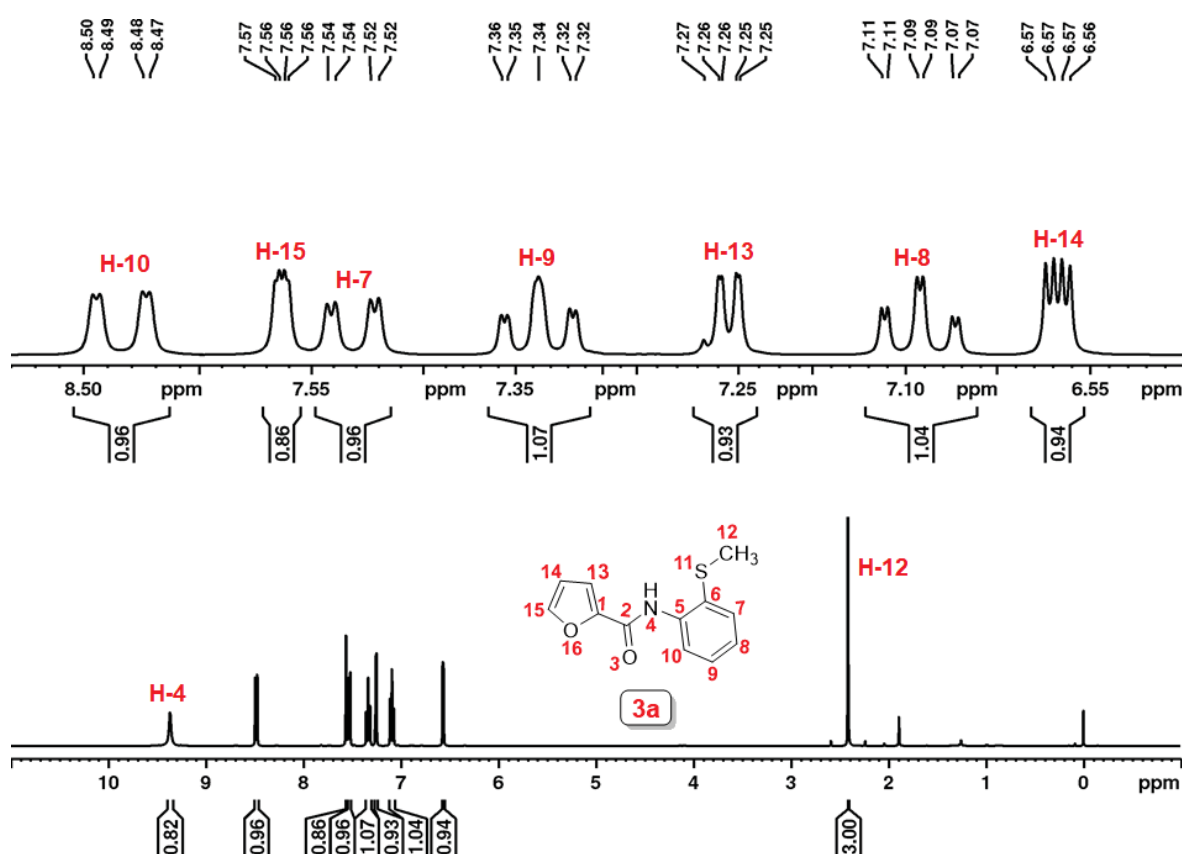


Figure 6: ^1H NMR spectrum (400 MHz, CDCl_3) of *N*-(2-(methylthio)phenyl)furan-2-carboxamide (**3a**).

The overall ^{13}C NMR spectrum of compound **3a** (Figure 7) shows 12 signals for all observable carbons. Most signals are in the region above 110 ppm, while only one signal at 19.1 ppm is related to methyl group bonded to sulfur atom (C-12). The quaternary carbons C-1, C-2, C-5 and C-6 give rise to 4 small peaks, where the signal at 156.1 ppm is characteristic of a carboxylic carbon of an amide group (C-2). Also, the signal at 148.0 ppm is related to the carbon C-1. In the other hand, the

signal at 138.2 ppm arises from the carbon C-5 and the signal at 125.4 ppm from carbon C-6 bonded to sulfur. In order to assign the remaining signals of each carbon atom in the molecular structure of **3a**, the HSQC (Heteronuclear Single Quantum Correlation) correlation map was obtained (Figure 8). In the figure 8 it was possible to observe that the correlations between ^1H and ^{13}C were observed in the region of characteristic peaks of aromatic rings and one hydrogen carbon on aliphatic region.

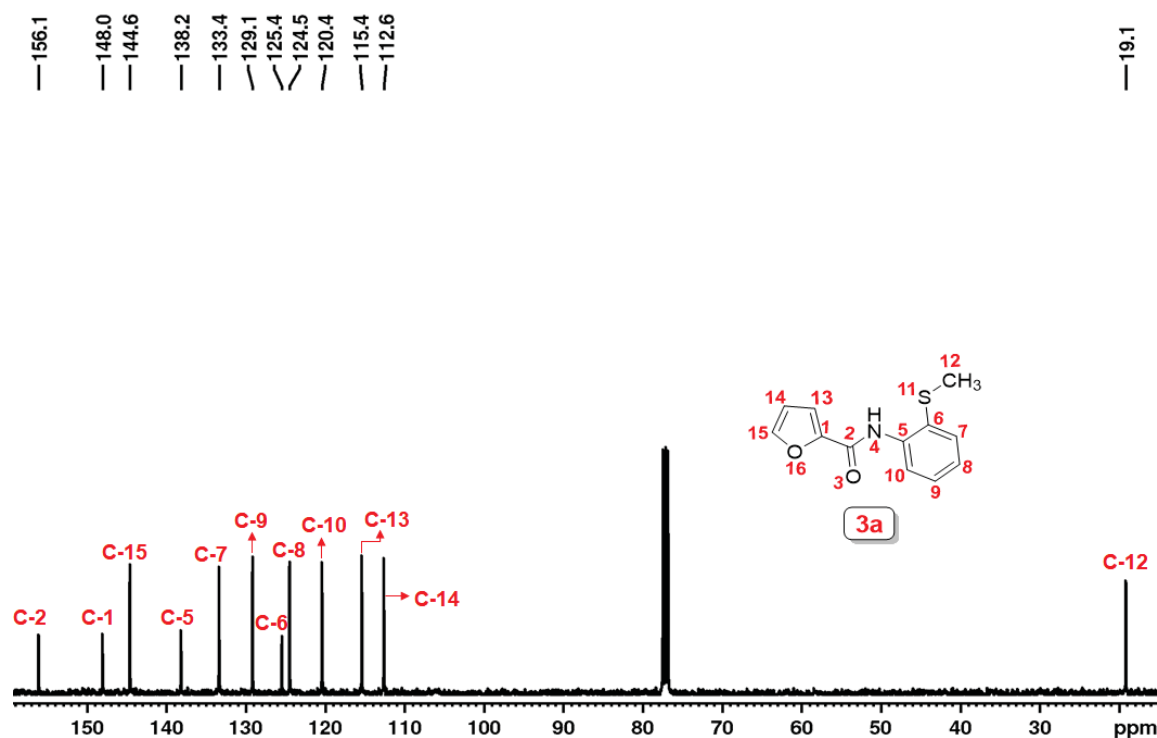


Figure 7: ^{13}C NMR spectrum (100 MHz, CDCl_3) of *N*-(2-(methylthio)phenyl)furan-2-carboxamide (**3a**).

Considering the broad range of ^{13}C NMR chemical shifts, we expand the region between 15,0 ppm – 155.0 ppm (Figure 8) in the HSQC correlation map to establish the direct ^1H - ^{13}C connections. The correlation between the doublet of doublets H-10 was found with the signal at 120.4 ppm in the ^{13}C spectra. As expected, the signal related to hydrogen H-4 does not have any correlation with carbon atoms. In the other hand, the H-15 depicted correlation with the carbon (C-15) signal at 144.6 ppm and the H-7 next to it with the signal at 133.4 ppm related to the carbon C-7. Additionally, the triplet of doublets of H-9 is correlated to the C-9 at 129.1 ppm and the doublet of doublets for the H-13 hydrogen with the signal at 115.4 ppm (C-13). Finally, the triplet of doublets of H-8 is correlated to the signal at 124.5 ppm (C-8), the doublet of doublets of H-14 was observed at 112.6 ppm (C-14) and the singlet of H-12 showed direct correlation at 19.1 ppm (C-12).

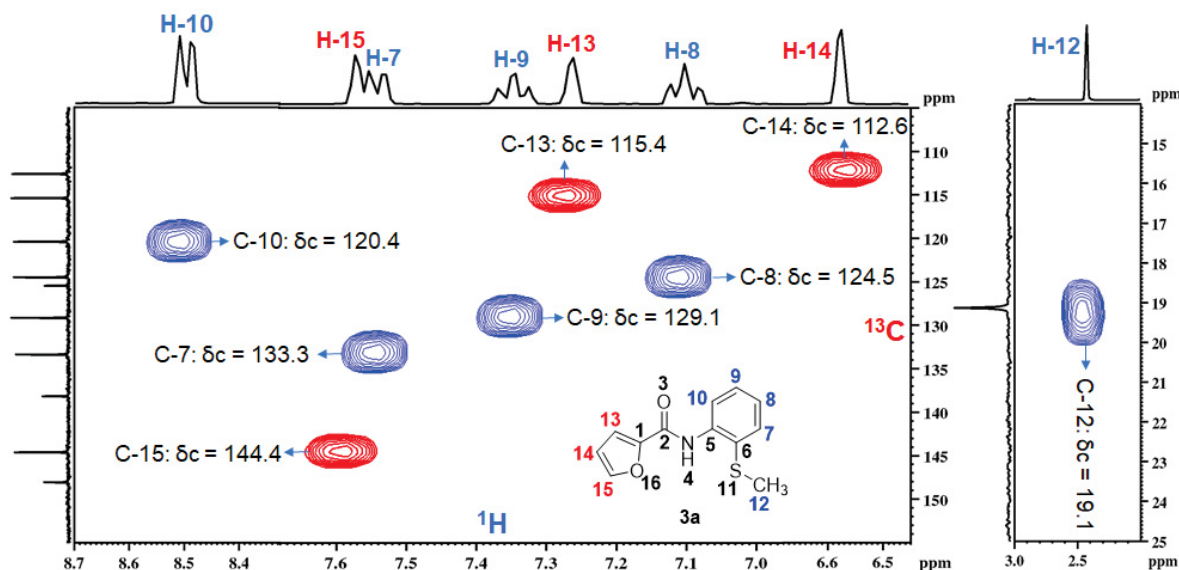


Figure 8: ^1H - ^{13}C HSQC correlation map (^1H , 400 MHz; ^{13}C , 100 MHz) of *N*-(2-(methylthio)phenyl)furan-2-carboxamide (**3a**).

Further confirmation of **3a** was established by Heteronuclear (^1H - ^{13}C) Multiple Bond Correlation (HMBC) experiments (Figure 9). In this sense, the long-range ^1H - ^{13}C correlations for **3a** were identified in the benzene system, where the H-10 at 8.50 ppm have shown correlation to C-8 (124.5 ppm), and C-6 (125.4 ppm). Next to it, the H-7 at 7.53 ppm was correlated to C-9 (129.1 ppm) and C-5 (138.1 ppm). The triplet of doublet at 7.36 ppm related to H-9 have shown correlation with C-7 (133.4 ppm) and C-5 (138.1 ppm). In the same order, the triplet of doublet of H-8 was correlated with C-10 (120.4 ppm), and C-6 (125.4 ppm). Similarly, H-12 at 2.42 ppm was correlated to C-6 (125.4 ppm). In the furan fragment of **3a** the H-15 at 7.57 ppm revealed correlation to C-14 (112.6 ppm), C-13 (115.4 ppm), and C-1 (148.0 ppm). In addition, the H-13 at 7.25 ppm was correlated to C-14 (112.6 ppm), C-15 (144.6 ppm) and C-1 (148.0 ppm). Finally, a correlation was detected for H-14 at 6.57 ppm to C-13 (115.4 ppm), C-15 (144.6 ppm) and C-1 (148.0 ppm).

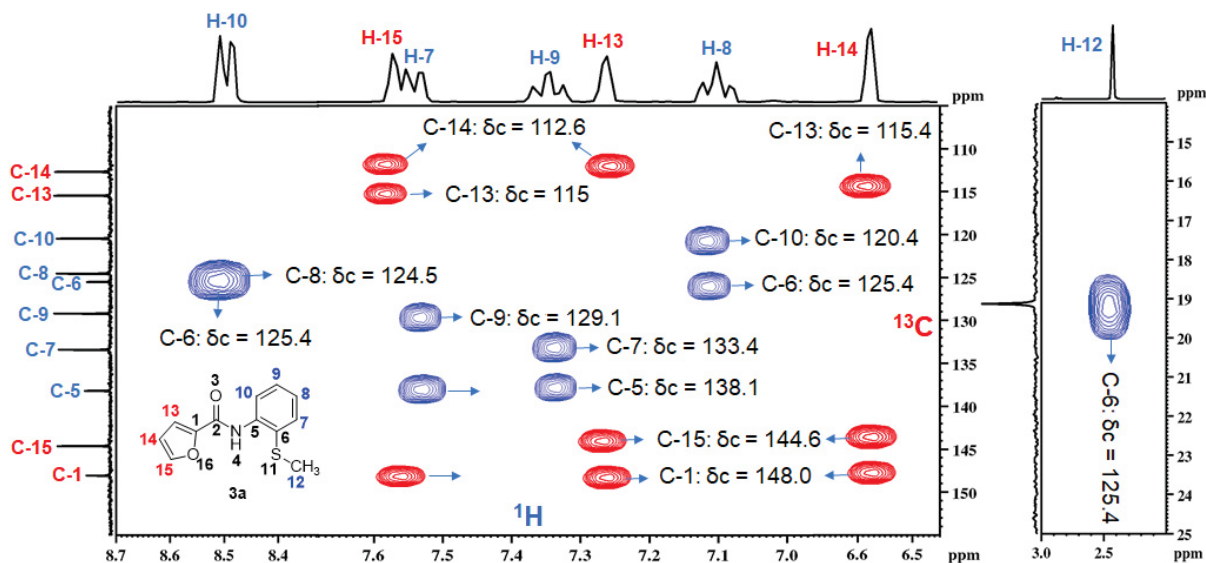


Figure 9: ^1H - ^{13}C HMBC correlation map (^1H , 400 MHz; ^{13}C , 100 MHz) of *N*-(2-(methylthio)phenyl)furan-2-carboxamide (**3a**).

Similarly, the characterization of *N*-2-(4,5-phenyl)furan-2-carboxamide (**5a**) by ^1H NMR (Figure 10) shows the relative integrals to 13 hydrogen atoms, most of them lying in the aromatic region, while 4 hydrogen atoms of methylene groups are in lower frequencies region. The singlet at 13.01 ppm (br. s, 1H) belongs to the hydrogen atom of amide group. While a doublet of doublet at 8.87 ppm (dd, $J = 8.4, 0.7$ Hz, 1H) is related to the H-10 hydrogen atom. The doublet of doublets is related to H-7 hydrogen atom lying at 7.87 (dd, $J = 7.9, 1.5$ Hz, 1H). Similarly, another doublet of doublets at 7.57 ppm (m, 1H) associated to H-18 hydrogen atom. In addition, a triplet of doublets at 7.49 ppm (td, $J = 7.9, 1.5$ Hz, 1H) belongs to H-9 hydrogen atom. A doublet of doublets at 7.22 ppm (dd, $J = 3.5, 1.2$ Hz, 1H) is related to the H-16 hydrogen atom. Next to it, a triplet of doublets at 7.09 ppm (td, $J = 7.6, 1.2$ Hz, 1H) related to H-8 hydrogen atom. On the other hand, the doublet of doublets at 6.54 ppm (dd, $J = 3.5, 1.7$ Hz, 1H) is attached to H-17 hydrogen atom. Also, two signals at lower frequencies region were observed for methylene groups. In this way, the triplet at 4.40 ppm (t, $J = 9.6$ Hz, 2H) belongs to H-14, H-14' hydrogen atoms. While the final triplet at 4.20 (t, $J = 9.6$ Hz, 2H) related to H-13, H-13' hydrogen atoms.

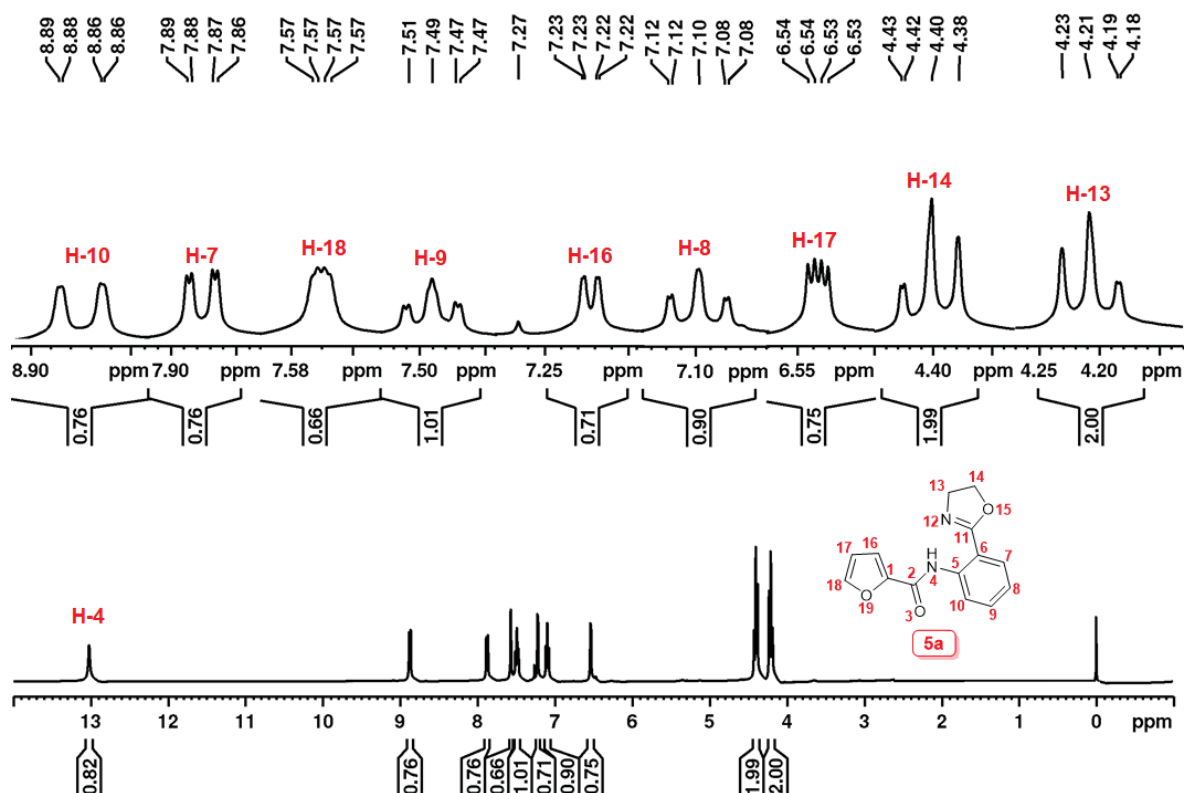


Figure 10: ^1H NMR spectrum (400 MHz, CDCl_3) of *N*-2-(4,5-phenyl)furan-2-carboxamide (**5a**).

The ^{13}C NMR spectrum of compound *N*-2-(4,5-phenyl)furan-2-carboxamide (**5a**). (Figure 11) shows 14 signals for all apparent carbons. Most signals are in the region above 110 ppm, while only two signals at 50-70 ppm is related to the carbon of methylene groups (C-13, and C-14). The 5 small peaks of C-1, C-2, C-5, C-6 and C-11 related to the quaternary carbons in which the signal at 164.7 ppm is related to the carbon (C-11), while the signal at 157.1 ppm is characteristic of a carboxylic carbon of an amide group (C-2). Also, the signal at 148.7 ppm is from the carbon C-1. On the other hand, the signal at 139.7 ppm arises from the carbon C-5 and the signal at 113.6 ppm from carbon C-6. In order to assign the remaining signals of each carbon atom in the molecular structure of **5a**, which consist of the signal at 144.7 ppm belongs to the C-18 of furan ring. While the signal at 132.5 related to the C-7 carbon atom. Similarly, the signal at 129.2 ppm arises for C-9 carbon atom. In the other hand the signal at 122.5 ppm associated for C-8 carbon atom and the signal at 120.0 ppm for C-10 carbon atom. However, the signal at 114.7 ppm related to C-16 and the signal at 112.0 ppm belongs to C-17 carbon atom of furan fragments in the compound **5a**. Finally, the lower frequency region consists of two signals at 66.3 ppm and 54.7 ppm related to C-14 and C-13 ppm carbon atoms respectively of methylene fragment. The HSQC correlation map to identify the direct ^1H - ^{13}C

connections and Heteronuclear (^1H - ^{13}C) Multiple Bond Correlation (HMBC) experiments of this compound is in the experimental section.

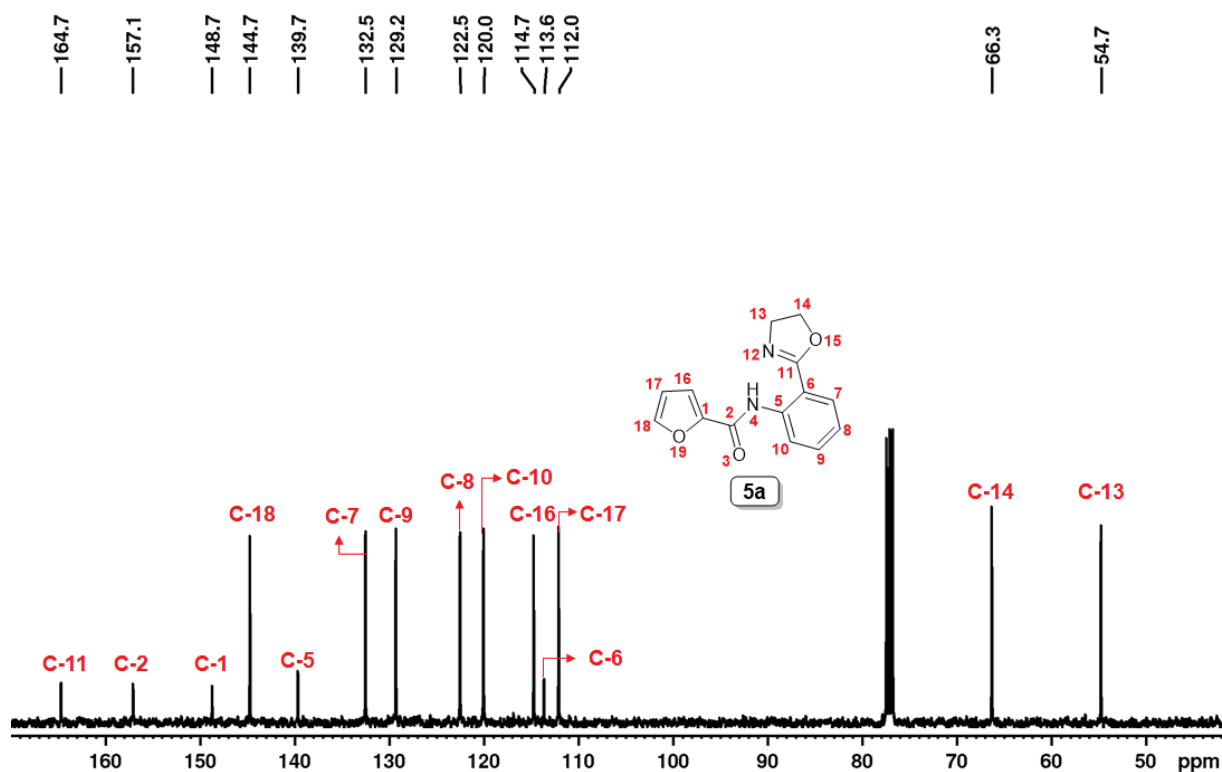
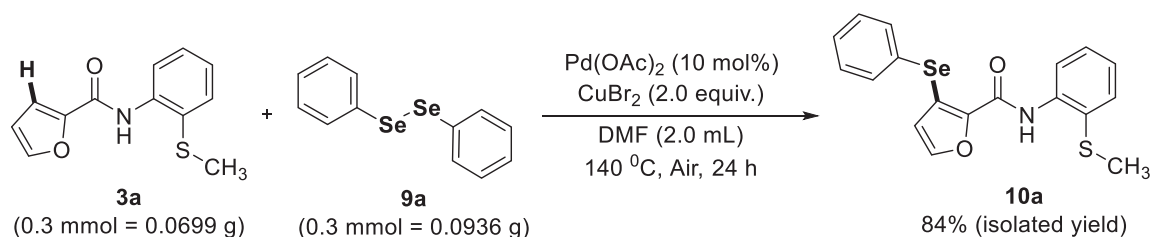


Figure 11: ^{13}C NMR spectrum (100 MHz, CDCl_3) of *N*-2-(4,5-phenyl)furan-2-carboxamide (**5a**).

2.4 REGIOSELECTIVE C3 DIRECT CHALCOGENYLATION OF CHALCOGENOPHENES USING 2-(METHYLTHIO)AMIDES AS DIRECTING GROUP

The study of regioselective C3 direct chalcogenylation of chalcogenophenes and arenes using 2-(methylthio)amides as directing groups started with several tests employing the amide (**3a**) and diphenyl diselenide (**9a**) as model reagents. We started the experiments based on the Kambe conditions,⁴⁹ where the chelate-assisted direct chalcogenylation was successfully developed in several heteroarenes with the easily removable 2-pyrimidine group (Scheme 17). Encouraged by this report, we employed the same conditions with $\text{Pd}(\text{OAc})_2$ (10 mol%), CuBr_2 (2.0 Equivalents), **3a** (0.3 mmol) and **9a** (0.3 mmol) in DMF (solvent) at 140 °C for 24 h (Scheme 24). To your surprise, this first reaction afforded 84% yield of the compound **10a** after isolation by column chromatography.



Scheme 24: Kambe conditions employed for the C3 regioselective direct selenylation of (**3a**).

The preliminary test proved that both Pd(OAc)₂ and CuBr₂ were efficient for the expected reaction. The product **10a** was characterized by low resolution Mass Spectrometry (MS), ¹H and ¹³C Nuclear Magnetic Resonance (NMR) Spectroscopy, Heteronuclear (¹H-¹³C) Single Quantum Correlation (HSQC), Heteronuclear (¹H-¹³C) Multiple Bond Coherence (HMBC) experiments and single-crystal X-ray diffraction (for **10b**). The reaction regioselectivity at C3 position of the furan ring was carefully evaluated by these analyses, since the direct selenylation at C4 or C5 might also happen.

Initially, it was observed by low-resolution Mass Spectrometry (MS) under electron impact (EI, 70 eV) the molecular ion with *m/z* 389, as expected for molecular structure of compound **10a** (Figure 12). The natural isotope distribution of selenium (six natural isotopes) could also be observed in the molecular ion, and the peak with exact mass ratio *m/z* 389 arises from the most abundant selenium isotope, ⁸⁰Se (49.61%).⁵⁵ The ion fragments are in accordance with the molecular structure (Figure 12), and the isotope distribution of selenium can also be seen in the ion fragments with higher intensity. Furthermore, the fragment ion with *m/z* 342 arises again from the simple heterolytic Csp²-S cleavage, related to the loss of CH₃S radical and the ion peak with *m/z* 250 arises from the conventional homolytic Csp²-N cleavage of amides.

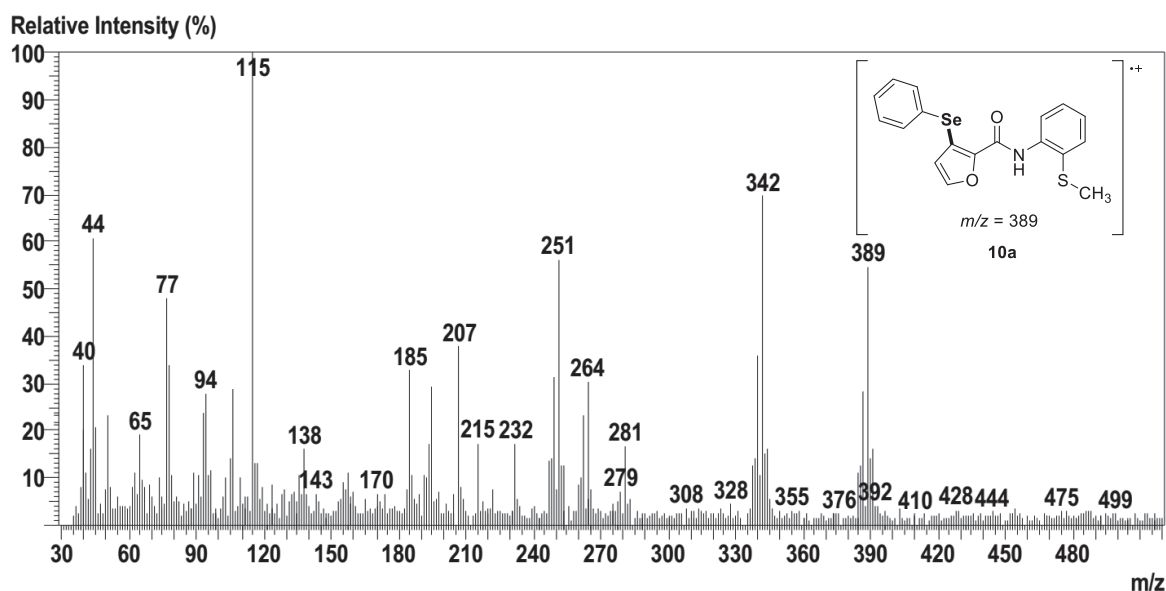
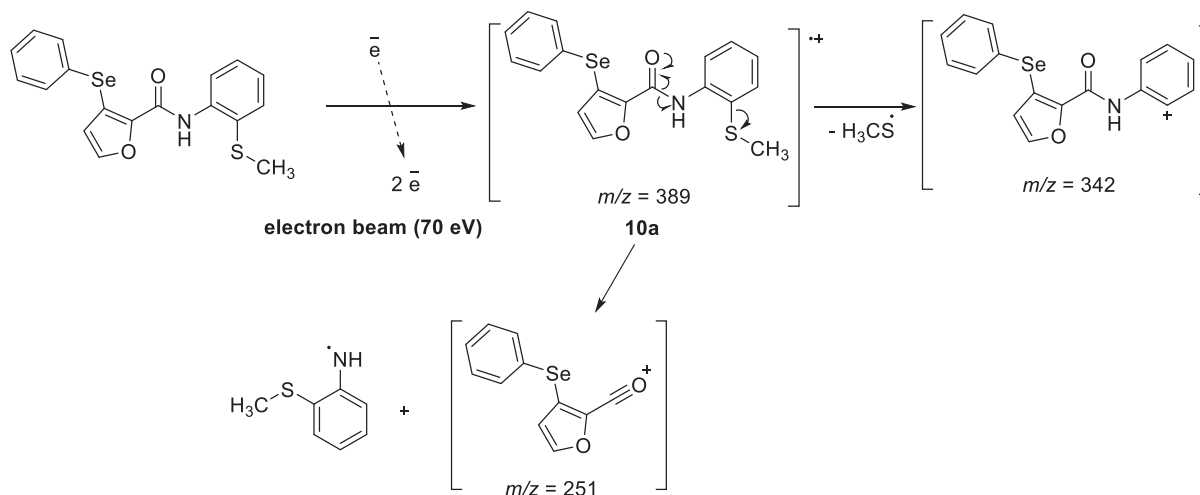


Figure 12: Low-resolution mass spectrum (EI, 70 eV) of *N*-(2-methylthio)phenyl-3-(phenylselanyl)furan-2-carboxamide (**10a**).

The ^1H NMR spectrum of **10a** (Figure 13) shows that the integrals are in accordance with 15 hydrogens of this compound. Additionally, the signals again at higher frequencies are related to hydrogens bonded to heteroaromatic and aromatic rings. The broad singlet at 9.32 ppm (br. s, 1H) is related to H-4 hydrogen atom bonded to nitrogen atom of the amide group. The singlet at 2.40 ppm (s, 3H) with relative integral for three hydrogen atoms belongs to H-12 hydrogen atom. Additionally, a doublet of doublets was observed at 8.55 ppm (dd, $J = 8.3, 1.4$ Hz, 1H) for the H-10, and the multiplet between 7.74 ppm - 7.71 ppm (m, 2H) is related to the hydrogen atoms H-19 and H-23. In addition, the expected doublet of doublets for the H-7 hydrogen atom was observed at 7.53 (dd, $J, = 7.8, 1.4$ Hz, 1H). The multiplet between 7.45 ppm - 7.29 ppm (m, 5H) is related to the hydrogens H-9, H-20, H-21,

H-22, H-15, and the triplet of doublets at 7.08 ppm (td, $J = 7.6, 1.4$ Hz, 1H) is from the hydrogen H-8. As we can see, the signal patterns for **10a** were more complex, since the molecular fragment PhSe- increases the molecular complexity. Although, the C3 regioselectivity can be confirmed by the doublet at 5.99 ppm (d, $J = 1.9$ Hz, 1H), related to the H-14 hydrogen. This doublet shows only a coupling constant 3J of 1.9 Hz, which the small value is in accordance with the vicinal coupling between the hydrogens H-14 and H-15, suggesting the reaction regioselectivity at C3 position (C-13 carbon).

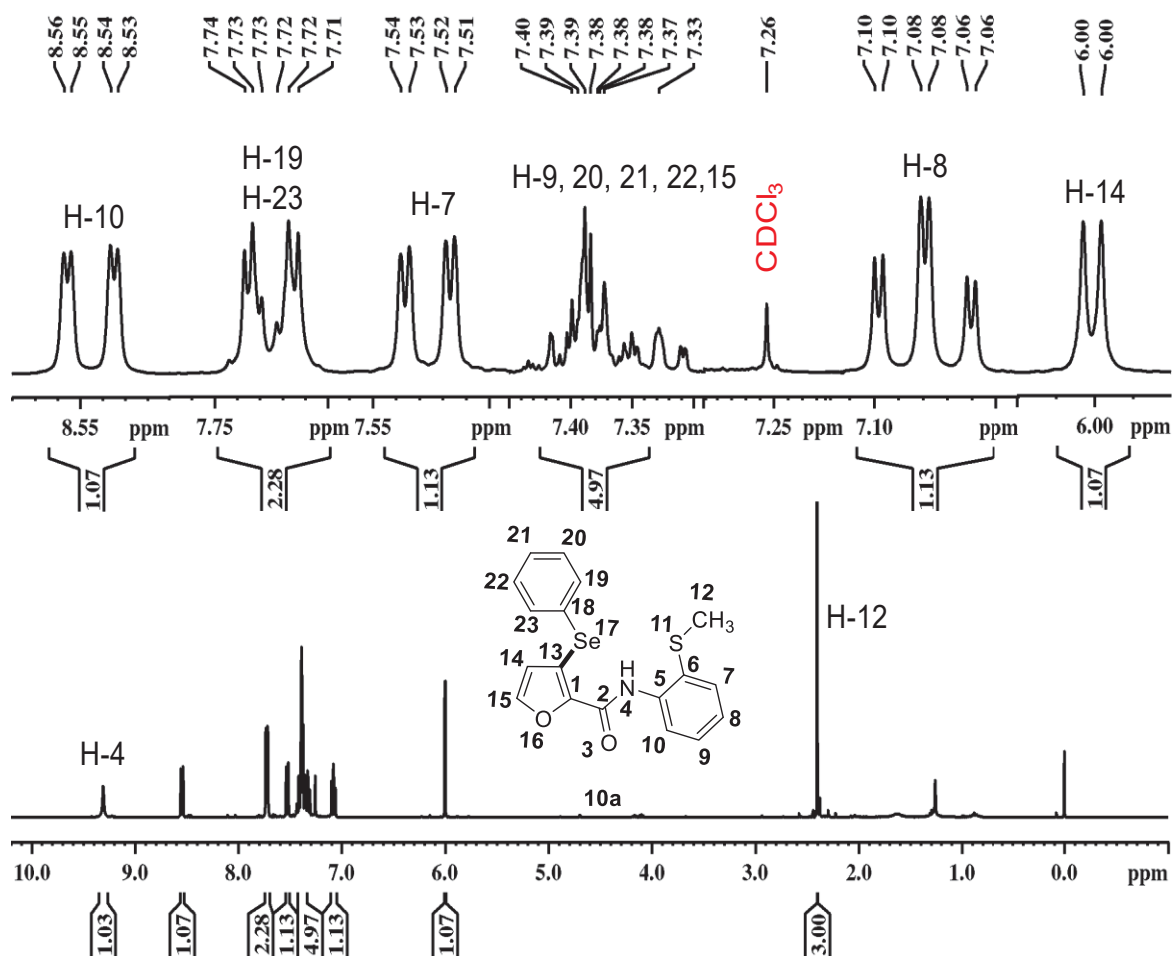


Figure 13: ^1H NMR spectrum (400 MHz, CDCl_3) of *N*-(2-methylthio)phenyl-3-(phenylselanyl)furan-2-carboxamide (**10a**).

The ^{13}C NMR spectrum of compound **10a** (Figure 14) shows the 16 signals for all 18 carbons of the expected molecular structure. About them, 15 signals are in the high frequency region of aromatic rings between 115 to 160 ppm, while only one signal of methyl group is at 20 ppm (C-12) at aliphatic region.

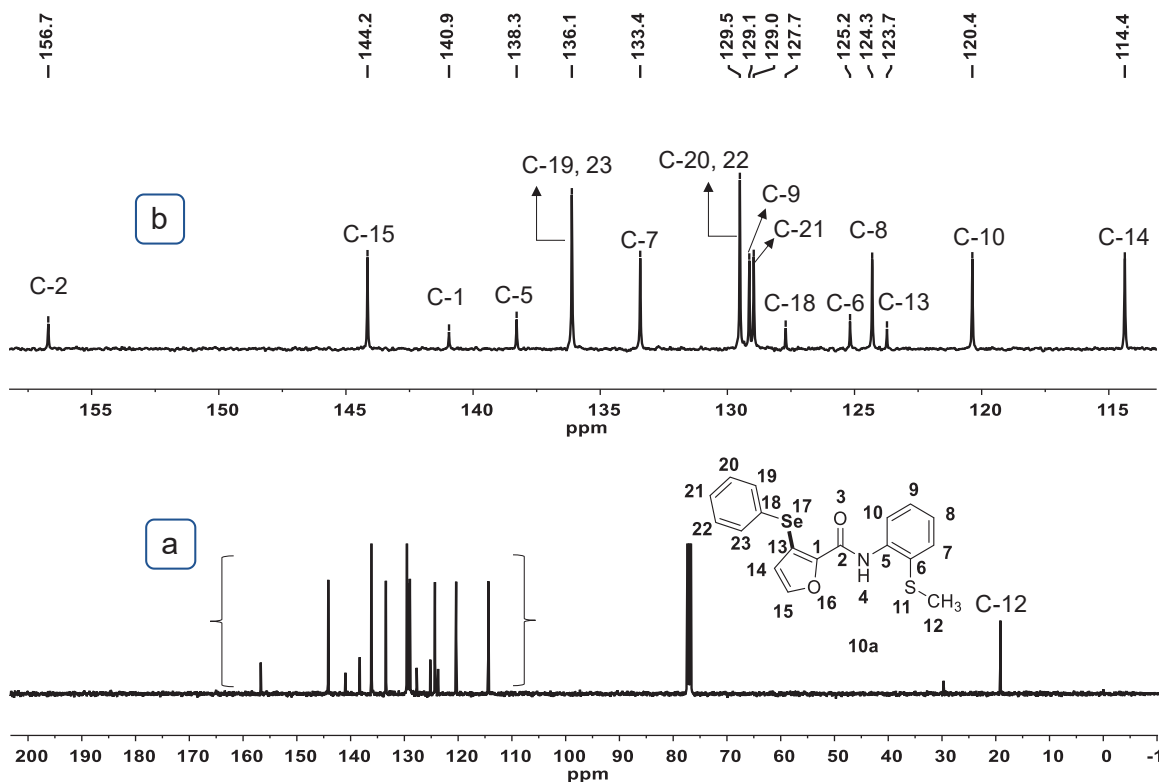


Figure 14: ^{13}C NMR spectrum (100 MHz; CDCl_3) of *N*-(2-methylthio)phenyl-3-(phenylselanyl)furan-2-carboxamide (**10a**).

It was also observed 6 signals with lower intensity at 156.7, 140.9, 138.3, 127.8, 125.2 and 123.7 ppm related to the quaternary carbon atoms of the molecular structure. The signal at 156.7 ppm arises from the carbon atom C-2, and the signal at 140.9 ppm is from C-1. Additionally, the signal at 138.3 ppm is related to C-5, and the signal at 125.2 ppm to C-6. Moreover, the signal at 127.8 ppm arises from the carbon C-18 and the signal at 123.7 ppm from the carbon C-13. The HSQC correlation map was evaluated to establish the direct bonded ^1H - ^{13}C atoms (Figure 15). It was observed that H-10 was directly correlated to the carbon at 120.4 ppm (C-10), and H-19 and H-23 were directly correlated to the signal at 136.1 ppm (C-19 and C-23). In addition, H-7 was correlated to the carbon at 133.4 ppm (C-7), while H-15 is directly correlated to the carbon at 144.2 ppm (C-15). Furthermore, the H-9, H-20, H-21, and H-22 showed direct correlations to the signals at 129.1 ppm, 129.5 ppm, and 129.0 ppm, respectively. On the other hand, H-8 was directly correlated to the carbon at 124.3 ppm (C-8). Finally, H-14 is correlated to the carbon at 114.4 ppm (C-14) and H-12 revealed direct correlation to carbon at 19.1 ppm (C-12).

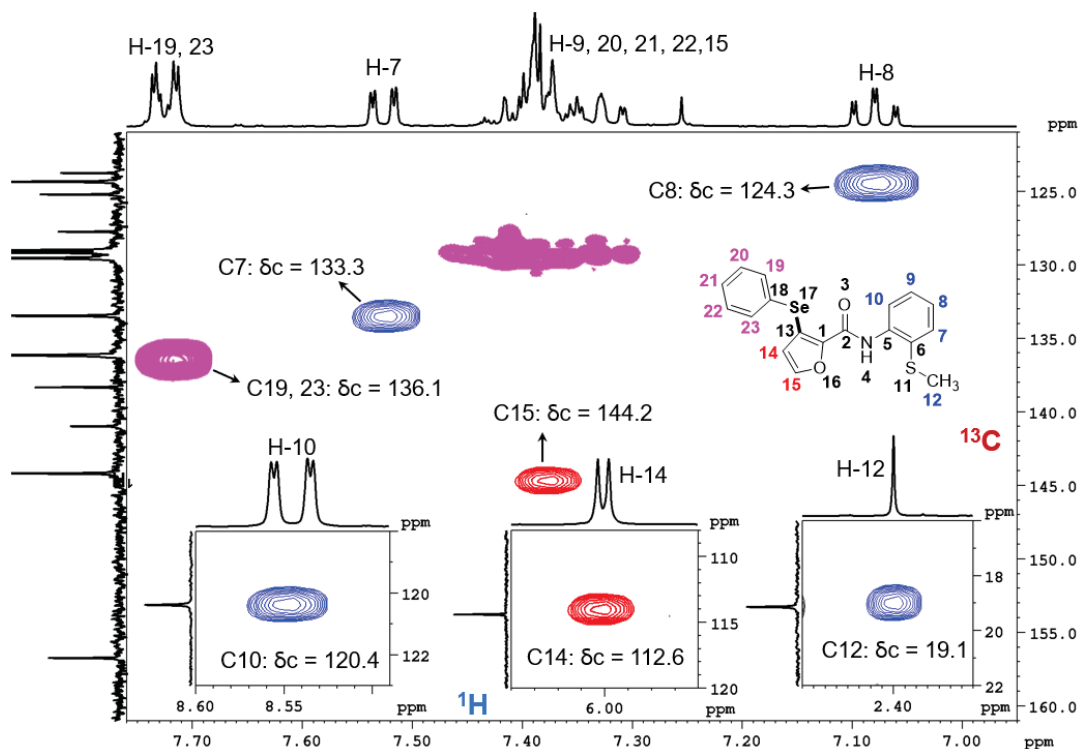


Figure 15: ^1H - ^{13}C direct correlation HSQC map (400 vs. 100 MHz, CDCl_3) of *N*-(2-methylthio)phenyl-3-(phenylselanyl)furan-2-carboxamide (**10a**).

The compound **10a** was further evaluated by Heteronuclear (^1H - ^{13}C) Multiple Bond Correlation (HMBC) mapping (Figure 16). Based on this map, the H-10 showed correlation with C-6 (125.2 ppm) and C-8 (124.3 ppm). By prospecting the HSQC (Figure 15), the multiplet between 7.75 ppm - 7.70 ppm related to hydrogens H-19 and H-23 were correlated mutually to the same signal at 136.1 ppm, and to C-21 (129.0 ppm). On the other hand, the doublet of doublet related to H-7 was correlated to C-9 (129.1 ppm) and C-5 (138.3 ppm). Similarly, the H-9, 20, 21, 22, 15 at 7.45-7.29 ppm showed correlations with C-13 (123.7 ppm), C-20, C-22 (129.5 ppm), C-7 (133.4 ppm), and C-5 (138.3 ppm). In the same way, H-8 depicted correlation with C-10 (120.4 ppm), C-6 (125.2 ppm) and C-7 (133.4 ppm). The H-14 was correlated to the C-13 (123.7 ppm), C-1 (140.9 ppm), and C-15 (144.2 ppm). Finally, the H-12 of the methyl group was correlated only with C-6 (125.2 ppm).

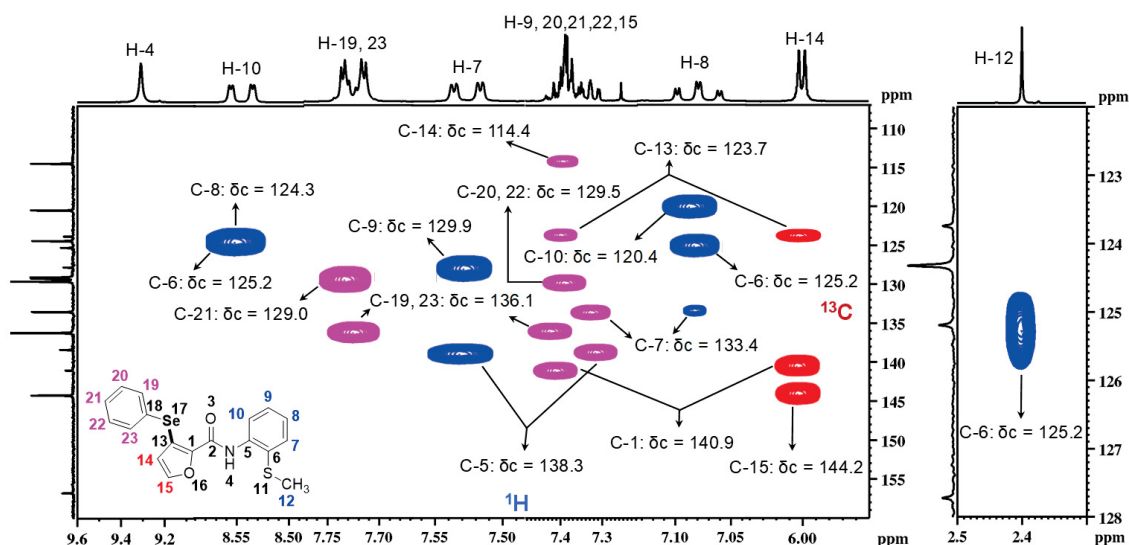


Figure 16: ^1H - ^{13}C HMBC correlation map (400 MHz and 100 MHz, CDCl_3) of *N*-(2-methylthio)phenyl-3-(phenylselanyl)furan-2-carboxamide (**10a**).

In order to further prove the reaction regioselectivity, the structural characterization of the scope compound **10b** (solid at room temperature) was based on the NMR analysis and confirmed by single-crystal X-ray diffraction of **10b**, which has proven the C3 regioselectivity on the direct selanylation (Figure 17)

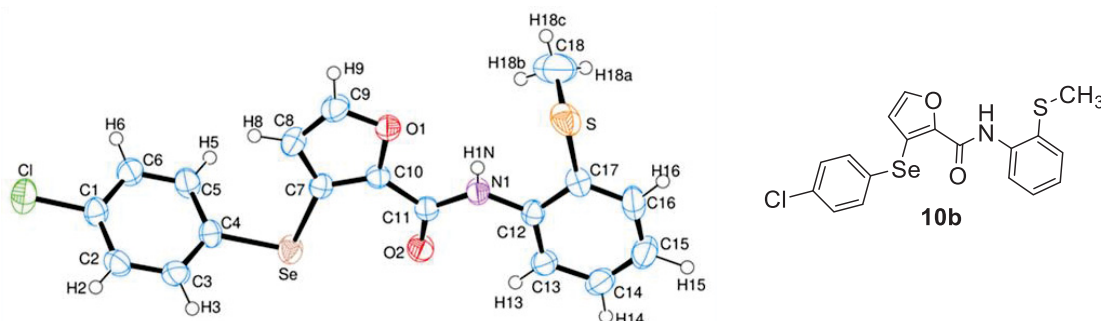


Figure 17: ORTEP diagram of compound (**10b**).

We have also observed by single-crystal X-ray diffraction that the furan fragment and the 2-(methylthio)amide group are almost planar, with dihedral angles up to 9.8° ($\text{C7-C10-C11-O2} = 9.8^\circ$ and $\text{C11-N1-C12-C13} = 6.3^\circ$), and two weak hydrogen bonds were detected between H1N-S and O2-H13 . The packing of **10b** molecules viewed along *b* axis are showing these intramolecular hydrogen bonds (double-dotted lines) between the sulfur atom and the amide hydrogen (H1N) and between the oxygen atom of carboxyl group (O2) and the *ortho* hydrogen of the 2-(methylthio)amide group (H13) (Figure 18). Interestingly, the aryl group bonded to

selenium atom and the furan ring are bent each other, with a dihedral angle of $58.2(3)^\circ$ ($C5-C4-Se-C7 = 58.2(3)^\circ$ and $C3-C4-Se-C7 = -124.3(3)^\circ$).

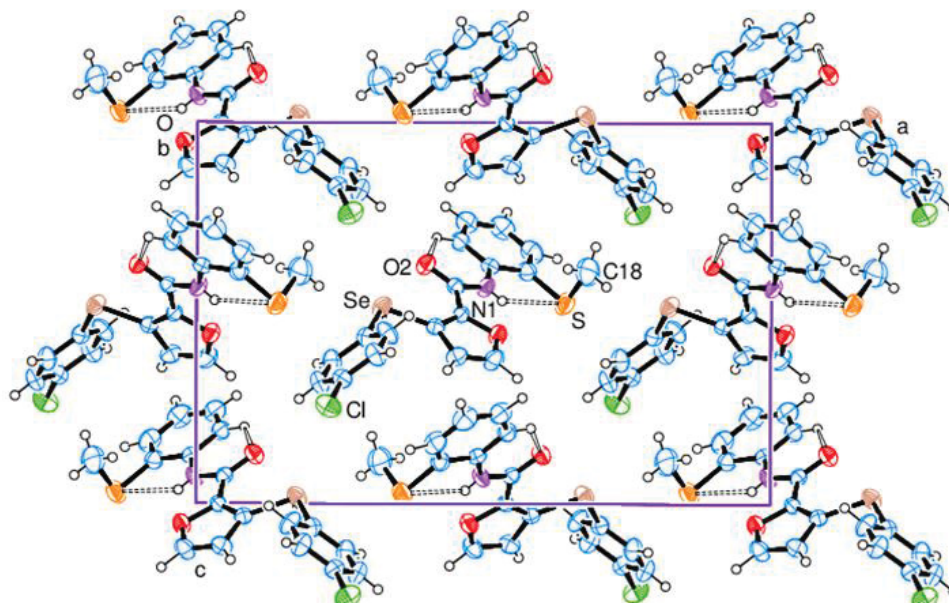
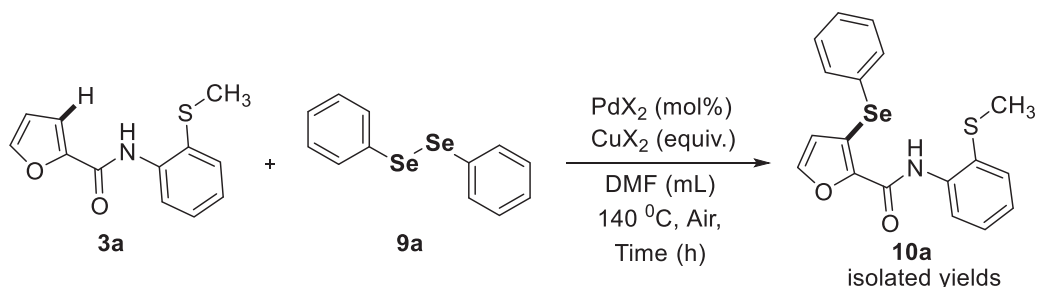


Figure 18: Packing of molecules of $(C_{18}H_{14}ClNO_2SSe)$ (**10b**), viewed along b axis showing the intramolecular hydrogen bonds (double-dotted lines). Thermal ellipsoids are drawn at the 50% probability level.

In order to optimize the reaction conditions, several experiments were developed changing the source and the amount of palladium catalyst and copper additive, as well as the stoichiometry between the reagents **3a** and **9a** (Table 2). The reaction was also evaluated in different solvents, time, temperature and atmosphere of the system. The yields of **10a** in the table 2 were obtained after isolation of the expected product by column chromatography (gradient 1% to 5% of ethyl acetate in hexane).

Table 2: Optimization of the reaction conditions for C3 regioselective direct selenylation of (**3a**).



Entry ^[a]	3a mmol	9a mmol	Catalyst (mol. %)	Additive (equiv.)	Time (h)	Yield (%) ^[b]
1	0.3	0.3	Pd(OAc) ₂ (10)	CuBr ₂ (2)	24	84
2	0.15	0.3	Pd(OAc) ₂ (10)	CuBr ₂ (2)	24	63
3	0.3	0.15	Pd(OAc) ₂ (10)	CuBr ₂ (2)	24	50
4	0.3	0.6	Pd(OAc) ₂ (10)	CuBr ₂ (2)	24	51
5	0.3	0.3	Pd(OAc) ₂ (10)	CuBr ₂ (1)	24	53
6	0.3	0.3	Pd(OAc) ₂ (10)	-----	24	7
7	0.3	0.3	-----	CuBr ₂ (2)	24	--
8	0.3	0.3	Pd(OAc) ₂ (10)	CuBr ₂ (2)	12	53
9	0.3	0.3	Pd(OAc) ₂ (10)	CuBr ₂ (2)	30	71
10	0.3	0.3	PdCl ₂ (10)	CuBr ₂ (2)	24	trace
11	0.3	0.3	Pd(TFA) ₂ (10)	CuBr ₂ (2)	24	trace
12	0.3	0.3	Pd(OAc) ₂ (10) PPh ₃ (40 mol%)	CuBr ₂ (2)	24	55
13	0.3	0.3	PdCl ₂ (MeCN) ₂ 10)	CuBr ₂ (2)	24	22
14	0.3	0.3	PdCl ₂ (PhCN) ₂ 10)	CuBr ₂ (2)	24	28
15	0.3	0.3	Pd(PPh ₃) ₄ (10)	CuBr ₂ (2)	24	60
16	0.3	0.3	PdCl ₂ (PPh ₃) ₂ (10)	CuBr ₂ (2)	24	43
17	0.3	0.3	Pd(OAc) ₂ (10)	Cu(OTf) ₂ (2)	24	28
18	0.3	0.3	Pd(OAc) ₂ (10)	CuCl ₂ (0.2)	24	80
19	0.3	0.3	Pd(OAc) ₂ (10)	CuBr (0.2)	24	67
20	0.3	0.3	Pd(OAc) ₂ (10)	CuCl (0.2)	24	73

^[a] **Reaction conditions:** The reaction mixture of *N*-(2-(methylthio)phenyl)furan-2-carboxamide (**3a**) (table), diphenyl diselenide (**9a**) (table 2), Pd(OAc)₂ (table), CuBr₂ (table) in 2 mL DMF (dry) solvent was heated at 140 °C temperature under air atmosphere for the time depicted in table 2 ^[b] isolated yields.

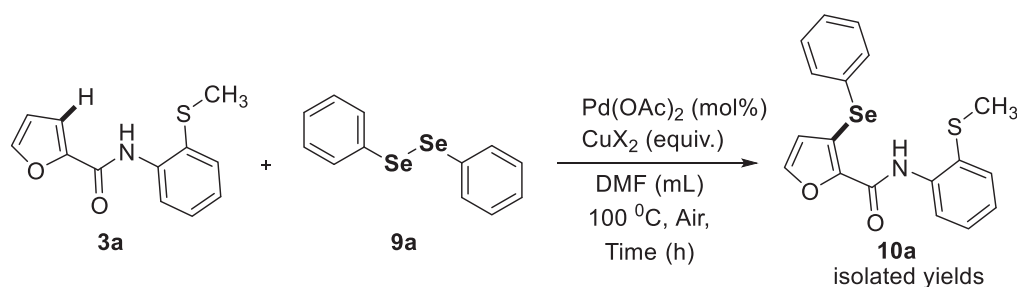
In order to evaluate the effect of stoichiometry between the substrates (**3a**, **9a**), the reaction was performed changing the amount of **3a** (0.15 mmol) and **9a** (0.3 mmol) with Pd(OAc)₂ (10 mol%) and CuBr₂ (2.0 Equivalents) in air atmosphere using DMF as solvent (Table 2, entry 2). It was observed that after 24 h of reaction at 140 °C, 63% yield of **10a** was attained. Similarly, decreasing the amount of **9a** (0.15

mmol) under same condition of entry 1 (table 2), the product was decreased to 50% (Table 2, entry 3). However, when the amount of **9a** was increase to (0.6 mmol), 51% yield of **10a** was obtained (Table 2, entry 4). By using an equimolar relationship between **3a** and **9a**, but with half of CuBr₂ (1 equiv.), the isolated yield of **10a** was reduced to 53% (Table 2, entry 5). Under the same reaction condition of entry 1 (Table 2) but without CuBr₂ the reaction yield was obtained only 7% (Table 2, entry 6), and without Pd(OAc)₂, no product was detected (Table 2, entry 7). Similarly, the reaction time was analyzed under same conditions, and after 12 h the yield of **10a** was reduced to 53% (Table 2, entry 8). Additionally, after 30 h the product yield was 71% (Table 2, entry 9).

When the reaction was developed with other Pd(II) sources such as: (PdCl₂ or Pd(TFA)₂) (Table 2, entries 10 and 11), only traces of the product **10a** were observed by GC-MS. Further screening of the reaction catalyst was developed with other Pd(II) or Pd(0) sources (Table 2, entries 12-16), however, these experiments gave lower yields of **10a**. The screening of different copper additives (Table 2, entries 17-20) was also evaluated, although none of them allowed yields higher than 80%.

It was observed that the reaction temperature plays a crucial role in this reaction. In this way, when the reaction was developed at 120 °C the yield dropped to 71% (Table 3, entry 1). Although, when the reaction temperature was decreased to 100 °C, the yield of the corresponding product increased to 92% (Table 3, entry 2).

Table 3: Optimization of the reaction conditions for C3 regioselective direct selenylation of (**3a**)



Entry ^[a]	<i>Pd(OAc)</i> ₂ (mol %)	Additive (equiv.)	Solvent (2 mL)	Temp (°C)	Time (h)	Yield (%) ^[b]
1	(10)	CuBr ₂ (2)	DMF	120	24	71
2	(10)	CuBr ₂ (2)	DMF	100	24	92
3	(10)	CuBr ₂ (2)	DMF	80	24	71
4	(10)	CuBr ₂ (2)	DMF	100	12	76
5 ^[c]	(10)	CuBr ₂ (2)	DMF	100	24	76
6	(10)	CuBr ₂ (2)	DMSO	100	24	82
7	(10)	CuBr ₂ (2)	Toluene	100	24	26
8	(10)	CuBr ₂ (2)	MeCN	100	24	21
9	(10)	CuBr ₂ (2)	THF	100	24	15
10	(10)	CuBr ₂ (2)	EtOH	100	24	0
11	(10)	----	DMSO	100	24	15
12 ^[d]	(10)	----	DMF	100	24	16
13 ^[d]	(10)	----	DMSO	100	24	17
14	(5)	CuBr ₂ (2)	DMF	100	24	85
15	(5)	CuBr ₂ (1)	DMF	100	24	88
16	(5)	CuBr ₂ (0.5)	DMF	100	24	87
17	(2.5)	CuBr ₂ (0.5)	DMF	100	24	88
18	(2.5)	CuBr ₂ (0.025)	DMF	100	24	26
19 ^[d]	(2.5)	CuBr ₂ (0.025)	DMF	100	24	16
20	(2.5)	CuBr₂ (0.33)	DMF	100	24	98
21 ^[e]	(2.5)	CuBr ₂ (0.33)	DMF	100	24	70
22 ^[c]	(2.5)	CuBr ₂ (0.33)	DMF	100	24	68
23	(2.5)	AgNO ₃ (0.33)	DMF	100	24	traces

^[a] **Reaction conditions:** The reaction mixture of *N*-(2-(methylthio)phenyl)furan-2-carboxamide (**3a**) (table), diphenyl diselenide (**9a**) (table 3), Pd(OAc)₂ (table), CuBr₂ (table) in 2 mL of DMF (dry) solvent was heated under air atmosphere for the time and temperature depicted in table 3. ^[b] Isolated yields ^[c] Argon atmosphere ^[d] Oxygen atmosphere ^[e] 0.15 mmol of **9a**

Further reduction of the temperature to 80 °C, the yield of **10a** reduced to 71% (Table 3, entry 3). Similarly, when the reaction was carried out for 12 h, 76% yield of product **10a** was obtained (Table 3, entry 4). The best condition until now (Table 3, entry 2) was also evaluated under inert atmosphere of argon, and the product yield

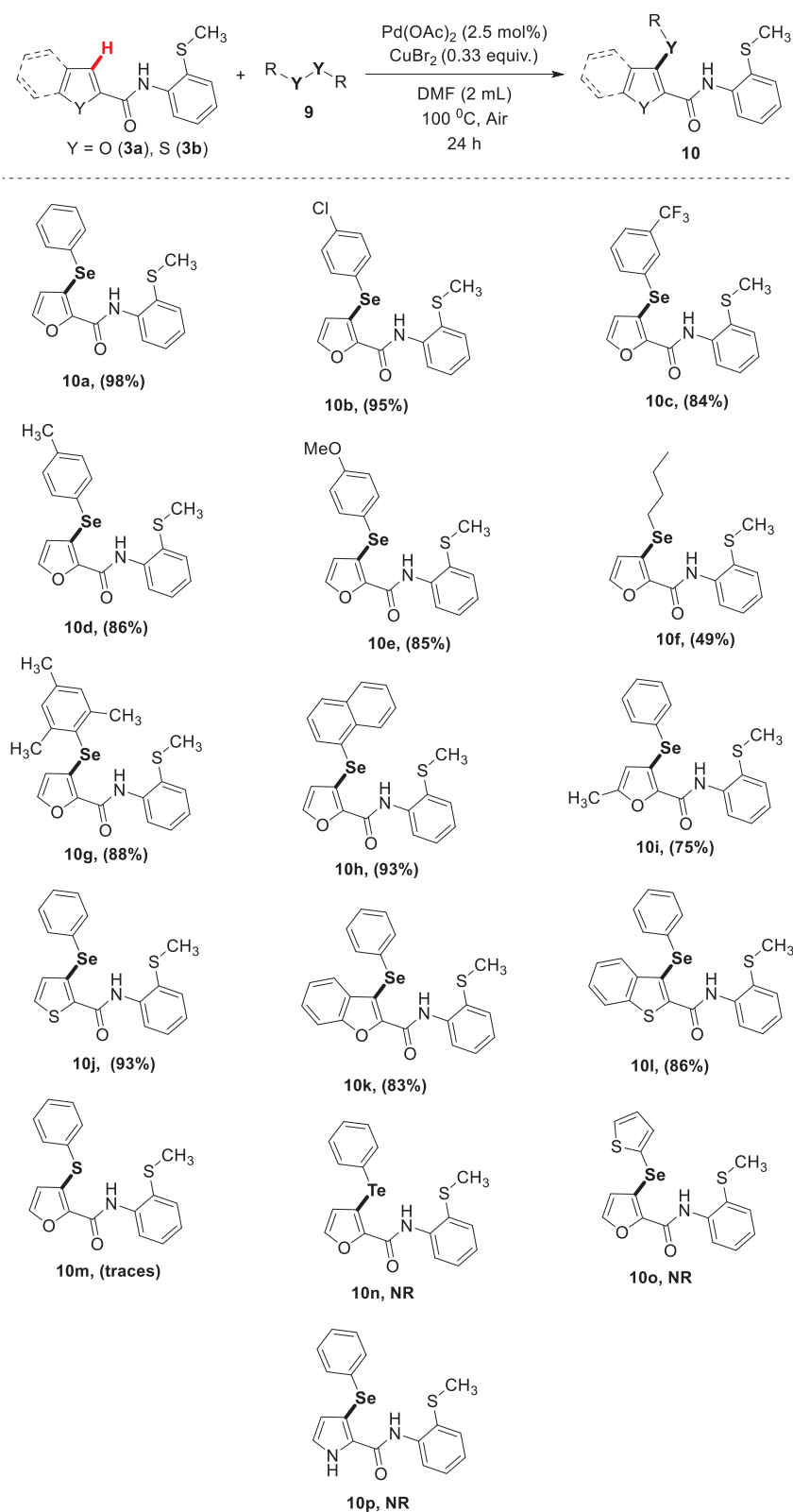
was 76% (Table 3, entry 5^c). Considering the entry 2 in the table 3, the comparative effect of different solvents was evaluated (Table 3, entries 6-10). It was observed that in DMSO the product **10a** was obtained 82% yield, while in other solvents lower yields were detected. To investigate the role of CuBr₂, when the reaction was examined in DMSO solvent without CuBr₂, the product yield decreased to 15% (Table 3, entry 11). The same condition of entry 11 (table 3) was evaluated under oxygen atmosphere (O₂) using DMSO and DMF as solvents, lower yields were detected from both experiments (Table 3, entries 12-13).

Surprisingly, when the amount of Pd(OAc)₂ catalyst was reduced to 5 mol% (Table 3, entry 14) under the same condition of entry 2 (table 3), 85% yield of **10a** was obtained. By using Pd(OAc)₂ (5 mol%) and CuBr₂ (1 equiv.), the product yield was also slightly increased to 88% (Table 3, entry 15). Further reduction in the amount of CuBr₂ (0.5 equiv.) afforded 87% yield of **10a** (Table 3, entry 16). Similarly, when the amount of Pd(OAc)₂ catalyst was reduced to 2.5 mol%, 88% yield of the expected product was attained (Table 3, entry 17). When a catalytic amount of CuBr₂ (2.5 mol% or 0.025 equiv.) was evaluated, only 26% yield of **10a** was obtained (Table 3, entry 18). In addition, a catalytic amount (2.5 mol%) of both Pd(OAc)₂ and CuBr₂ under oxygen atmosphere (O₂) gave 16% yield of the product (Table 3, entry 19^d). In the next reaction, the amount of Pd(OAc)₂ 2.5 mol% was used with 0.33 Equivalent of CuBr₂, and the yield of product **10a** was significantly increased to 98% (Table 3, entry 20). When the amount of diphenyl diselenide (**9a**) was reduced to half (0.15 mmol) the product yield also decreased to 70% (Table 3, entry 21^e). The same reaction condition of entry 20 was evaluated under inert atmosphere of argon, and it provided only 68% product yield (Table 3, entry 22^c). When the reaction was carried out in silver nitrate (AgNO₃) additive, it gave only traces of the expected product (Table 3, entry 23) In this way entry 20 (table 3) gave the excellent yield of **10a** to 98% and was selected for the optimization of scope.

After establishing the optimal reaction conditions (Table 3, entry 20), next we directed our attention to explore the versatility of this transformation with several 2-(methylthio)amides and diorganoyl diselenides (Table 4). It was observed good to excellent yields when diaryl diselenides containing electron-withdrawing or electron-donating groups were employed (Table 4, **10a-e**, **10g**). Additionally, sterically hindered diaryl diselenides also provide excellent yields of the expected products under the optimized reaction condition (Table 4, **10g** and **10h**). Although only a

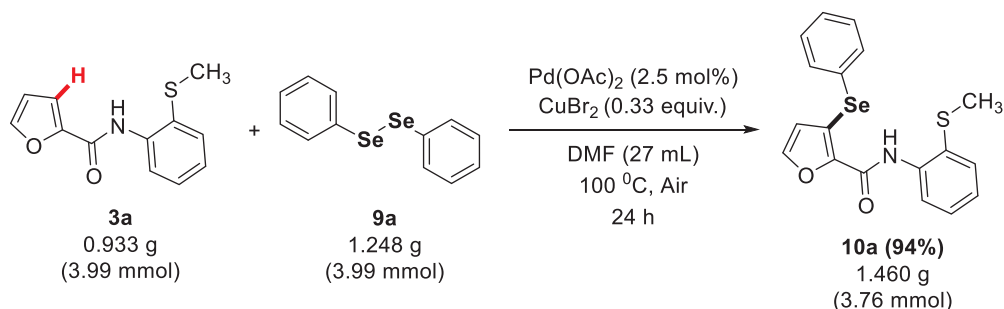
moderate yield of **10f** (Table 4) was obtained when dibutyl diselenide was employed. However, the substituted furan at 5-position by methyl of 2-(methylthio)amides afforded good yield (Table 4, **10i**). Moreover, 2-(methylthio)amides containing heterocycles such as benzo[*b*]furan, thiophene and benzo[*b*]thiophene were also effective substrates provided excellent results under standard reaction conditions (Table 4, **10j-l**). The reaction with diphenyl disulfide was not effective and we observed only traces of the expected compound **10m** (Table 4). Similarly, the reaction between 2-(methylthio)amides and diphenyl ditelluride did not afford the expected product **10n** (Table 4). Additionally, the 2,2'-diselenobisthiophene did not produce the expected product of compound **10o** (Table 4) under the optimized conditions. While 2-(methylthio)amides containing *N*-heteroarenes are also not successful in this transformation (Table 4, **10p**).

Table 4: Scope of the C3-selective direct chalcogenylation of chalcogenophenes and benzo[*b*]chalcogenophenes.



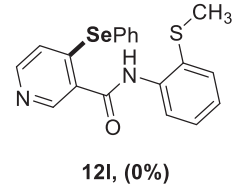
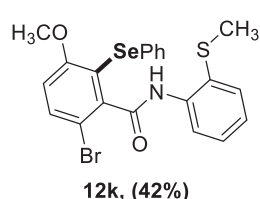
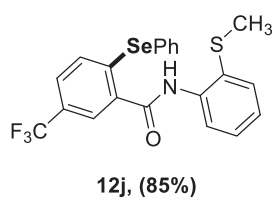
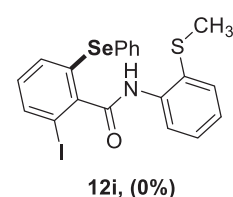
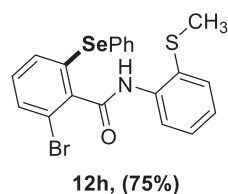
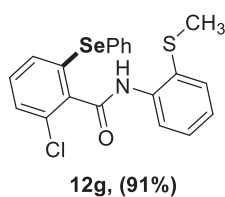
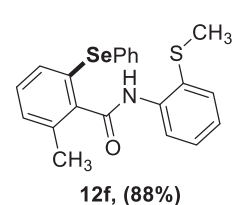
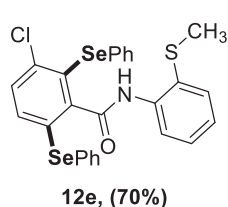
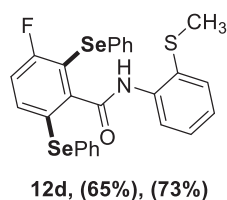
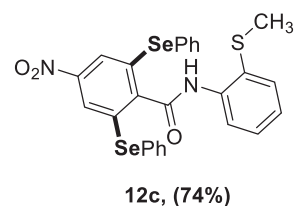
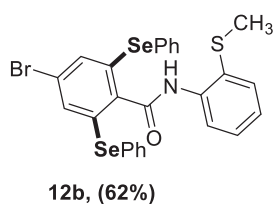
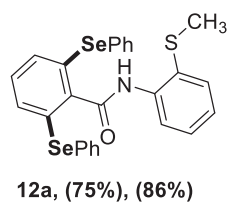
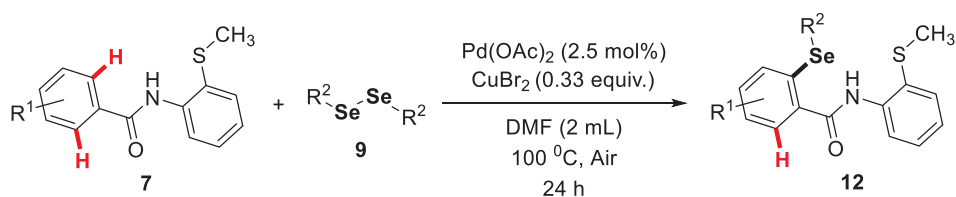
Reaction conditions: The reaction mixture of *N*-(2-(methylthio)phenyl)amide (3a-f) (0,3 mmol), diorganoyl diselenides (9a) (0.3 mmol), Pd(OAc)₂ (2.5 mol%), CuBr₂ (0.33 equiv., 0.1 mmol) in 2 mL of DMF (dry) solvent was heated at 100 °C under air atmosphere for 24 h. (table 4). Isolated yields

To evaluate the reaction practicality, a gram scale experiment of the optimized condition was carried out. In this way, the reaction with 0.933 g of **3a** (3.99 mmol) and 1.248 g of **9a** (3.99) mmol provided (94%, 1.460 g, 3.76 mmol) of the desired product of **10a** under the standard reaction system (scheme 25).



Scheme 25 : Gram-scale C3-selective direct selanylation of chalcogenophenes.

The substrate scope of this transformation was further explored, in this way benzamides containing 2-(methylthio)amide directing group were also investigated (Table 5). The substrates were effective under the optimal reaction conditions. The reaction proceeded efficiently and provided double *ortho* direct selanylation when both positions were available (Table 5, **12a-e**). When the reaction stoichiometry was investigated by using 1.0 equivalent of **9a**, moderated yields of the expected product of double *ortho* selanylation was obtained (Table 5, **12a-e**). However, the yield of product **12a** was increased to 86% when 2.0 equivalents of **9a** was used (Table 5, **12a**). In contrast, the sterically bulky group at *meta* position creates steric hindrance at one of the reaction sites, the mono-*ortho* direct selanylation was observed in excellent yield exclusively at the less sterically congested position (Table 5, **12j**). As expected, the benzamides with one of the *ortho* positions blocked afforded the desired mono-*ortho* direct selanylation in excellent yields (Table 5, **12f-h**, **12k**). However, the iodo substituent at *ortho*-position and nitrogen contain heterocyclic amides were not successful in this transformation (table 5, **12i**, **12l**). Lastly, the methodology was successfully applied to benzamides bearing chloro and bromo groups (Table 5, **12b**, **12d-e**, **12g**, **12h** and **12k**), which can allow several further transformations for example coupling reactions.

Table 5: Scope of *ortho* direct selenylation of benzamides.

Reaction conditions: The reaction mixture of benzamides (**7a-l**) (0.3 mmol), diphenyl diselenide (**9a**) (0.3 mmol), Pd(OAc)₂ (2.5 mol%), CuBr₂ (0.33 equiv., 0.1 mmol) in 2 mL of DMF (dry) solvent was heated at 100 °C under air atmosphere for 24 h. (**table 5**). Isolated yields

All the above results suggest that the reaction requires at least 2.0 Equivalents of the PhSe fragment (0.3 mmol of **9a**), and further excess of diphenyl diselenide (**9a**) reduced the yields of **10a**. Furthermore, the reaction requires 0.33 Equivalent of CuBr₂, and it was observed that both Pd(OAc)₂ and CuBr₂ play a pivotal role on this transformation. The product **10a** was not detected in the absence of Pd(OAc)₂, and

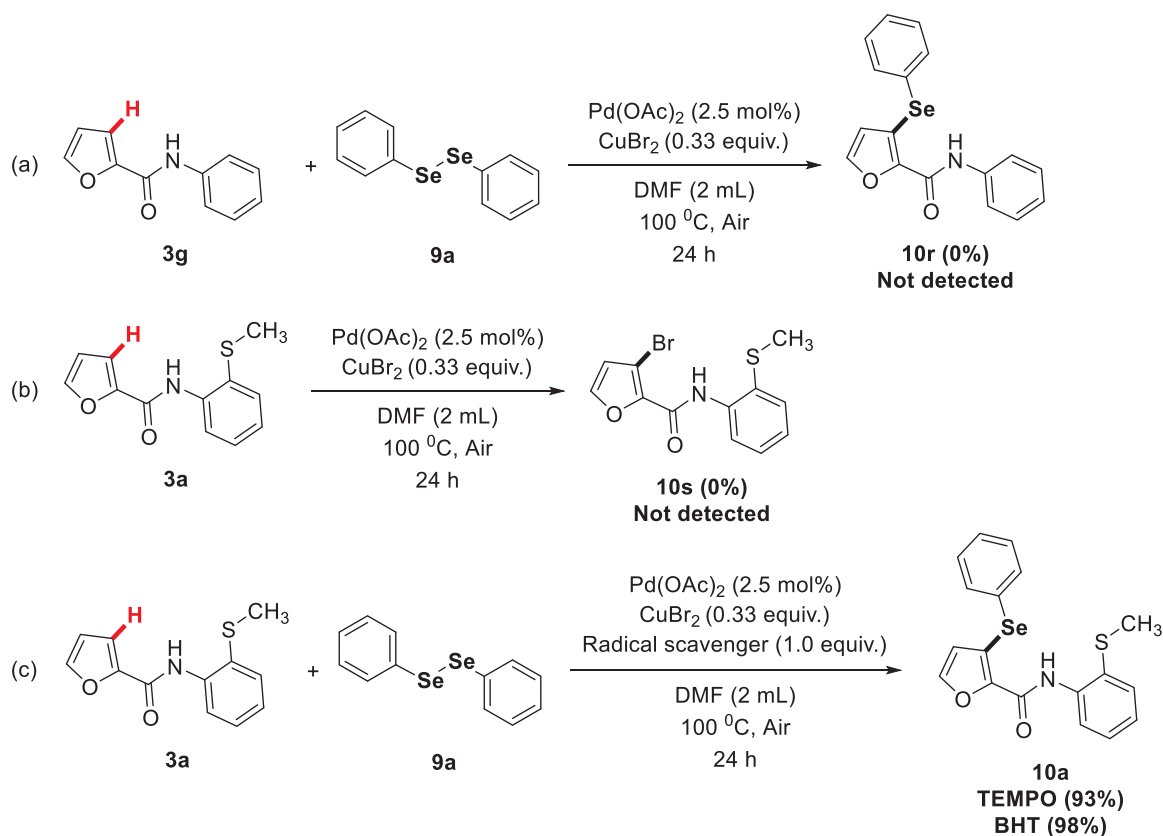
without CuBr₂ the reaction does not proceed efficiently (Table 2, entries 6-7), even using catalytic amount CuBr₂ (0.025 Equivalent), oxygen atmosphere and DMSO solvent as an oxidant (Table 3, entries 11-13, 19) the reaction gave low yields. Also, under the inert atmosphere of argon, lower yield of product **10a** was obtained (Table 3, entry 22). Additionally, it seems that the DMF solvent and the acetate ligand from the palladium source have an important role in the reaction. It was also observed that the presence of phosphine ligands in the system has a detrimental effect in the reaction yields (Table 2, entries 12, 15-16).

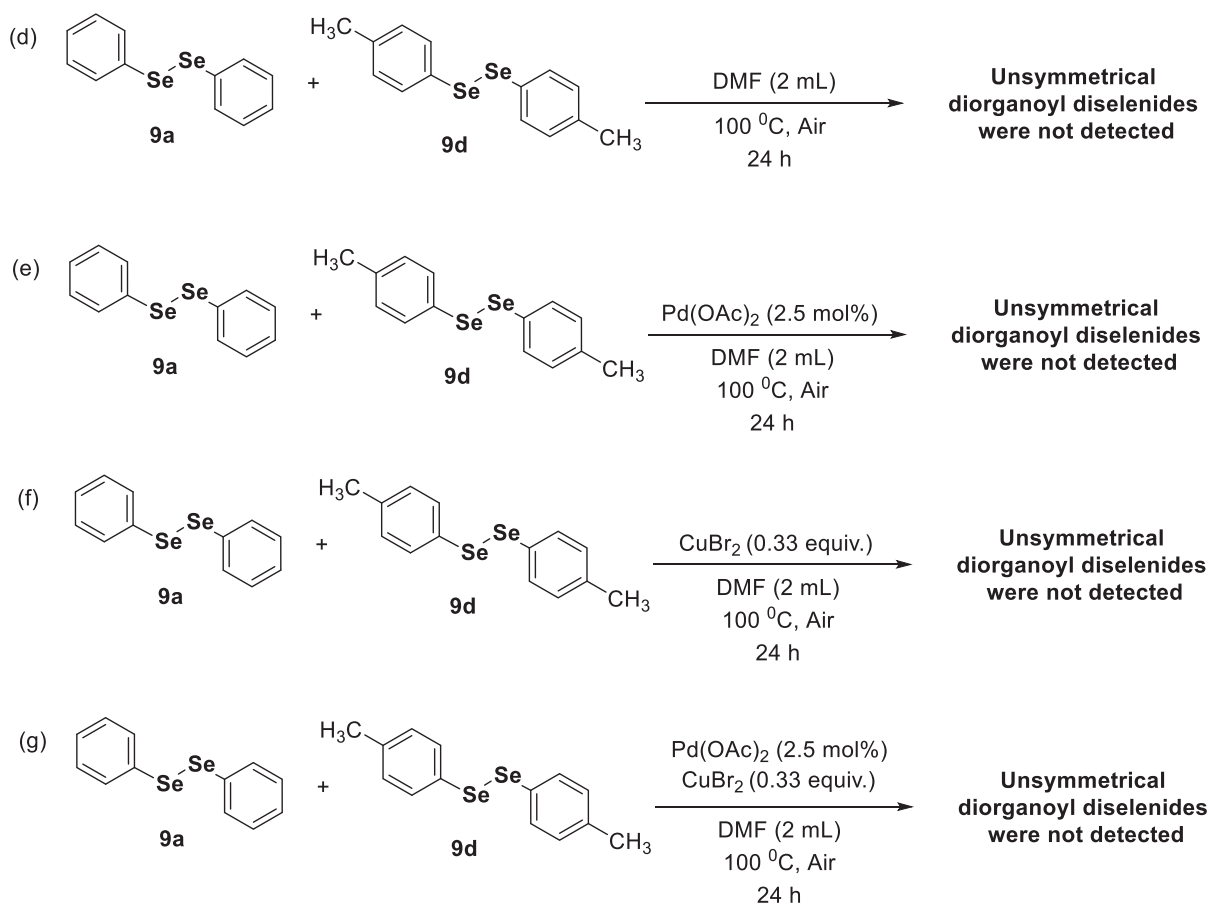
The reaction mechanism of direct chalcogenylations involving the combination of Pd(II), Cu(II), and diorganoyl dichalcogenides was studied by the groups of Kambe,⁴⁸ Nishihara,⁵⁶ Glorius,⁵⁷ and Ma.⁵⁸ Regarding the chelation-assisted palladium-catalyzed direct chalcogenylation, the evidences obtained until now are scarce to fully prove the oxidation state of palladium at some steps of the mechanism and also to make clear the role of copper. Therefore, we carried out some control experiments to understand the role of each reagent in this transformation. The first test showed that the thiomethyl moiety of the directing group was essential for the reaction to occur, which demonstrates that a Pd(II) palladacycle has a crucial role in the mechanism (Scheme 26a). Only the starting materials **3a** and **9a** were detected by GC-MS of the reaction crude from this experiment. On the other hand, the second experiment under optimized reaction conditions without diphenyl diselenide (**9a**) suggests that a first C-H bromination is not involved in the reaction mechanism (Scheme 26b). Therefore, the conventional coupling via palladium or copper catalysis between the heteroaryl bromide (**10s**) and diphenyl diselenide (**9a**) can be ruled out.^{8a} Again, only the starting material **3a** was recovered from this experiment.

We also observed that the optimized reaction conditions with TEMPO (2,2,6,6-tetramethyl-1-piperidinyloxy) or BHT (2,6-di-*tert*-butyl-4-methylphenol) did not affect the outcome of the reaction (Scheme 26c); therefore, the reaction is unlikely to involve a single-electron transfer.

In addition, the dependence of reaction yield with O₂ from air may suggests that Cu(II) acts as oxidant of Pd(0) to Pd(II) (Table 3, entry 22), and that O₂ is the oxidant of Cu(0) to Cu(II).⁵⁹ On the other hand, the role of O₂ could be also related to regeneration of Cu(II) from in situ produced Cu(0) or Cu(I) coming from other paths, since it is well-know that Cu(II)-chalcogenolates are unstable under atmosphere conditions.⁶⁰ Interestingly, we did not detect the product **10a** employing Ag(I) as

additive (Table 3, entry 23), even though Ag(I) being well recognized as an oxidizing agent of Pd(0) to Pd(II), and this result may suggest that Cu(II) is not acting as terminal oxidizing agent to Pd(0) in the catalytic cycle. One possibility might be the interaction between the borderline Lewis acid Cu(II) and the soft selenium Lewis base on the diorganoyl diselenides (**9a**) reducing the Se-Se bond order,^{57,61} and then allowing the oxidative addition of a Pd(II) palladacycle intermediate to a Lewis acid-base adduct [**9a**-Cu(II)] to produce a Pd(IV) complex (Scheme 27). However, the absence of the unsymmetrical diaryl diselenide when diphenyl diselenide (**9a**) and 1,2-di-*p*-tolyl diselane (**9d**) were mixed under the optimized conditions or even with only Pd(OAc)₂ or CuBr₂ (Scheme 26d-g), does not support the involvement of the Lewis acid-base adduct [**9a**-Cu(II)] in our system.⁵⁷ This data indicates that Se-Se bond was not cleaved out of the main catalytic cycle, a reaction expected to occur in the presence of two structural different diorganoyl diselenides if the Lewis acid-base adducts were involved.⁵⁷





Scheme 26: Control experiments.

The reaction under optimized condition was monitored by Gas Chromatography coupled with Mass Spectrometry (GC-MS) in order to detect any possible intermediates during the course of reaction (Figure 19). The reaction test consisted of taking aliquots for GC-MS analysis every two hours (5 aliquots) and then after 24 h of reaction. The chromatogram shows the consumption of substrates **3a** and **9a** and the formation of product **10a**. Initially, the reaction was run at room temperature and after two hour of reaction the first aliquot was taked, and it gives two elution bands of starting materials **3a** and **9a**. Then, after two hours of reaction, the temperature was risid to 100 °C. After this time, observed again two elution bands of substrates **3a** and **9a**. The product **10a** arised in the third aliquot of the reaction, after 6 h from the beginning and its concentration increased in in the aliquots 4 and 5. After 24 h of reaction, the last aliquot was taken and analyzed in GC-MS, providing two elution bands of substrate **9a** and product **10a**, while the starting material **3a** was completely converted into the product **10a**. We did not detect any intermediate or side product during the course of reaction.

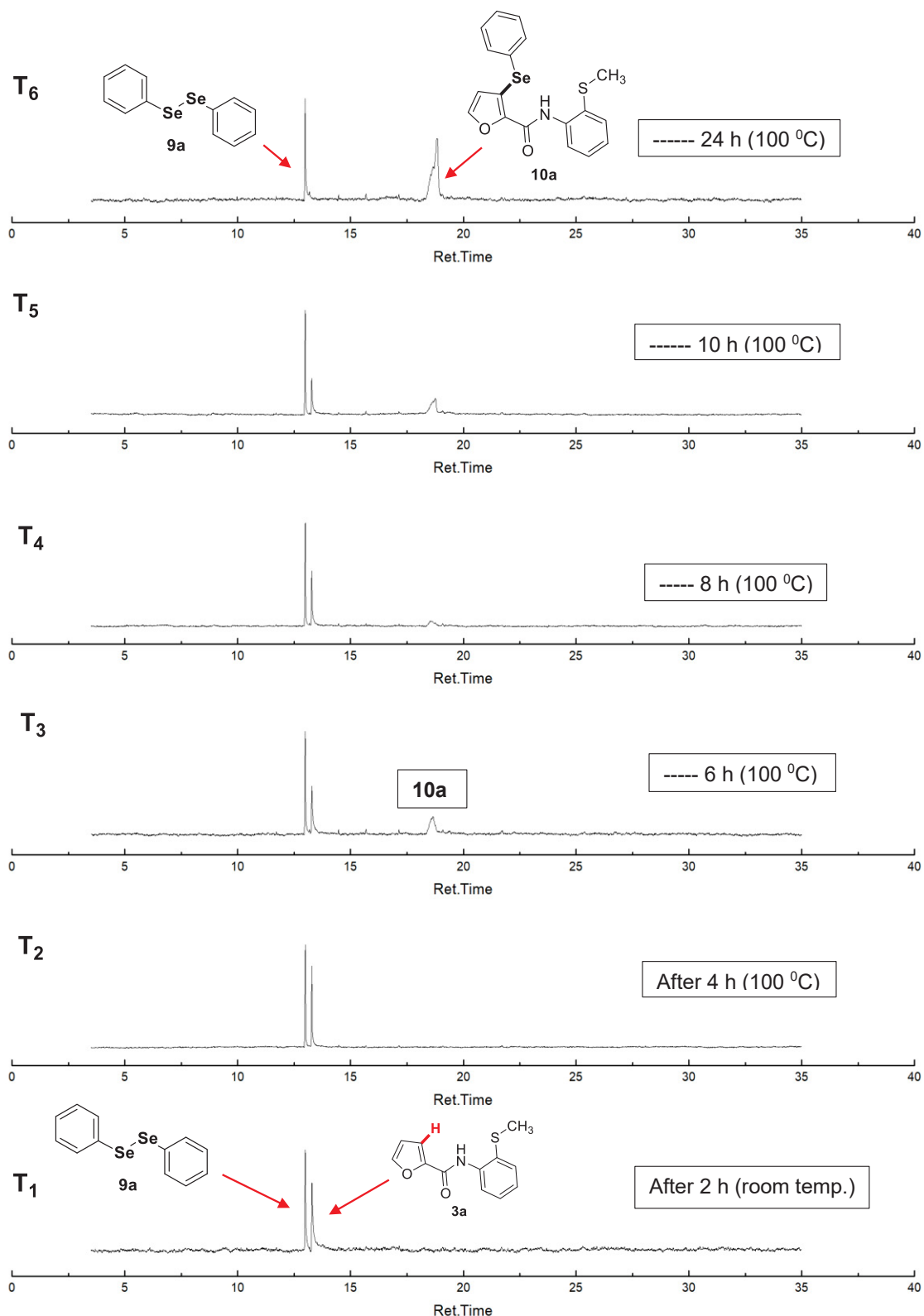
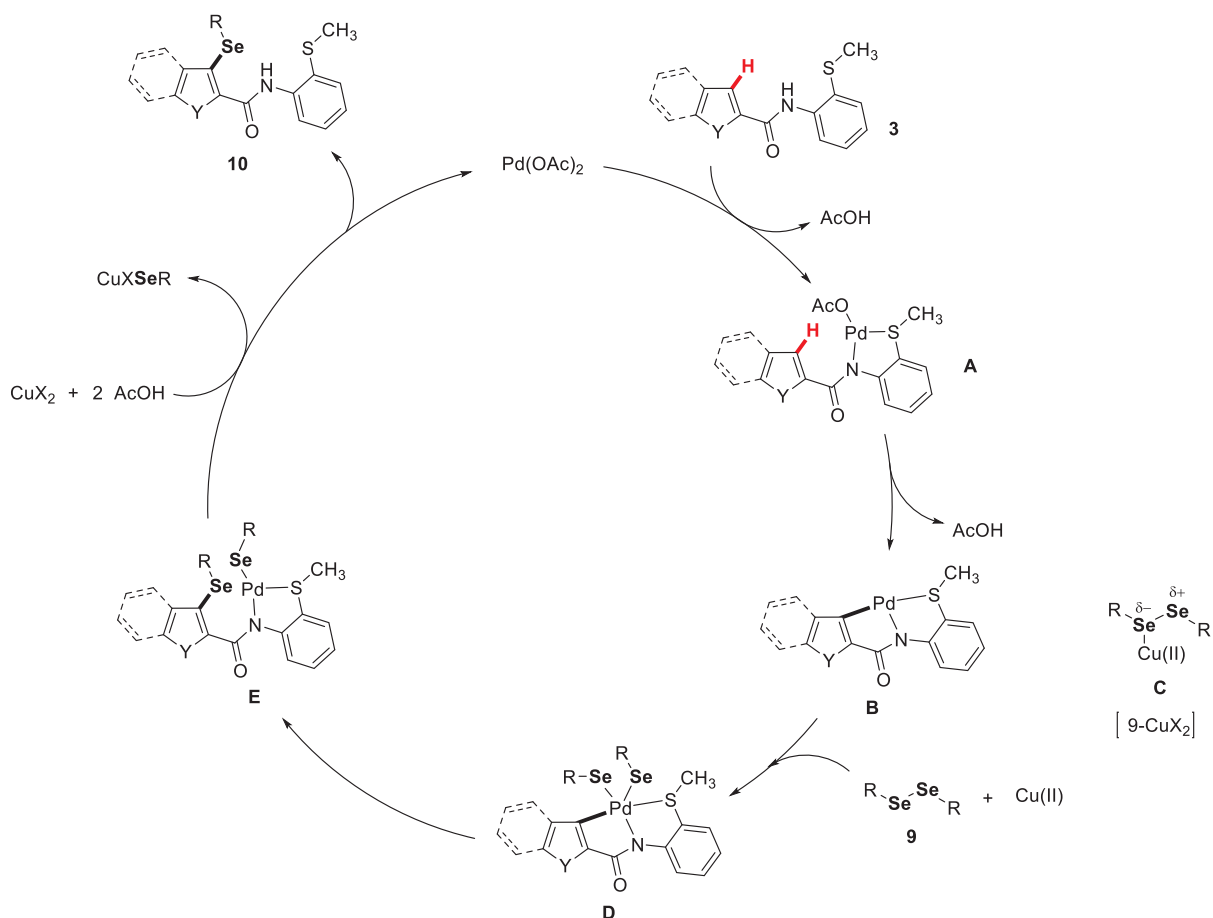


Figure 19: Reactional follow-up via Gas Chromatography coupled to Mass Spectrometry.

Based on the evidence acquired here and previous reports,^{48,56,57,58} a plausible catalytic cycle is proposed in Scheme 27. To begin with, the coordination of the bidentate 2-(methylthio)amide directing group to Pd(OAc)₂ followed by release of

AcOH produces the Pd(II) chelated complex **A**. Then, a C-H activation takes place producing the five-membered Pd(II) metallacycle intermediate (**B**). The reaction yield shows a strong dependence on the acetate ligand (Table 2, entries 11-16) which could be rationalized by a C-H activation step via concerted metallation-deprotonation (CMD). Subsequently, the oxidative addition of Pd(II) to diorganoyl diselenide (**9**) leads to a Pd(IV) intermediate (**D**). The involvement of the Lewis acid-base complex [**9**-CuX₂] (**C**) was ruled out of the main catalytic cycle since we have not detected any unsymmetrical diorganoyl diselenides when diphenyl diselenide (**9a**) and 1,2-di-*p*-tolyl diselane (**9d**) were mixed under the optimized conditions or even with only Pd(OAc)₂ or CuBr₂ (Scheme 26d-g). Next, a reductive elimination releases the intermediate **E**. During the release of the product **10**, the CuX₂ can undergo ligand exchange with Pd(II) to sequester the organoselenide byproduct, along with the simultaneous regeneration of Pd(OAc)₂ catalyst for a further catalytic cycle.⁶² This is the most supported pathway until now since the reaction requires 1.0 equivalent of diorganoyl diselenide to afford high yields, which means that only one RSe fragment from the diorganoyl diselenides was incorporated in the final product **10**.

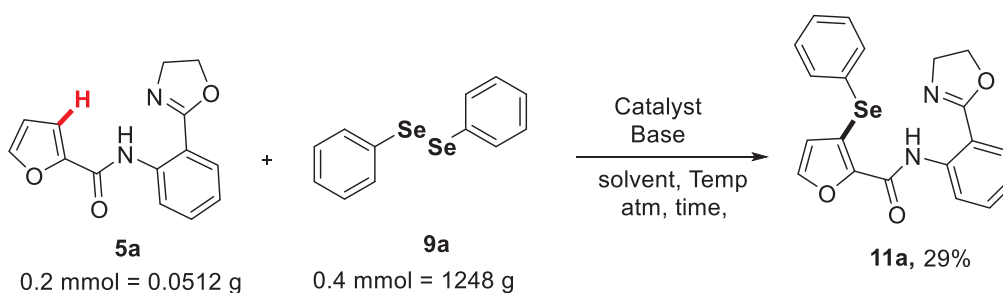


Scheme 27: Proposed catalytic cycle.

2.5 REGIOSELECTIVE C3 DIRECT CHALCOGENYLATION OF CHALCOGENOPHENES USING 2-(4,5-DIHYDROOXAZOL-2-YL)AMIDES AS DIRECTING GROUP

The regioselective C3 direct chalcogenylation of chalcogenophenes using 2-(4,5-dihydrooxazol-2-yl)amides as directing group begins with many tests using the *N*-2-(4,5-phenyl)furan-2-carboxamide (**5a**) and diphenyl diselenide (**9a**) as model reagents (Scheme 28). The methodology for this transformation was taken on the bases of “Yu” condition where the Cu-mediated protocol was applied, which allows chelation-assisted direct amination in arenes using benzamide.⁶³ Stimulated by this transformation the same reaction condition were employed with $\text{Cu}(\text{OAc})_2$ (1.0 Equivalent), Na_2CO_3 (2.0 Equivalents), **5a** (0.2 mmol) and **9a** (0.4 mmol) in DMSO at 80 °C for 6 h (Scheme 28). The first test of this transformation gave 29% yield of

compound **11a** after column chromatography using ethyl acetate 10% in hexane as eluent.



Scheme 28 : Yu conditions employed for the C3 regioselective direct selenylation of (**5a**).

The initial test gave a piece of evidence that both $\text{Cu}(\text{OAc})_2$ and Na_2CO_3 were effective for this reaction. The product **11a** was characterized by ^1H and ^{13}C Nuclear Magnetic Resonance (NMR) Spectroscopy, High Resolution Mass Spectrometry (HMRS) and single-crystal X-ray diffraction. The regioselectivity at C3 position of the furan ring was confirmed by the above characterization.

Initially, the compound **11a** was characterized by ^1H NMR spectrum which confirm 16 hydrogen atoms (Figure 20) from the relative integrals. In this way, a broad singlet at 12.98 ppm assigned to the hydrogen of the amide group and the doublet of doublet at 8.94 ppm (dd, $J = 8.5, 0.9$ Hz, 1H) to the hydrogen H-10. The next doublet of doublets at 7.87 ppm (dd, $J = 7.9, 1.6$ Hz, 1H) belongs to hydrogen H-7. While a multiplet at 7.75-7.72 ppm related to the two hydrogens H-22 and H-26. In the other hand a triplet of doublet at 7.48 ppm (td, $J = 8.6, 1.6$ Hz, 1H) associated to hydrogen H-9. The multiplet from 7.42 to 7.35 ppm related to four hydrogens H-18, H-23, H-24, H-25. Additionally, the other triplet of doublets at 7.10 ppm (td, $J = 7.8, 0.9$ Hz, 1H) for hydrogen H-8. The doublet at 5.95 ppm (d, $J = 1.8$ Hz, 1H) was assigned to hydrogen H-17. In addition, the triplet at lower frequency region at 4.39 ppm (t, $J = 9.6, 2\text{H}$) belongs to the hydrogens H-14, H-14' and the triplet at 4.19 ppm (t, $J = 9.1, 2\text{H}$) to the hydrogens H-13, H-13' of methylene fragment in the compound **11a**.

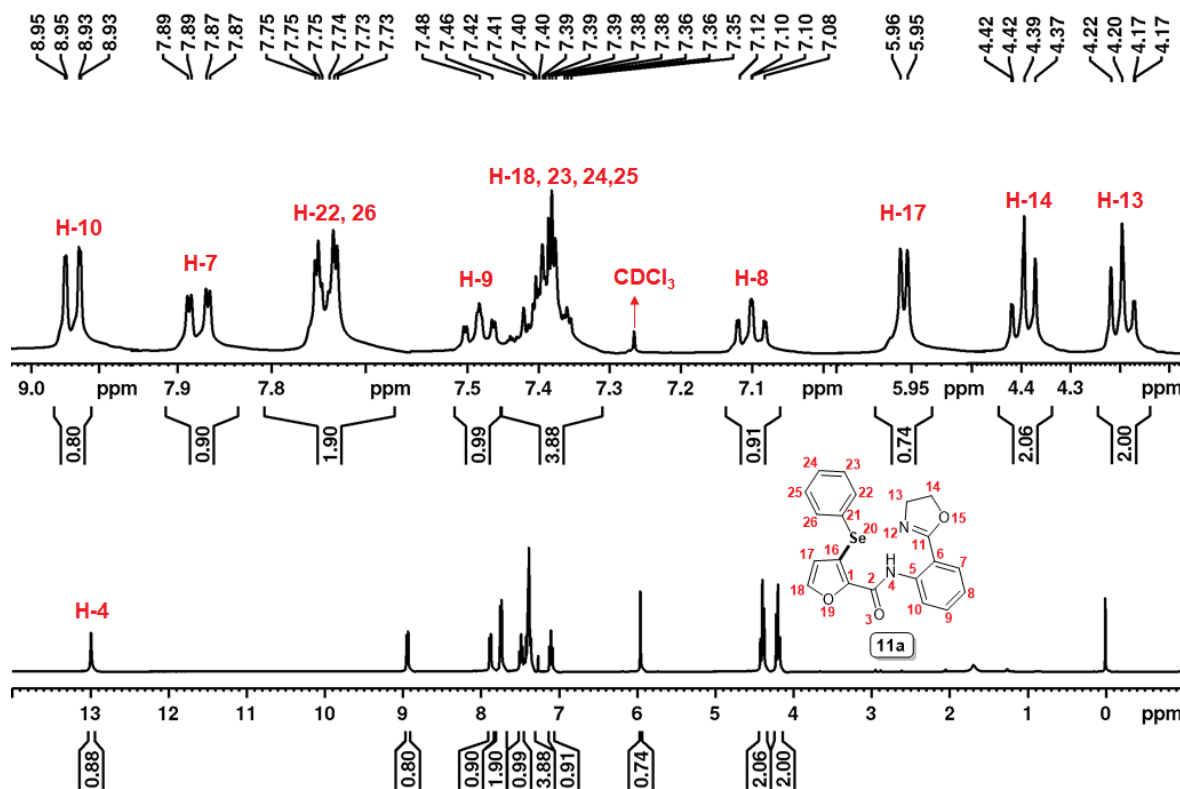


Figure 20: ^1H NMR spectrum (400 MHz, CDCl_3) of *N*-(2-(4,5-dihydrooxazol-2-yl)phenyl)-3-(phenylselanyl)furan-2-carboxamide (**11a**).

The signals in ^{13}C NMR spectrum (Figure 21) of compound **11a** confirmed 20 carbon atoms, in which most of them lies in the region above 110 ppm and only two signals at 50 to 70 ppm assigned to the carbon of methylene group. In the other hand, the 7 small signals of compound **11a** belongs to the quaternary carbon of C-1, C-2, C-5, C-6, C-11, C-16, and C-21 respectively. In order to elaborate all signals in the compound **11a** of ^{13}C NMR spectrum, the signal observed at 164.6 ppm related to C-11 carbon and at 157.8 ppm to C-2 carbon atom. Similarly, the signal at 144.1 ppm associated to C-18 and the two small signals at 141.5 ppm, 139.6 ppm to C-1 and C-5 carbon atoms respectively. Next to it the signal at 136.3 ppm related to C-22, C-26 two carbon atoms. While the signal at 132.4 ppm assigned to C-7 carbon atom. Additionally, the signal at 129.5 ppm also belongs to two carbon atoms (C-23, C-25). The signal at 129.2 ppm and at 128.9 ppm allocated for Carbon C-9 and C-24 respectively. In the other hand, the signals at 127.9 ppm and 123.9 ppm related to the quaternary carbon C-21 and C16. The next signal at 122.4 ppm to the C-8 carbon an at 120 ppm assigned to Carbon C-10. Finally, the signal in the aromatic region of arenes and hetero-arene at 113.9 ppm related to C-17 of furan ring while the signal at 113.6 ppm for C-6 carbon atom. However, the signal at low frequency

region at 66.2 ppm and 54.8 ppm belongs to C-14 and C-13 carbon atoms of methylene group in the compounds **11a**.

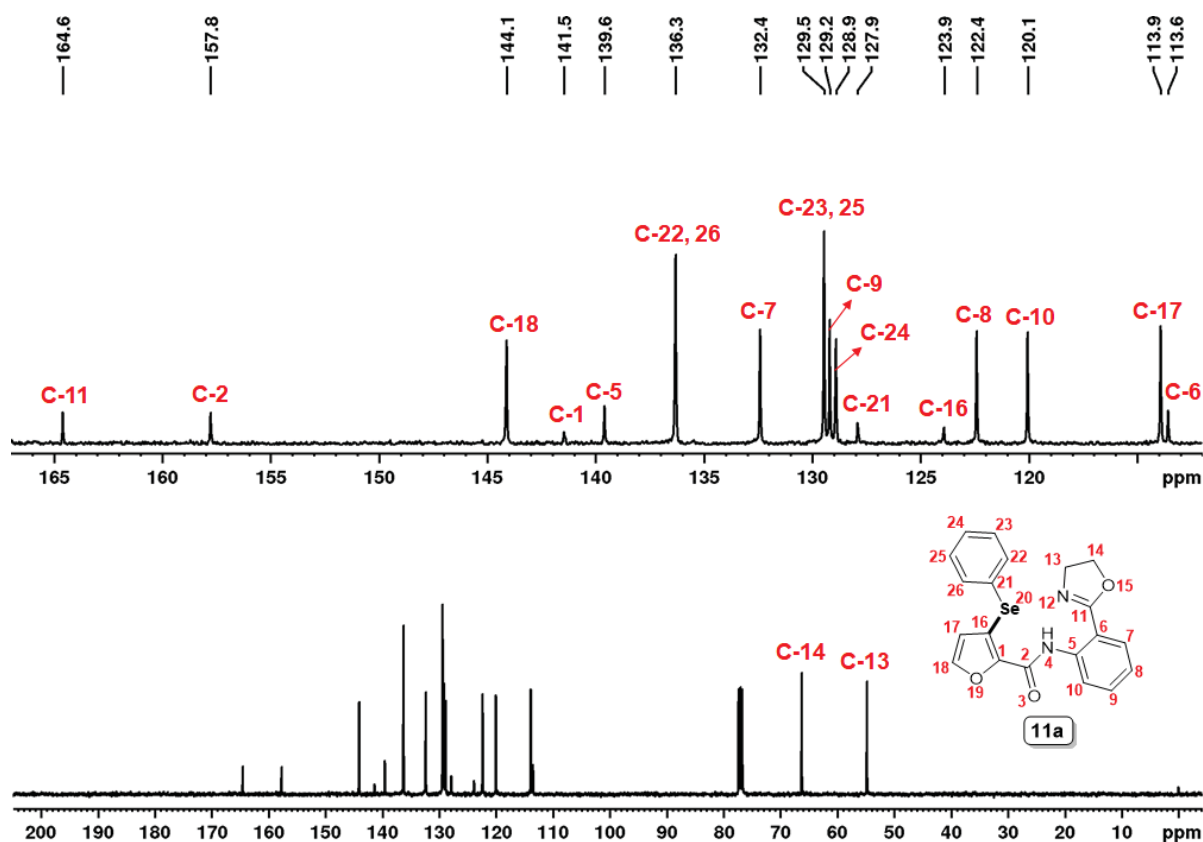


Figure 21: ^{13}C NMR spectrum (100 MHz; CDCl_3) of *N*-(2-(4,5-dihydrooxazol-2-yl)phenyl)-3-(phenylselanyl)furan-2-carboxamide (**11a**).

After NMR analysis the reaction regioselectivity was further confirmed by single-crystal X-ray diffraction of **11a**, which has proven the C3 regioselectivity on the direct selanylation (Figure 22).

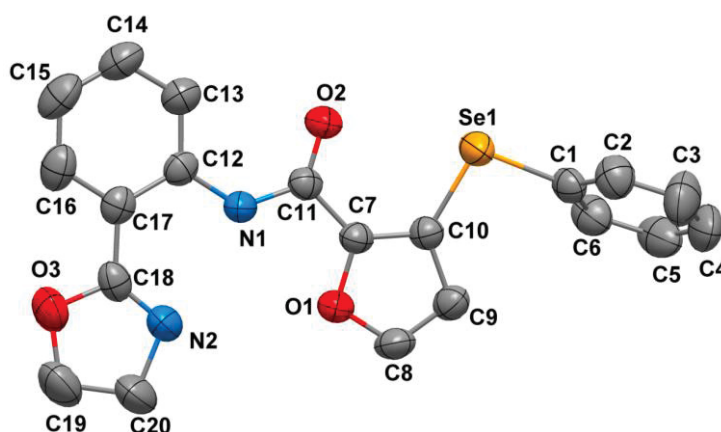
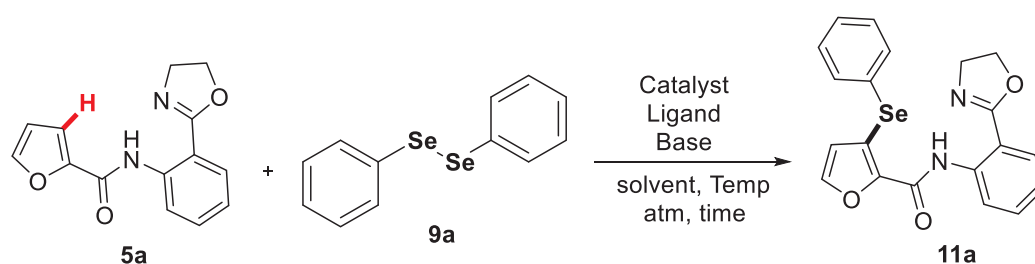


Figure 22: ORTEP diagram of compound **11a**.

After structural elucidation and confirmation of the product **11a**, the next step consisted of optimizing the reaction conditions (Table 6), evaluating the effects of stoichiometry between the substrates (**5a**) and (**9a**), catalyst, base, ligand, solvent, temperature, atmosphere, and time of the reaction. At the beginning, the reaction of *N*-(2-(4,5-dihydrooxazol-2-yl)phenyl)furan-2-carboxamide **5a** (0.2 mmol) with diphenyl diselenide **9a** (0.4 mmol) was performed in the presence of copper acetate $\text{Cu}(\text{OAc})_2$ (1.0 Equivalent) as catalyst and Na_2CO_3 (2.0 Equivalents) as base at 80 °C in DMSO for 6 h. The reaction was followed by thin-layer chromatography (TLC) and the product *N*-(2-(4,5-dihydrooxazol-2-yl)phenyl)-3-(phenylselenanyl)furan-2-carboxamide (**11a**) was isolated by column chromatography (gradient 1% to 10% of ethyl acetate in hexane) in 29% yield (Table 6, entry, 1).

Table 6: Optimization of the reaction conditions for C3 regioselective direct selenylation of (**5a**).



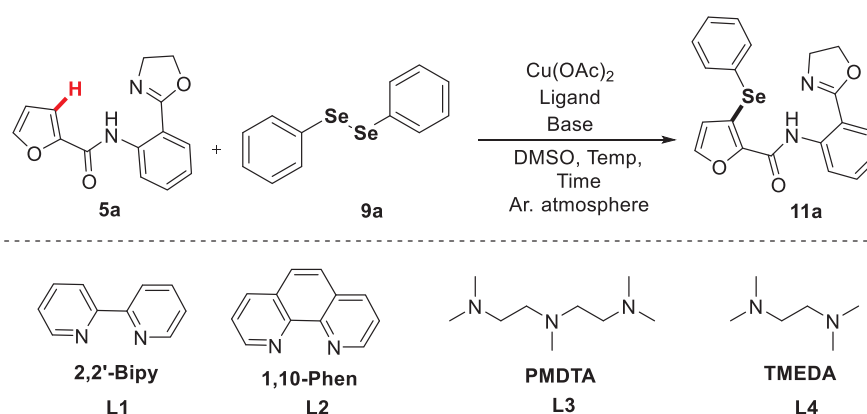
Entry ^[a]	5a (mmol)	9a (mmol)	$\text{Cu}(\text{OAc})_2$ (equiv.)	Na_2CO_3 (equiv.)	Temp (°C)	Time (h)	Yield (%) ^[b]
1	0.2	0.4	1.0	2.0	80	6	29
2	0.2	0.4	1.0	2.0	80	8	33
3	0.2	0.4	2.0	2.0	80	8	29
4	0.2	0.4	1.0	2.0	80	24	28
5	0.2	0.2	1.0	2.0	80	24	20
6	0.2	0.2	1.0	1.0	80	24	18
7	0.2	0.2	1.0	1.0	100	24	7
8 ^e	0.2	0.4	1.0	2.0	80	8	39
9 ^d	0.2	0.4	1.0	2.0	80	8	47
10 ^c	0.2	0.4	1.0	2.0	80	8	54

^[a] **Reaction conditions:** The reaction of **5a** with **9a** was evaluated in the presence of $\text{Cu}(\text{OAc})_2$ catalyst and Base in 2.0 mL of DMSO (dry) Solvent was heated under air atmosphere for the time and temperature mentioned in the table 6. ^[b] Isolated yields ^[c] inert atmosphere ^[d] oxygen atmosphere ^[e] 2,2'-bipyridine ligand (1 equiv., 0.2 mmol).

When the same reaction condition of (entry 1) table 6 was employed for 8 h, the product **11a** was slightly increased to 33% (Table 6, entry 2). While increasing the amount of $\text{Cu}(\text{OAc})_2$ catalyst up to 2 Equivalents, 29% yield was obtained (Table 6, entry 3). Similarly, under same condition of entry 1 (Table 6) but the reaction time was increased to 24 h, the yield of product **11a** was 28% (Table 6, entry 4). While the equimolar concentration of substrates **5a** and **9a** under the similar condition of 24 h reaction time gave 20% yield of **11a** (Table 6, entry 5). When the amount of base was decrease to (1.0 Equivalent), 18% yield was attained (Table 6, entry 6). The same reaction conditions of entry 6 (Table 6) was evaluated at 100 °C, temperature the yield decreased to 7% (Table 6, entry 7). However, by adding 1.0 equiv. 2,2'-bipyridine ligand under the same condition of (entry 2) table 6, the yield was improved to 39% (Table 5, entry 8). Similarly, the reaction condition of (entry 2) table 6 was evaluated under molecular oxygen (O_2) atmosphere the yield of **11a** was increased to 47% (Table 6, entry 9). While in inert atmosphere of argon, the product significantly increased to 54% (Table 6, entry 10).

The above results proved that the role of inert atmosphere and ligand significantly increased the yields of **11a**, in this way further screening of the reaction was practiced by using different ligands under inert atmosphere of argon in table 7.

Table 7: Optimization of the reaction conditions for C3 regioselective direct selanylation of (**5a**).



(Continuation)

Entry ^[a]	5a mmol	9a mmol	Ligand (equiv.)	$\text{Cu}(\text{OAc})_2$ (equiv.)	Base (equiv.)	Temp (°C)	Time (h)	Yield (%) ^[b]
1	0.2	0.4	L1 (1.0)	1.0	Na_2CO_3 (2.0)	80	8	64
2^[c]	0.2	0.4	L1 (1.0)	1.0	Na_2CO_3 (2.0)	80	8	53

(Conclusion)								
3	0.2	0.4	L1 (1.0)	1.0	<i>t</i> -BuOK (2.0)	80	8	47
4	0.2	0.4	L1 (1.0)	1.0	Na ₂ CO ₃ (2.0)	60	8	60
5	0.2	0.4	L1 (1.0)	1.0	Na ₂ CO ₃ (2.0)	60	24	54
6	0.2	0.4	L1 (0.1)	0.1	Na ₂ CO ₃ (2.0)	80	8	16
7	0.2	0.4	L2 (1.0)	1.0	Na ₂ CO ₃ (2.0)	80	8	68
8	0.2	0.4	L2 (1.0)	1.0	Na ₂ CO ₃ (2.0)	100	8	42
9	0.2	0.4	L2 (1.0)	1.0	Cs ₂ CO ₃ (2.0)	80	8	40
10	0.2	0.4	L2 (1.0)	1.0	K ₂ CO ₃ (2.0)	80	8	52
11	0.2	0.4	L2 (1.0)	1.0	Na ₂ CO ₃ (1.0)	80	8	40
12	0.2	0.2	L2 (1.0)	1.0	Na ₂ CO ₃ (1.0)	80	8	43
13	0.2	0.4	L2 (1.5)	1.5	Na ₂ CO ₃ (2.0)	80	8	50
14^[d]	0.2	0.4	L2 (1.0)	1.0	Na ₂ CO ₃ (2.0)	80	8	14
15	0.2	0.4	L2 (0.2)	0.2	Na ₂ CO ₃ (2.0)	80	8	5

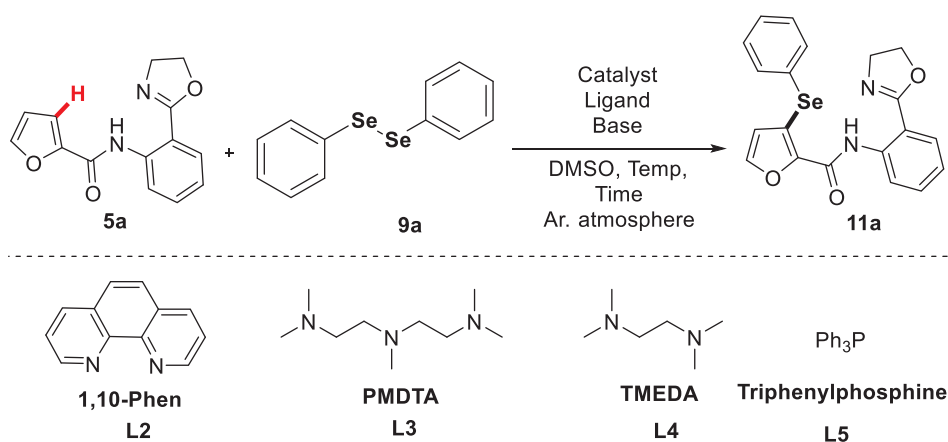
^[a] **Reaction conditions:** The reaction of **5a** with **9a** was evaluated in the presence of Cu(OAc)₂ catalyst (table) and Base (table) in 2.0 mL of DMSO (dry) Solvent was heated under inert atmosphere of argon for the time and temperature mentioned in the table 7. ^[b] Isolated yields ^[c] oxygen atmosphere ^[d] air atmosphere

The first experiment was performed using **5a** (2 mmol) and **9a** (0.4 mmol) in the presence of Cu(OAc)₂ (1.0 equiv.) as catalyst, 2,2'-bipyridine (1.0 Equivalent), as ligand and Na₂CO₃ as base in 2.0 mL DMSO at 80 °C temperature for 8 h under argon atmosphere, 64% yield of **11a** was obtained (Table 7, entry 1). The same reaction conditions of (Table 7, entry 1) under oxygen (O₂) atmosphere gave 53% yield (Table 7, entry 2). In the next test *t*-BuOK base was used, 47% yield was obtained (Table 7, entry 3). When the reaction was carried out at 60 °C of the temperature, 60% yield of **11a** was attained (Table 7, entry 4). While the reaction time increased to 24 h provided 54% yield (Table 7, entry 5). In the next test the catalytic amount of Cu(OAc)₂ (10 mol% or 0.1 Equivalent) catalyst and 2,2'-bipyridine (10 mol% or 0.1 Equivalent) afforded 16% yield (Table 7, entry 6). However, when the ligand 1,10-phenanthroline was used under the same reaction condition of (entry

1) Table 7, the yield was effectively increased to 68 % (Table 7, entry 7). Under similar condition of (Table 7, entry 7) but increased the temperature to 100 °C, 42% yield was achieved (Table 7, entry 8). The same reaction condition of (Table 7, entry 7) was evaluated using Cs₂CO₃ base, 40% yield was obtained (Table 7, entry 9). Similarly, when K₂CO₃ base was employed 52% yield was attained (Table 7, entry 10). In the next two test the stoichiometry of base and diphenyl diselenide **9a** was investigated, in this way when the amount of base Na₂CO₃ was decreased to 1.0 equivalent the yield was also decreased to 40% (Table 7, entry 11). Similarly, decreasing the amount of diphenyl diselenides **9a** to 0.2 mmol gave almost same results, only 43% yield of **11a** was attained (Table 7, entry 12). Furthermore, the stoichiometry of Cu(OAc)₂ catalyst and 1,10-phenanthroline Ligand (L2) was scrutinized, when the amount of both are increased to 1.5 equivalent, 50% yield of **11a** was produced (Table 7, entry 13). In the next test the reaction was analyzed in the presence of 1.0 Equivalent Cu(OAc)₂ catalyst, ligand (L2) and 2.0 Equivalent base at 80 °C temperature for 8 h under Air atmosphere the yield of product **11a** was decrease to 14% (Table 7 entry 14) it shows that the inert atmosphere is crucial for the reaction. Similarly, when catalytic amount (20 mol% or 0.2 Equivalent) of Cu(OAc)₂ catalyst and ligands (L2) were used, only 5% yields was obtained (Table 7, entry 15).

In an effort to increase the yield, further optimization under new reaction condition was investigated in table 8, in this way when the first experiment was performed in the presence of 1.0 Equivalent $\text{Cu}(\text{OAc})_2$ catalyst and bulky tridentate ligand (L3) of PMDTA (N,N,N',N'',N'' -pentamethyldiethylenetriamine) and 2.0 Equivalent of Na_2CO_3 base at 80 °C temperature for 8 h in an inert atmosphere of argon, 52% yields was obtained (Table 8, entry 1).

Table 8: Optimization of the reaction conditions for C3 regioselective direct selanylation of (**5a**).



(Continuation)

Entry ^[a]	5a mmol	9 mmol	Ligand (equiv.)	$\text{Cu}(\text{OAc})_2$ (equiv.)	Base (equiv.)	Temp (°C)	Time (h)	Yield (%) ^[b]
1	0.2	0.4	L3 (1.0)	1.0	Na_2CO_3 (2.0)	80	8	52
2	0.2	0.4	L5 (1.0)	1.0	Na_2CO_3 (2.0)	80	8	15
3	0.2	0.4	L4 (1.0)	1.0	Na_2CO_3 (2.0)	80	8	70
4	0.2	0.4	L4 (1.0)	1.0	-----	80	8	6
5	0.2	0.4	L4 (0.2)	0.2	Na_2CO_3 (2.0)	80	8	16
6	0.2	0.4	L4 (0.5)	0.5	Na_2CO_3 (2.0)	80	8	37
7	0.2	0.2	L4 (1.0)	1.0	Na_2CO_3 (2.0)	80	8	73
8	0.2	0.2	L4 (1.0)	1.0	Na_2CO_3 (1.0)	80	8	56
9	0.2	0.2	L4 (1.0)	1.0	Na_2CO_3 (2.0)	80	24	57
10	0.2	0.2	L4 (1.0)	1.0	Na_2CO_3 (2.0)	80	16	47
11	0.2	0.2	L4 (1.0)	1.0	Na_2CO_3 (2.0)	80	12	53

(Conclusion)								
11	0.2	0.2	L4 (1.0)	1.0	Cs ₂ CO ₃ (2.0)	80	8	55
12	0.2	0.2	L4 (1.0)	1.0	<i>t</i> -BuOK (2.0)	80	8	34
13	0.2	0.2	L4 (1.0)	1.0	K ₂ CO ₃ (2.0)	80	8	45
14	0.2	0.2	L4 (1.0)	1.0	DBU (2.0)	80	8	35

^[a] **Reaction conditions:** The reaction of **5a** with **9a** was evaluated in the presence of Cu(OAc)₂ catalyst (table) and Base (table) in 2.0 mL of DMSO (dry) Solvent was heated under inert atmosphere of argon for the time and temperature mentioned in the table 8. ^[b] Isolated yields

Similarly, when the reaction was analyzed in triphenylphosphine ligand (L5) only 15% yield was produced (Table 8, entry 2). However, when the reaction was scrutinized in TMEDA (*N,N,N',N'*-Tetramethylethylenediamine) ligand (L4) under the reaction condition of (entry 1) table 8, the yield was significantly increased to 70% (Table 8, entry 3). The reaction without base gave only 6% yield (Table 8, entry 4). While in the catalytic amount (20 mol% or 0.2 Equivalent) of Cu(OAc)₂ catalyst and ligands (L4) produced 16% yields (Table 8, entry 5). Furthermore, when the catalytic amount of Cu(OAc)₂ catalyst and ligands (L4) was increased to (50 mol % or 0.5 equivalent) the yield of product **11a** also increased slightly to 37% (Table 8, entry 6). However, the equimolar concentration of **5a** and **9a** used in the reaction provides 73% yields (Table 8, entry 7). Similarly, decreasing the amount of base Na₂CO₃ to 1.0 equivalent also decreased the yield to 56% (Table 8, entry 8). Considering the (entry 7) table 8 the best condition until now in the next tests the reaction time were evaluated but lower yield of product **11a** was detected (Table 8, entries 9-11). Similarly, the reaction was further scrutinized in different bases, lower yields were obtained, only Cs₂CO₃ afforded 55% yield (Table 8, entries 11-14). Further investigation of the reaction condition is underway.

3 CONCLUSIONS

Considering the results obtained so far, several conclusions and perspectives can be elaborated. In the context of the preparation of starting materials 2-methylthio amide and *N*-2-(4,5-phenyl)furan-2-carboxamide (**5a**) were prepared using steglich condition of DCC and DMAP, this methodology provided different heterocyclic amide from 65-93% yields, and different substituted aryl amide from 50- 70% yields. This methodology provides twenty different starting materials with 24 h reactions time. and with a smaller number of purification steps.

After synthesis of starting materials, an efficient new methodology was developed for regioselective C3 direct chalcogenylation of chalcogenophenes and arenes oriented by the 2-(methylthio)amide group and 2-(4,5-dihydrooxazol-2-yl)amides. The directing group assisted direct chalcogenylation is a new field in organochalcogen chemistry, and a wide variety of bidentate nitrogen-based directing groups could be explored. These directing groups range in structural complexity from simple to highly elaborate and possess differing coordination strengths to transition metal catalysts. Collectively, this set of directing groups could be compatible with many different transition metals, including Pd, Rh, Co, Cu, Ru and Ir. In order to verify the aptitude of 2-(methylthio)amide group for the direct chalcogenylation at C3 position in chalcogenophenes, the amide **3a** and diphenyl diselenide (**9a**) were choose as models reagents. The initial tests under palladium catalysis produced the *N*-(2-methylthio)phenyl-3-(phenylselanyl)furan-2-carboxamide (**10a**), which was characterized by means of Mass Spectrometry (MS), ¹H and ¹³C Nuclear Magnetic Resonance (NMR), Heteronuclear (¹H-¹³C) Single Quantum Correlation (HSQC) and Heteronuclear (¹H-¹³C) Multiple Bond Coherence (HMBC) experiments. In the compound **10a**, the H-14 signal in the ¹H NMR spectra was observed as a doublet (6.00 ppm) with ³J coupling constant of 1.8 Hz with H-15. Additionally, the structural characterization of **10b** by single-crystal X-ray diffraction also undoubtedly proved the C3-regioselectivity. The MS spectra displayed the molecular ion in accordance with the expected exact mass of the compound **10a**. The HSQC and HMBC experiments supported the molecular structure proposed (**10a**), and all the observable ¹H-¹³C correlations were disclosed. Similarly, the direct chalcogenylation at C3 position of 2-(4,5-dihydrooxazol-2-yl)amides (**5a**) with diphenyl diselenide (**9a**) as model reagent was observed, and the product (**11a**) was confirmed by ¹H and ¹³C Nuclear Magnetic Resonance (NMR), and single-crystal X-ray diffraction analysis.

After several experiments, the best conditions for the preparation of **10a** in 98% isolated yield employed Pd(OAc)₂ (2.5 mol%) and CuBr₂ as additive (0.33 Equivalents) in DMF (dry) as solvent at 100 °C for 24 h. The scope of this methodology was evaluated, and as a result of this transformation 22 new compounds were formed while 8 compounds were not produce the expected products. In summary this protocol provides moderate to excellent yields of selanylated compounds **10** but it also shows certain limitation that the reaction does not reliable for sulfenylation and tellurized moieties.

In addition, the reaction was monitored by gas chromatography coupled to mass spectrometry (GC-MS). In order to clarify the reaction mechanism, several tests were conducted but the clear mechanism wasn't identified. However, as a result of these tests a plausible mechanism of the reaction was presented. Similarly, after the confirmation of *N*-(2-(4,5-dihydrooxazol-2-yl)phenyl)-3-(phenylselanyl)furan-2-carboxamide (**11a**), the optimization of reaction was evaluated and until now 73% yields of **11a** shows the best condition employed Cu(OAc)₂ (1.0 Equivalent) catalyst, Na₂CO₃ (2.0 Equivalent) base and TMEDA (1.0 Equivalent) ligand in 2 mL DMSO solvent under inert atmosphere of argon (Ar) at 80 °C temperature for 8 h. Further optimization of the reaction is in progress and after that the scope will be under consideration.

4 EXPERIMENTAL SECTION

The experimental section contains general information and procedure employed in the synthesis of starting materials 2-(methylthio)amide. In this way all experiments of this project were carried out in the Laboratory of Polymers and Molecular Catalysis (LaPoCa) at the Department of Chemistry of the Federal University of Paraná (UFPR).

4.1 GENERAL INFORMATION

In this work, the reagents; thiomethyl aniline, several organic acids, *N,N'*-Dicyclohexylcarbodiimide (DCC), and 4-Dimethylaminopyridine (DMAP) were purchased from sigma Aldrich. Through them, except the recrystallized acids, further reagents were used without purification. Similarly, the solvents such as *N,N'*-dimethylformamide (DMF), dimethyl sulfoxide (DMSO), dichloromethane (DCM), Tetrahydrofuran (THF), toluene, ethanol, and so far were purified dried and degassed, performing classical approaches⁶⁴. Solvents used in liquid-liquid extraction and as eluents for chromatographic purification were distilled before use. The reactions were monitored by thin-layer chromatography (TLC) using silica gel 60 F254 aluminum sheets, and the visualization of the spots was by UV light (254 nm) or stained with iodine. Column chromatography was performed on silica gel (230–400 mesh). The low-resolution mass spectra (MS) were measured on a gas chromatograph coupled to a Shimadzu GC-2010 Plus mass spectrometer with mass spectrometry detection model QP2010 SE, and the chromatographic column used is the Agilent model VF-5MS (30 mx 0.32 mm, 015 μm). High resolution mass spectra (HMRS) were recorded in positive ion mode (APCI) using a Bruker micrOTOF-QIII spectrometer.

4.1.1 Single-crystal X-ray diffraction analysis

The single crystals X-ray diffraction analysis for **10b** was scrutinised in DMF solvent by slow evaporation at room temperature using Bruker D8 Venture diffractometer, equipped with a Photon 100 CMOS detector, Mo-K α radiation ($\lambda = 0.71073 \text{ \AA}$) and graphite monochromator. The data from **10b** was processed using

the APEX3 program.⁶⁵ The structure was determined by intrinsic phasing method in the SHELXT program⁶⁶ and also refined by full-matrix least-squares method, on F²'s, in SHELXL.⁶⁷ The non-hydrogen atoms were refined with anisotropic thermal parameters. The hydrogen atoms were located in different maps followed by refining isotropically and freely. Scattering factors for neutral atoms were taken from reference.⁶⁸ Computer programs used in this analysis have been noted above and were run through WinGX⁶⁹ and figures that refer to the compound **10a** were made using program ORTEP.⁶⁹

Table 9: Crystal data and structure refinement for **10b** (C₁₈H₁₄ClNO₂SSe)

Elemental formula	C ₁₈ H ₁₄ Cl N O ₂ S Se
Molar Mass / g.mol ⁻¹	422.77
Temperature	296(2) K
Wavelength	0.71073 Å
Crystal system, space group	Orthorhombic, Pna2 ₁
Unit cell dimensions	
a / Å	a = 19.0177(9) Å α = 90
b / Å	b = 7.2938(3) Å β = 90
c / Å	c = 12.6350(6) Å γ = 90
Volume / Å ³	1752.62(14)
Calculated density	4, 1.602 Mg/m ³
F(000)	848
Absorption coefficient	2.424 mm ⁻¹
Crystal colour, shape	yellow parallelepiped
Crystal size	0.226 x 0.198 x 0.066 mm
Theta range for data collection	3.0 to 26.0 °
Limiting indices	-23 ≤ h ≤ 23, -8 ≤ k ≤ 8, -15 ≤ l ≤ 15
Completeness to theta = 25.2 °	99.8 %
Absorption correction	Semi-empirical from equivalents
Max. and min. transmission	0.7455 and 0.6571
Reflections collected / unique	67332 / 3416 [R(int) = 0.051]
No. of 'observed' reflections	(I > 2σI) 3147
Structure determined by:	intrinsic phasing, in SHELXT
Refinement:	Full-matrix least-squares on F ²
Data / restraints / parameters	3416 / 6 / 273
Goodness-of-fit on F ²	1.057
Final R indices ('observed' data)	R ₁ = 0.021, wR ₂ = 0.042
Final R indices (all data)	R ₁ = 0.025, wR ₂ = 0.043
	Reflections weighted:
w = [σ ² (Fo ²) + (0.0184*P) ² + 0.2246*P] ⁻¹ where P = (Fo ² + 2Fc ²)/3	
Absolute structure parameter	0.016(3)
Extinction coefficient	n/a
Largest diff. peak and hole	0.15 and -0.20 e. Å ⁻³
Location of largest difference peak	on C10-C11 bond

*Calculation according to the definition of the SHELXS-2013 programme

Table 10: Crystal data and structure refinement for **11a** (C₂₀H₁₆N₂O₃Se)
(Continuation)

Elemental formula	C ₂₀ H ₁₆ N ₂ O ₃ Se
Formula weight	411.31
Temperature	299(2) K
Wavelength	0.71073 Å
Crystal system, space group	Triclinic, P-1
Unit cell dimensions	a = 11.5375(10) Å α = 73.538(2)° b = 13.1083(10) Å β = 88.909(3) ° c = 13.8710(13) Å γ = 64.945(3) °
Volume	1810.2(3) Å ³
Z, Calculated density	4, 1.509 Mg/m ³
F(000)	832
Absorption coefficient	2.096 mm ⁻¹
Crystal colour, shape	colorless, prism
Crystal size	0.168 x 0.156 x 0.120 mm
On the diffractometer:	
Theta range for data collection	.63 to 23 °.
Limiting indices	-12 ≤ h ≤ 12, -14 ≤ k ≤ 14, -15 ≤ l ≤ 15
Completeness to theta = 23°	99.8 %
Absorption correction	Semi-empirical from equivalents
Max. and min. transmission	0.7451 and 0.6978
Reflections collected / unique	75644 / 5033 [R(int) = 0.064]
No. of 'observed' reflections (I > 2σI)	3959
Structure determined by: intrinsic phasing methods, in SHELXS Refinement:	
Full-matrix least-squares on F ²	
Data / restraints / parameters	5033 / 0 / 597
Goodness-of-fit on F ²	1.047
Final R indices ('observed' data)	R ₁ = 0.036, wR ₂ = 0.089
Final R indices (all data)	R ₁ = 0.053, wR ₂ = 0.095

	(Conclusion)
Reflections weighted:	
$w=[s^2(F_o^2)+(0.0535P)^2 + 0.9317]^{-1}$	where $P=(F_o^2+2F_c^2)/3$
Extinction coefficient	n/a
Largest diff. peak and hole	0.36 and -0.43 e. Å ⁻³
Location of largest difference peak	near N(2) atom

*Calculation according to the definition of the SHELXS-2013 programe

4.1.2 Nuclear Magnetic Resonance (NMR) Spectroscopy

The ¹H and ¹³C NMR spectra were obtained at the Laboratory of Nuclear Magnetic Resonance Department of Chemistry (LabNMR-DQUI) in Federal University of Paraná (UFPR) using Bruker spectrometers of the Ascend Nuclear 400 MHz model, operating at a frequency of 400 MHz for hydrogen and 100 MHz for carbon and DPX200 operating at a frequency of 200 MHz for the hydrogen core and 50 MHz for carbon. The chemical shifts (δ) are related in part per million (ppm) relative to tetramethylsilane (TMS, used as an internal standard for ¹H-NMR spectra) and CDCl₃ (for ¹³C NMR spectra), by placing in brackets at multiplicity (s = singlet, bs = broad singlet, d = doublet, t = triplet, q = quartet, quint = quintuplet, sex = sextet, m = multiplet, dd = doublet doublet, dt = doublet triplet, td = triple doublet), the number of hydrogens deduced from the relative integral and the coupling constant (J) expressed in Hertz (Hz).

4.2 EXPERIMENTAL PROCEDURES

4.2.1 General procedure A for the synthesis of 2-(methylthio)amide (**3a**, **3b**, **3d**, **3e**, **3f**, **8a**, **8b**, **8c**, **8d**, **8e**, **8f**, **8g**, **8h**, **8i**, **8j**, **8k**)

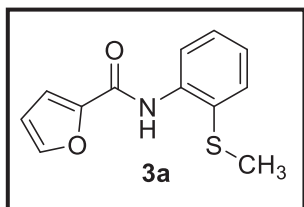
In a dry 250 mL 2-necked flask provided with magnetic stirring at room temperature under argon atmosphere, in which 2-furic acid (**1a**, 1.0 equiv, 10 mmol, 1.12 g) was added with 2-(methylthio)aniline (**2**, 1.0 equiv, 10 mmol, 1.39 g) in the presence of *N,N'*-Dicyclohexylcarbodiimide (DCC) (1.2 equiv, 12 mmol, 2.47 g) and 4-Dimethylaminopyridine (DMAP) (0.1 equiv, 1.0 mmol, 0.122 g) in 20 ml of anhydrous dichloromethane. The reaction solution was allowed to stir for 24h under argon atmosphere. After this time, 20 ml dichloromethane (DCM) was added to dilute the reaction and the solution was passed through a layer of silica. Then, it was added dichloromethane (60 mL), and the solution was washed with saturated NaHCO₃ solution (3 x 30 mL). The organic phase was dried over MgSO₄ and concentrated in vacuo. *N*-(2-(methylthio)phenyl)furan-2-carboxamide (**3a**) was obtained. Then, the crude was purified by column chromatography using silica gel, ethyl acetate and hexane was used as the eluent. The *N*-(2-(methylthio)phenyl)furan-2-carboxamide (**3a**) was obtained in 79% yield. Similarly, the other starting materials was also synthesized using same methodology (Table 1).

4.2.2 General procedure A for the synthesis of 2-(4,5-dihydrooxazol-2-yl)aniline

To a schilink flask with magnetic stir bar, isotoic anhydride (20 mmol), 2-chloroethyl amine hydrochloric acid (HCl) (20 mmol) and triethyl amine 7.0 mL was added in DMF (20 mL) solvent. The reaction mixture was stir for 2.5 h at 80 °C. after that the reaction residue was washed with distilled water (60 mL) and dichloromethane (CH₂Cl₂) (3x10). The organic layer was separated and dried over MgSO₄ and concentrated in vacuo. Then the crude was purified by column chromatography using hexane and ethyl acetate as eluent. The 2-(4,5-dihydrooxazol-2-yl)aniline was obtained 94% yield.

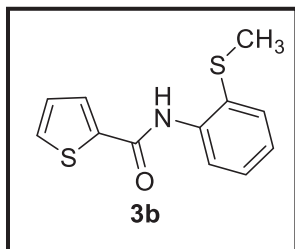
5.1 Characterized Data of starting materials:

***N*-2-(methylthio)phenylfuran-2-carboxamide (3a):** ^[70] Yield: 79%, white solid,



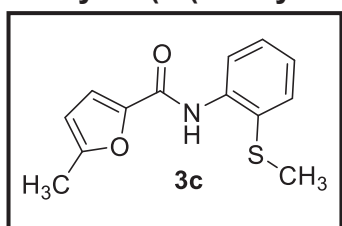
m.p. 77.1-77.6 °C; ¹H NMR (400 MHz, CDCl₃): δ 9.37 (br. s, 1H), 8.48 (dd, *J* = 8.2 and 1.2 Hz, 1H), 7.56 (dd, *J* = 1.6 and 0.8 Hz, 1H), 7.53 (dd, *J* = 7.8 and 1.4 Hz, 1H), 7.34 (td, *J* = 7.9 and 1.4 Hz, 1H), 7.25 (dd, *J* = 3.6 and 0.8 Hz, 1H), 7.09 (td, *J* = 7.6 and 1.2 Hz, 1H), 6.57 (dd, *J* = 3.4 and 1.8 Hz, 1H), 2.41 (s, 3H); ¹³C{H} NMR (100 MHz, CDCl₃): δ 156.1, 148.0, 144.6, 138.2, 133.4, 129.1, 125.4, 124.5, 120.4, 115.4, 112.6, 19.1; MS (EI) *m/z* (Rel. Int., %): [M⁺] 233 (10), 186 (35), 95 (100), 65(12), 45 (12), 39 (65).

***N*-2-(methylthio)phenylthiophene-2-carboxamide (3b):** ^[70] Yield: 66%, white



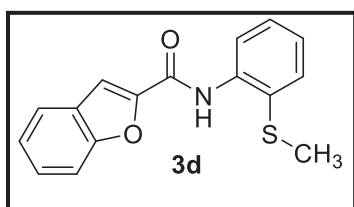
solid, m.p. 109.0-109.4 °C; ¹H NMR (400 MHz, CDCl₃): δ 9.14 (br. s, 1H), 8.46 (dd, *J* = 8.0 and 1.2 Hz, 1H), 7.68 (dd, *J* = 3.8 and 1.0 Hz, 1H), 7.57 (dd, *J* = 5.2 and 1.2 Hz, 1H), 7.54 (dd, *J* = 7.8 and 1.4 Hz, 1H), 7.35 (td, *J* = 7.8 and 1.2 Hz, 1H), 7.15 (dd, *J* = 5.0 and 3.8 Hz, 1H), 7.09 (td, *J* = 7.6 and 1.2 Hz, 1H), 2.41 (s, 3H); ¹³C{H} NMR (100 MHz CDCl₃, 100 MHz): δ 159.7, 139.6, 138.5, 133.6, 131.1, 129.4, 128.4, 128.0, 125.1, 124.5, 120.3, 19.3; MS (EI) *m/z* (Rel. Int., %): [M⁺] 249 (10), 202 (48), 111 (100), 39 (29).

5-methyl-*N*-2-(methylthio)phenylfuran-2-carboxamide (3c): Yield: 67%, white



solid, m.p. 60.5-61.0°C; ¹H NMR (400 MHz, CDCl₃): δ 9.23 (br. s, 1H), 8.46 (dd, *J* = 8.0, and 1.2 Hz, 1H), 7.52 (dd, *J* = 7.8 and 1.4 Hz, 1H), 7.33 (td, *J* = 7.8 and 1.2 Hz, 1H), 7.15 (d, *J* = 3.2 Hz, 1H), 7.08 (td, *J* = 7.6 and 1.2 Hz, 1H), 6.17 (dd, *J* = 3.4 and 1.0 Hz, 1H), 2.42 (s, 6H); ¹³C{H} NMR (100 MHz CDCl₃): δ 156.2, 155.3, 146.4, 138.3, 133.2, 129.1, 125.4, 120.5, 116.6, 109.0, 19.0, 14.0; MS (EI) *m/z* (Rel. Int., %): [M⁺] 247 (24), 200 (74), 109 (100), 53 (44); HRMS (ESI) *m/z* calcd for C₁₃H₁₄NO₂S [M+H]⁺ 248.0745, found 248.0748.

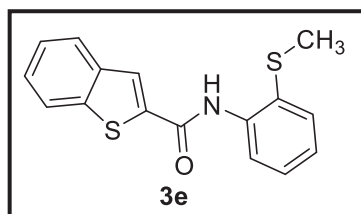
***N*-2-(methylthio)phenylbenzo[*b*]furan-2-carboxamide (3d):**^[70] Yield: 93%, white



solid, m.p. 97.5-97.8 °C; ¹H NMR (400 MHz, CDCl₃): δ 9.60 (br. s, 1H), 8.52 (dd, *J* = 8.0 and 1.2 Hz, 1H), 7.70 (ddd, *J* = 7.8, 1.2 and 0.4 Hz, 1H), 7.59-7.62 (m, 2H), 7.55

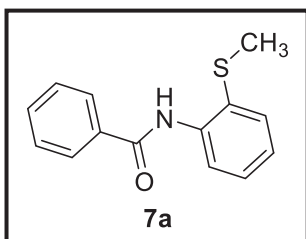
(dd, $J = 7.8$ and 1.4 Hz, 1H), 7.46 (ddd, $J = 8.6$, 7.2 and 1.2 Hz, 1H), 7.30-7.38 (m, 2H), 7.12 (td, $J = 7.6$ and 1.2 Hz, 1H), 2.46 (s, 3H). $^{13}\text{C}\{\text{H}\}$ NMR (100 MHz, CDCl_3): δ 156.7, 155.0, 148.8, 138.0, 133.3, 129.1, 127.7, 127.2, 125.9, 124.8, 123.9, 122.8, 120.7, 112.1, 111.5, 19.1. MS (EI) m/z (Rel. Int., %): $[\text{M}^+]$ 283 (30), 236 (100), 207 (5), 145 (66), 106 (7), 89 (52), 63 (10), 39 (5).

***N*-(2-(methylthio)phenyl)benzo[*b*]thiophene-2-carboxamide (3e):**^[70] Yield: 84%,



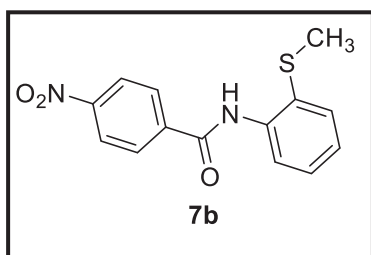
yellowish brown solid, m.p. 111.8-112.1 °C; ^1H NMR (400 MHz, CDCl_3): δ 9.26 (br. s, 1H), 8.49 (dd, $J = 8.2$ and 1.2 Hz, 1H), 7.92 (s, 1H), 7.87-7.90 (m, 2H), 7.55 (dd, $J = 7.8$ and 1.2 Hz, 1H), 7.40-7.47 (m, 2H), 7.36 (td, $J = 7.2$ and 1.6 Hz, 1H), 7.11 (td, $J = 7.6$ and 1.2 Hz, 1H), 2.43 (s, 3H); $^{13}\text{C}\{\text{H}\}$ NMR (100 MHz, CDCl_3): δ 160.1, 141.2, 139.1, 139.1, 138.4, 133.6, 129.4, 126.7, 125.6, 125.3, 125.1, 124.7, 122.8, 120.4, 19.4; MS (EI) m/z (Rel. Int., %): $[\text{M}^+]$ 299 (20), 252 (70), 161 (100), 133 (34), 89 (58), 63 (7), 39 (5).

***N*-(2-(Methylthio)phenyl)benzamide (7a):**^[70] Yield: 50%, white solid, m.p. 98.8-



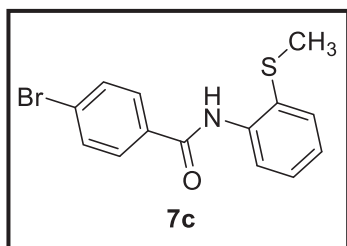
99.0 °C; ^1H NMR (400 MHz, CDCl_3): δ 9.23 (br. s, 1H), 8.53 (dd, $J = 8.4$ and 1.2 Hz, 1H), 7.94-7.97 (m, 2H), 7.48-7.58 (m, 4H), 7.35 (td, $J = 7.8$ and 1.6 Hz, 1H), 7.09 (td, $J = 7.6$ and 1.2 Hz, 1H), 2.40 (s, 3H); $^{13}\text{C}\{\text{H}\}$ NMR (100 MHz, CDCl_3): δ 165.1, 138.7, 134.9, 133.3, 132.0, 129.2, 128.9, 127.1, 125.5, 124.5, 120.5, 19.2; MS (EI) m/z (Rel. Int., %): $[\text{M}^+]$ 243 (26), 196 (74), 105 (100), 77 (75), 51 (14).

***N*-(2-(methylthio)phenyl)-4-nitrobenzamide (7b):**^[71] Yield: 61%, yellowish solid,



m.p. 128.4-129.9 °C; ^1H NMR (400 MHz, CDCl_3): δ 9.27 (br. s, 1H), 8.49 (d, $J = 8.4$ Hz, 1H), 8.38 (d, $J = 8.8$ Hz, 2H), 8.11 (d, $J = 8$ Hz, 2H), 7.57 (dd, $J = 7.8$ and 1.4 Hz, 1H), 7.39 (td, $J = 7.9$ and 1.4 Hz, 1H), 7.17 (td, $J = 7.6$ and 1.2 Hz, 1H), 2.44 (s, 3H); $^{13}\text{C}\{\text{H}\}$ NMR (CDCl_3 , 100 MHz): δ 163.0, 149.9, 140.4, 137.9, 133.2, 129.2, 128.3, 125.9, 125.3, 124.1, 120.6, 19.3; MS (EI) m/z (Rel. Int., %): $[\text{M}^+]$ 288 (23), 241 (100), 195 (16), 150 (36), 120 (16), 104 (38), 94 (26), 76 (15), 50 (7); HRMS (ESI) m/z calcd for $\text{C}_{14}\text{H}_{13}\text{N}_2\text{O}_3\text{S}$ $[\text{M}+\text{H}]^+$ 289.0647, found 289.0646.

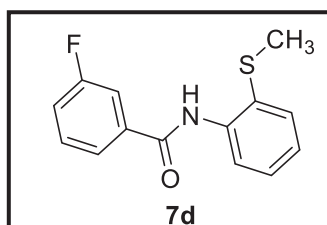
4-bromo-*N*-(2-(methylthio)phenyl)benzamide (7c):^[71] Yield: 55%, white solid, m.p.



117.2-117.6 °C; ¹H NMR (600 MHz, CDCl₃): δ 9.18 (s, 1H), 8.49 (d, *J* = 8.4 Hz, 1H), 7.82 (d, *J* = 8.5 Hz, 2H), 7.65 (d, *J* = 8.5 Hz, 2H), 7.54 (dd, *J* = 7.8 and 1.4 Hz, 1H), 7.36 (td, *J* = 7.8 and 1.3 Hz, 1H), 7.12 (td, *J* = 7.6 and 1.2 Hz, 1H), 2.41 (s, 3H); ¹³C NMR{H} (150 MHz, CDCl₃): δ

164.2, 138.3, 133.7, 133.3, 132.2, 129.2, 128.7, 126.8, 125.6, 124.7, 120.5, 19.2; MS (EI) *m/z* (Rel. Int., %): [M⁺] 321 (16), 274 (100), 183 (90), 155 (42), 104 (16), 94 (20), 76 (44), 50 (22), 39 (10); HRMS (ESI) *m/z* calcd for C₁₄H₁₃BrNOS [M+H]⁺ 321.9901, found 321.9900.

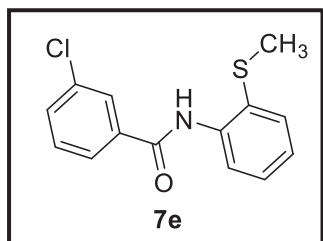
3-fluoro-*N*-(2-(methylthio)phenyl)benzamide (7d):^[70] Yield: 68%, white solid, m.p.



78.5-78.9 °C; ¹H NMR (400 MHz, CDCl₃): δ 9.19 (s, 1H), 8.49 (dd, *J* = 8.4 and 1.2 Hz, 1H), 7.70 (dd, *J* = 7.6 and 0.8 Hz, 1H), 7.65-7.69 (m, 1H), (dd, *J* = 7.6 and 1.6 Hz, 1H), 7.49 (td, *J* = 7.9 and 5.7 Hz, 1H), 7.36 (td, *J* = 7.8 and 1.2

Hz, 1H), 7.26 (tdd, *J* = 8.2, 2.6 and 0.8 Hz, 1H), 7.12 (td, *J* = 7.6, and 1.6 Hz, 1H), 2.41 (s, 3H); ¹³C{H} NMR (100 MHz, CDCl₃): δ 163.8, 162.9 (d, ¹*J*_{C-F} = 246.8 Hz), 138.3, 137.2 (d, ³*J*_{C-F} = 6.6 Hz), 133.3, 130.6 (d, ³*J*_{C-F} = 7.8 Hz), 129.2, 125.7, 124.7, 122.4 (d, ⁴*J*_{C-F} = 2.3 Hz), 120.5, 119.1 (d, ²*J*_{C-F} = 21.4 Hz), 114.7 (d, ²*J*_{C-F} = 23.1 Hz), 19.2; MS (EI) *m/z* (Rel. Int., %): [M⁺] 261 (22), 214 (100), 123 (96), 95 (66), 65 (7), 39 (5).

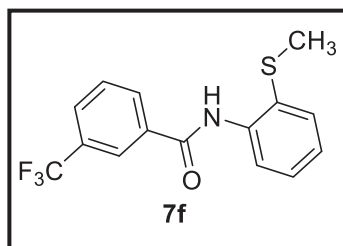
3-chloro-*N*-(2-(methylthio)phenyl)benzamide (7e):^[72] Yield: 44%, white solid, m.p.



113.8-114.4 °C; ¹H NMR (600 MHz, CDCl₃): δ 9.17 (br. s, 1H), 8.48 (dd, *J* = 8.2 and 0.9 Hz, 1H), 7.94 (t, *J* = 1.8 Hz, 1H), 7.80 (ddd, *J* = 7.7, 1.7 and 1.1 Hz, 1H), 7.53-7.55 (m, 2H), 7.45 (t, *J* = 7.8 Hz, 1H), 7.36 (td, *J* = 7.8 and 1.4 Hz, 1H), 7.13 (td, *J* = 7.6 and 1.4 Hz, 1H), 2.42 (s, 3H); ¹³C{H}

NMR (150 MHz, CDCl₃): δ 163.8, 138.2, 136.6, 135.2, 133.2, 132.0, 130.2, 129.2, 127.7, 125.7, 124.9, 124.8, 120.6, 19.2; MS (EI) *m/z* (Rel. Int., %): [M⁺] 277 (16), 230 (100), 207 (14), 139 (88), 111 (56), 75 (19), 44 (8), 39 (4); HRMS (ESI) *m/z* calcd for C₁₄H₁₃ClONS [M+H]⁺ 278.0406, found 278.0406.

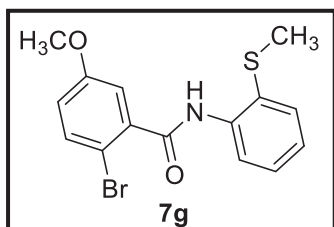
***N*-2-(methylthio)phenyl-3-(trifluoromethyl)benzamide (7f):** ^[71] Yield: 70%, white



solid, m.p.68.8-69.2 °C; ¹H NMR (400 MHz, CDCl₃): δ 9.23 (br. s, 1H), 8.49 (dd, *J* = 8.0 and 0.8 Hz, 1H), 8.24 (s, 1H), 8.11 (d, *J* = 8.0 Hz, 1H), 7.83 (d, *J* = 8.0 Hz, 1H), 7.67 (t, *J* = 7.8 Hz, 1H), 7.55 (dd, *J* = 7.8 and 1.6 Hz, 1H), 7.38 (td, *J* = 7.8 and 1.4 Hz, 1H), 7.14 (td, *J* = 7.6 and 1.2 Hz, 1H),

2.43 (s, 3H); ¹³C{H} NMR (100 MHz, CDCl₃): δ 163.7, 138.1, 135.8, 133.2, 131.6 (q, ²*J*_{C-F} = 32.7 Hz), 130.0, 129.5, 129.2, 128.6 (q, ³*J*_{C-F} = 3.6 Hz), 125.8, 124.9, 124.4 (q, ³*J*_{C-F} = 4.0 Hz), 123.6 (q, ¹*J*_{C-F} = 271.0 Hz), 120.6, 19.2; MS (EI) *m/z* (Rel. Int., %): [M⁺] 311 (20), 264 (100), 207 (10), 173 (68), 145 (60), 94 (11), 44 (12).

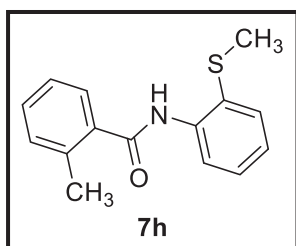
2-bromo-5-methoxy-*N*-2-(methylthio)phenylbenzamide (7g): Yield: 52%, white



solid, m.p. 82.1-82.6 °C; ¹H NMR (400 MHz, CDCl₃): δ 8.81 (br. s, 1H), 8.51 (d, *J* = 8.4, Hz, 1H), 7.54 (dd, *J* = 7.6 and 1.2 Hz, 1H), 7.52 (d, *J* = 8.8 Hz, 1H), 7.37 (t, *J* = 7.6 Hz, 1H), 7.19 (d, *J* = 3.2 Hz, 1H), 7.13 (td, *J* = 7.6 and 1.2

Hz, 1H), 6.89 (dd, *J* = 8.8 and 3.2 Hz, 1H), 3.83 (s, 3H), 2.39 (s, 3H); ¹³C{H} NMR (100 MHz, CDCl₃): δ 165.4, 159.1, 138.7, 138.2, 134.4, 133.3, 129.1, 125.9, 124.9, 120.8, 118.1, 114.8, 109.4, 55.7, 19.5; MS (EI) *m/z* (Rel. Int., %): [M⁺] 353 (10), 304 (32), 272 (72), 215 (64), 170 (22), 155 (12), 106 (11), 94 (53), 78 (75), 63 (100), 45 (37), 40 (18); HRMS (ESI) *m/z* calcd for C₁₅H₁₅BrNO₂S [M+H]⁺ 352.0007, found 352.0004.

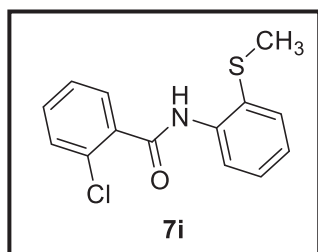
2-methyl-*N*-2-(methylthio)phenylbenzamide (7h):^[73] Yield: 31%, white solid, m.p.



63.9-64.2 °C; ¹H NMR (400 MHz, CDCl₃): δ 8.65 (br. s, 1H), 8.50 (d, *J* = 7.6 Hz, 1H), 7.56 (d, *J* = 7.2 Hz, 1H), 7.51 (dd, *J* = 7.8 and 1.0 Hz, 1H), 7.28-7.40 (m, 4H), 7.11 (td, *J* = 7.6 and 1.2 Hz, 1H), 2.56 (s, 3H), 2.37 (s, 3H); ¹³C{H} NMR (100 MHz, CDCl₃): δ 167.8, 138.4, 136.7, 136.2, 132.8, 131.4, 130.4,

128.8, 126.8, 126.0, 125.7, 124.6, 120.6, 20.1, 18.9; MS (EI) *m/z* (Rel. Int., %): [M⁺] 257 (13), 210 (58), 119 (100), 91 (56), 65 (26), 39 (6).

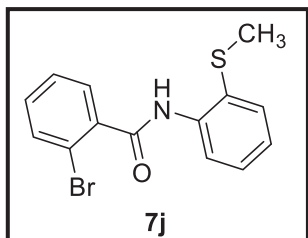
2-chloro-*N*-2-(methylthio)phenylbenzamide (7i):^[72] Yield: 67%, white solid, m.p.



55.8-56.7 °C; ¹H NMR (400 MHz, CDCl₃): δ 8.99 (br. s, 1H), 8.52 (d, *J* = 8.0 Hz, 1H), 7.76 (dd, *J* = 7.2 and 1.6 Hz, 1H), 7.53 (dd, *J* = 7.8, and 1.1 Hz, 1H), 7.33-7.46 (m, 4H), 7.12

(td, $J = 7.6$ and 1.2 Hz, 1H), 2.38 (s, 3H); $^{13}\text{C}\{\text{H}\}$ NMR (100 MHz, CDCl_3): δ 164.6, 138.3, 135.5, 133.2, 131.7, 130.8, 130.5, 130.2, 129.0, 127.3, 125.9, 124.9, 120.9, 19.3; MS (EI) m/z (Rel. Int., %): $[\text{M}^+]$ 277 (16), 230 (100), 139 (95), 111 (38), 75 (14), 65 (6); HRMS (ESI) m/z calcd for $\text{C}_{14}\text{H}_{13}\text{ClONS}$ $[\text{M}+\text{H}]^+$ 278.0406, found 278.0408.

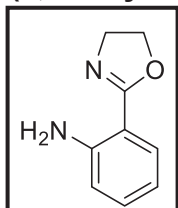
2-bromo-*N*-(2-(methylthio)phenyl)benzamide (7j): Yield: 66%, white solid, m.p.



60.3-60.9 °C; ^1H NMR (400 MHz, CDCl_3): δ 8.77 (br. s, 1H), 8.52 (d, $J = 8.4$ Hz, 1H), 7.63-7.67 (m, 2H), 7.53 (d, $J = 8.0$ Hz, 1H), 7.42 (t, $J = 7.4$ Hz, 1H), 7.31-7.37 (m, 2H), 7.13 (td, $J = 7.6$ and 1.2 Hz, 1H), 2.38 (s, 3H); $^{13}\text{C}\{\text{H}\}$ NMR (100 MHz, CDCl_3): δ 165.7, 138.2, 138.1, 133.7, 133.3, 131.6, 129.6,

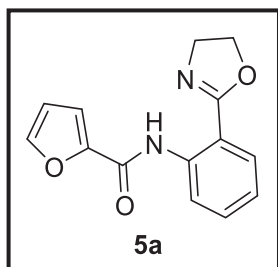
129.1, 127.8, 125.9, 124.9, 120.8, 119.4, 19.5; MS (EI) m/z (Rel. Int., %): $[\text{M}^+]$ 321 (15), 274 (100), 242 (13), 183 (93), 155 (35), 76 (24), 65 (11), 39 (5); HRMS (ESI) m/z calcd for $\text{C}_{14}\text{H}_{13}\text{BrNOS}$ $[\text{M}+\text{H}]^+$ 321.9901, found 321.9903.

2-(4,5-dihydrooxazol-2-yl)aniline 4:^[74] Yield 94% brown liquid. ^1H NMR (400 MHz,



CDCl_3): δ (ppm) = 7.69 (dd, $J = 7.9, 1.5$ Hz, 1H), 7.18 (td, $J = 15.4, 5.6$ Hz, 1H), 6.70- 6.62 (m, 2H), 6.04 (s, 2H), 4.29 (td, $J = 9.3$ Hz, 2H), 4.08 (t, $J = 9.3$ Hz, 2H); $^{13}\text{C}\{\text{H}\}$ NMR (100 MHz, CDCl_3): δ (ppm) = 164.8, 148.5, 132.0, 129.6, 116.0, 115.7, 109.2, 65.8, 55.0.

***N*-(2-(4,5-dihydrooxazol-2-yl)phenyl)furan-2-carboxamide (5a)**:^[75] Yield: 69%,



yellow solid. ^1H NMR (CDCl_3 , 600 MHz) δ (ppm) = 13.01 (br. s, 1H); 8.87 (d, $J = 8.4$ Hz, 1H); 7.88 (dd, $J = 7.8$ and 1.2 Hz, 1H); 7.56 (m, 1H); 7.49 (td, $J = 7.8$ and 1.8 Hz, 1H); 7.22 (dd, $J = 3.6$ and 1.2 Hz, 1H); 7.09 (td, $J = 7.6$ and 1.2 Hz, 1H); 6.54 (dd, $J = 3.6$ and 1.8 Hz, 1H); 4.40 (t, $J = 9.6$ Hz, 2H); 4.20 (t, $J = 9.6$

Hz, 2H). $^{13}\text{C}\{\text{H}\}$ NMR (CDCl_3 , 150 MHz) δ (ppm) = 164.7, 157.1, 148.7, 144.8, 139.6, 132.5, 129.2, 122.5, 119.9, 114.7, 113.5, 112.0, 66.3, 54.7. $\text{C}_{14}\text{H}_{12}\text{N}_2\text{O}_3$ $[\text{M}+\text{H}]^+$

4.2.3 General procedure B for the synthesis of compounds 10:

To a screw-caped vial with magnetic stir bar, 2-(methylthio)amide (**3a–3f**, **7a–7k**) (0.3 mmol, 1.0 equiv.), dioganyl dichalcogenide (**9a–j**) (0.3 mmol, 1.0 equiv.), $\text{Pd}(\text{OAc})_2$ (2.5 mol%) (0.0017 g, 0.03 mmol) and CuBr_2 (0.1 mmol, 0.33 equiv.) were added in dry DMF (2.0 mL) under air atmospheric condition. After this the reaction system was heated at 100 °C for the reaction time (T) described in the tables 1 and 2. Then, the

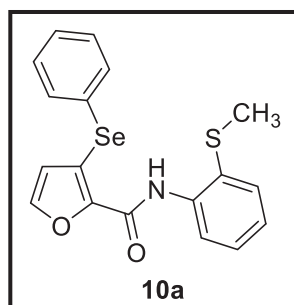
reaction was cooled to the room temperature and filter through a plug of celite. After that the reaction mixture was washed with ethyl acetate (3x 10 mL), and saturated brine solution (60 mL). The organic phase was dried over magnesium sulfate (MgSO₄) and concentrated under reduced pressure. The products were further purified by flash chromatography using hexane as eluent.

4.2.4 General procedure C for the synthesis of compounds 11:

To a Schlenk charge with magnetic stir bar, *N*-(2-(4,5-dihydrooxazol-2-yl)phenyl)furan-2-carboxamide (**5a**) (0.2 mmol) and diphenyl diselenide (**9a**) (0.2 mmol) were added. At the same time Cu(OAc)₂ (1.0 equivalent) catalyst, Na₂CO₃ (0.2 mmol) base and TMEDA (1.0 equivalent) ligand were also added under inert atmosphere of argon (Ar) in 2.0 mL DMSO solvent at 80 °C temperature for 8 h. After that the reaction was cooled to room temperature and washed with ethyl acetate (3x 10 mL) and saturated solution of brine and sodium thiosulphate (80 mL). The organic layer was dried over magnesium sulfate (MgSO₄) and concentrated under reduced pressure. The products were further purified by flash chromatography using hexane as eluent.

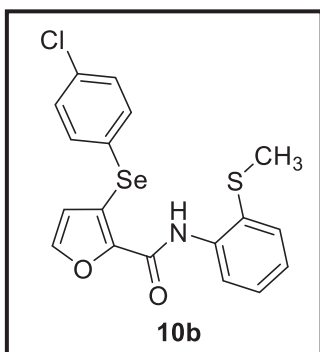
4.2.5 Characterized data of scope compounds:

***N*-(2-(methylthio)phenyl)-3-(phenylselanyl)furan-2-carboxamide (10a):** Yield:



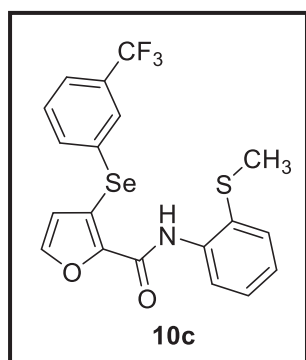
98% (0,114 g), brown solid, m.p.: 49.6 – 49.9 °C; ¹H NMR (400 MHz, CDCl₃): δ 9.32 (s, 1H), 8.55 (dd, *J* = 8.4 and 1.2 Hz, 1H), 7.72-7.74 (m, 2H), 7.53 (dd, *J* = 7.8 and 1.4 Hz, 1H), 7.32-7.45 (m, 5H), 7.09 (td, *J* = 7.6 and 1.6 Hz, 1H), 5.99 (d, *J* = 2.0 Hz, 1H), 2.40 (s, 3H); ¹³C{¹H} NMR (100 MHz, CDCl₃): δ 156.7, 144.1, 140.8, 138.2, 136.1, 133.4, 129.5, 129.1, 128.9, 127.6,

125.1, 124.3, 123.8, 120.3, 114.3, 19.1; MS (EI) *m/z* (Rel. Int., %): [M⁺] 389 (50), 342 (68), 264 (33), 251 (56), 215 (11), 195 (28), 185 (27), 138 (15), 115 (100), 106 (23), 93 (22), 77 (35), 65 (16), 51 (15), 45 (11), 39 (11); HRMS (ESI) *m/z* calcd for C₁₈H₁₆NO₂SSe [M+H]⁺ 390.0061, found 390.0067.

3-((4-chlorophenyl)selanyl)-N-(2-(methylthio)phenyl)furan-2-carboxamide (10b):

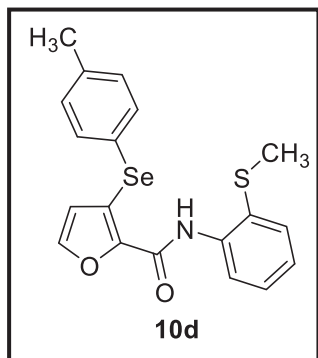
Yield: 95 % (0.120 g), brown crystals, m.p.: 138.3 – 139.1 °C; ¹H NMR (400 MHz, CDCl₃): δ 9.30 (br. s, 1H), 8.53 (dd, *J* = 8.2 and 1.2 Hz, 1H), 7.65 (d, *J* = 8.4 Hz, 2H), 7.53 (dd, *J* = 7.8 and 1.4 Hz, 1H), 7.41 (d, *J* = 1.6 Hz, 1H), 7.31-7.37 (m, 3H), 7.09 (td, *J* = 7.6 and 1.6 Hz, 1H), 5.99 (d, *J* = 2.0 Hz, 1H), 2.41 (s, 3H); ¹³C{H} NMR (100 MHz, CDCl₃): δ 156.6, 144.3, 141.0, 138.1, 137.4, 135.4, 133.4, 129.7, 129.1, 125.8, 125.2, 124.4,

123.2, 120.3, 114.1, 19.1; MS (EI) *m/z* (Rel. Int., %): [M⁺] 423 (75), 376 (100), 285 (68), 264 (70), 232 (33), 185 (45), 149 (62), 138 (32), 106 (35), 93 (39), 77 (22), 45 (20), 39 (10); HRMS (ESI) *m/z* calcd for C₁₈H₁₅ClNO₂S₂Se [M+H]⁺ 423.9672, found 423.9656. **Crystal Data for 10b:** C₁₈H₁₄ClNO₂S₂Se, (M = 422.77 g/mol): Orthorhombic, space group Pna2₁ (no.33), Unit cell dimensions: a = 19.0177(9) Å, b = 7.2938(3) Å, c = 12.6350(6) Å, α = β = γ = 90 °, Volume (V) = 1752.62(14) Å³. Z = 4, Calculated density (D_c) = 1.602 Mg m⁻³, F(000) = 848, Temperature (T) = 296(2) K, Absorption coefficient: μ(Mo-Kα) = 2.424 mm⁻¹, Wavelength: λ(Mo-Kα) = 0.71073 Å.

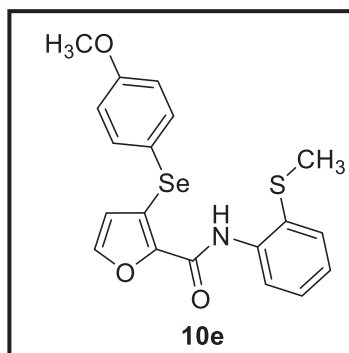
N-(2-(methylthio)phenyl)-3-((3-(trifluoromethyl)phenyl)selanyl)furan-2-

carboxamide (10c): Yield: 86% (0.117 g), brown solid, m.p.: 96.0 – 96.7 °C; ¹H NMR (400 MHz, CDCl₃): δ 9.33 (br. s, 1H), 8.53 (dd, *J* = 8.0 and 1.2 Hz, 1H), 7.99 (s, 1H), 7.91 (d, *J* = 7.6 Hz, 1H), 7.68 (d, *J* = 8.0 Hz, 1H), 7.49-7.55 (m, 2H), 7.44 (d, *J* = 1.6 Hz, 1H), 7.34 (td, *J* = 7.8 and 1.6 Hz, 1H), 7.10 (td, *J* = 7.6 and 1.2 Hz, 1H), 5.99 (d, *J* = 1.6 Hz, 1H), 2.41 (s, 3H); ¹³C{H} NMR (100 MHz, CDCl₃): δ 156.6, 144.5, 141.3,

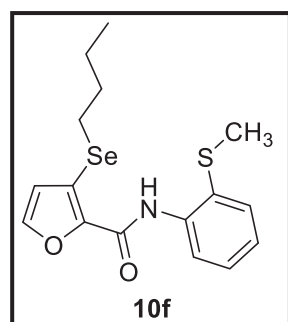
139.2, 138.1, 133.4, 132.5 (q, ³J_{C-F} = 3.8 Hz), 131.8 (q, ²J_{C-F} = 32.5 Hz), 129.9, 129.2, 128.9, 125.7 (q, ³J_{C-F} = 3.8 Hz), 125.3, 124.5, 123.5 (q, ¹J_{C-F} = 271.19 Hz), 122.3, 120.4, 114.1, 19.1; MS (EI) *m/z* (Rel. Int., %): [M⁺] 457 (60), 410 (100), 319 (50), 263 (25), 232 (23), 183 (57), 138 (28), 106 (28), 93 (41), 65 (15), 39 (10); HRMS (ESI) *m/z* calcd for C₁₉H₁₅F₃NO₂S₂Se [M+H]⁺ 457.9935, found 457.9908.

N-(2-(methylthio)phenyl)-3-(p-tolylselanyl)furan-2-carboxamide (10d): Yield: 89%

(0.107 g), brownish solid, m.p.: 91.7 – 92.3 °C; ¹H NMR (600 MHz, CDCl₃): δ 9.30 (br. s, 1H), 8.55 (dd, *J* = 8.4 and 1.2 Hz, 1H), 7.62 (d, *J* = 7.8 Hz, 2H), 7.53 (dd, *J* = 7.8 and 1.2 Hz, 1H), 7.37 (d, *J* = 2.4 Hz, 1H), 7.33 (td, *J* = 7.8 and 1.8 Hz, 1H), 7.19 (d, *J* = 7.8 Hz, 2H), 7.08 (td, *J* = 7.5 and 1.4 Hz, 1H), 5.98 (d, *J* = 1.8 Hz, 1H), 2.40 (s, 3H), 2.39 (s, 3H); ¹³C{H} NMR (150 MHz, CDCl₃) δ 156.7, 144.1, 140.6, 139.2, 138.3, 136.3, 133.4, 130.3, 129.1, 125.1, 124.4, 124.3, 123.9, 120.3, 114.3, 21.3, 19.1; MS (EI) *m/z* (Rel. Int., %): [M⁺] 403 (98), 356 (63), 265 (100), 229 (38), 209 (32), 185 (30), 128 (62), 91 (58), 65 (28), 39 (18); HRMS (ESI) *m/z* calcd for C₁₉H₁₈NO₂S₂Se [M+H]⁺ 404.0218, found 404.0181.

3-((4-methoxyphenyl)selanyl)-N-(2-(methylthio)phenyl)furan-2-carboxamide

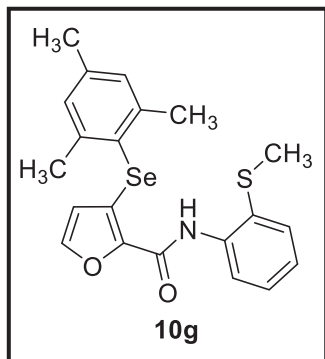
(10e): Yield: 87% (0.109 g), white solid, m.p.: 104.8 – 105.1 °C; ¹H NMR (400 MHz, CDCl₃): δ 9.29 (br. s, 1H), 8.55 (dd, *J* = 8.0 and 1.2 Hz, 1H), 7.67 (d, *J* = 8.8 Hz, 2H), 7.53 (dd, *J* = 7.6 and 1.2 Hz, 1H), 7.37 (d, *J* = 2.0 Hz, 1H), 7.33 (td, *J* = 7.8 and 1.2 Hz, 1H), 7.08 (td, *J* = 7.6 and 1.2 Hz, 1H), 6.91 (d, *J* = 8.4 Hz, 2H), 5.95 (d, *J* = 1.6 Hz, 1H), 3.84 (s, 3H), 2.41 (s, 3H); ¹³C{H} NMR (100 MHz, CDCl₃): δ 160.5, 156.8, 144.1, 140.4, 138.3, 138.1, 133.5, 129.2, 125.1, 124.3, 120.3, 117.9, 115.2, 114.2, 55.4, 19.2; MS (EI) *m/z* (Rel. Int., %): [M⁺] 419 (100), 372 (15), 281 (98), 264 (96), 245 (34), 238 (52), 207 (70), 187 (26), 136 (21), 108 (26), 77 (32), 44 (38), 39 (20), HRMS (ESI) *m/z* calcd for C₁₉H₁₈NO₃S₂Se [M+H]⁺ 420.0167, found 420.0169.

3-(butylselanyl)-N-(2-(methylthio)phenyl)furan-2-carboxamide (10f): Yield: 51%

(0.056 g), dark brown liquid; ¹H NMR (400 MHz, CDCl₃): δ 9.34 (br. s, 1H), 8.53 (dd, *J* = 8.2 and 1.0 Hz, 1H), 7.51-7.53 (m, 2H), 7.31 (td, *J* = 7.9 and 1.4 Hz, 1H), 7.07 (td, *J* = 7.6 and 1.2 Hz, 1H), 6.56 (d, *J* = 2.0 Hz, 1H), 2.92 (t, *J* = 7.6 Hz, 2H), 2.40 (s, 3H), 1.77 (quint, *J* = 7.4 Hz, 2H), 1.49 (sext, *J* = 7.4 Hz, 2H), 0.95 (t, *J* = 7.4 Hz, 3H); ¹³C{H} NMR (100 MHz, CDCl₃): δ 156.6, 144.3, 142.0, 138.3, 133.3, 129.1, 125.1, 124.2, 121.1, 120.3, 113.6, 32.0, 25.5, 23.0, 19.1, 13.5; MS (EI) *m/z* (Rel. Int., %): [M⁺] 369 (50), 322 (76),

266 (12), 231 (12), 207 (26), 175 (63), 139 (100), 121 (26), 94 (31), 41 (24). HRMS (ESI) m/z calcd for $C_{16}H_{20}NO_2SSe$ $[M+H]^+$ 370.0374, found 370.0362.

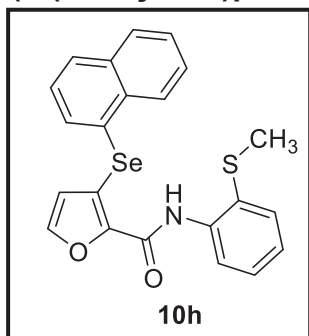
3-(mesitylseyanyl)-*N*-(2-(methylthio)phenyl)furan-2-carboxamide (10g): Yield:



90% (0.116 g), light brown solid, m.p.: 87.4 – 88.0 °C; 1H NMR (600 MHz, $CDCl_3$): δ 9.31 (br. s, 1H), 8.61 (dd, J = 8.1 and 1.2 Hz, 1H), 7.53 (dd, J = 7.8 and 1.8 Hz, 1H), 7.32-7.35 (m, 2H), 7.08 (td, J = 7.6 and 1.2 7.8 Hz, 1H), 7.01 (s, 2H), 5.72 (d, J = 1.8 Hz, 1H), 2.48 (s, 6H), 2.41 (s, 3H), 2.32 (s, 3H); $^{13}C\{H\}$ NMR (150 MHz, $CDCl_3$): δ 156.9, 144.1, 143.7, 140.9, 139.5, 138.4, 133.5, 129.2, 128.8, 126.0,

124.9, 124.5, 124.1, 120.1, 113.8, 24.3, 21.1, 19.2; MS (EI) m/z (Rel. Int., %): $[M^+]$ 431 (30), 350 (10), 293 (14), 264 (17), 211 (24), 139 (100), 119 (55), 91 (10); HRMS (ESI) m/z calcd for $C_{21}H_{22}NO_2SSe$ $[M+H]^+$ 432.0531, found 432.0535.

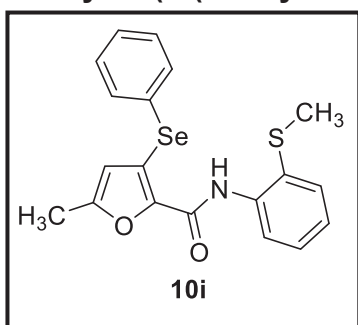
***N*-(2-(methylthio)phenyl)-3-(naphthalen-1-ylselyanyl)furan-2-carboxamide (10h):**



Yield: 93% (0.122 g), brown solid, m.p.: 113.2 – 113.5°C; 1H NMR (400 MHz, $CDCl_3$): δ 9.33 (br. s, 1H), 8.61 (dd, J = 8.0 and 1.2 Hz, 1H), 8.40-8.45 (m, 1H), 8.08 (dd, J = 6.8 and 1.2 Hz, 1H), 7.96 (d, J = 8.0 Hz, 1H), 7.87-7.91 (m, 1H), 7.52-7.55 (m, 3H), 7.46 (dd, J = 8.2 and 7.0 Hz, 1H), 7.36 (td, J = 7.8 and 1.6 Hz, 1H), 7.24-7.25 (m, 1H), 7.10 (td, J = 7.6 and

1.6 Hz, 1H), 5.59 (d, J = 2.0 Hz, 1H), 2.41 (s, 3H); $^{13}C\{H\}$ NMR (100 MHz, $CDCl_3$): δ 156.9, 144.0, 140.8, 138.3, 136.5, 135.0, 134.2, 133.5, 130.7, 129.2, 128.6, 128.5, 127.3, 126.8, 126.5, 125.9, 125.1, 124.3, 124.0, 120.3, 114.6, 19.2; MS (EI) m/z (Rel. Int., %): $[M^+]$ 439 (58), 392 (15), 301 (20), 281 (62), 264 (30), 221 (14), 207 (100), 165 (50), 128 (24), 115 (38), 96 (18), 77 (14), 44 (20); HRMS (ESI) m/z calcd for $C_{22}H_{18}NO_2SSe$ $[M+H]^+$ 440.0218, found, 440.0199.

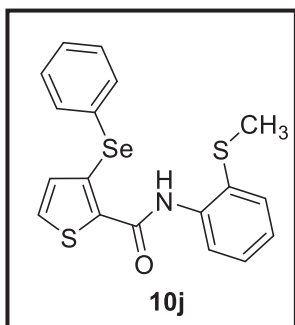
5-methyl-*N*-(2-(methylthio)phenyl)-3-(phenylselyanyl)furan-2-carboxamide (10i):



Yield: 78% (0.094 g), brown solid, m.p.: 123.5 – 124.0 °C; 1H NMR (400 MHz, $CDCl_3$): δ 9.19 (br. s, 1H), 8.53 (dd, J = 8.4 and 1.2 Hz, 1H), 7.70-7.73 (m, 2H), 7.52 (dd, J = 7.8 and 1.4 Hz, 1H), 7.35-7.44 (m, 3H), 7.32 (td, J = 8.0 and 1.2 Hz, 1H), 7.07 (td, J = 7.6 and 1.2 Hz, 1H), 5.63 (q, J = 1.2 Hz, 1H), 2.40 (s, 3H), 2.30 (d, J = 1.2 Hz,

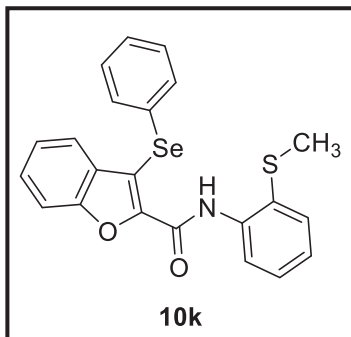
3H); $^{13}\text{C}\{\text{H}\}$ NMR (100 MHz, CDCl_3): δ 156.7, 154.9, 139.5, 138.3, 136.1, 133.2, 129.4, 129.0, 128.8, 127.8, 125.1, 124.9, 124.1, 120.4, 110.8, 19.0, 13.9; MS (EI) m/z (Rel. Int., %): $[\text{M}^+]$ 403 (28), 356 (40), 265 (60), 207 (85), 128 (20), 77 (18), 43 (100); HRMS (ESI) m/z calcd for $\text{C}_{19}\text{H}_{18}\text{NO}_2\text{SSe}$ $[\text{M}+\text{H}]^+$ 404.0218, found 404.0201.

***N*-(2-(methylthio)phenyl)-3-(phenylselanyl)thiophene-2-carboxamide (10j):** Yield:

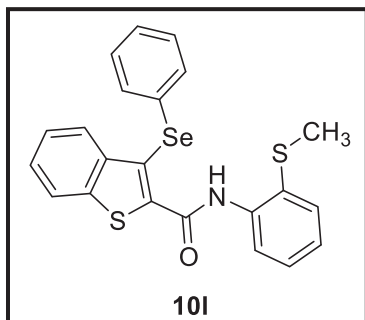


93% (0.113 g), orange brownish solid, m.p. 138.3-139.1; ^1H NMR (400 MHz, CDCl_3): δ 9.45 (br. s, 1H), 8.44 (dd, J = 8.0 and 1.2 Hz, 1H), 7.62-7.64 (m, 2H), 7.52 (dd, J = 7.8 and 1.4 Hz 1H), 7.31-7.37 (m, 5H), 7.09 (td, J = 7.6 and 1.2 Hz, 1H), 6.68 (d, J = 5.2 Hz, 1H), 2.35 (s, 3H); $^{13}\text{C}\{\text{H}\}$ NMR (100 MHz, CDCl_3): δ 160.3, 138.4, 134.7, 133.6, 133.3, 132.5, 131.0, 129.9, 129.6, 129.0, 128.9, 128.5, 125.8, 124.6, 121.0, 19.1; MS (EI) m/z (Rel. Int., %): $[\text{M}^+]$ 403 (95), 356 (68), 265 (100), 229 (38), 209 (32), 185 (30), 128 (62) 106 (30), 91 (62), 65 (30), 39 (20); HRMS (ESI) m/z calcd for $\text{C}_{18}\text{H}_{16}\text{NOS}_2\text{Se}$ $[\text{M}+\text{H}]^+$ 405.9833, found 405.9836.

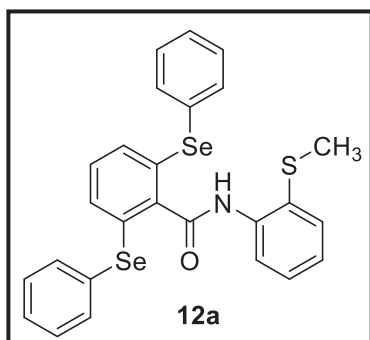
***N*-(2-(methylthio)phenyl)-3-(phenylselanyl)benzofuran-2-carboxamide (10k):**



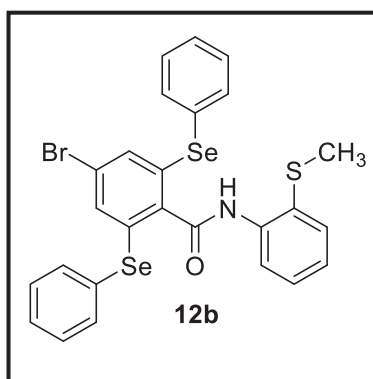
Yield: 84% (0.110 g), yellowish white solid, m.p.: 108.3 – 108.5 °C; ^1H NMR (400 MHz, CDCl_3): δ 9.80 (br. s, 1H), 8.58 (dd, J = 8.2 and 1.0 Hz, 1H), 7.64-7.66 (m, 2H), 7.58 (d, J = 8.4 Hz, 1H), 7.55 (dd, J = 7.8 and 1.4 Hz, 1H), 7.39 (ddd, J = 7.8, 7.8 and 1.2 Hz, 1H), 7.27-7.35 (m, 4H), 7.12 (td, J = 7.6 and 1.2 Hz, 1H), 7.07 (td, J = 7.6 and 0.8 Hz, 1H), 6.82 (d, J = 7.6 Hz, 1H), 2.42 (s, 3H); $^{13}\text{C}\{\text{H}\}$ NMR (100 MHz, CDCl_3): δ 157.1, 154.4, 144.6, 138.1, 134.0, 133.3, 129.5, 129.3, 129.0, 128.2, 128.1, 127.6, 125.8, 124.7, 123.6, 122.8, 120.8, 113.8, 112.2, 19.1; MS (EI) m/z (Rel. Int., %): $[\text{M}^+]$ 439 (53), 392 (44), 314 (27), 301 (62), 282 (100), 235 (40), 207 (39), 165 (90), 106 (16), 77 (28), 44 (22), 39 (8); HRMS (ESI) m/z calcd for $\text{C}_{22}\text{H}_{18}\text{NO}_2\text{SSe}$ $[\text{M}+\text{H}]^+$ 440.0218, found 440.0195.

***N*-(2-(methylthio)phenyl)-3-(phenylselanyl)benzo[*b*]thiophene-2-carboxamide**

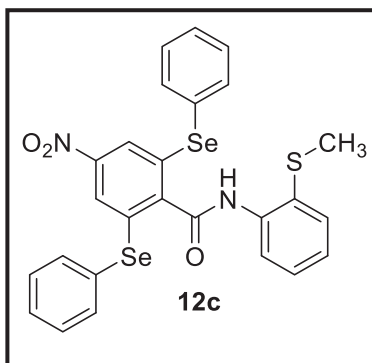
(101): Yield: 91% (0.124 g), brown solid, m.p.: 113.9 – 114.9 °C; ^1H NMR (400 MHz, CDCl_3): δ 10.78 (br. s, 1H), 8.41 (dd, J = 8.4 and 0.8 Hz, 1H), 7.98 (d, J = 8.0 Hz, 1H), 7.91 (d, J = 8.0 Hz, 1H), 7.45-7.49 (m, 2H), 7.40 (ddd, J = 8.1, 6.9 and 1.2 Hz, 1H), 7.32 (td, J = 7.8 and 1.6 Hz, 1H), 7.24-7.26 (m, 2H), 7.15-7.18 (m, 3H), 7.10 (td, J = 7.6 and 1.2 Hz, 1H), 2.19 (s, 3H); $^{13}\text{C}\{^1\text{H}\}$ NMR (100 MHz, CDCl_3): δ 160.1, 144.9, 141.9, 140.2, 138.2, 132.9, 131.1, 129.6, 129.4, 128.5, 127.1, 126.9, 126.1, 125.5, 125.0, 122.6, 122.1, 117.7, 18.9; MS (EI) m/z (Rel. Int., %): [M^+] 455 (7), 408 (6), 317 (40), 298 (100), 288 (16), 237 (24), 208 (20), 165 (8), 132 (6), 77 (11), 44 (5); HRMS (ESI) m/z calcd for $\text{C}_{22}\text{H}_{18}\text{NOS}_2\text{Se}$ [$\text{M}+\text{H}$] $^+$ 455.9990, found 455.9948.

***N*-(2-(methylthio)phenyl)-2,6-bis(phenylselanyl)benzamide (12a):** Yield: 76%

(0.126 g), brown solid, m.p.: 109.6 – 110.1 °C; ^1H NMR (600 MHz, CDCl_3): δ 8.65 (br. s, 1H), 8.55 (d, J = 8.4 Hz, 1H), 7.51-7.54 (m, 5H), 7.37 (t, J = 7.6 Hz, 1H), 7.26-7.29 (m, 6H), 7.18 (d, J = 7.8 Hz, 2H), 7.10 (td, J = 7.6 and 1.2 Hz, 1H), 7.04 (t, J = 7.8 Hz, 1H), 2.29 (s, 3H); $^{13}\text{C}\{^1\text{H}\}$ NMR (150 MHz, CDCl_3): δ 166.1, 140.9, 138.3, 134.4, 133.8, 131.8, 131.2, 130.6, 129.8, 129.5, 129.2, 128.1, 125.5, 124.8, 120.8, 19.8; MS (EI) m/z (Rel. Int., %): [M^+] 555 (66), 508 (11), 415 (22), 398 (18), 339 (100), 308 (11), 260 (24), 232 (43), 207 (17), 180 (14), 152 (68), 105 (7), 94 (19), 77 (26), 51 (12), 39 (5); HRMS (ESI) m/z calcd for $\text{C}_{26}\text{H}_{22}\text{NOSSe}_2$ [$\text{M}+\text{H}$] $^+$ 555.9747, found 555.9740.

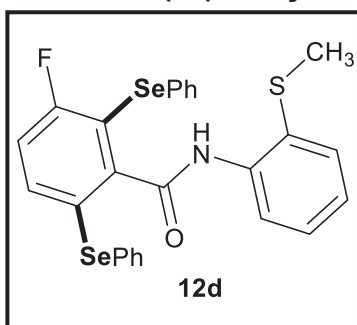
4-bromo-*N*-(2-(methylthio)phenyl)-2,6-bis(phenylselanyl)benzamide (12b):

Yield: 62% (0.118 g), brown solid, m.p. 117.0-117.4 °C; ^1H NMR (600 MHz, CDCl_3): δ 8.68 (br. s, 1H), 8.52 (d, J = 8.4 Hz, 1H), 7.53-7.57 (m, 5H), 7.31-7.39 (m, 7H), 7.21 (s, 2H), 7.13 (td, J = 7.8 and 1.2 Hz, 1H), 2.34 (s, 3H); $^{13}\text{C}\{^1\text{H}\}$ NMR (150 MHz, CDCl_3): δ 165.4, 138.5, 138.2, 135.0, 133.8, 133.6, 133.2, 129.8, 129.3, 128.9, 128.8, 125.7, 125.0, 124.7, 120.8, 20.0; HRMS (ESI) m/z calcd for [$\text{M}+\text{H}$] $^+$ $\text{C}_{26}\text{H}_{21}\text{BrNOSSe}_2$, 633.8852, found 633.8889.

***N*-(2-(methylthio)phenyl)-4-nitro-2,6-bis(phenylselanyl)benzamide (12c):** Yield:

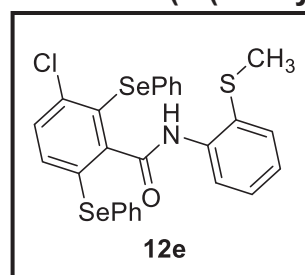
64% (0.115 g), yellow bluish solid, m.p.: 83.5 – 84.0 °C; ¹H NMR (400 MHz, CDCl₃): δ 8.75 (br. s, 1H), 8.54 (dd, *J* = 8.4 and 1.2 Hz, 1H), 7.80 (s, 2H), 7.56 (m, 5H), 7.34-7.43 (m, 7H), 7.17 (td, *J* = 7.6 and 1.2 Hz, 1H), 2.39 (s, 3H); ¹³C{¹H} NMR (100 MHz, CDCl₃): δ 164.6, 148.6, 143.3, 137.7, 135.6, 134.7, 133.8, 130.1, 129.5, 129.3, 127.8, 125.9, 125.4, 124.3, 121.0, 20.0; HRMS (ESI)

m/z calcd for C₂₆H₂₁N₂O₃SSe₂ [M+H]⁺ 600.9598, found 600.9407.

3-fluoro-*N*-(2-(methylthio)phenyl)-2,6-bis(phenylselanyl)benzamide (12d): Yield:

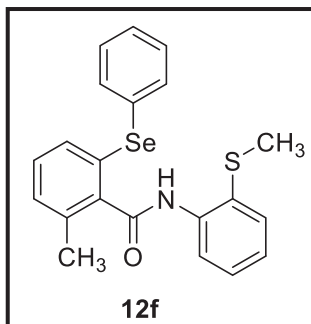
65% (0.111g), white solid, m.p.: 70.0 – 70.5 °C; ¹H NMR (400 MHz, CDCl₃): δ 8.52 (dd, *J* = 8.0 and 1.2 Hz, 1H), 8.46 (br. s, 1H), 7.47-7.51 (m, 3H), 7.34-7.45 (m, 4H), 7.23-7.29 (m, 3H), 7.15-7.21 (m, 3H), 7.10 (td, *J* = 7.6 and 1.2 Hz, 1H), 7.03 (dd, *J* = 8.4 and 8.0 Hz, 1H), 2.19 (s, 3H); ¹³C{¹H}NMR (100 MHz, CDCl₃): δ 165.2 (d, ⁴*J*_{C-F} = 2.2

Hz), 162.3 (d, ¹*J*_{C-F} = 247.3 Hz), 146.8, 138.2, 137.1 (d, ³*J*_{C-F} = 7.8 Hz), 133.7, 133.6 (d, ³*J*_{C-F} = 9.4 Hz), 132.1, 130.4 (d, ⁴*J*_{C-F} = 4.0 Hz), 129.5, 129.3, 129.2, 128.0, 127.5, 125.5, 124.8, 124.8, 120.8, 117.7 (d, ²*J*_{C-F} = 25.0 Hz), 115.5 (d, ²*J*_{C-F} = 24.4 Hz), 19.6; HRMS (ESI) *m/z* calcd for C₂₆H₂₁FNOSse₂ [M+H]⁺ 573.9653, found 573.9685.

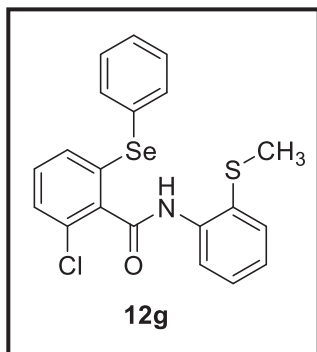
3-chloro-*N*-(2-(methylthio)phenyl)-2,6-bis(phenylselanyl)benzamide (12e): Yield:

70% (0.123 g), white solid, m.p.: 88.5 – 88.9 °C; ¹H NMR (400 MHz, CDCl₃): δ 8.50 (dd, *J* = 8.4 and 1.2 Hz, 1H), 8.46 (br. s, 1H), 7.52-7.55 (m, 2H), 7.49 (dd, *J* = 7.6 and 1.2 Hz, 1H), 7.27-7.37 (m, 8H), 7.16-7.18 (m, 3H), 7.09 (td, *J* = 7.6 and 1.2 Hz, 1H), 2.19 (s, 3H); ¹³C{¹H} NMR (100 MHz, CDCl₃): δ

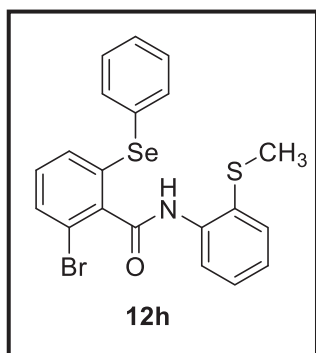
165.6, 146.9, 140.1, 138.3, 135.1, 134.5, 133.7, 131.4, 131.3, 131.1, 129.7, 129.6, 129.4, 129.3, 128.4, 127.3, 127.2, 125.5, 124.8, 120.8, 19.7; HRMS (ESI) *m/z* calcd for C₂₆H₂₁ClNOSse₂ [M+H]⁺ 589.9357, found 589.9400.

2-methyl-N-(2-(methylthio)phenyl)-6-(phenylselanyl)benzamide (12f): Yield: 88%

(0.109 g), brown liquid; ^1H NMR (400 MHz, CDCl_3): δ 8.52 (dd, $J = 8.0$ and 1.2 Hz, 1H), 8.41 (br. s, 1H), 7.46-7.50 (m, 3H), 7.35 (ddd, $J = 8.2$, 7.4 and 1.6 Hz, 1H), 7.22-7.25 (m, 4H), 7.16-7.17 (m, 2H), 7.11 (td, $J = 7.6$ and 1.3 Hz, 1H), 2.46 (s, 3H), 2.29 (s, 3H); $^{13}\text{C}\{\text{H}\}$ NMR (100 MHz, CDCl_3): δ 167.2, 140.3, 138.0, 135.7, 133.4, 133.0, 131.6, 130.8, 129.9, 129.6, 129.3, 128.9, 127.6, 125.8, 124.8, 121.0, 19.6, 19.2; MS (EI) m/z (Rel. Int., %): $[\text{M}^+]$ 413 (25), 366 (6), 275 (100), 256 (28), 232 (29), 215 (4), 195 (5), 165 (17), 152 (15), 139 (3), 94 (7), 65 (5); HRMS (ESI) m/z calcd for $\text{C}_{21}\text{H}_{20}\text{NOSse}[\text{M}+\text{H}]^+$ 414.0425, found 414.0462.

2-chloro-N-(2-(methylthio)phenyl)-6-(phenylselanyl)benzamide (12g): Yield: 91%

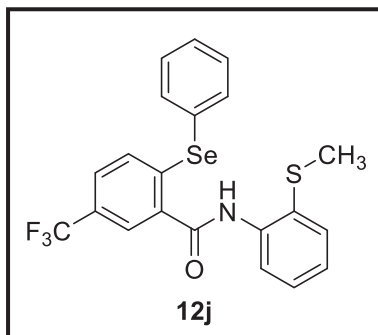
(0.118 g), brownish solid, m.p.: $84.5 - 85.0$ °C; ^1H NMR (600 MHz, CDCl_3): δ 8.62 (br. s, 1H), 8.56 (dd, $J = 8.4$ and 1.2 Hz, 1H), 7.53-7.56 (m, 2H), 7.39 (td, $J = 7.8$ and 1.2 Hz, 1H), 7.28-7.34 (m, 5H), 7.21 (dd, $J = 7.8$ and 1.2 Hz, 1H), 7.16-7.18 (m, 1H), 7.13 (td, $J = 7.6$ and 1.2 Hz, 1H), 2.35 (s, 3H); $^{13}\text{C}\{\text{H}\}$ NMR (150 MHz, CDCl_3): δ 164.4, 138.2, 138.0, 134.7, 133.7, 133.1, 131.4, 131.3, 130.8, 129.6, 129.6, 129.3, 128.4, 128.2, 125.7, 125.0, 120.9, 19.6; MS (EI) m/z (Rel. Int., %): $[\text{M}^+]$ 433 (44), 386 (32), 356 (5), 295 (100), 276 (24), 260 (16), 232 (30), 215 (24), 186 (4), 152 (34), 139 (16), 94 (15), 77 (18), 51 (8), 45 (7); HRMS (ESI) m/z calcd for $\text{C}_{20}\text{H}_{17}\text{ClNOSse}[\text{M}+\text{H}]^+$ 433.9879, found 433.9904.

2-bromo-N-(2-(methylthio)phenyl)-6-(phenylselanyl)benzamide (12h): Yield: 75%

(0.107 g), brown liquid; ^1H NMR (600 MHz, CDCl_3): δ 8.54 – 8.56 (m, 2H), 7.54 (ddd, $J = 7.8$, 1.8 and 1.8 Hz, 2H), 7.49 (dd, $J = 7.8$ and 1.2 Hz, 1H), 7.38 (td, $J = 7.8$ and 1.2 Hz, 1H), 7.26-7.31 (m, 5H), 7.13 (td, $J = 7.6$ and 1.2 Hz, 1H), 7.09 (t, $J = 8.1$ Hz, 1H), 2.34 (s, 3H); $^{13}\text{C}\{\text{H}\}$ NMR (150 MHz, CDCl_3): δ 165.2, 140.2, 138.1, 134.5, 133.5, 132.6, 132.1, 131.4, 131.1, 129.6, 129.2, 128.4, 128.1, 125.7, 124.9, 120.9, 119.8, 19.7; MS (EI) m/z (Rel. Int.): $[\text{M}^+]$ 477 (22), 430 (16), 398 (4), 339 (38), 322 (12), 274 (6), 260 (52), 232 (56), 215 (16), 180 (23), 152 (98), 139 (24), 109 (11), 94 (100), 77 (84),

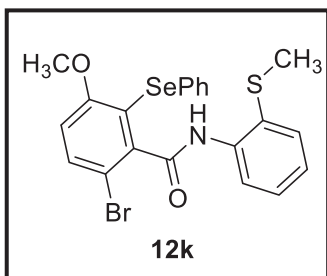
65 (42), 51 (55), 45 (38), 39 (22); HRMS (ESI) m/z calcd for $C_{20}H_{17}BrNOSSe$ $[M+H]^+$ 477.9374, found 477.9411.

***N*-(2-(methylthio)phenyl)-2-(phenylselanyl)-5-(trifluoromethyl)benzamide (12j):**



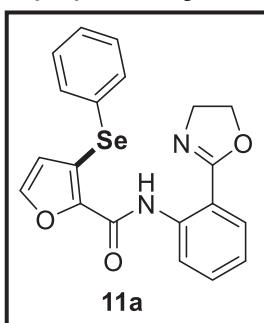
Yield: 85% (0.119 g), white solid, m.p.: 132.0 – 132.3 °C; 1H NMR (400 MHz, $CDCl_3$): δ 9.10 (br. s, 1H), 8.49 (d, J = 8.0 Hz, 1H), 7.92 (s, 1H), 7.70 (d, J = 6.4 Hz, 2H), 7.56 (dd, J = 7.8 and 1.4 Hz, 1H), 7.38-7.46 (m, 5H), 7.14-7.18 (m, 2H), 2.44 (s, 3H); $^{13}C\{H\}$ NMR (100 MHz, $CDCl_3$): δ 165.0, 143.0, 138.0, 136.9, 133.8, 133.2, 131.1, 130.0, 129.4, 129.1, 128.7, 127.6 (q, $^2J_{C-F}$ = 32.6), 127.6 (q, $^3J_{C-F}$ = 3.6 Hz), 126.0, 125.1, 123.9 (q, $^3J_{C-F}$ = 3.8 Hz), 123.7 (q, $^1J_{C-F}$ = 270.3 Hz), 120.8, 19.3; MS (EI) m/z (Rel. Int., %): $[M^+]$ 467 (70), 420 (66), 390 (6), 342 (27), 329 (98), 310 (26), 281 (45), 232 (41), 207 (100), 191 (11), 152 (35), 133 (9), 94 (34), 77 (33), 44 (56), 40 (20); HRMS (ESI) m/z calcd for $C_{21}H_{17}F_3NOSSe$ $[M+H]^+$ 468.0143, found 468.0184.

6-bromo-3-methoxy-*N*-(2-(methylthio)phenyl)-2-(phenylselanyl)benzamide



(12k): Yield: 42% (0.064 g), brownish solid, m.p.: 89.7 – 90.1 °C; 1H NMR (600 MHz, $CDCl_3$): δ 8.52 (dd, J = 8.4 and 1.2 Hz, 1H), 8.41 (br. s, 1H), 7.59 (d, J = 8.4 Hz, 1H), 7.50 (dd, J = 7.8 and 1.8 Hz, 1H), 7.34-7.38 (m, 3H), 7.14-7.15 (m, 3H), 7.10 (td, J = 7.6 and 1.2 Hz, 1H), 6.86 (d, J = 8.4 Hz, 1H), 3.75 (s, 3H), 2.22 (s, 3H); $^{13}C\{H\}$ NMR (150 MHz, $CDCl_3$): δ 164.2, 158.3, 144.0, 137.3, 133.7, 132.7, 130.5, 130.2, 128.3, 128.0, 125.8, 124.5, 123.8, 119.8, 116.5, 112.5, 108.8, 55.5, 18.6; HRMS (ESI) m/z calcd for $C_{21}H_{19}BrNO_2SSe$ $[M+H]^+$ 507.9480, found 507.9519.

***N*-(2-(4,5-dihydrooxazol-2-yl)phenyl)-3-(phenylselanyl)furan-2-carboxamide**



(11a): Yield: 0.454 g (73%) white solid. 1H NMR ($CDCl_3$, 400 MHz) δ (ppm). = 12.98 (s, 1H); 8.94 (dd, J = 8.5, 0.9 Hz, 1H); 7.87 ppm (dd, J = 7.9, 1.6 Hz, 1H); 7.75-7.72 ppm (m, 2H); 7.48 ppm (ddd, J = 8.6, 1.6 Hz, 1H); 7.42 to 7.35 ppm (m, 4H); 7.10 ppm (ddd, J = 7.8, 0.9 Hz, 1H); 5.95 ppm (d, J = 1.8 Hz, 1H); 4.39 ppm (dd, J = 9.1, 1.2 Hz, 2H); 4.19 ppm (dd, J = 9.1, 1.2

Hz, 2H). **¹³C NMR** (CDCl₃, 100 MHz) δ (ppm) = 164.6, 157.8, 144.1, 141.5, 139.6, 136.3, 132.4, 129.5, 129.2, 128.9, 127.9, 123.9, 122.4, 120.0, 113.9, 113.6, 66.2, 54.8.

5.2.2 Selected spectra

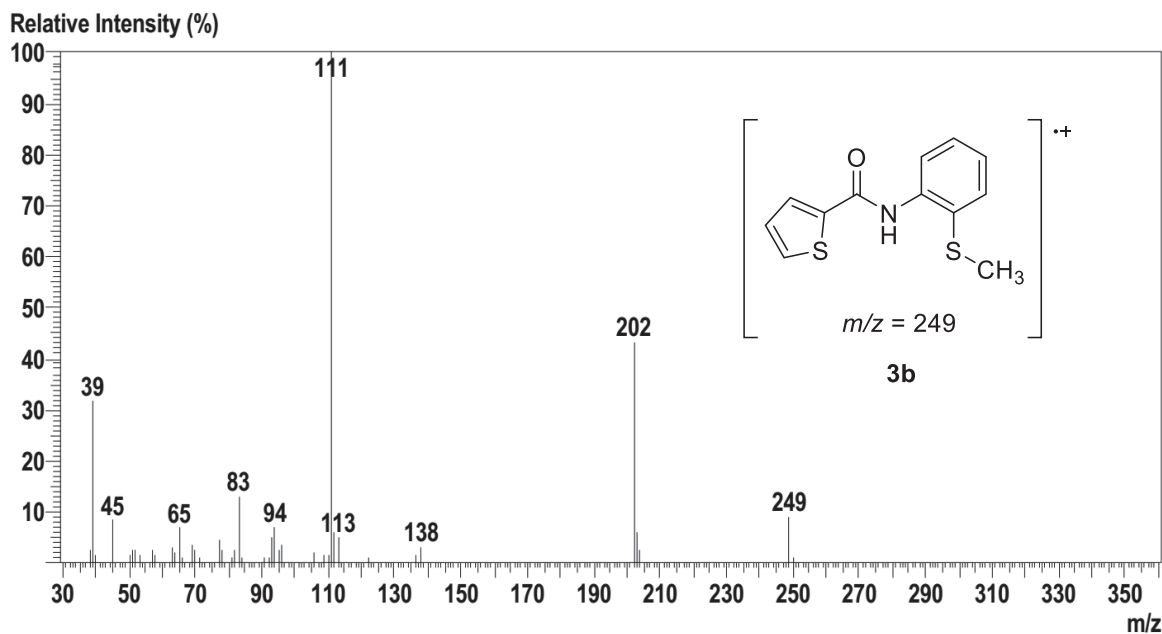


Figure 23: Mass spectrum (EI, 70 eV) of compound *N*-(2-(methylthio)phenyl)thiophene-2-carboxamide (**3b**).

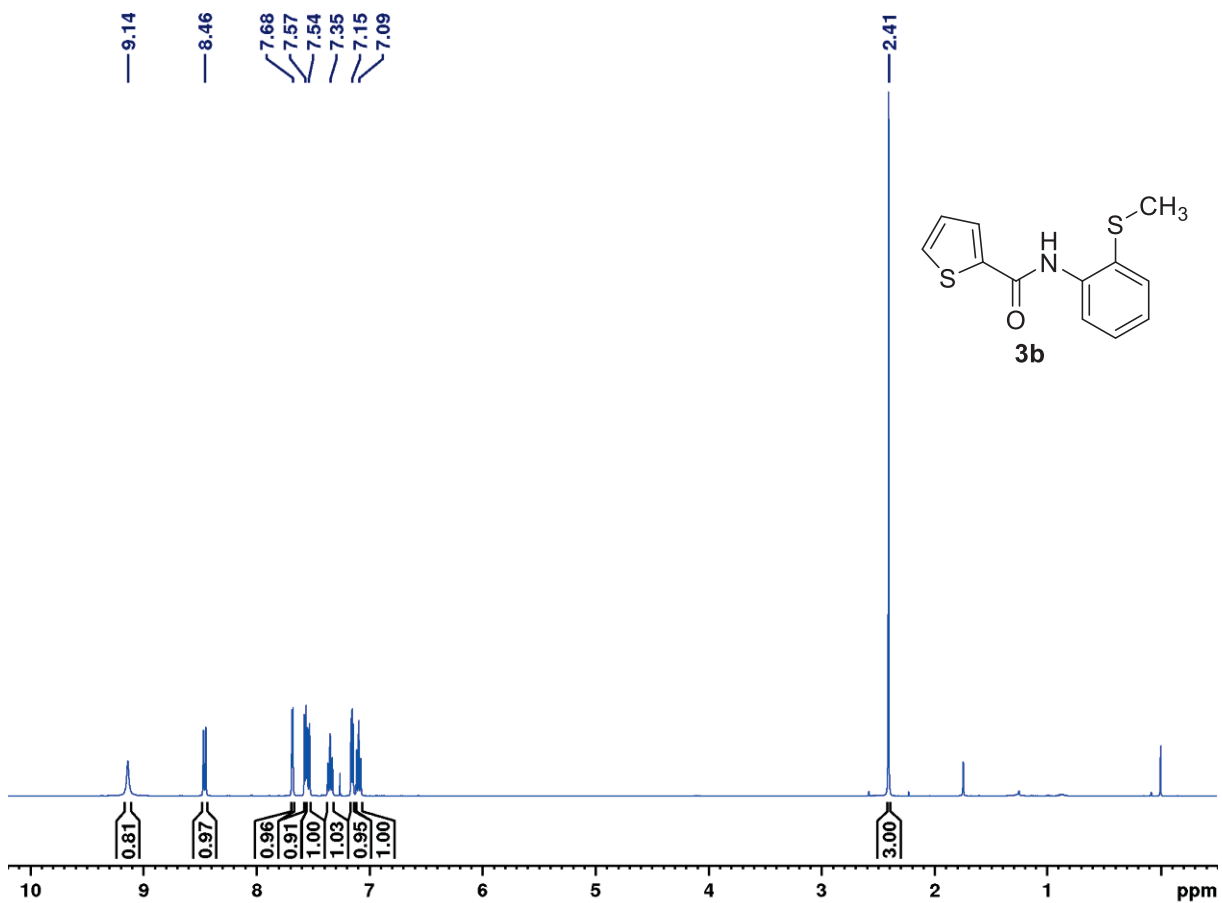


Figure 24: ^1H NMR spectrum (400 MHz, CDCl_3) of compound *N*-(2-(methylthio)phenyl)thiophene-2-carboxamide (**3b**).

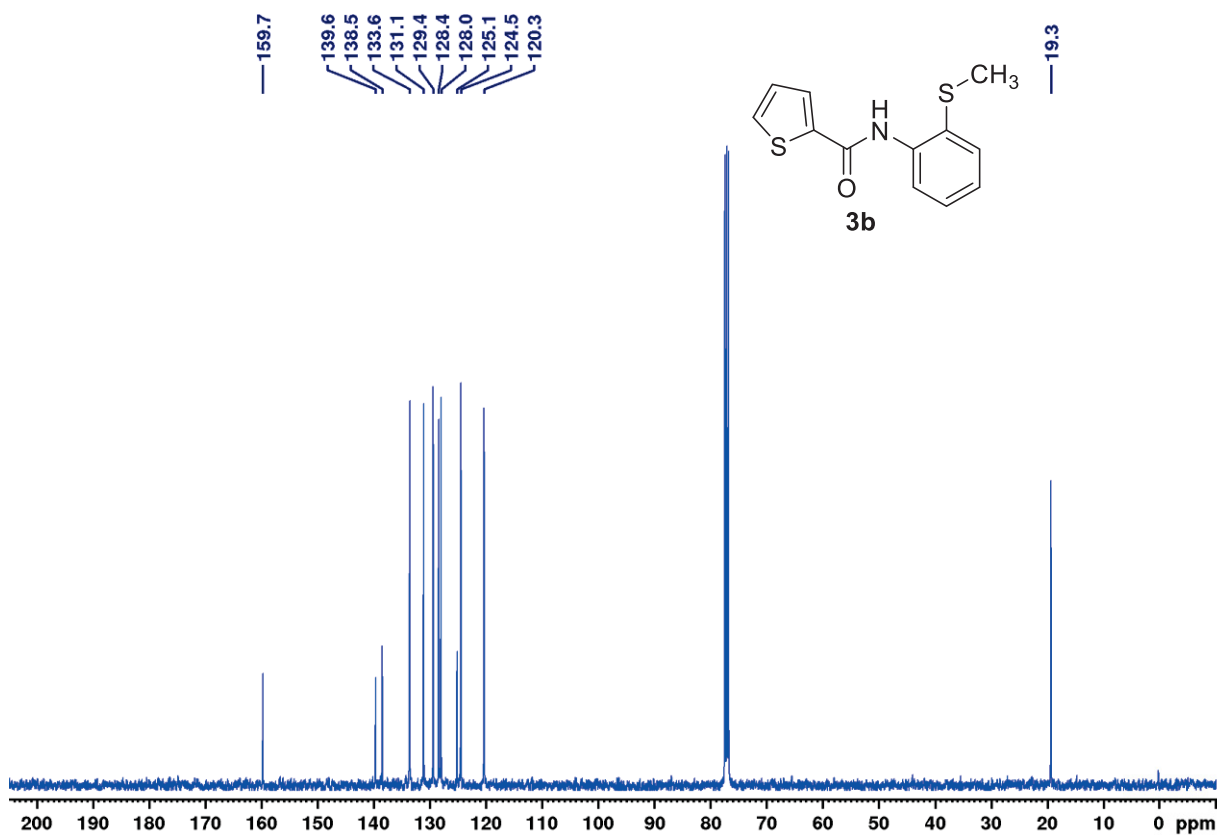


Figure 25: ¹³C NMR spectrum (100 MHz, CDCl₃) of compound *N*-(2-(methylthio)phenyl)thiophene-2-carboxamide (**3b**).

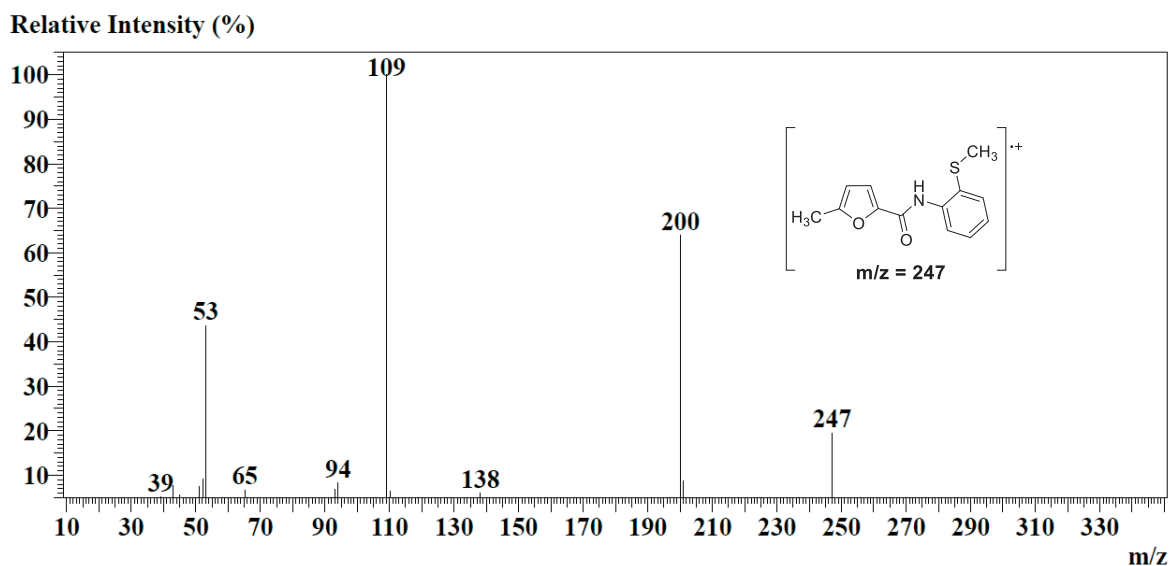


Figure 26: Mass spectrum (EI, 70 eV) of 5-methyl-*N*-(2-(methylthio)phenyl)furan-2-carboxamide (**3c**).

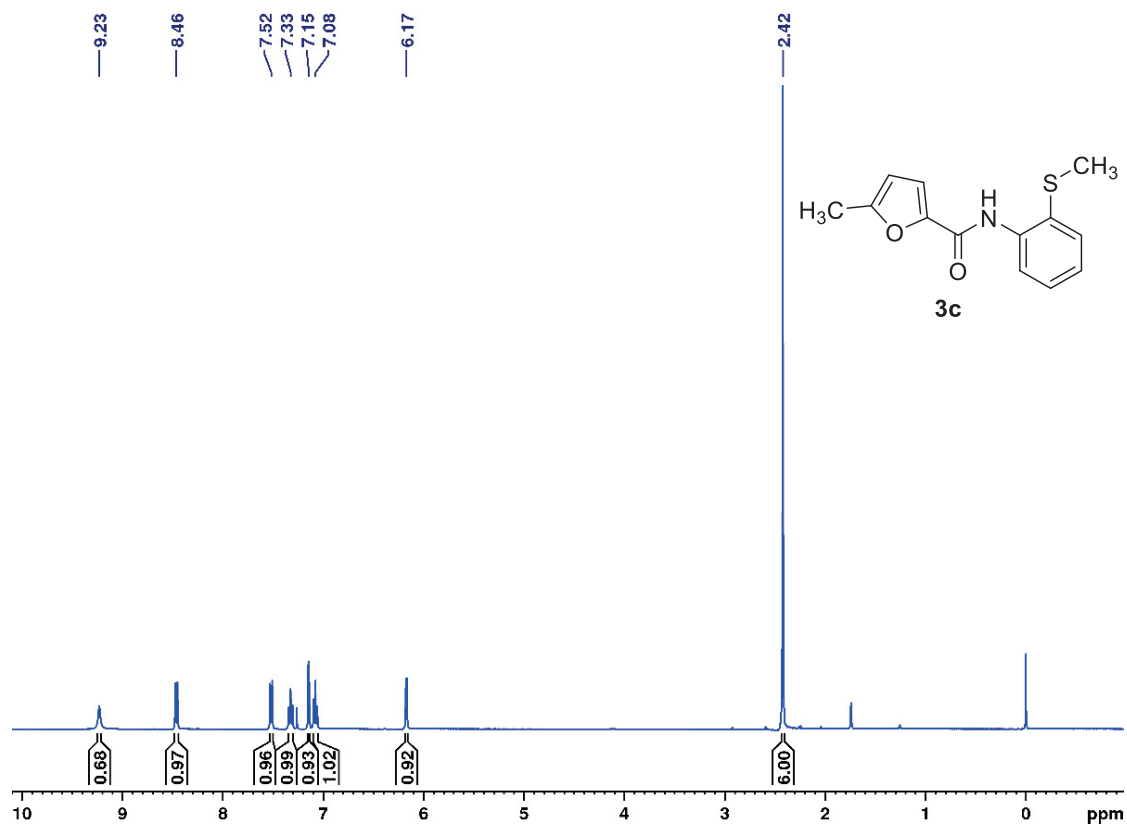


Figure 27: ¹H NMR Spectrum (400 MHz, CDCl₃) of 5-methyl-*N*-(2-(methylthio)phenyl)furan-2-carboxamide (**3c**).

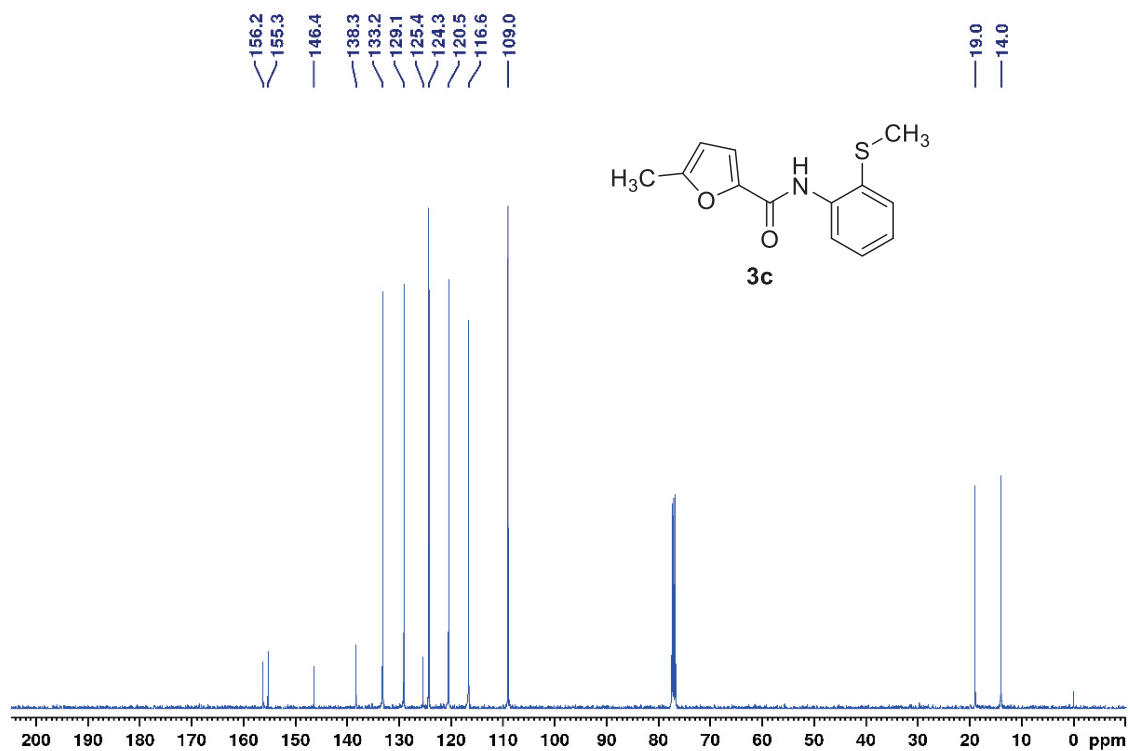


Figure 28: ¹³C NMR Spectrum (100 MHz, CDCl₃) of 5-methyl-*N*-(2-(methylthio)phenyl)furan-2-carboxamide (**3c**).

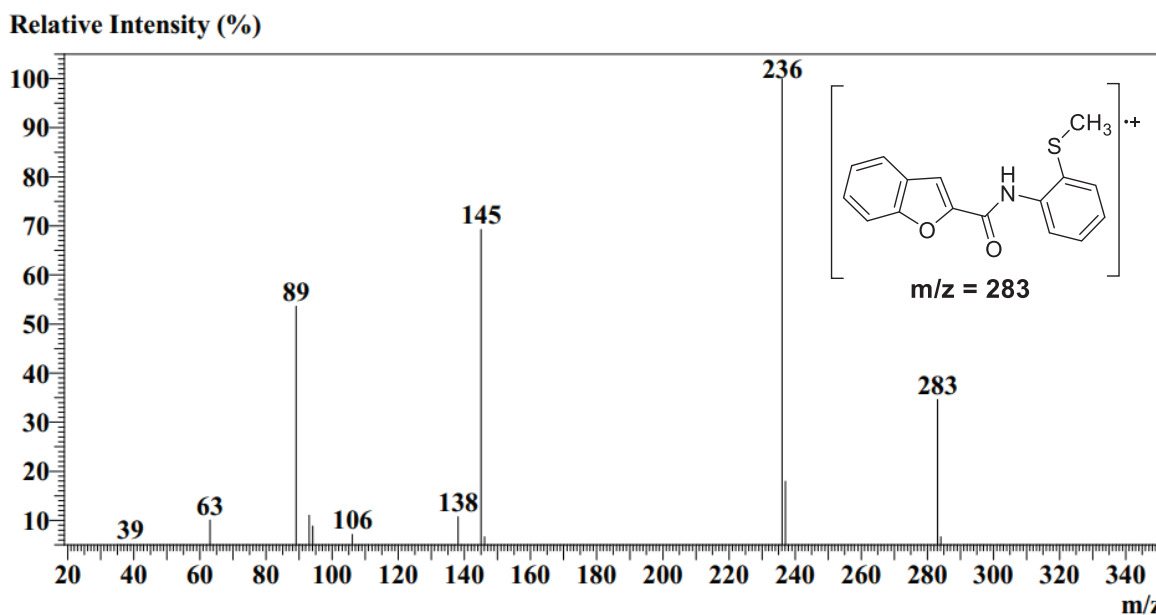


Figure 29: Mass spectrum (EI, 70 eV) of *N*-(2-(methylthio)phenyl)benzofuran-2-carboxamide (**3d**).

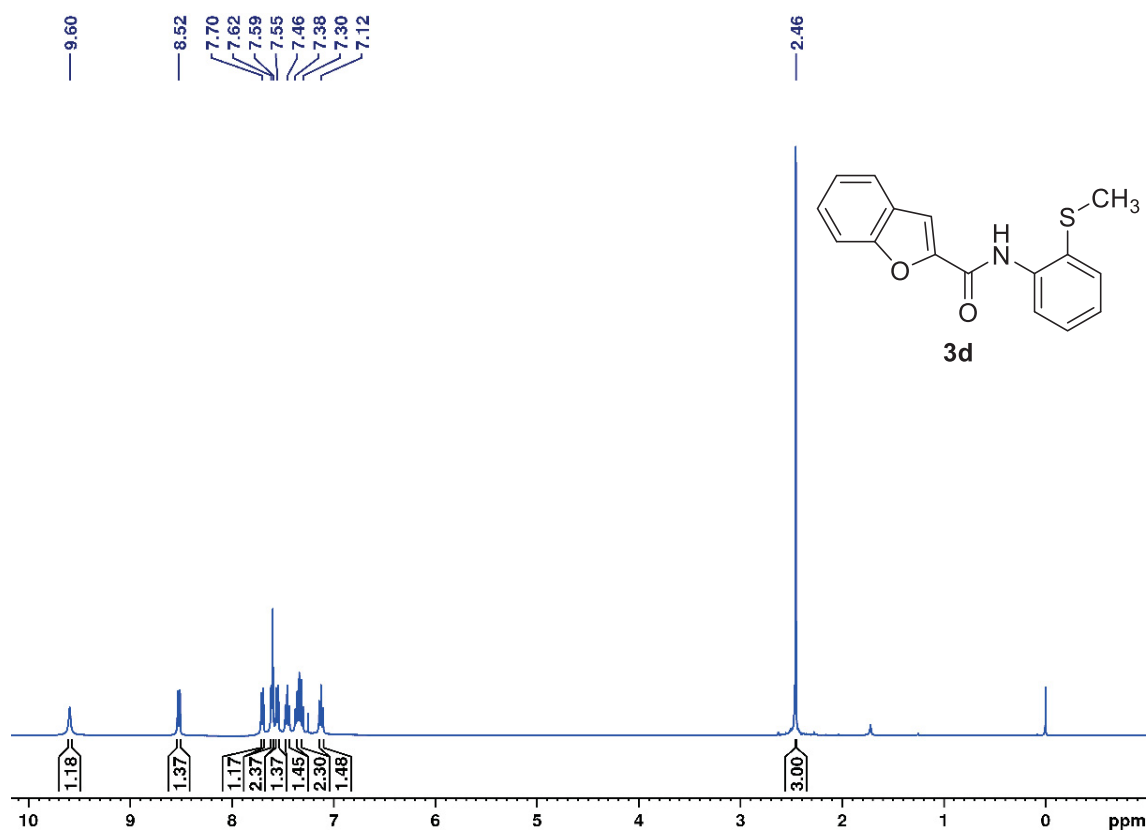


Figure 30: ¹H NMR Spectrum (400 MHz, CDCl₃) of *N*-(2-(methylthio)phenyl)benzofuran-2-carboxamide (**3d**).

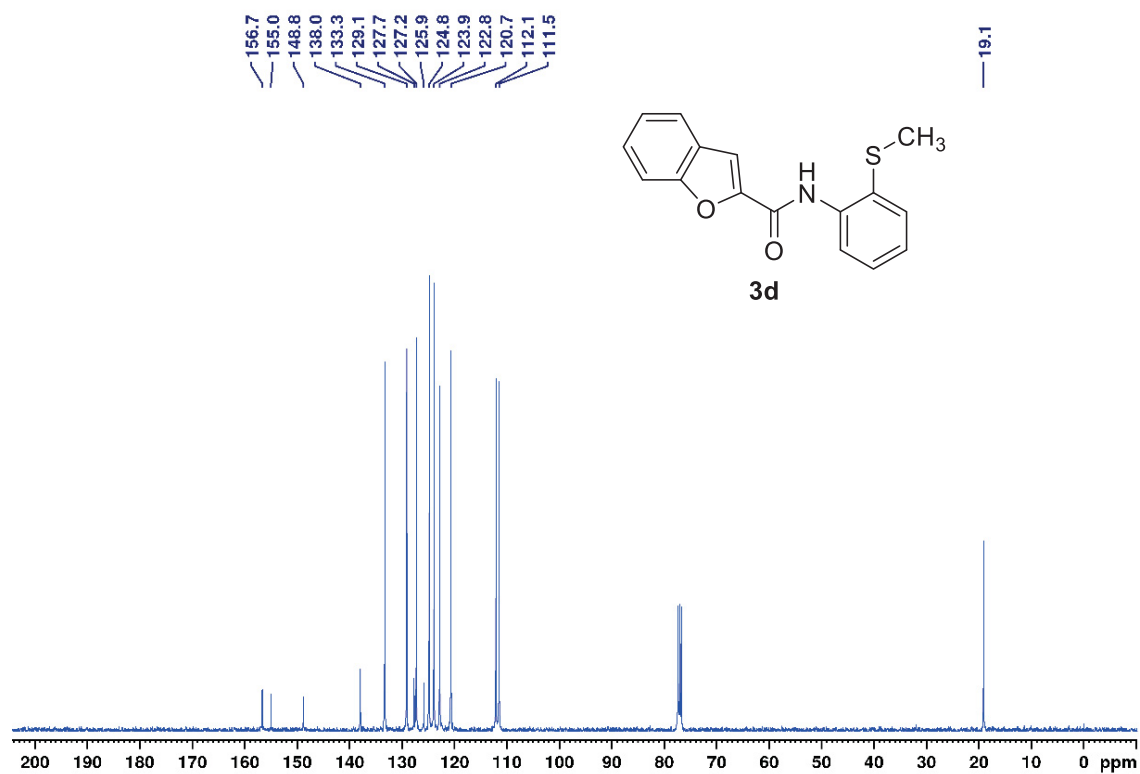


Figure 31: ^{13}C NMR Spectrum (100 MHz, CDCl_3) of *N*-(2-(methylthio)phenyl)benzofuran-2-carboxamide (**3d**).

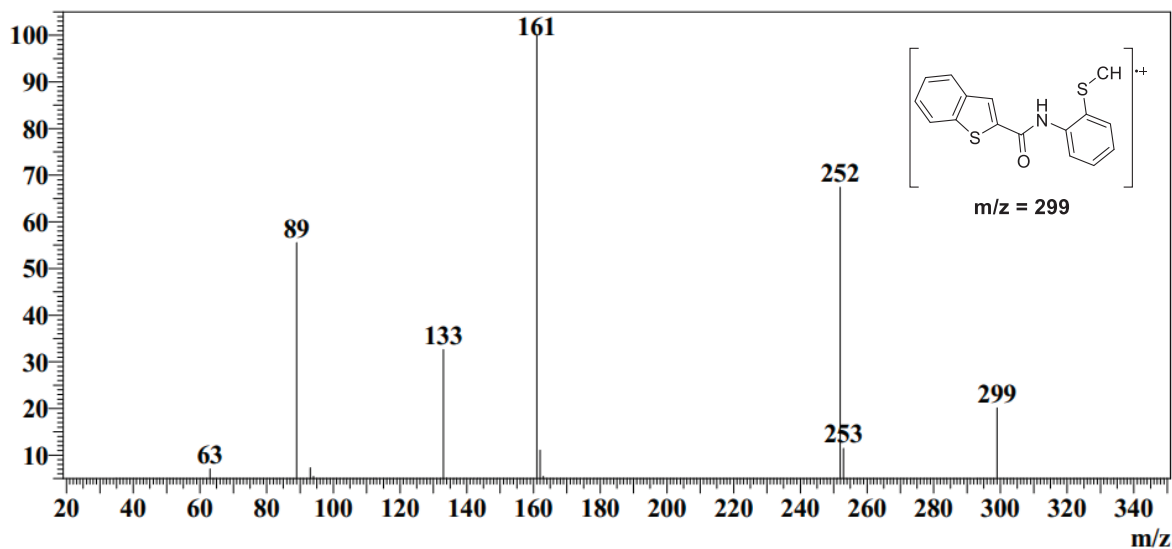


Figure 32: Mass spectrum (EI, 70 eV) of *N*-(2-(methylthio)phenyl)benzo[*b*]thiophene-2-carboxamide (**3e**).

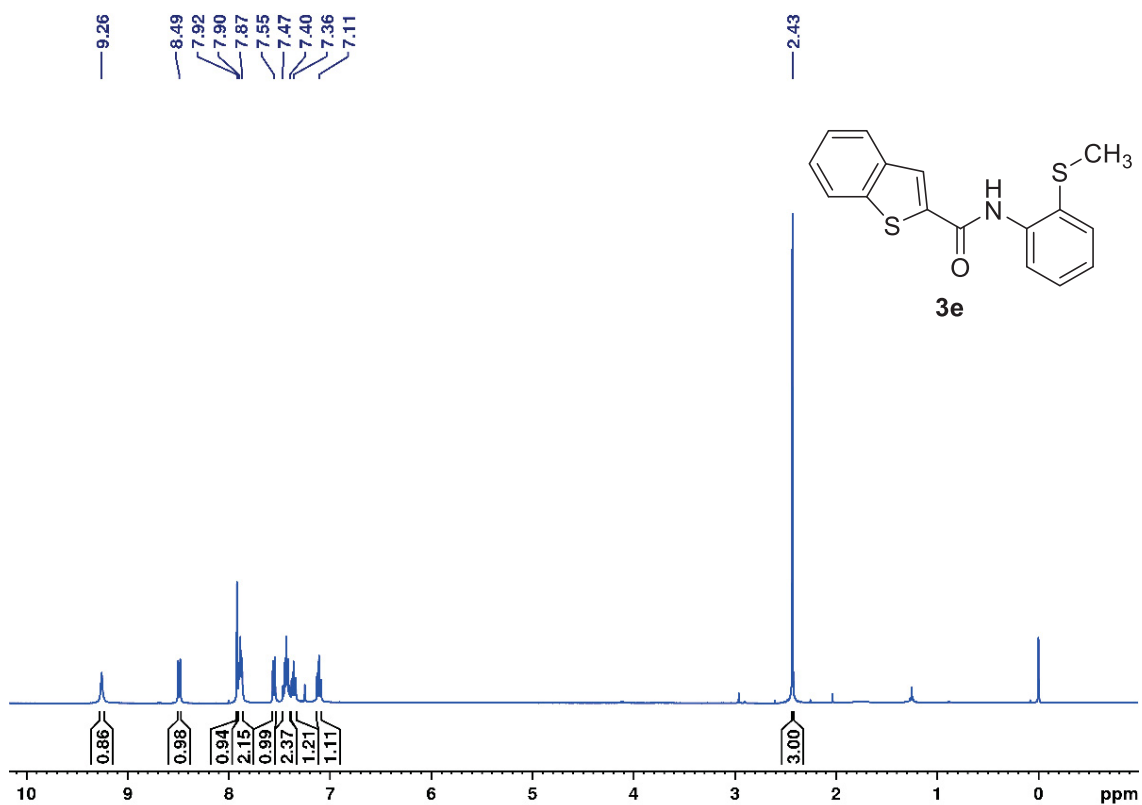


Figure 33: ¹H NMR Spectrum (400 MHz, CDCl₃) of *N*-(2-(methylthio)phenyl)benzo[*b*]thiophene-2-carboxamide (**3e**).

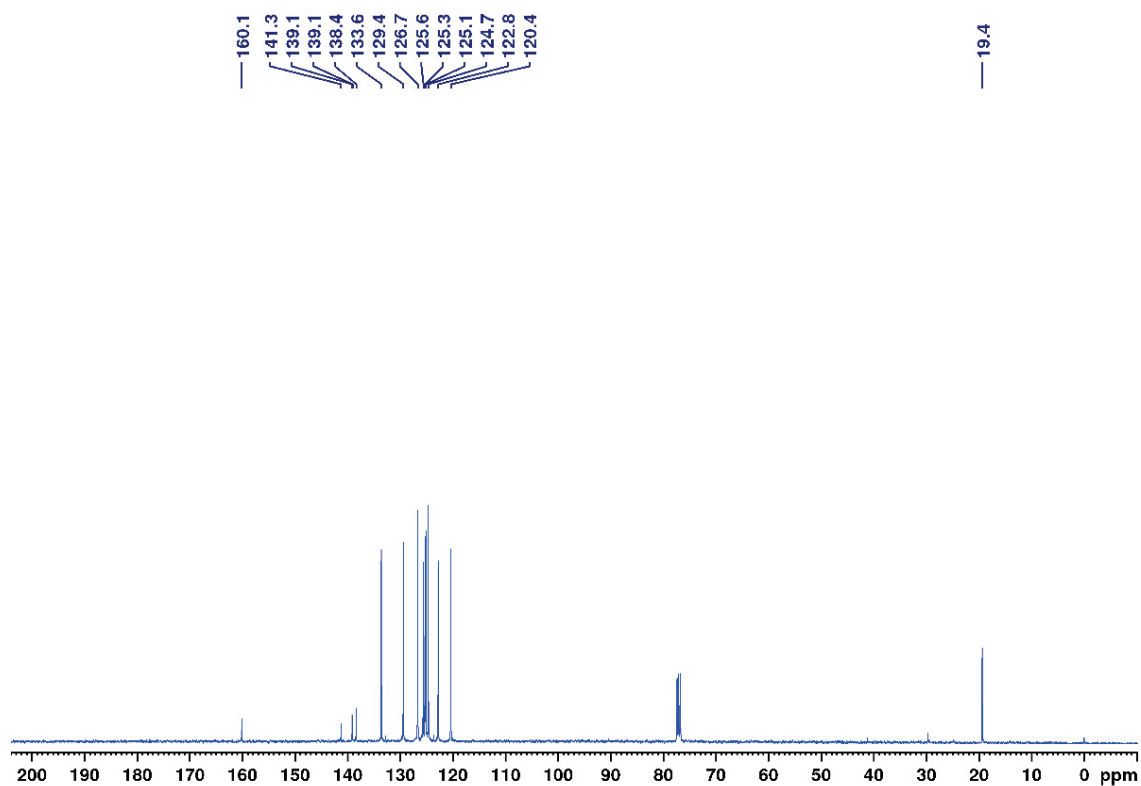


Figure 34: ¹³C NMR Spectrum (100 MHz, CDCl₃) *N*-(2-(methylthio)phenyl)benzo[*b*]thiophene-2-carboxamide (**3e**).

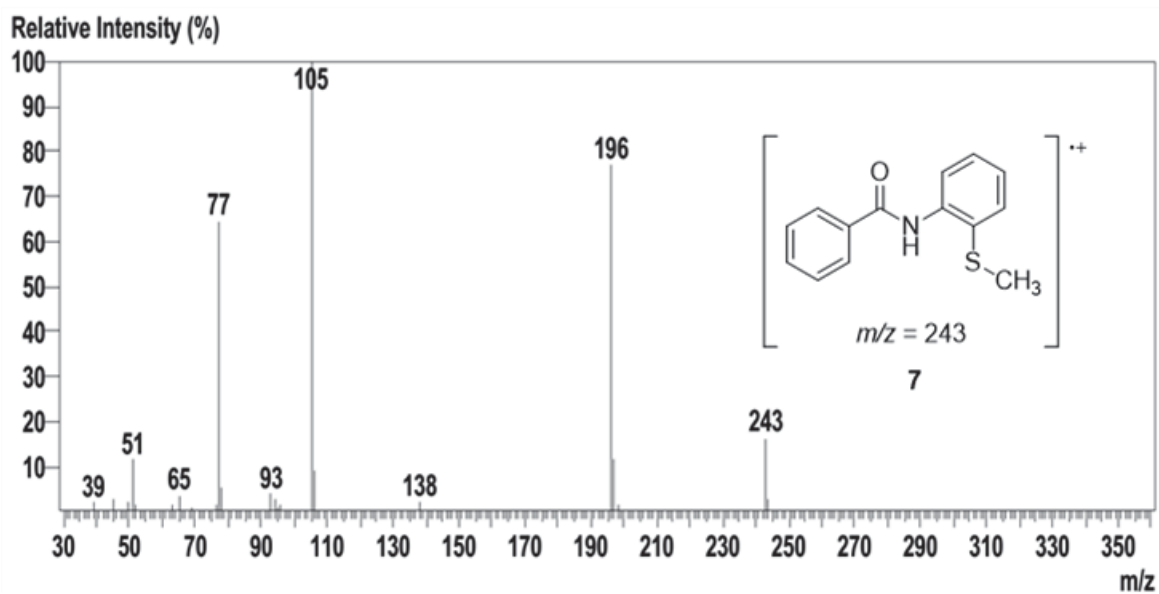


Figure 35: Mass spectrum (EI, 70 eV) of *N*-(2-(methylthio)phenyl)benzamide (7a).

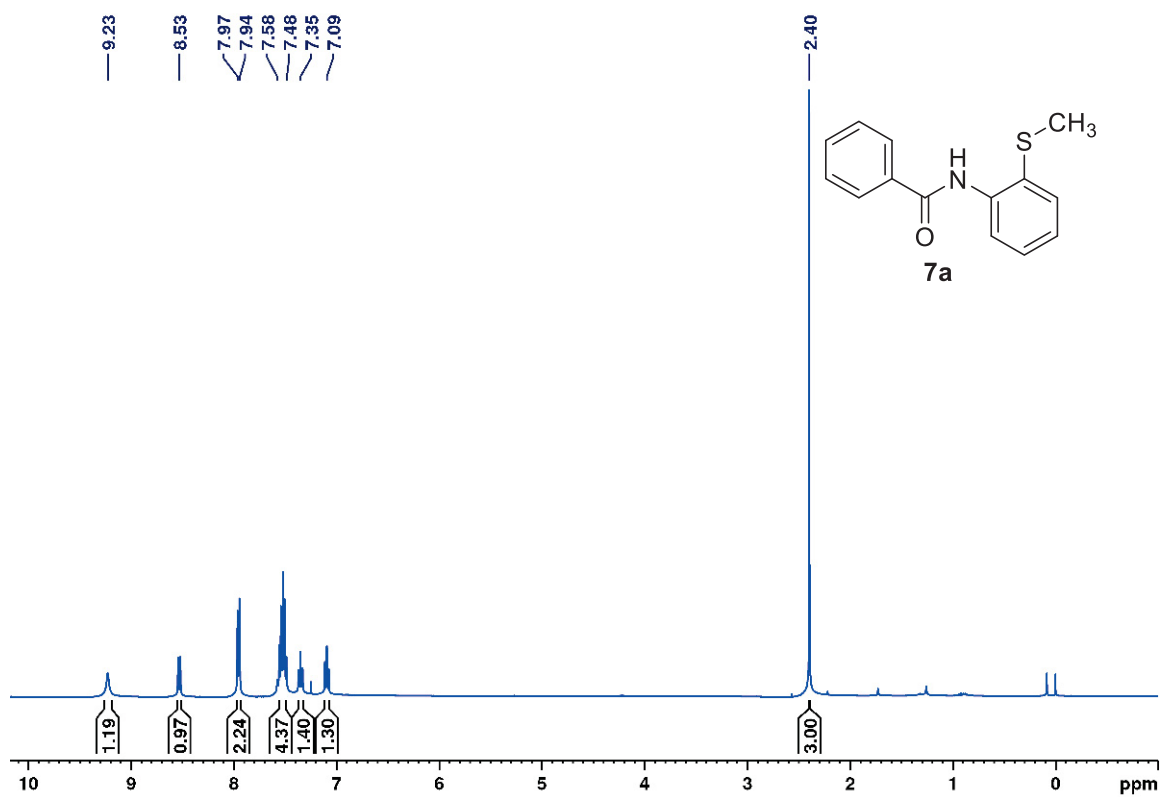


Figure 36: ^1H NMR spectrum (400 MHz, CDCl_3) of *N*-(2-(methylthio)phenyl)benzamide (7a).

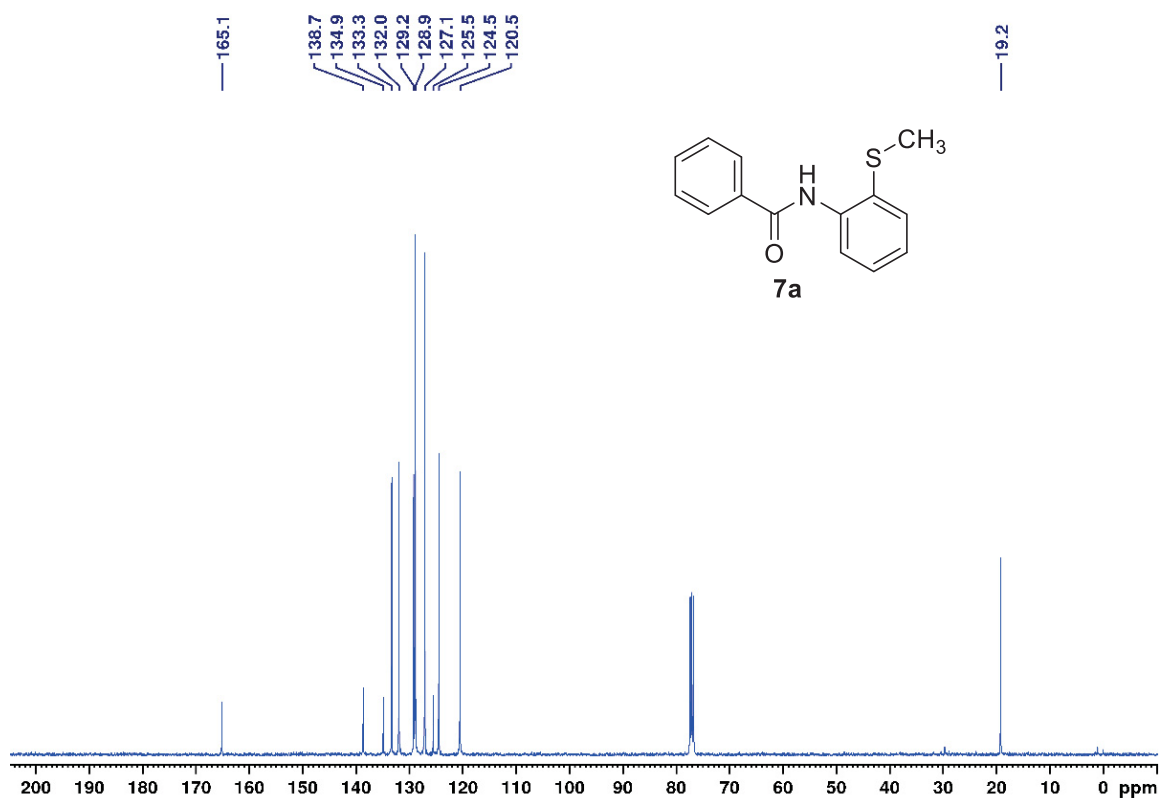


Figure 37: ¹³C NMR spectrum (100 MHz, CDCl₃) of *N*-(2-(methylthio)phenyl)benzamide (**7a**).

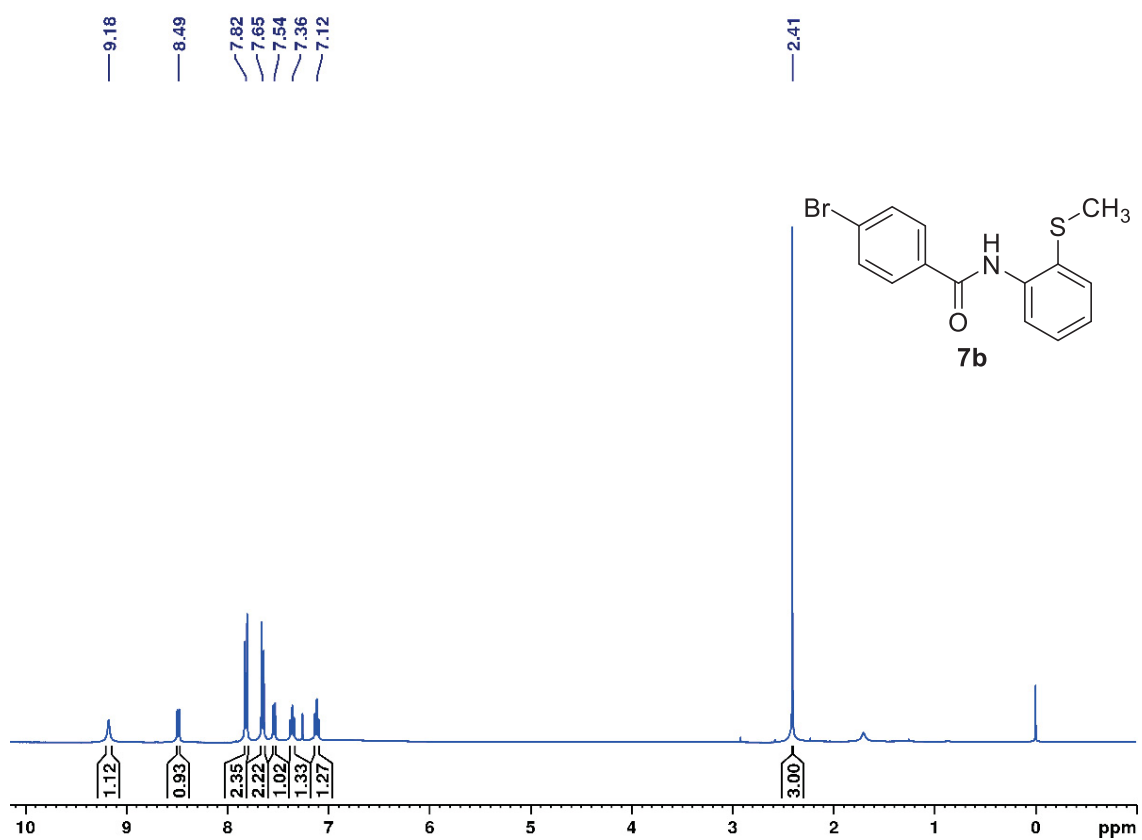


Figure 38: ¹H NMR spectrum (400 MHz, CDCl₃) of 4-bromo-*N*-(2-(methylthio)phenyl)benzamide (**7b**).

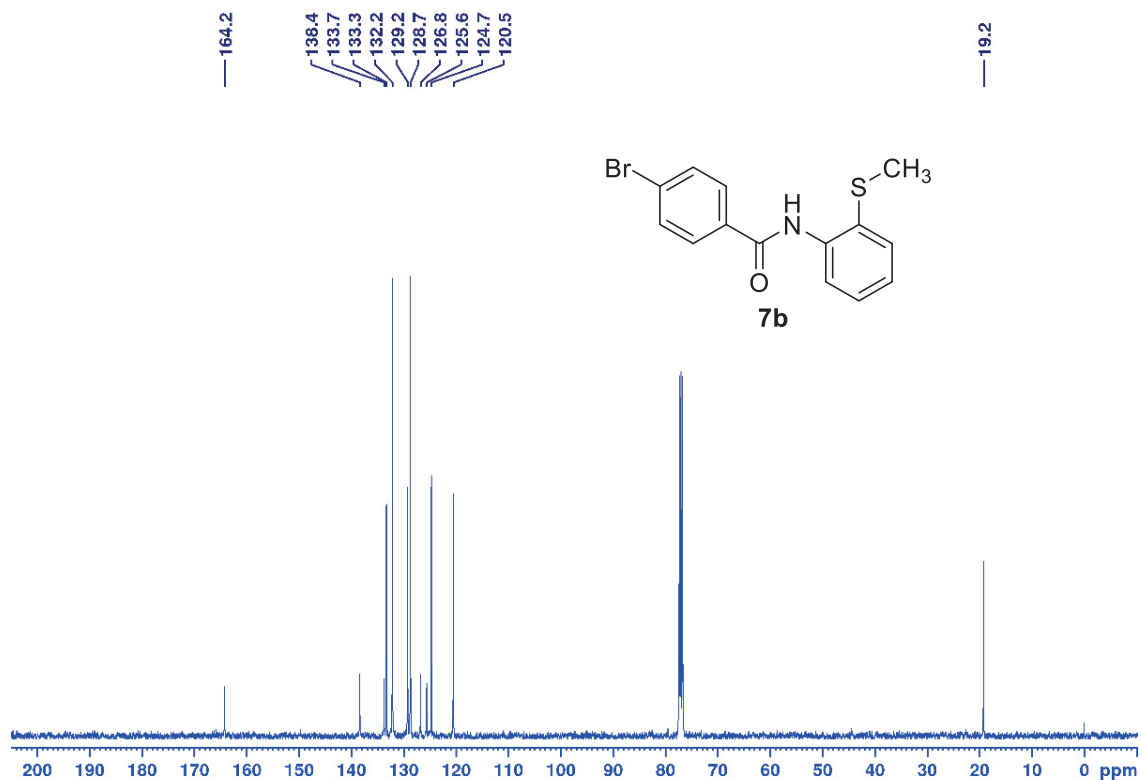


Figure 39: ¹³C NMR spectrum (100 MHz, CDCl₃) of 4-bromo-N-(2-(methylthio)phenyl)benzamide (7b).

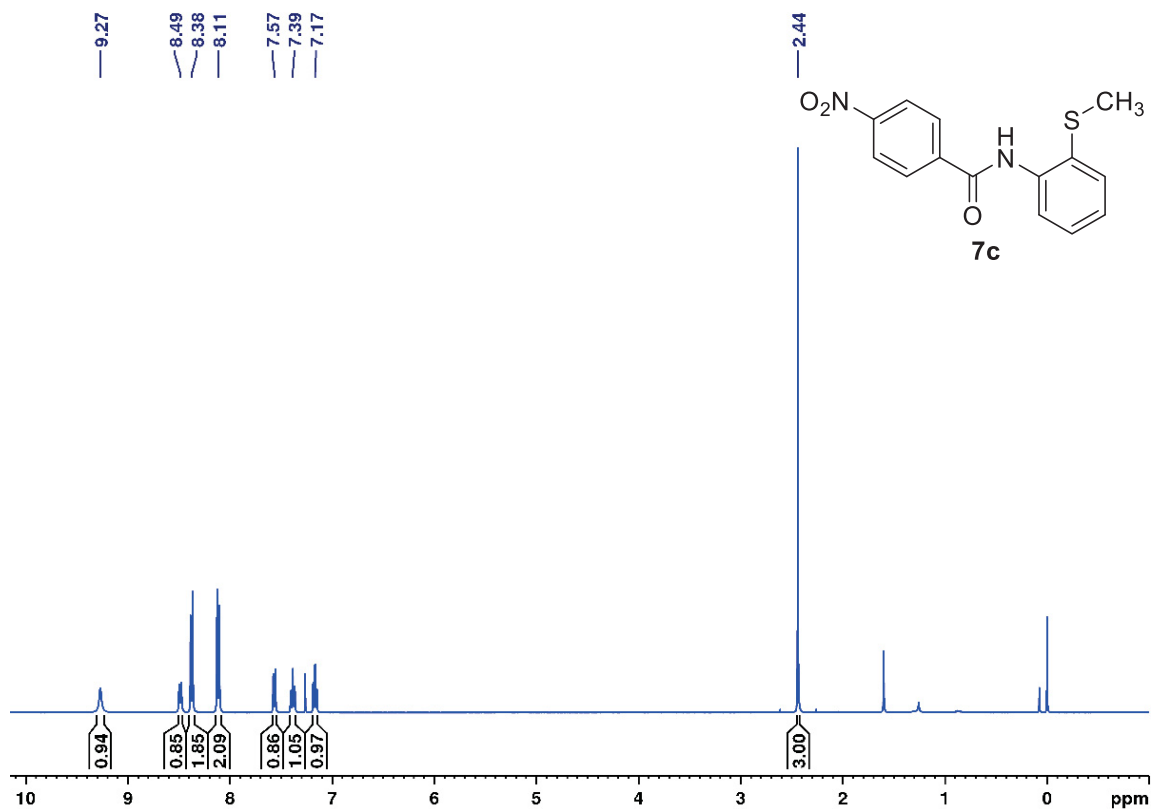


Figure 40: ¹H NMR spectrum (400 MHz, CDCl₃) of N-(2-(methylthio)phenyl)-4-nitrobenzamide (7c).

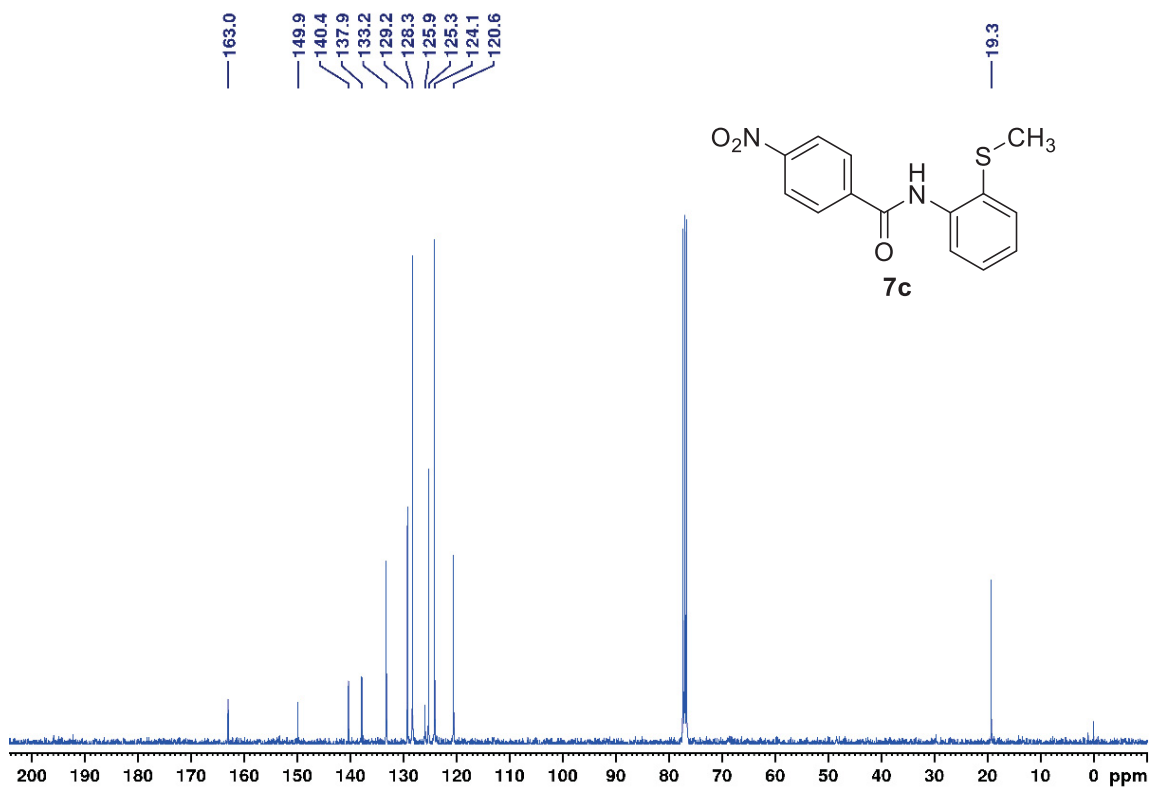


Figure 41: ^{13}C NMR spectrum (100 MHz, CDCl_3) of *N*-(2-(methylthio)phenyl)-4-nitrobenzamide (**7c**).

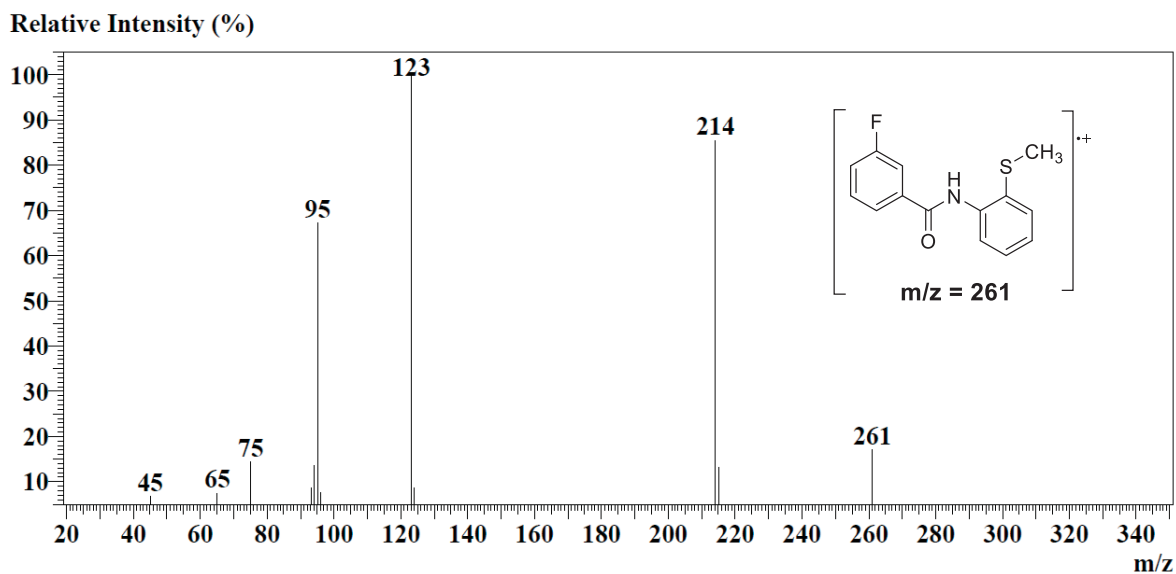


Figure 42: Mass spectrum (EI, 70 eV) of 3-fluoro-*N*-(2-(methylthio)phenyl)benzamide (**7d**).

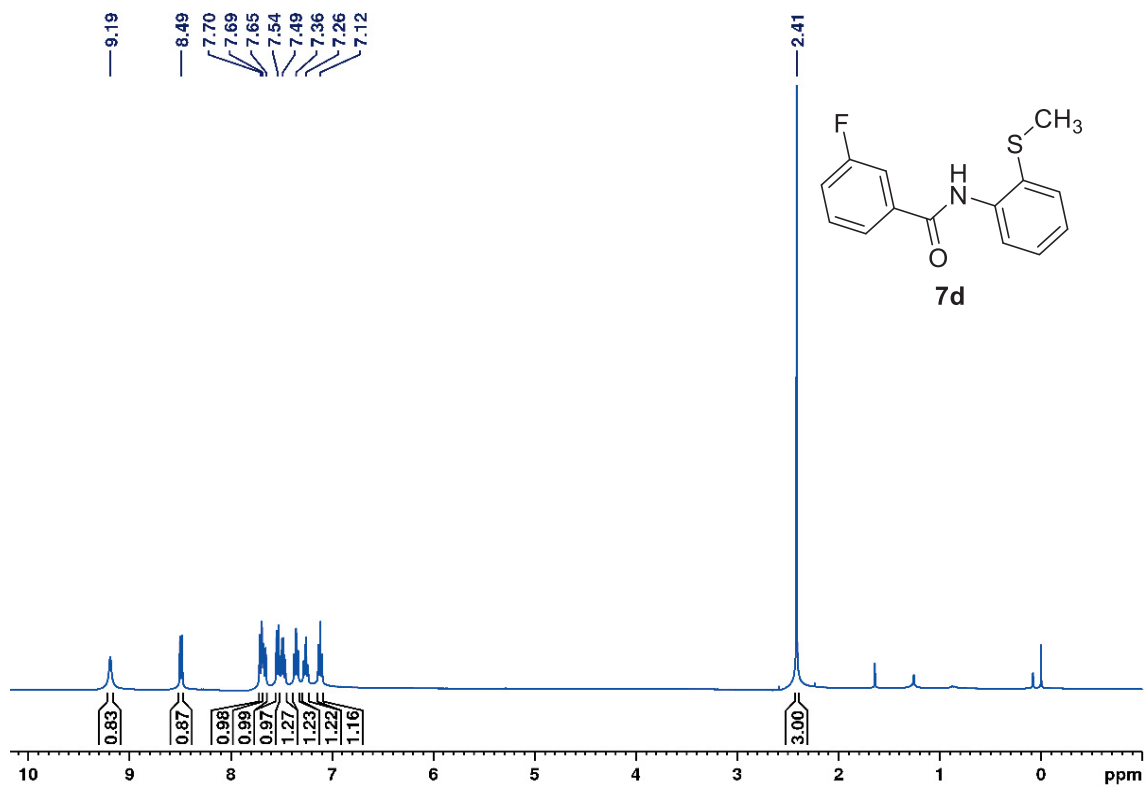


Figure 43: ^1H NMR spectrum (400 MHz, CDCl_3) of 3-fluoro-*N*-(2-(methylthio)phenyl)benzamide (**7d**).

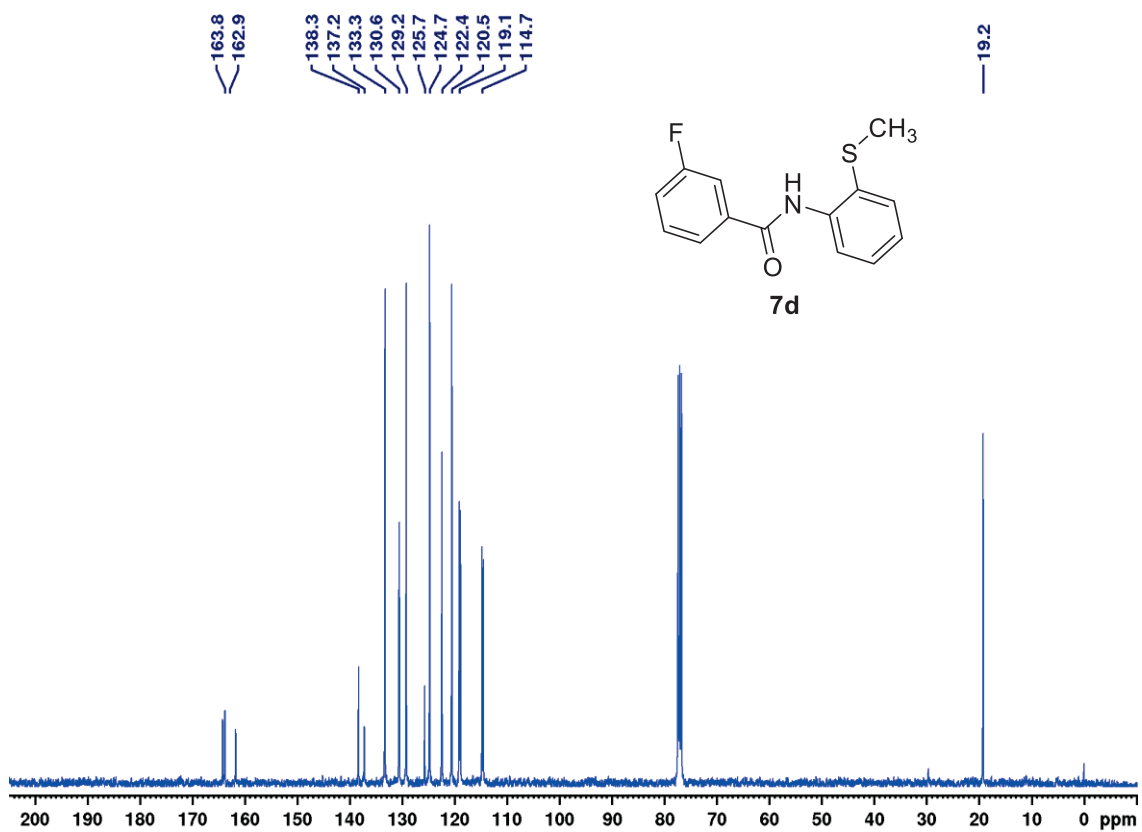


Figure 44: ^{13}C NMR spectrum (100 MHz, CDCl_3) of 3-fluoro-*N*-(2-(methylthio)phenyl)benzamide (**7d**).

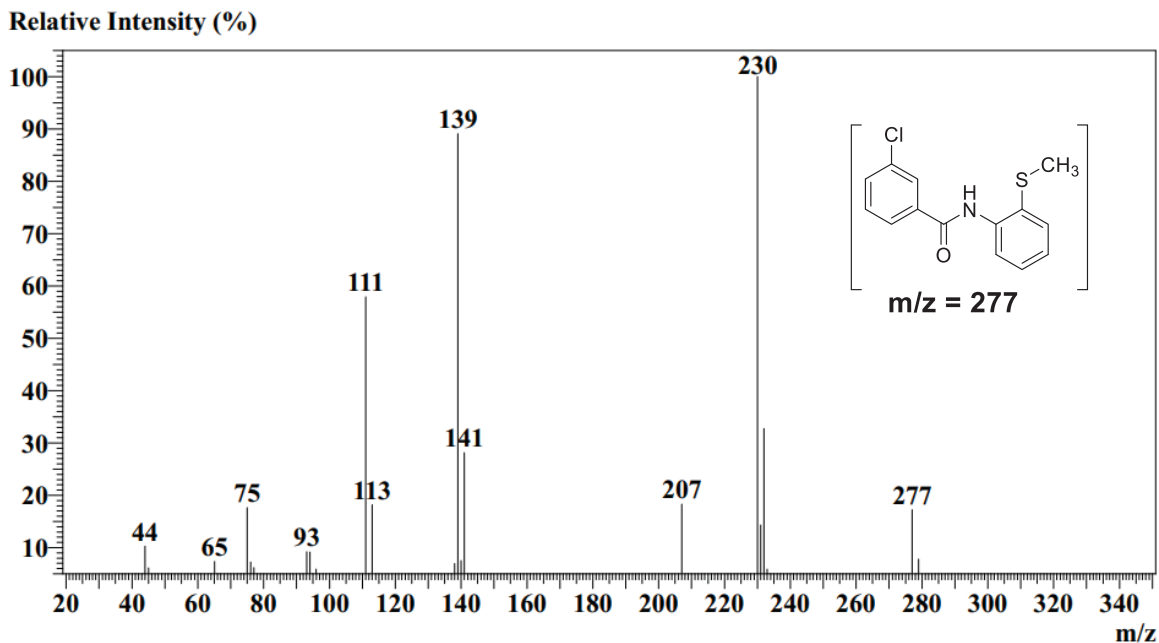


Figure 45: Mass spectrum (EI, 70 eV) of 3-chloro-*N*-(2-(methylthio)phenyl)benzamide (**7e**).

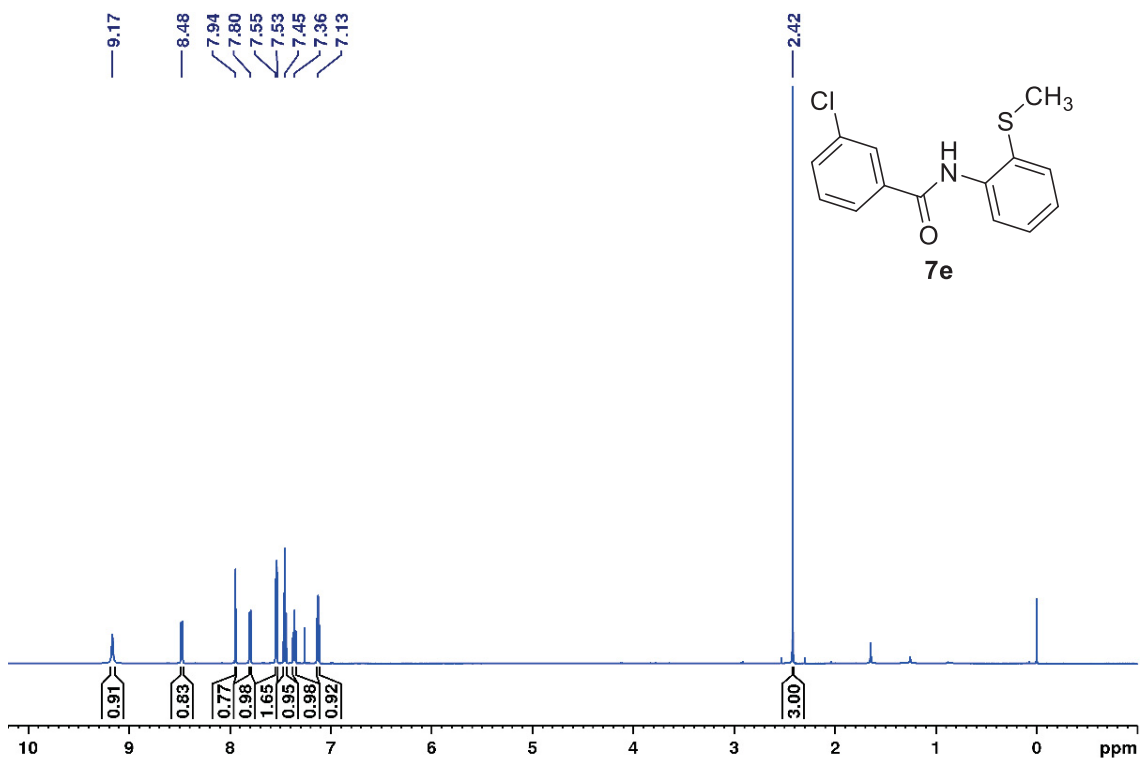


Figure 46: ¹H NMR spectrum (400 MHz, CDCl₃) of 3-chloro-*N*-(2-(methylthio)phenyl)benzamide (**7e**).

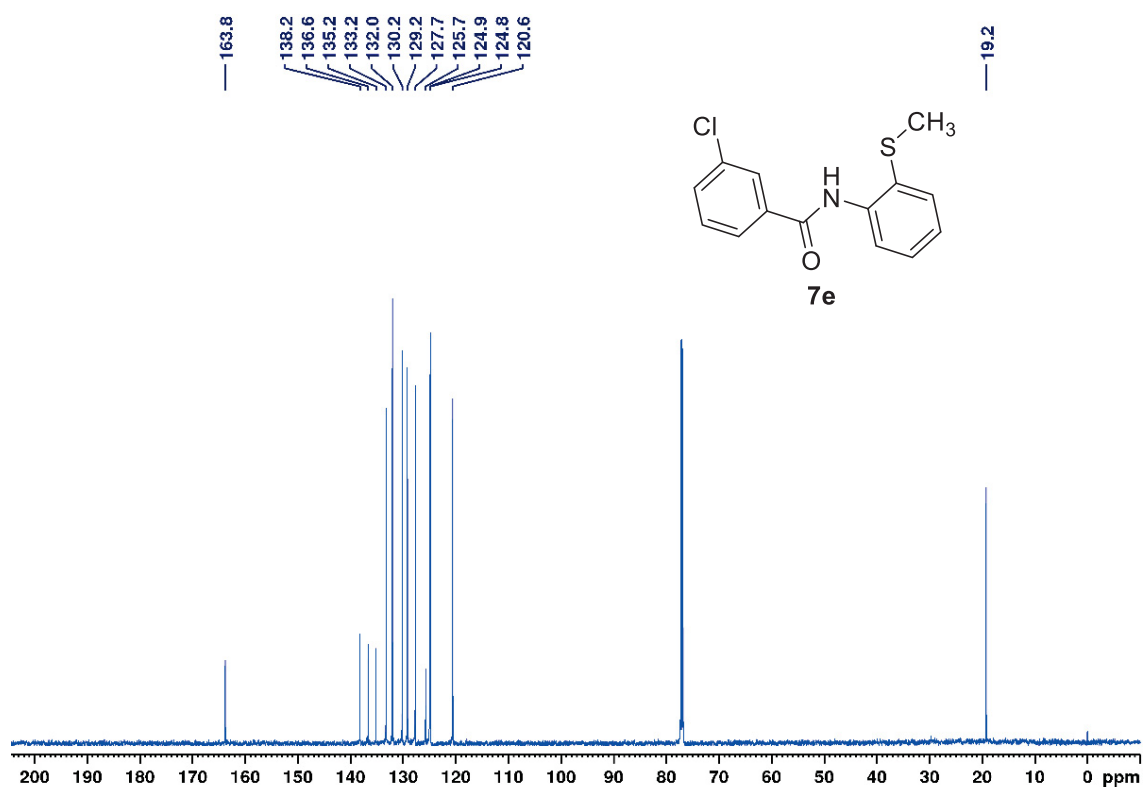


Figure 47: ¹³C NMR spectrum (100 MHz, CDCl₃) of 3-chloro-N-(2-(methylthio)phenyl)benzamide (7e).

Relative Intensity (%)

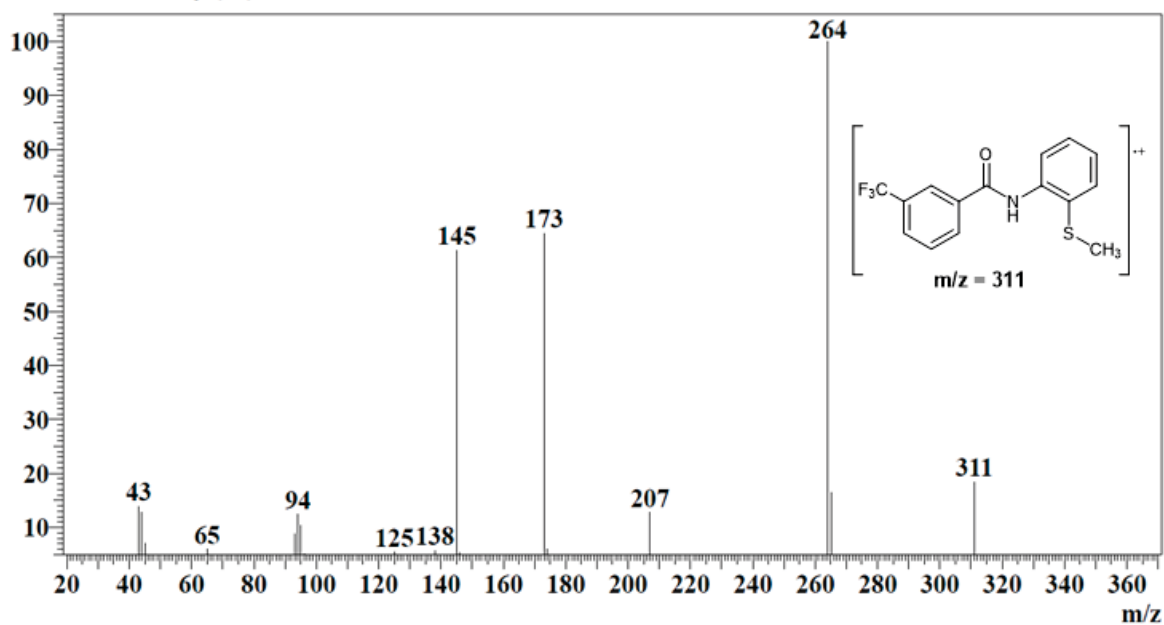


Figure 48: Mass spectrum (EI, 70 eV) of N-(2-(methylthio)phenyl)-2-(trifluoromethyl)benzamide (7f).

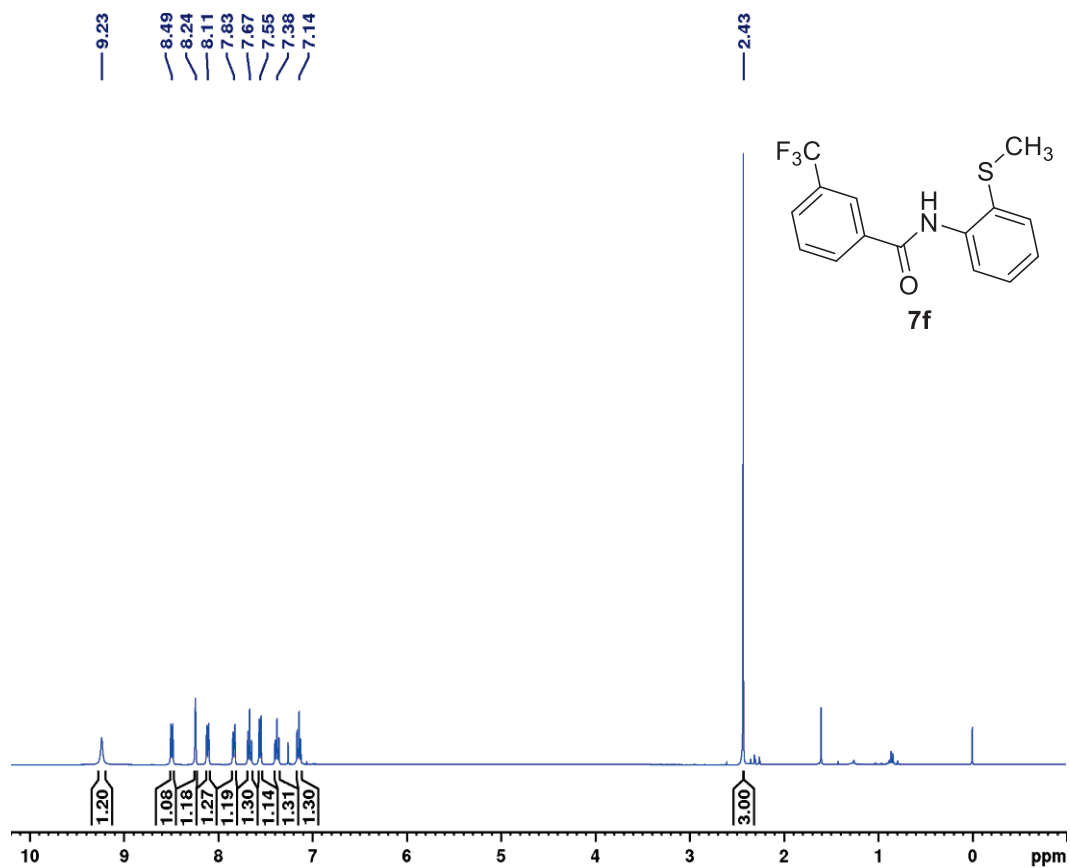


Figure 49: ¹H NMR spectrum (400 MHz, CDCl₃) *N*-(2-(methylthio)phenyl)-3-(trifluoromethyl)benzamide (**7f**).

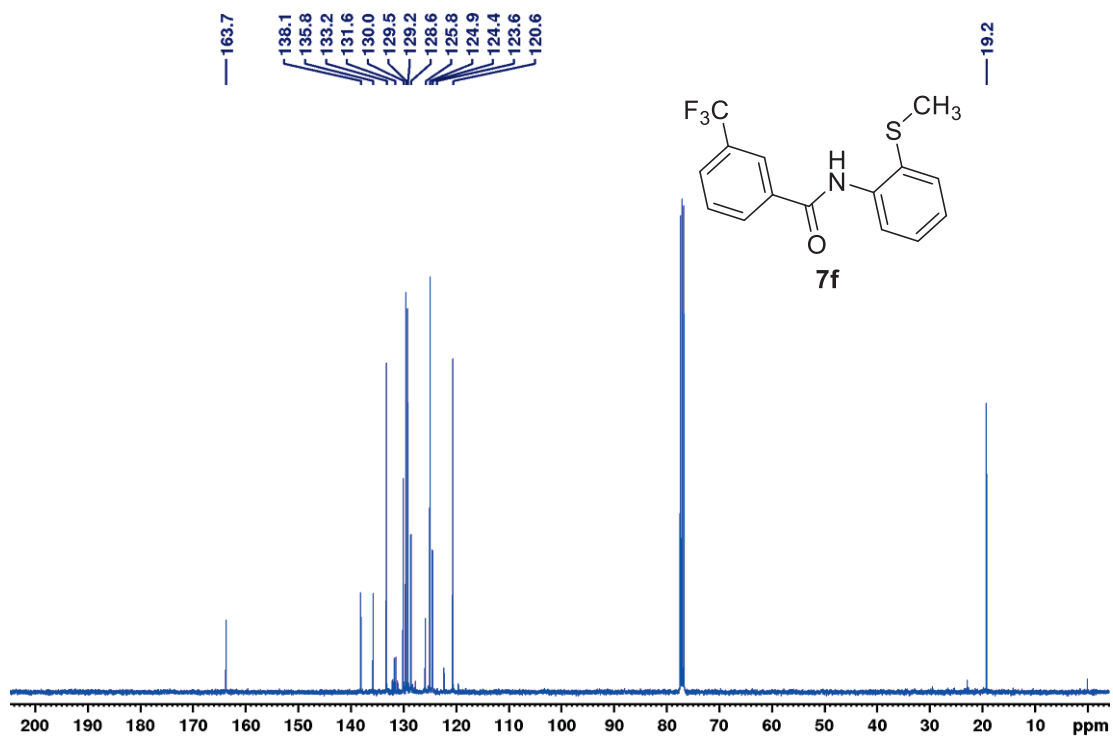


Figure 50: ¹³C NMR spectrum (100 MHz, CDCl₃) *N*-(2-(methylthio)phenyl)-3-(trifluoromethyl)benzamide (**7f**).

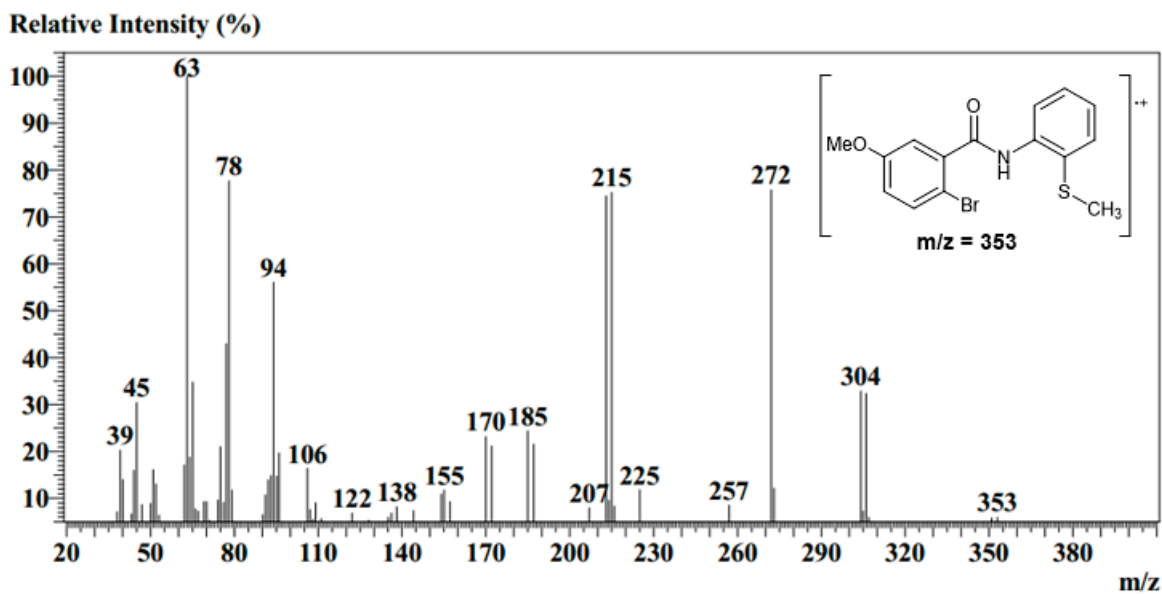


Figure 51: Mass spectrum (EI, 70 eV) 2-bromo-5-methoxy-*N*-(2-(methylthio)phenyl)benzamide (**7g**).

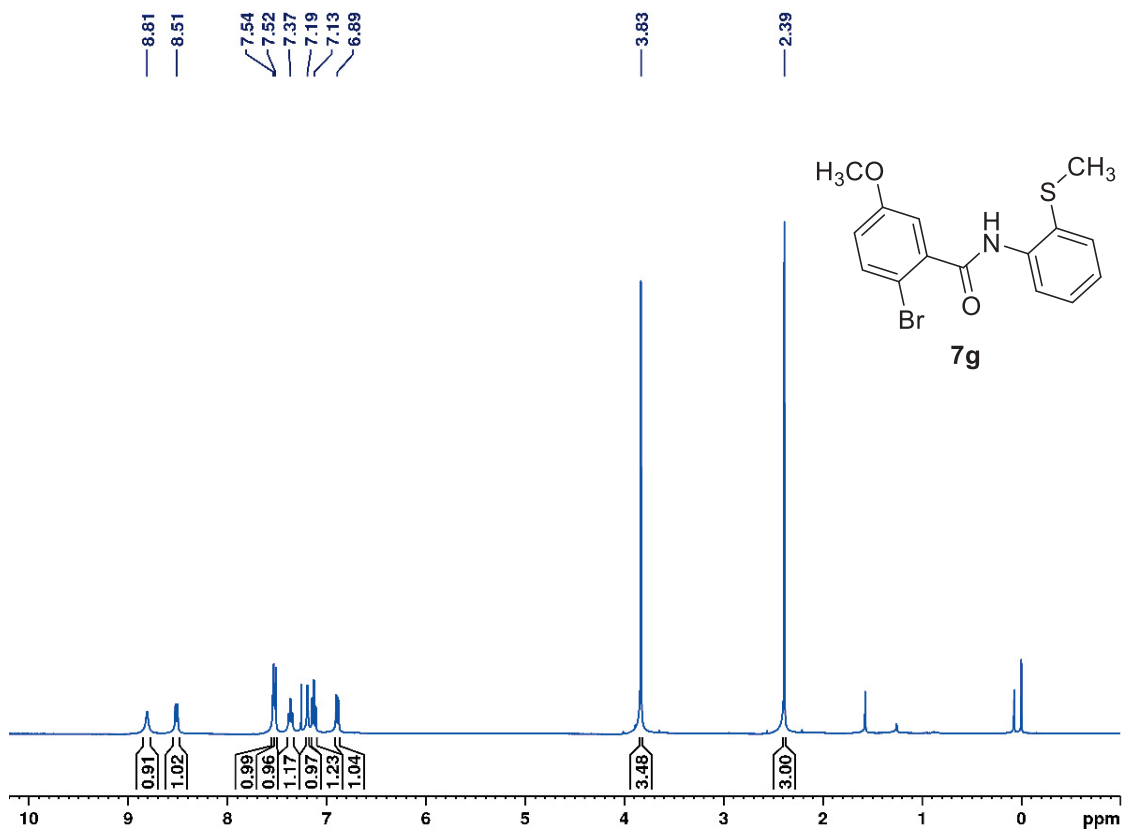


Figure 52: ^1H NMR spectrum (400 MHz, CDCl_3) 2-bromo-5-methoxy-*N*-(2-(methylthio)phenyl)benzamide (**7g**).

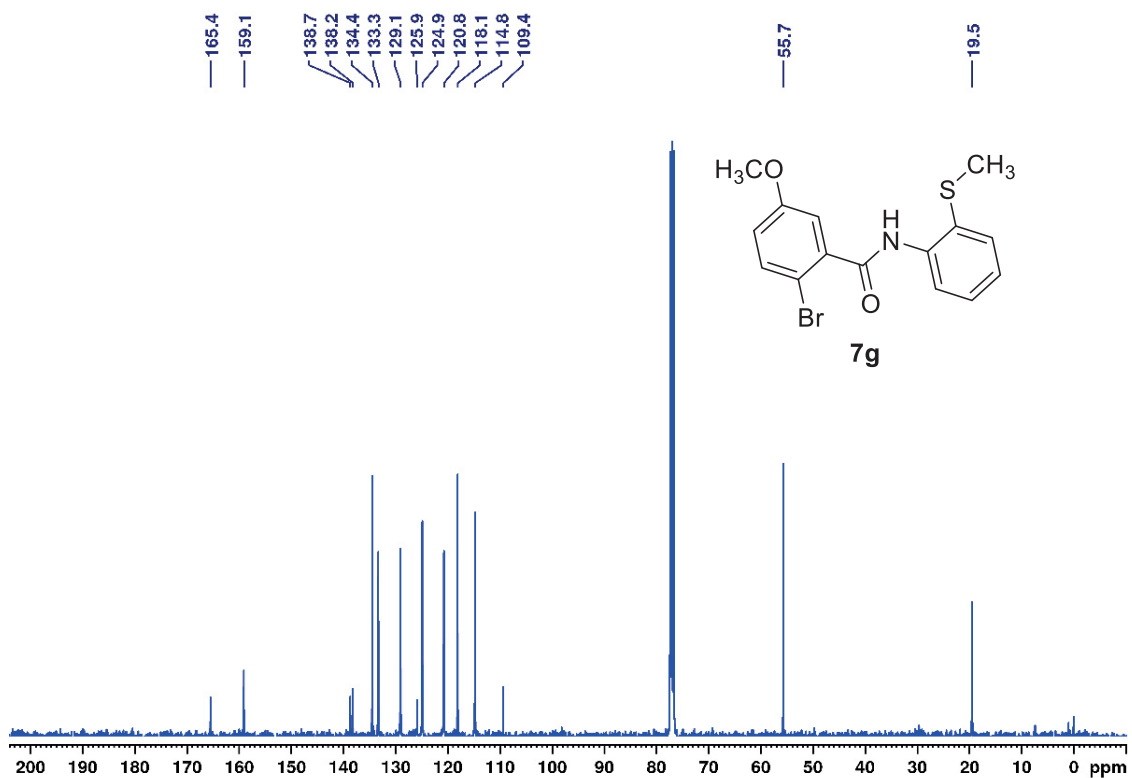


Figure 53: ¹³C NMR spectrum (100 MHz, CDCl₃) 2-bromo-5-methoxy-*N*-(2-(methylthio)phenyl)benzamide (**7g**).

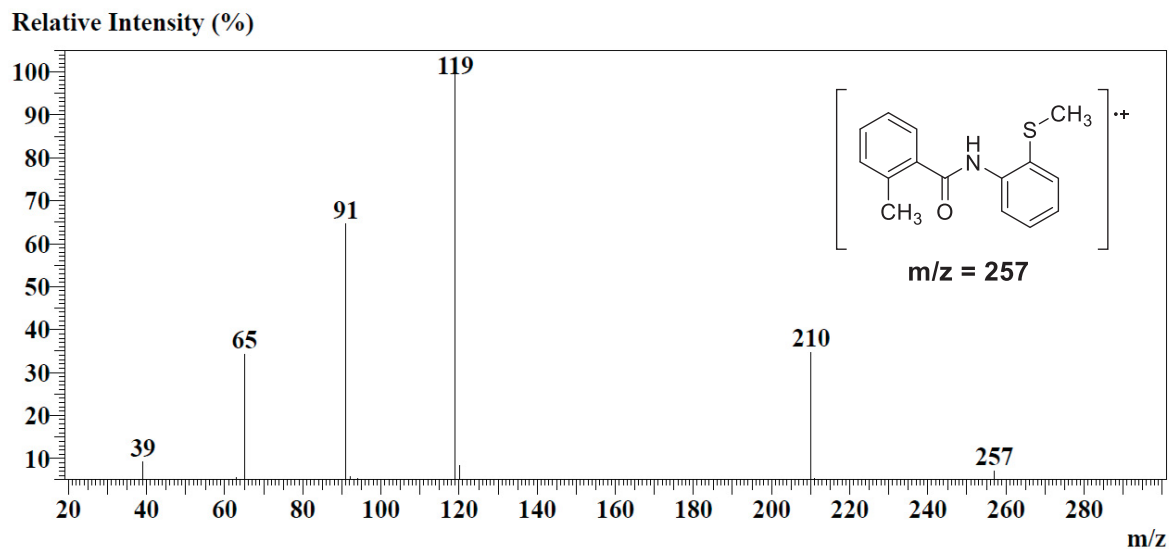


Figure 54: Mass spectrum (EI, 70 eV) of 2-methyl-*N*-(2-(methylthio)phenyl)benzamide (**7h**).

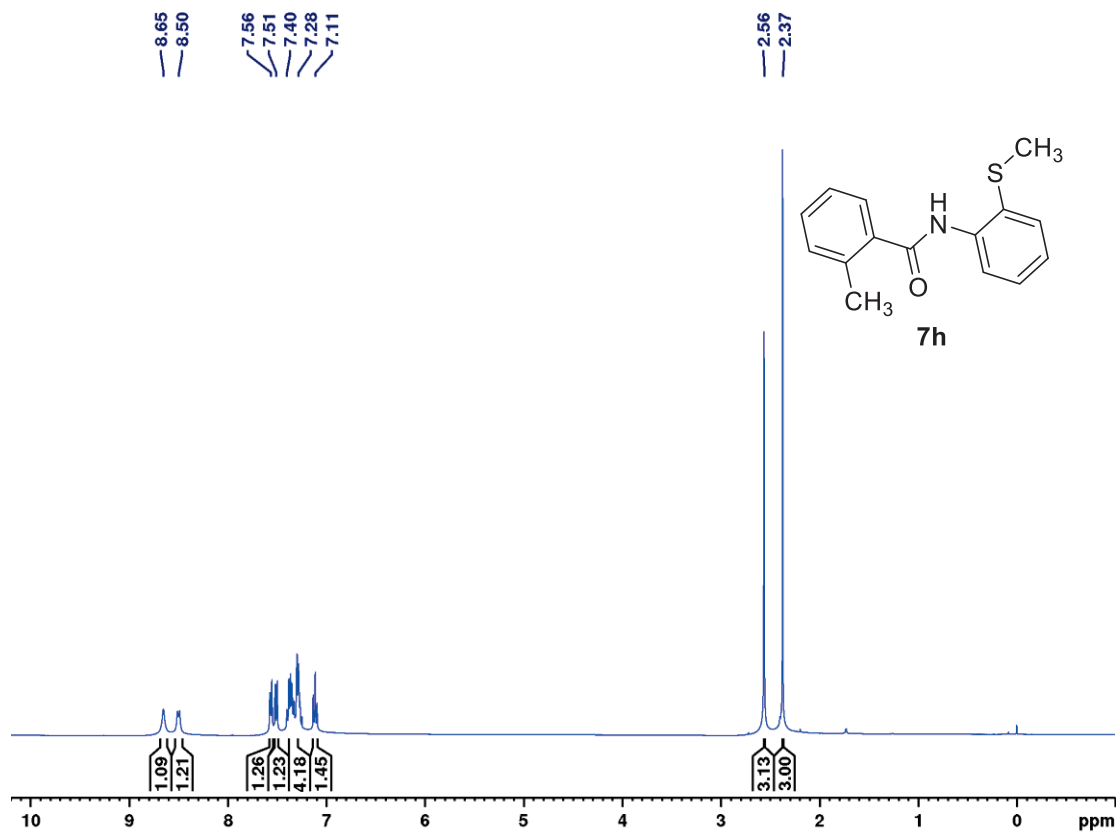


Figure 55: ¹H NMR (400 MHz, CDCl₃) of 2-methyl-N-(2-(methylthio)phenyl)benzamide (7h).

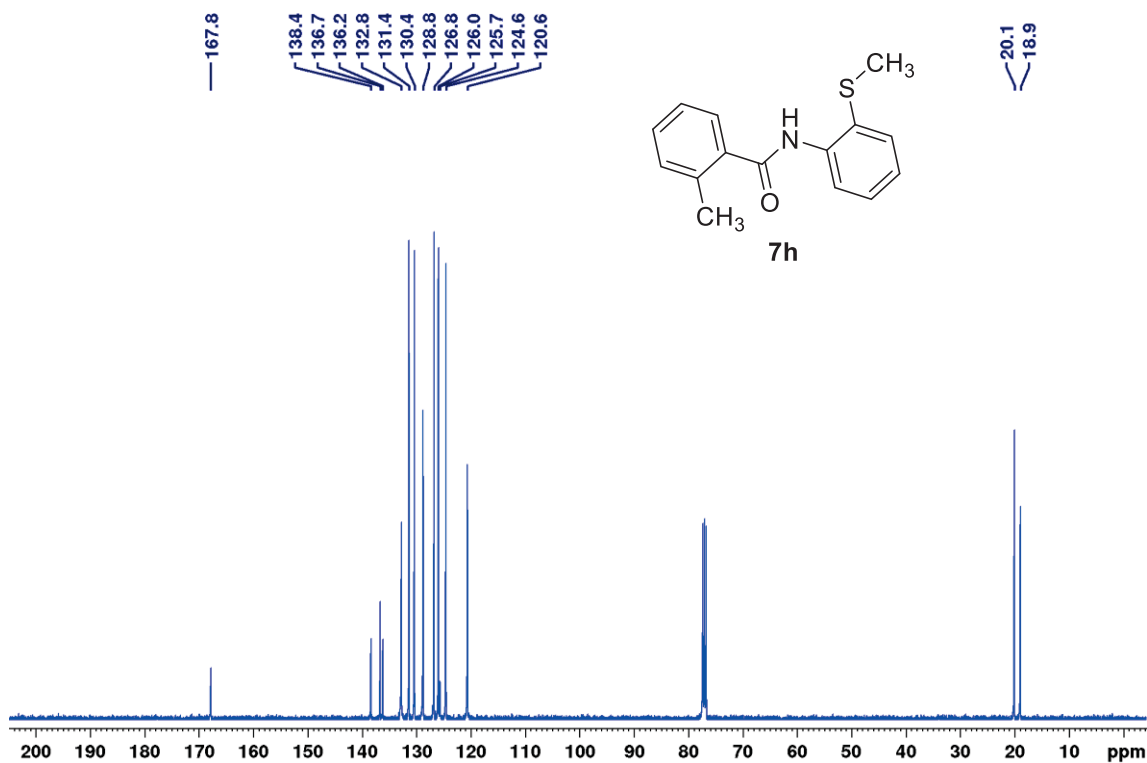


Figure 56: ¹³C NMR (100 MHz, CDCl₃) of 2-methyl-N-(2-(methylthio)phenyl)benzamide (7h).

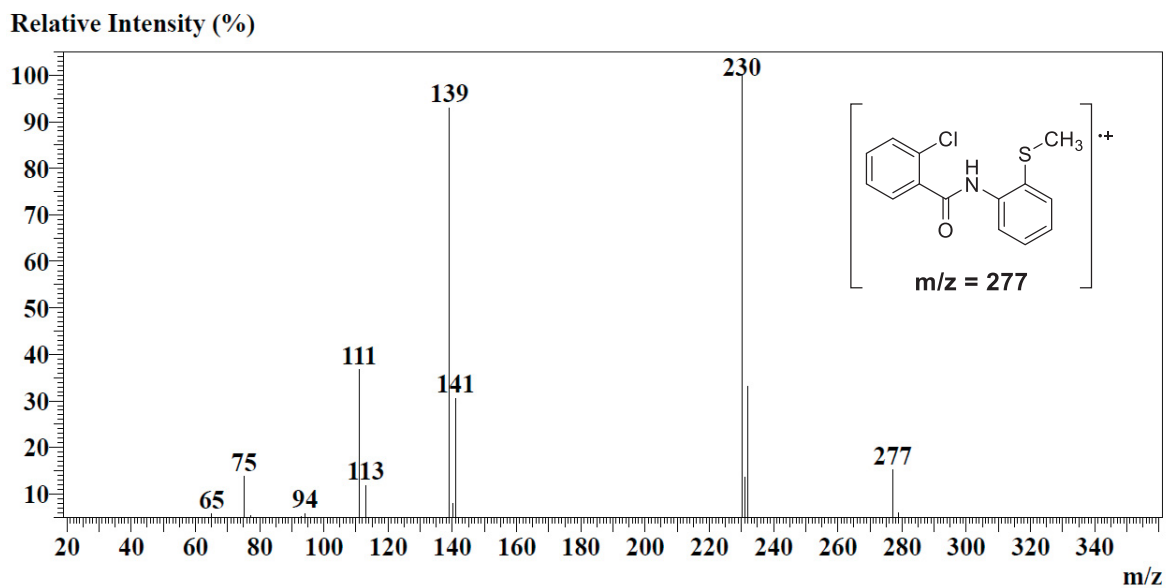


Figure 57: Mass spectrum (EI, 70 eV) of 2-chloro-*N*-(2-(methylthio)phenyl)benzamide (**7i**).

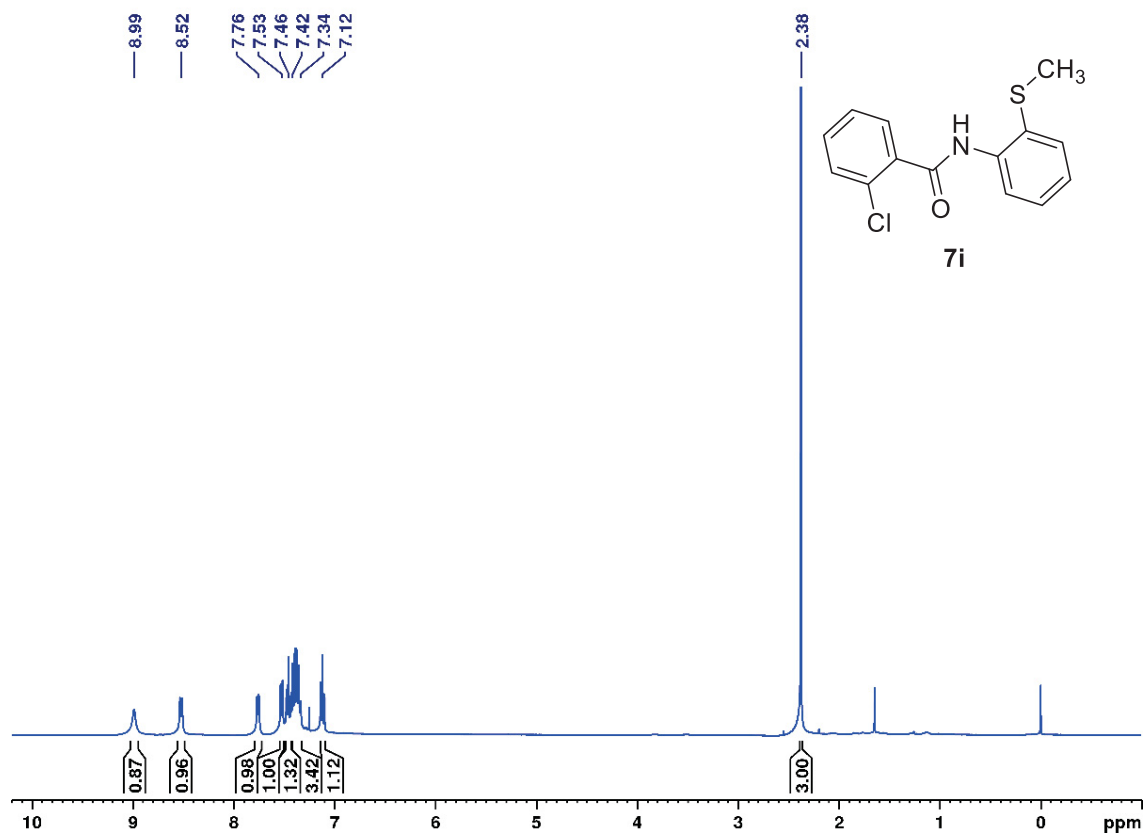


Figure 58: ^1H NMR (400 MHz, CDCl_3) of 2-chloro-*N*-(2-(methylthio)phenyl)benzamide (**7i**).

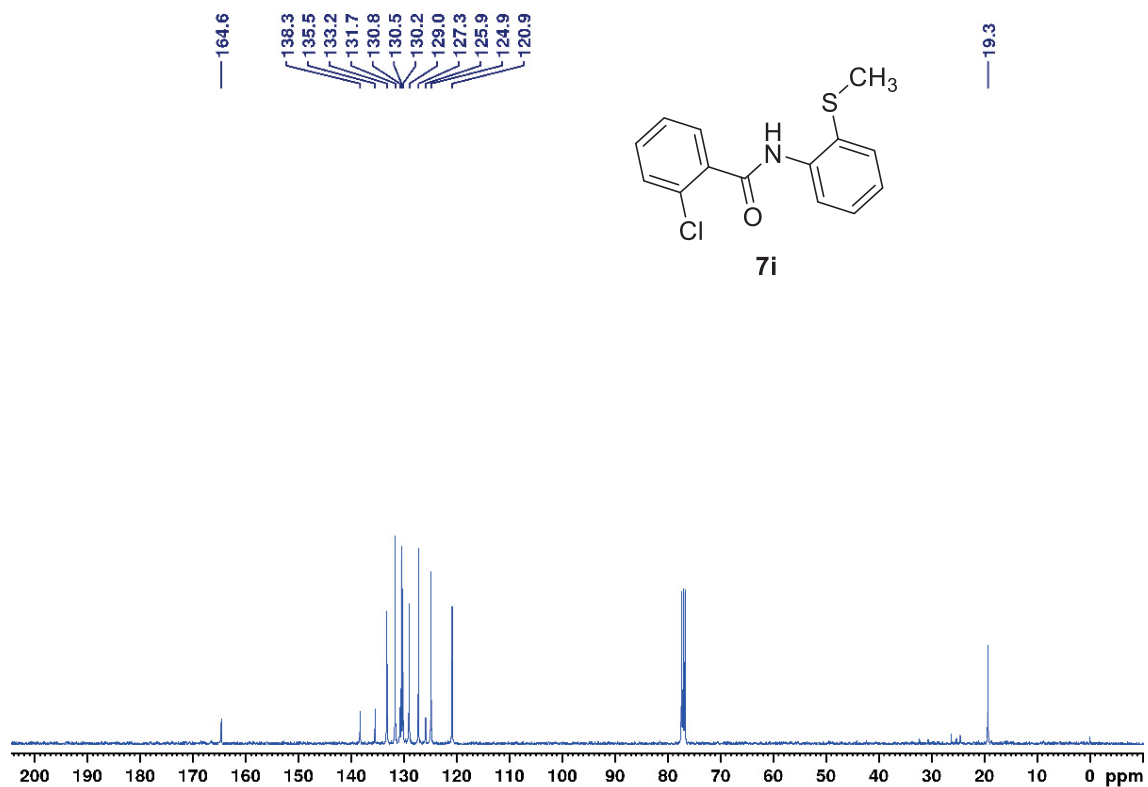


Figure 59: ^{13}C NMR (100 MHz, CDCl_3) of 2-chloro-*N*-(2-(methylthio)phenyl)benzamide (7i).

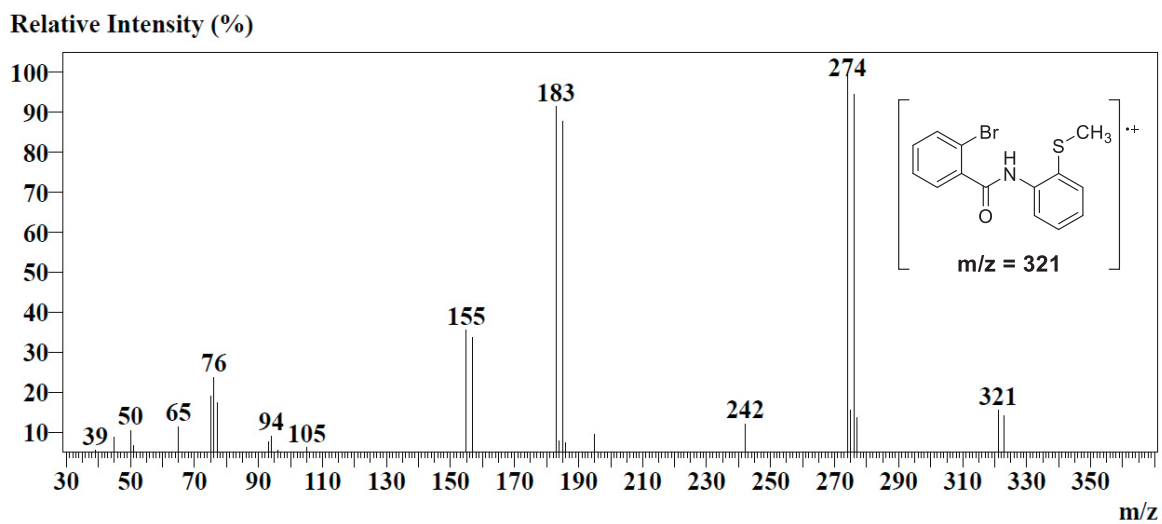


Figure 60: Mass spectrum (EI, 70 eV) of 2-bromo-*N*-(2-(methylthio)phenyl)benzamide (7j).

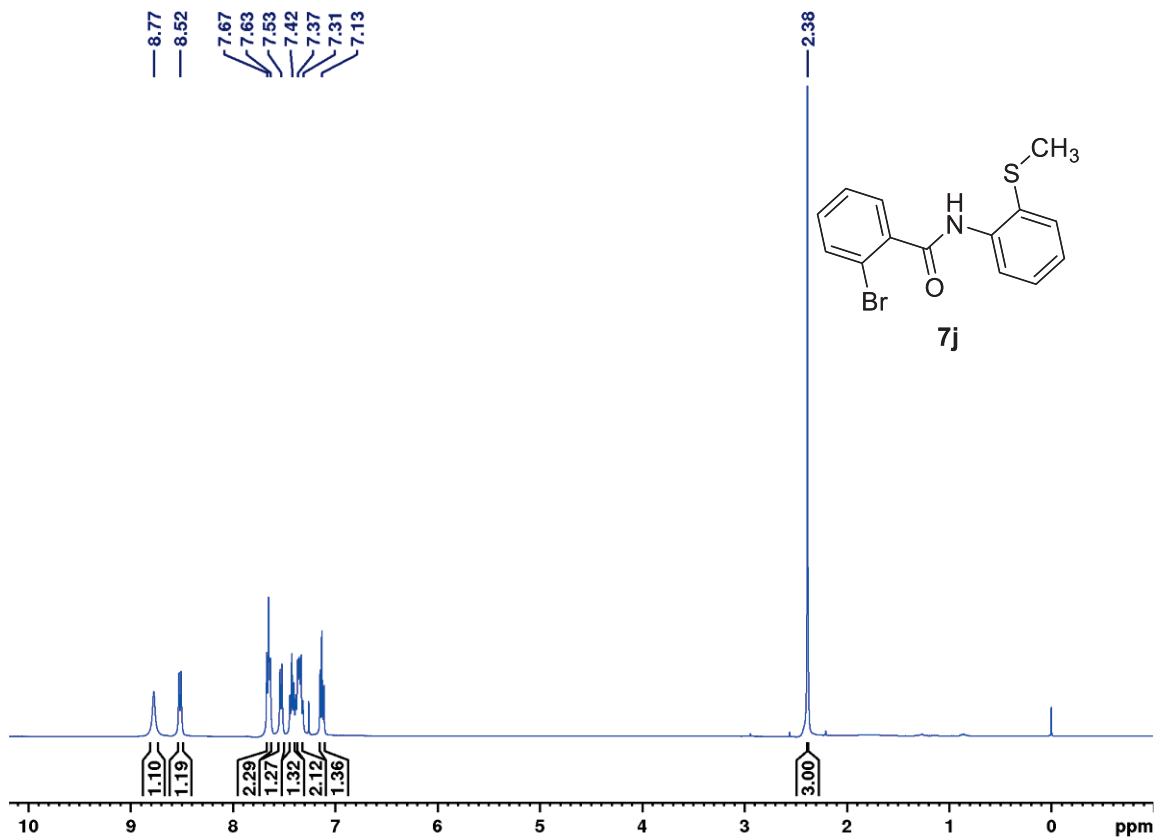


Figure 61: ¹H NMR (400 MHz, CDCl₃) of 2-bromo-N-(2-(methylthio)phenyl)benzamide (7j).

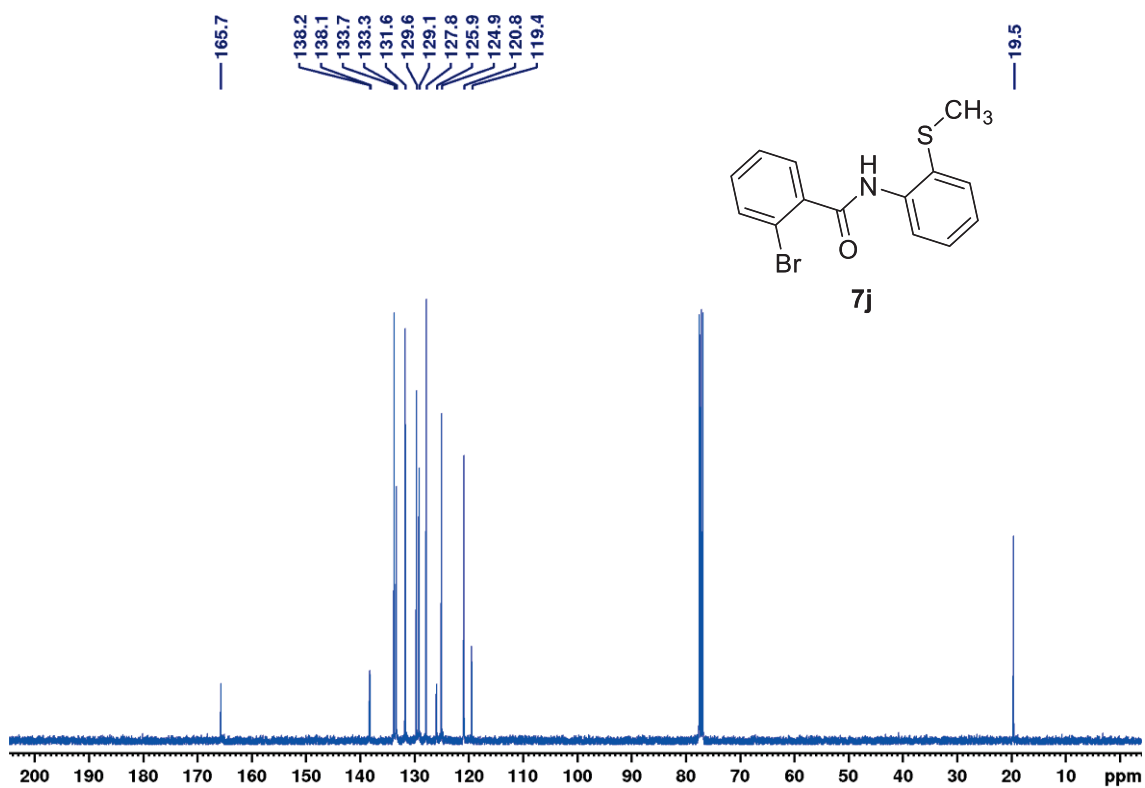


Figure 62: ¹³C NMR (100 MHz, CDCl₃) of 2-bromo-N-(2-(methylthio)phenyl)benzamide (7j).

Spectra of Compounds

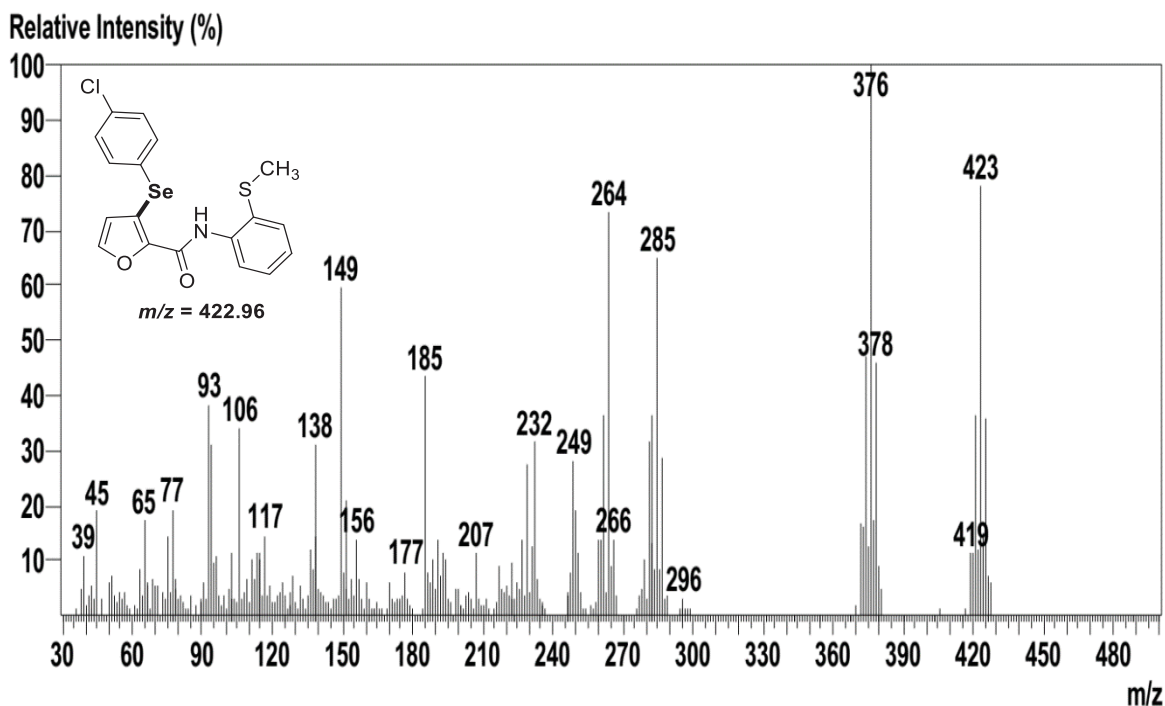


Figure 63: Mass spectrum (EI, 70 eV) of 3-((4-chlorophenyl)selenyl)-*N*-(2-(methylthio)phenyl)furan-2-carboxamide (**10b**).

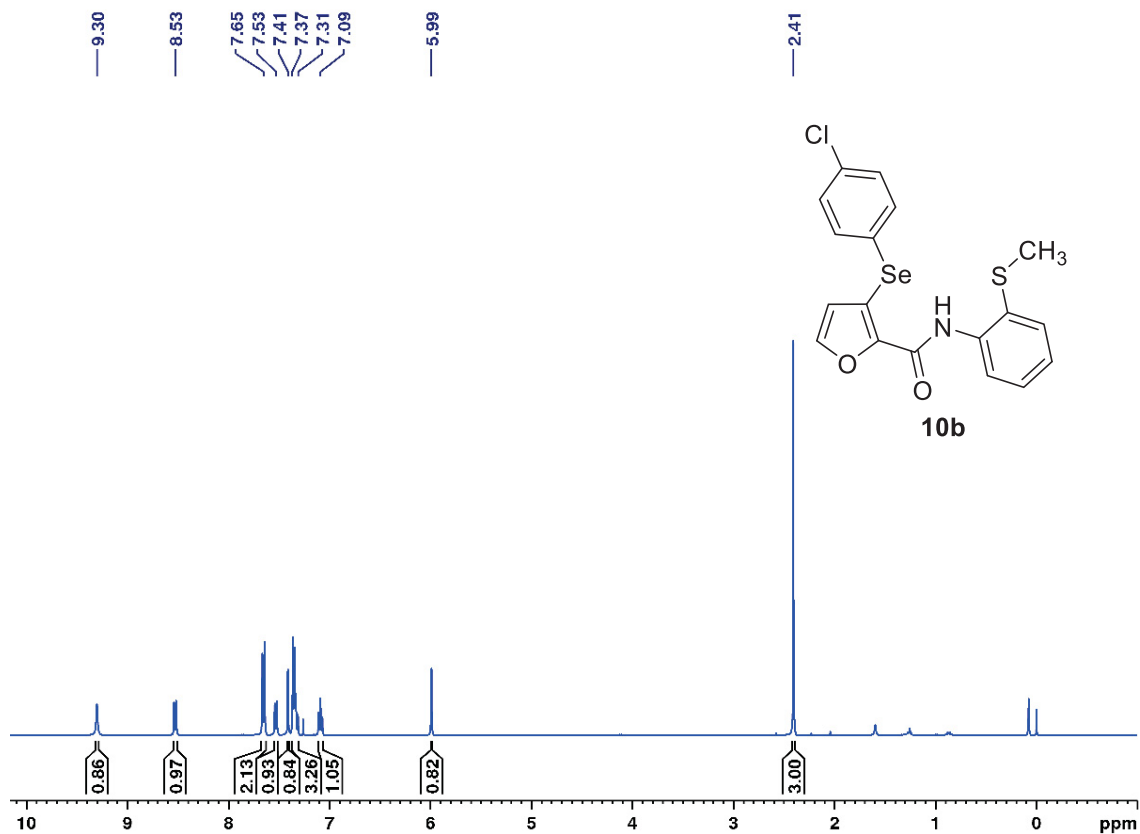


Figure 64: ^1H NMR spectrum (400 MHz, CDCl_3) of 3-((4-chlorophenyl)selenyl)-*N*-(2-(methylthio)phenyl)furan-2-carboxamide (**10b**).

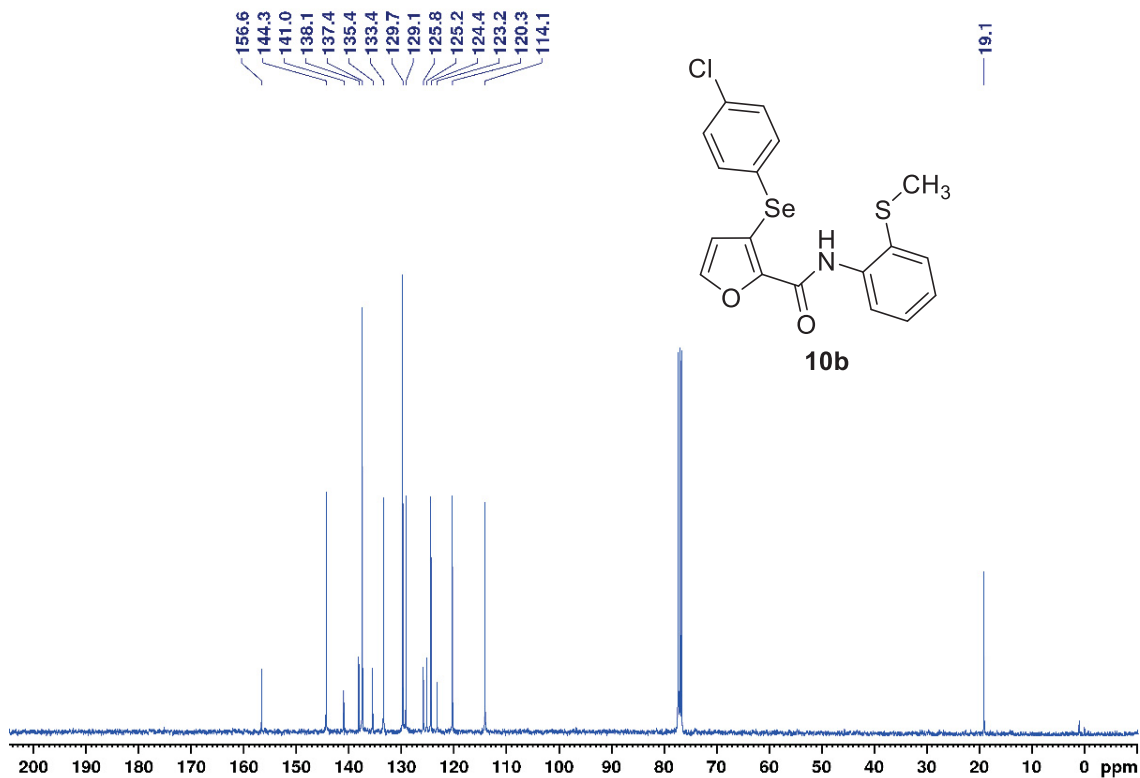


Figure 65: ¹³C NMR spectrum (100 MHz; CDCl₃) of 3-((4-chlorophenyl)selenyl)-*N*-(2-(methylthio)phenyl)furan-2-carboxamide (**10b**).

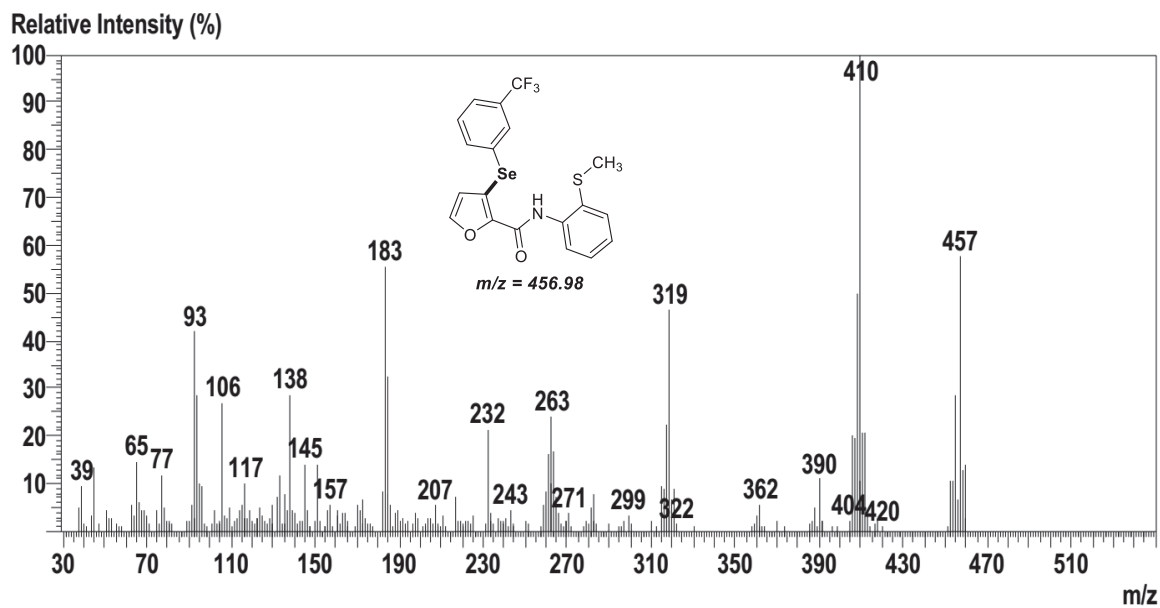


Figure 66: Mass spectrum (EI, 70 eV) of *N*-(2-(methylthio)phenyl)-3-((3-(trifluoromethyl)phenyl)selenyl)furan-2-carboxamide (**10c**).

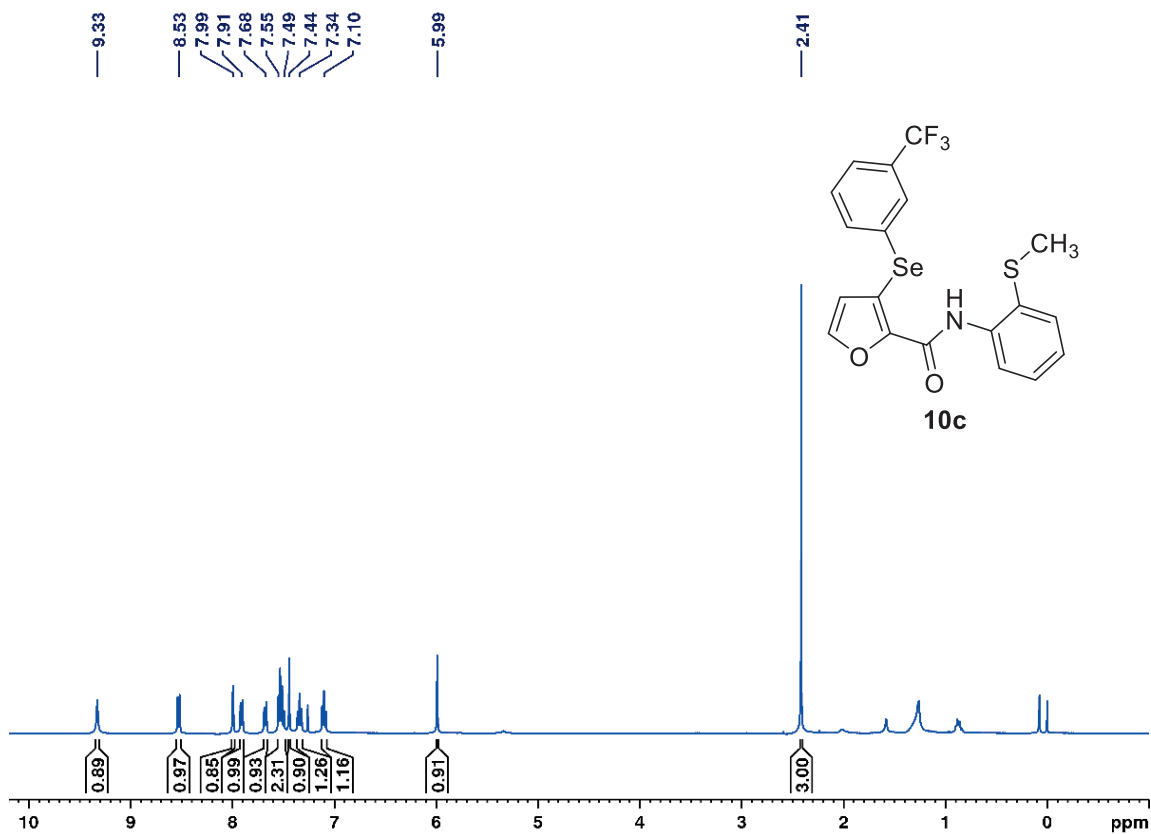


Figure 67: ¹H NMR spectrum (400 MHz, CDCl₃) of *N*-(2-(methylthio)phenyl)-3-((3-(trifluoromethyl)phenyl)selenanyl)furan-2-carboxamide (**10c**).

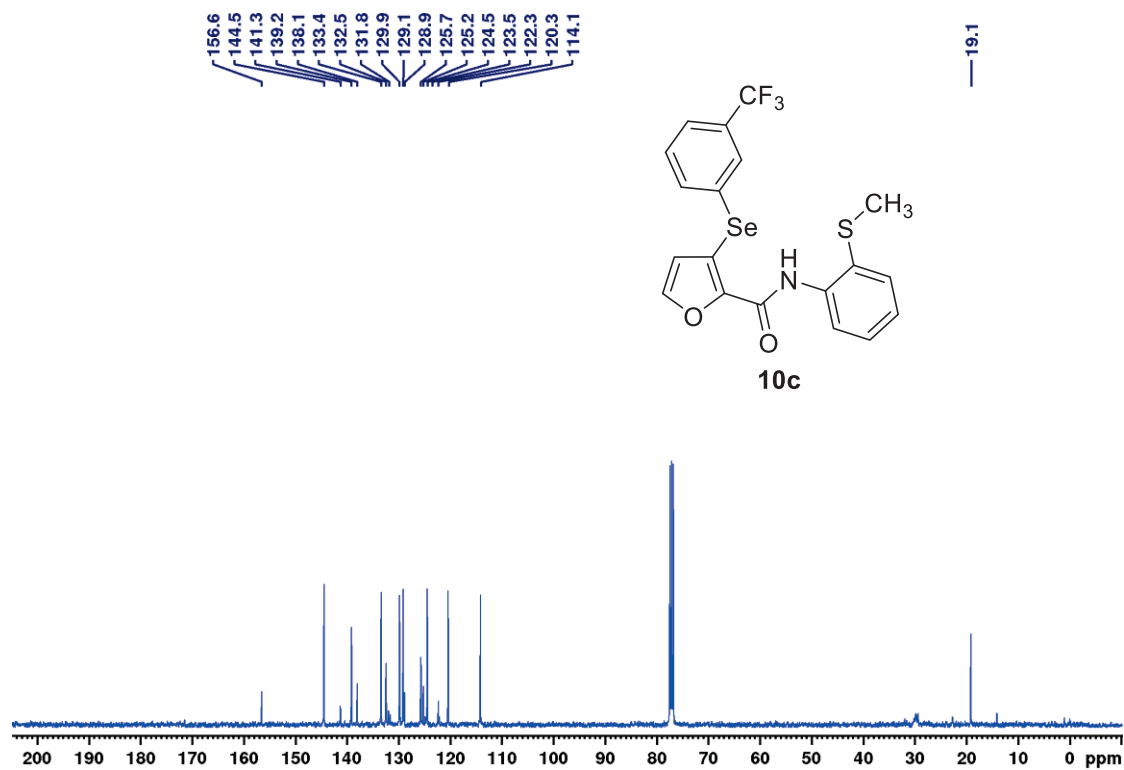


Figure 68: ¹³C NMR spectrum (100 MHz, CDCl₃) of *N*-(2-(methylthio)phenyl)-3-((3-(trifluoromethyl)phenyl)selenanyl)furan-2-carboxamide (**10c**).

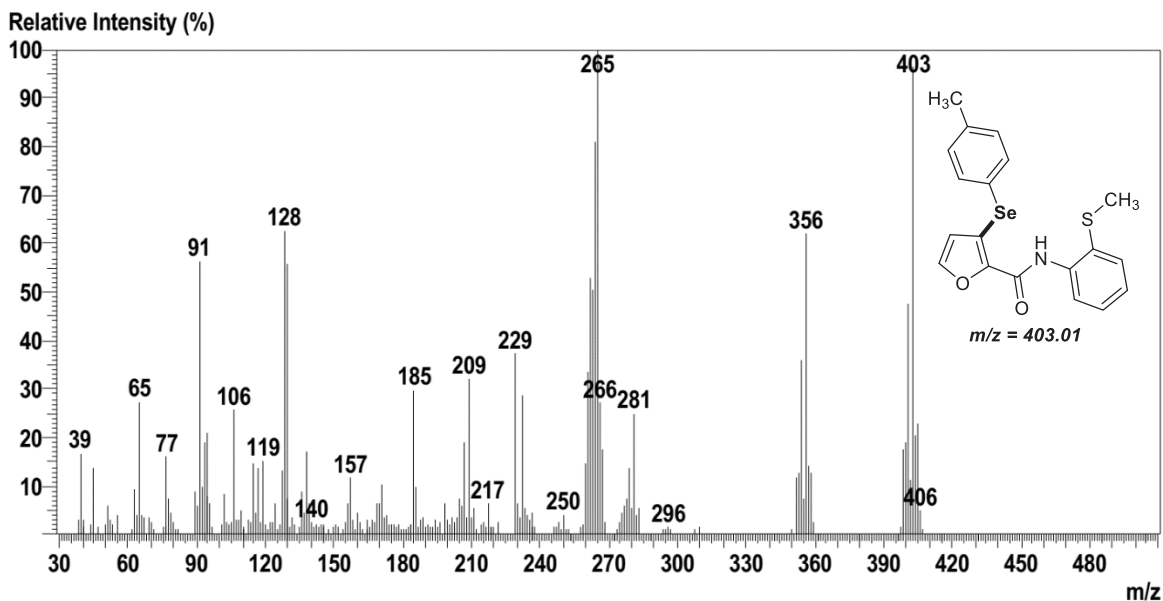


Figure 69: Mass spectrum (EI, 70 eV) of *N*-(2-(methylthio)phenyl)-3-(*p*-tolylselanyl)furan-2-carboxamide (**10d**).

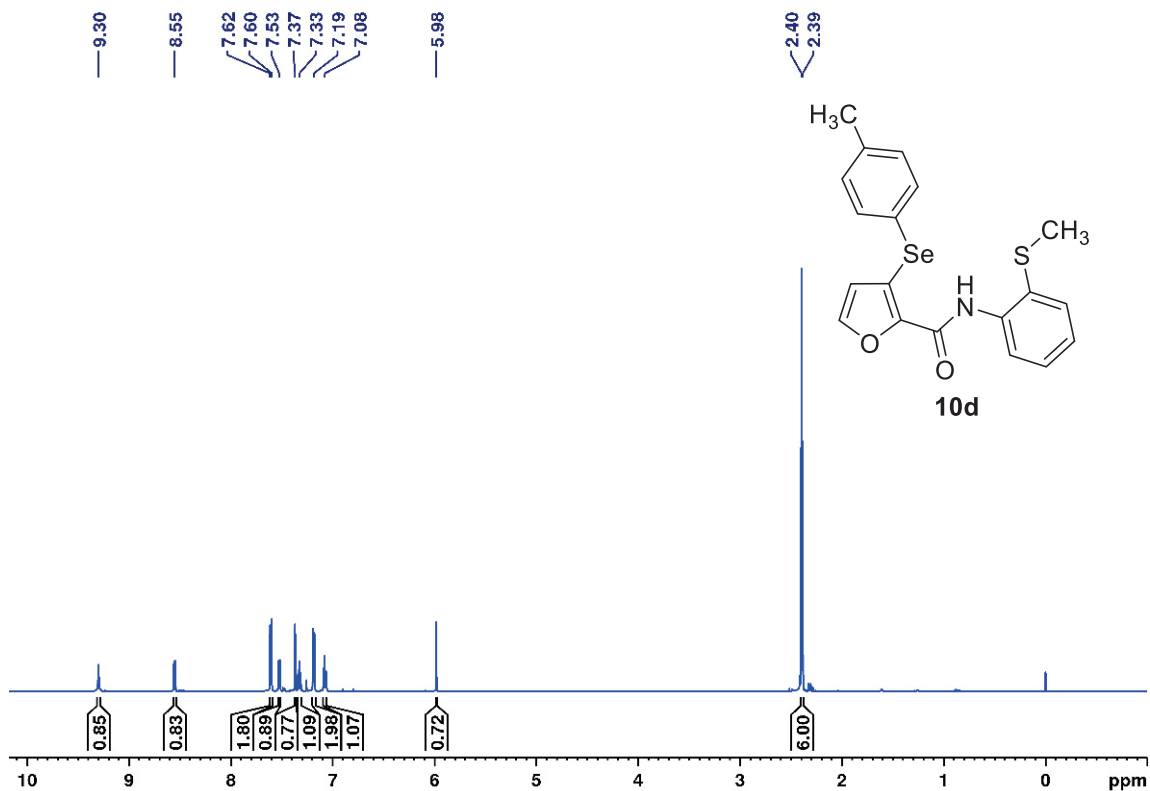


Figure 70: ^1H NMR spectrum (400 MHz, CDCl_3) of *N*-(2-(methylthio)phenyl)-3-(*p*-tolylselanyl)furan-2-carboxamide (**10d**).

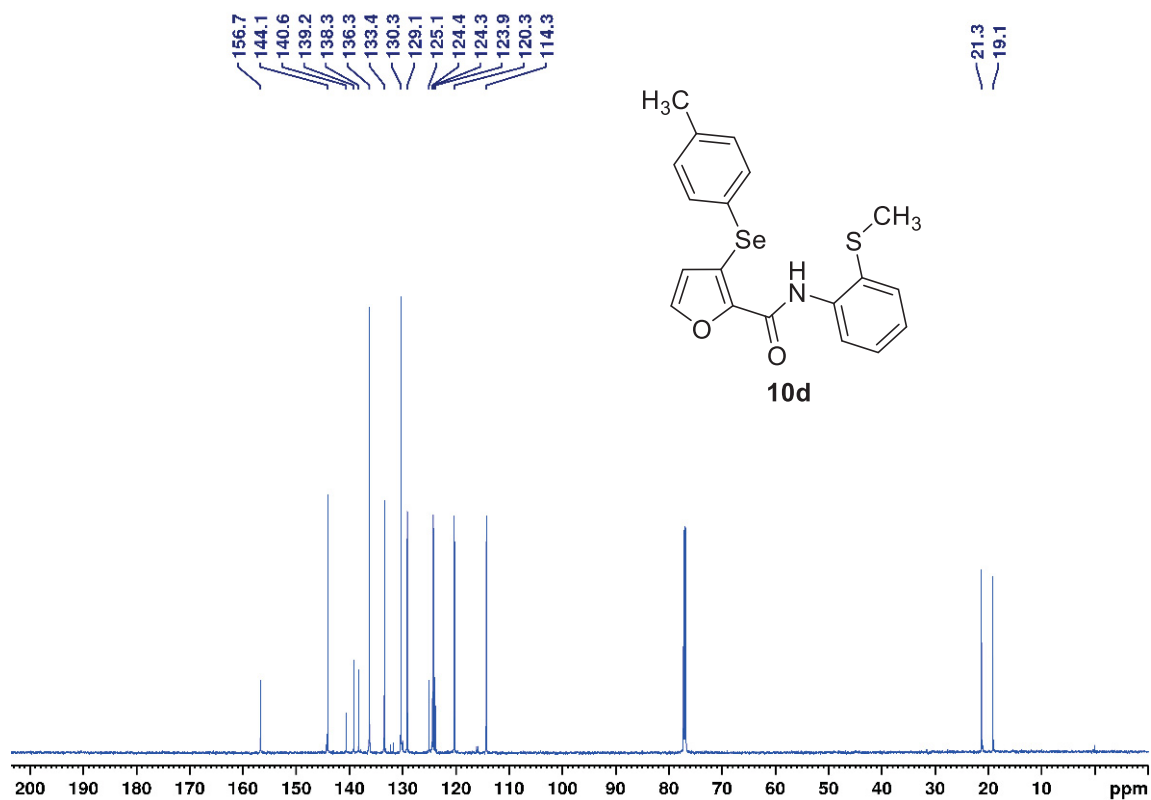


Figure 71: ¹³C NMR spectrum (100 MHz; CDCl₃) of *N*-(2-(methylthio)phenyl)-3-(*p*-tolylselanyl)furan-2-carboxamide (**10d**).

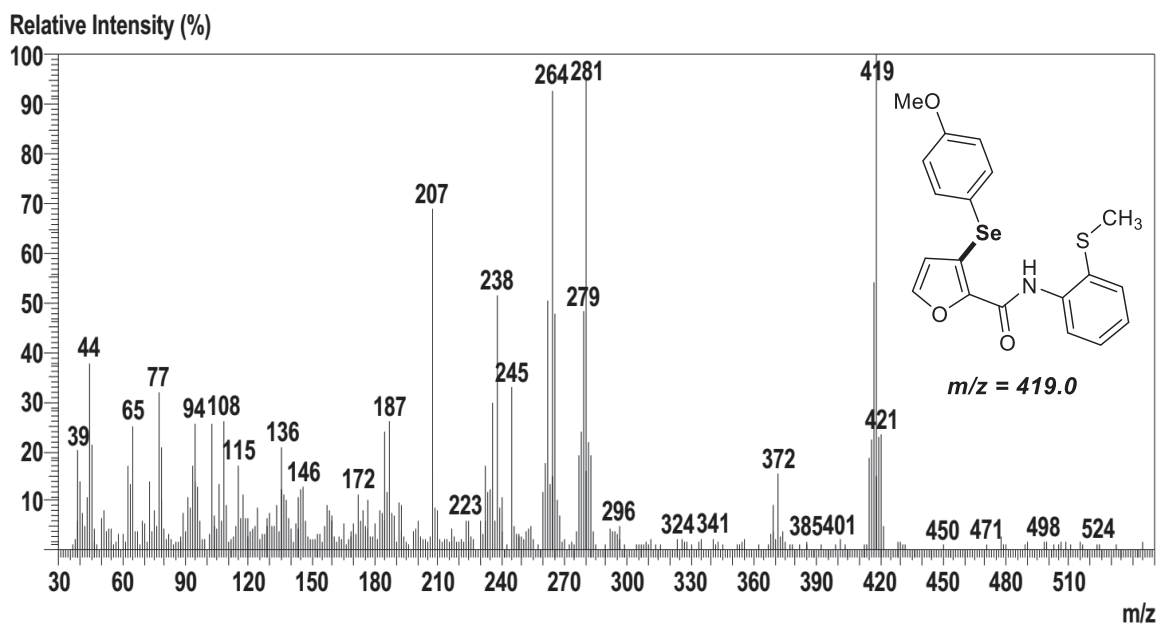


Figure 72: Mass spectrum (EI, 70 eV) of 3-((4-methoxyphenyl)selanyl)-*N*-(2-(methylthio)phenyl)furan-2-carboxamide (**10e**).

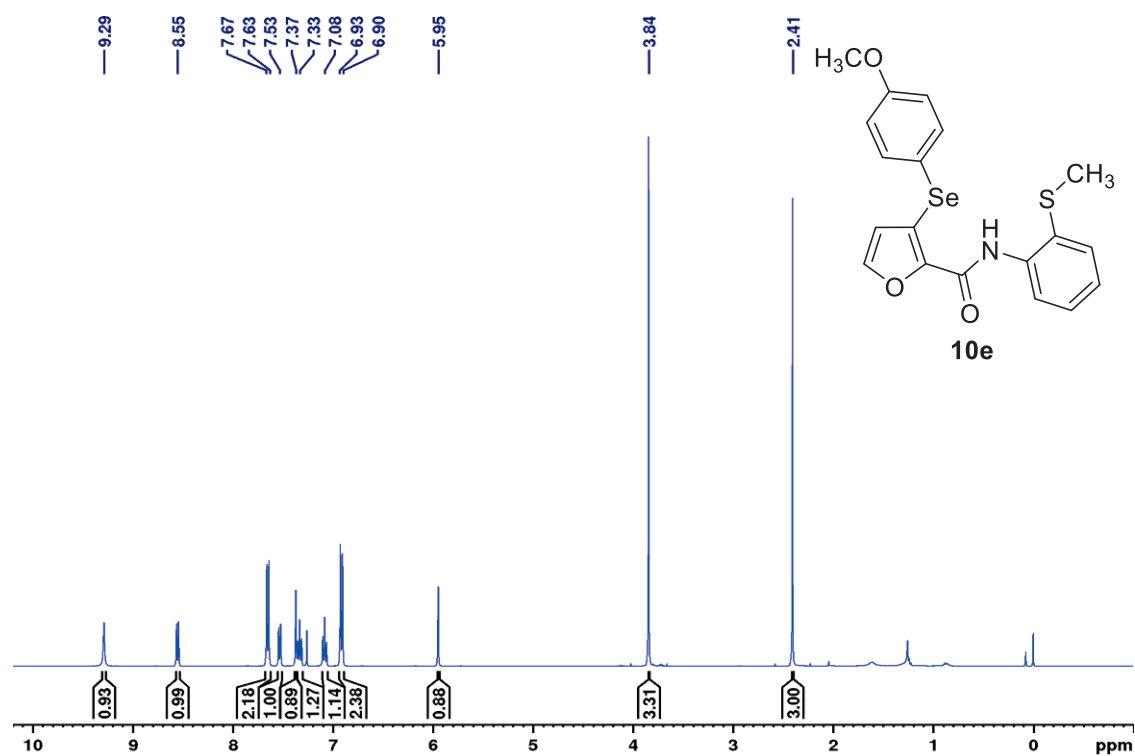


Figure 73: ¹H NMR spectrum (400 MHz, CDCl₃) of 3-((4-methoxyphenyl)selanyl)-N-(2-(methylthio)phenyl)furan-2-carboxamide (**10e**).

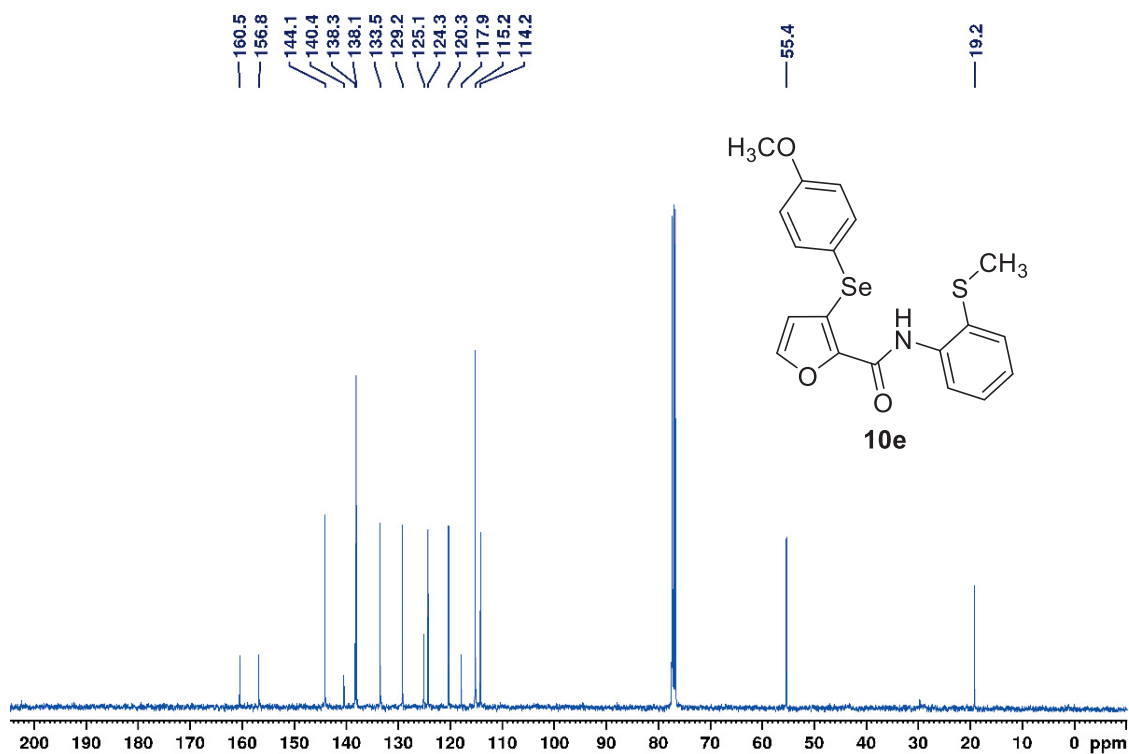


Figure 74: ¹³C NMR spectrum (100 MHz, CDCl₃) of 3-((4-methoxyphenyl)selanyl)-N-(2-(methylthio)phenyl)furan-2-carboxamide (**10e**).

Relative Intensity (%)

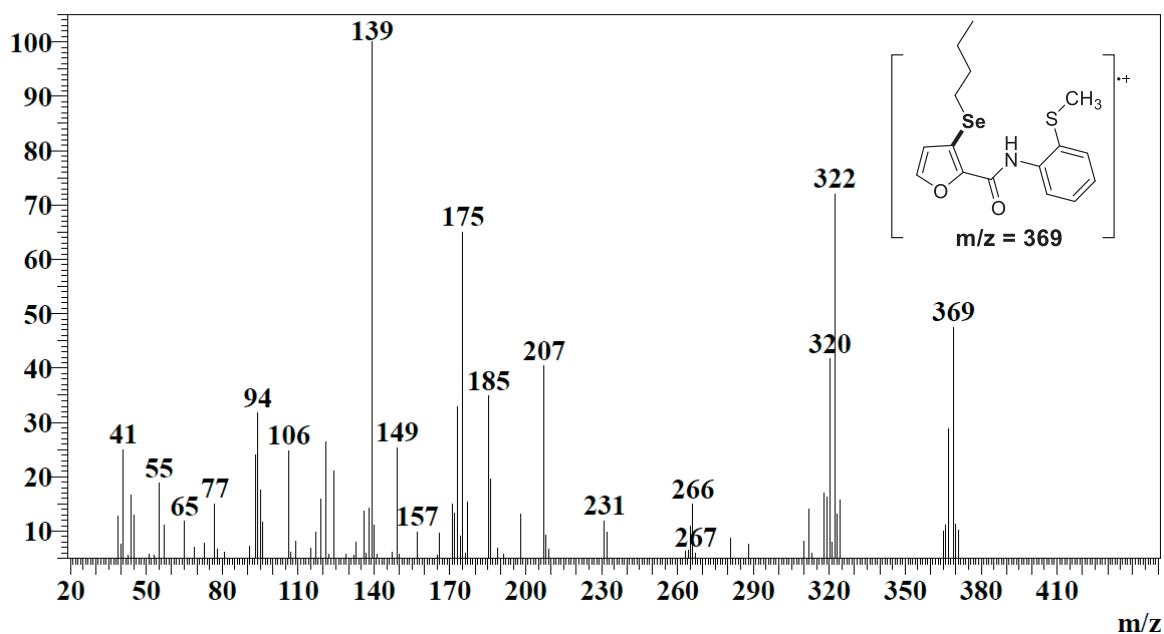


Figure 75: Mass spectrum (EI, 70 eV) of 3-(butylselanyl)-N-(2-(methylthio)phenyl)furan-2-carboxamide (**10f**).

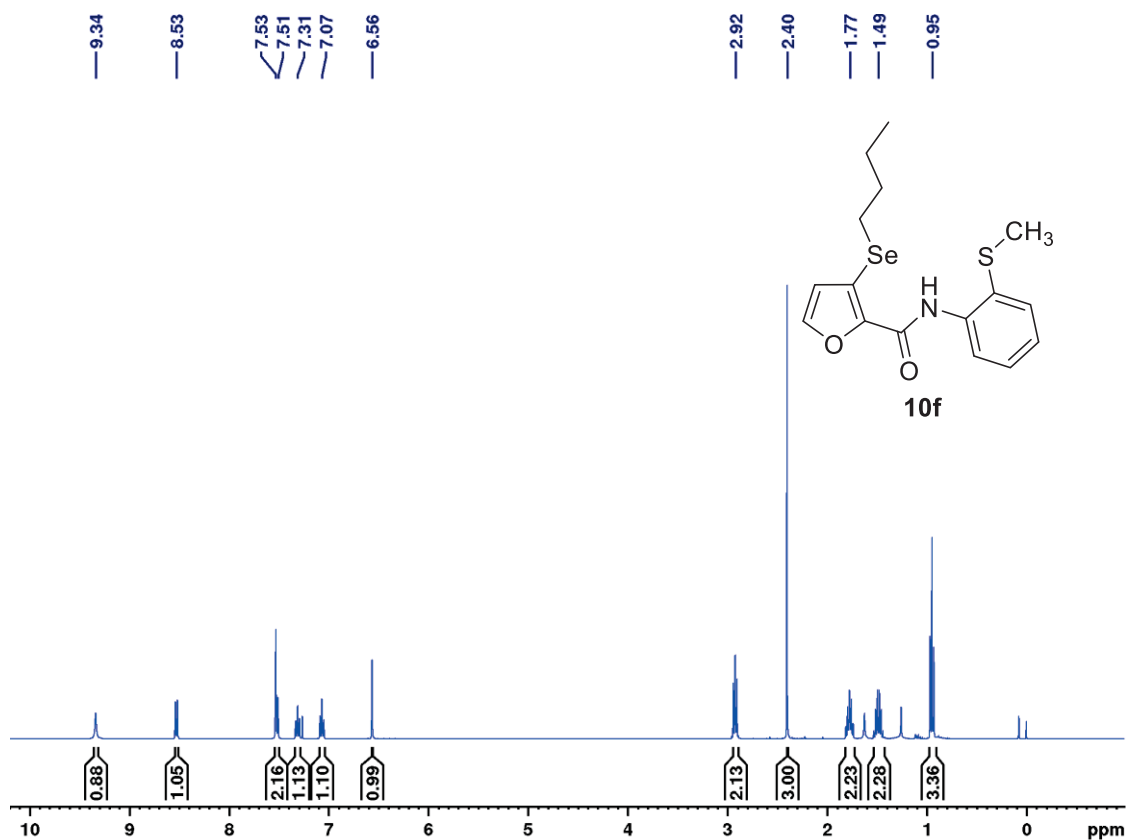


Figure 76: ^1H NMR spectrum (400 MHz, CDCl_3) of 3-(butylselanyl)-N-(2-(methylthio)phenyl)furan-2-carboxamide (**10f**).

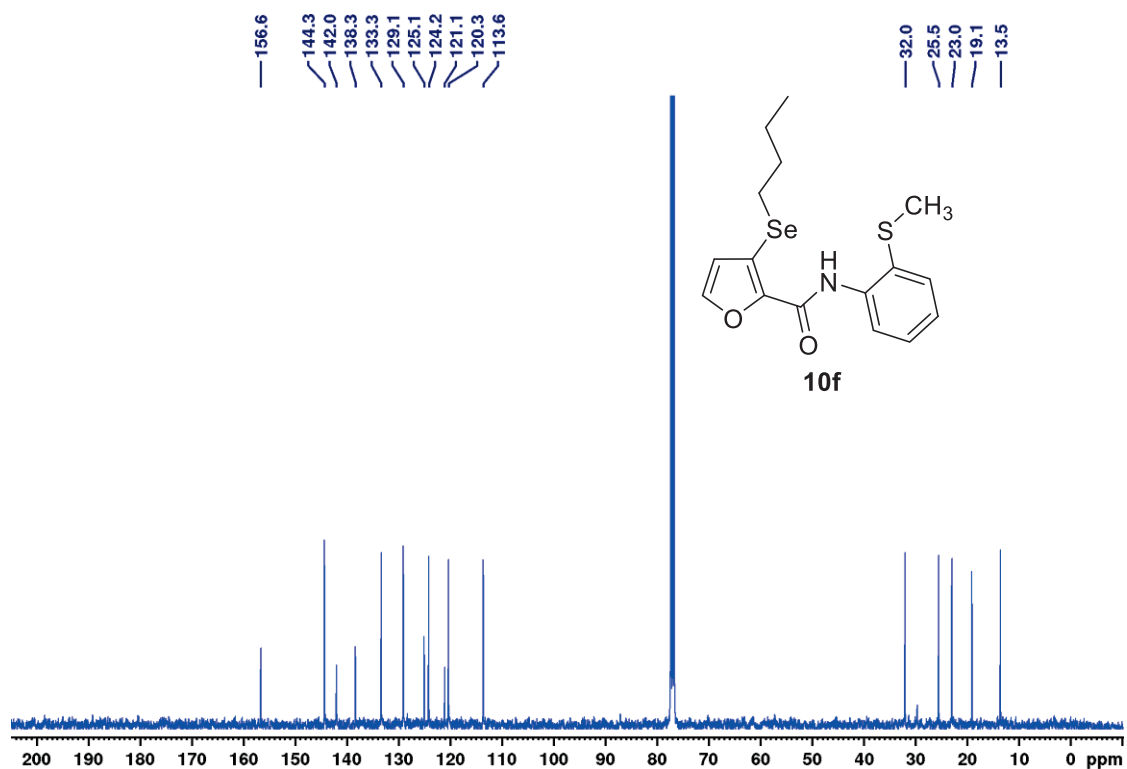


Figure 77: ^{13}C NMR spectrum (100 MHz; CDCl_3) of 3-(butylselanyl)-*N*-(2-(methylthio)phenyl)furan-2-carboxamide (**10f**).

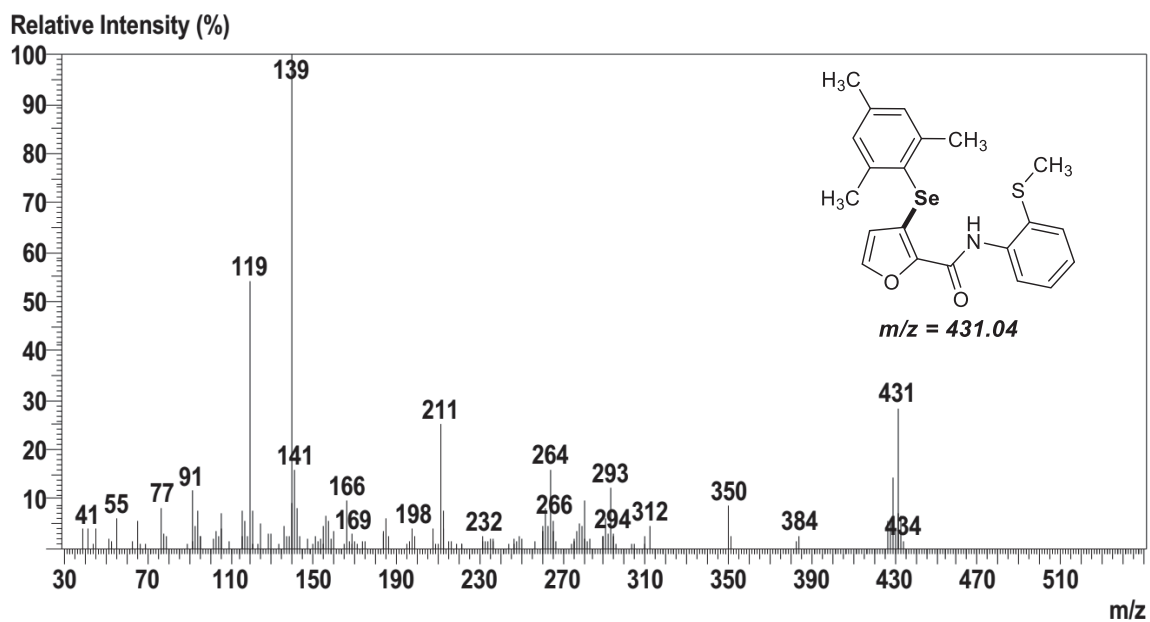


Figure 78: Mass spectrum (EI, 70 eV) of 3-(mesitylselanyl)-*N*-(2-(methylthio)phenyl)furan-2-carboxamide (**10g**).

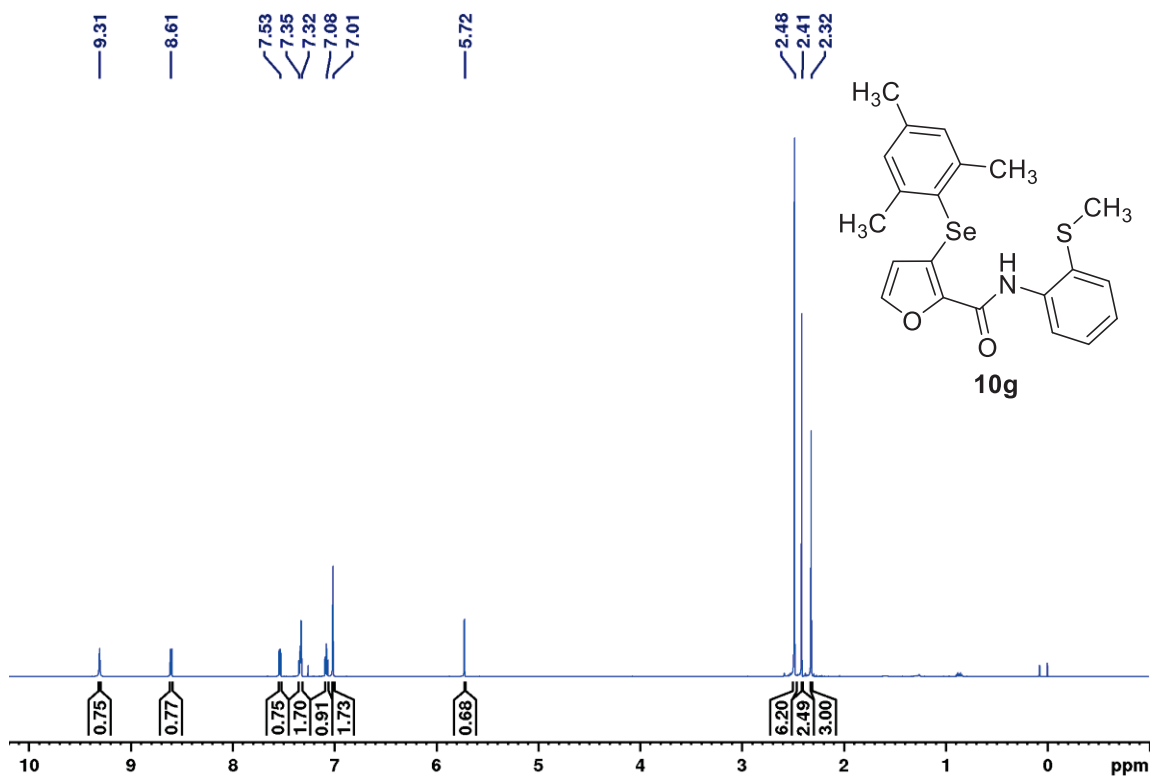


Figure 79: $^1\text{H NMR}$ spectrum (400 MHz, CDCl_3) of 3-(mesitylselanyl)-*N*-(2-(methylthio)phenyl)furan-2-carboxamide (**10g**).

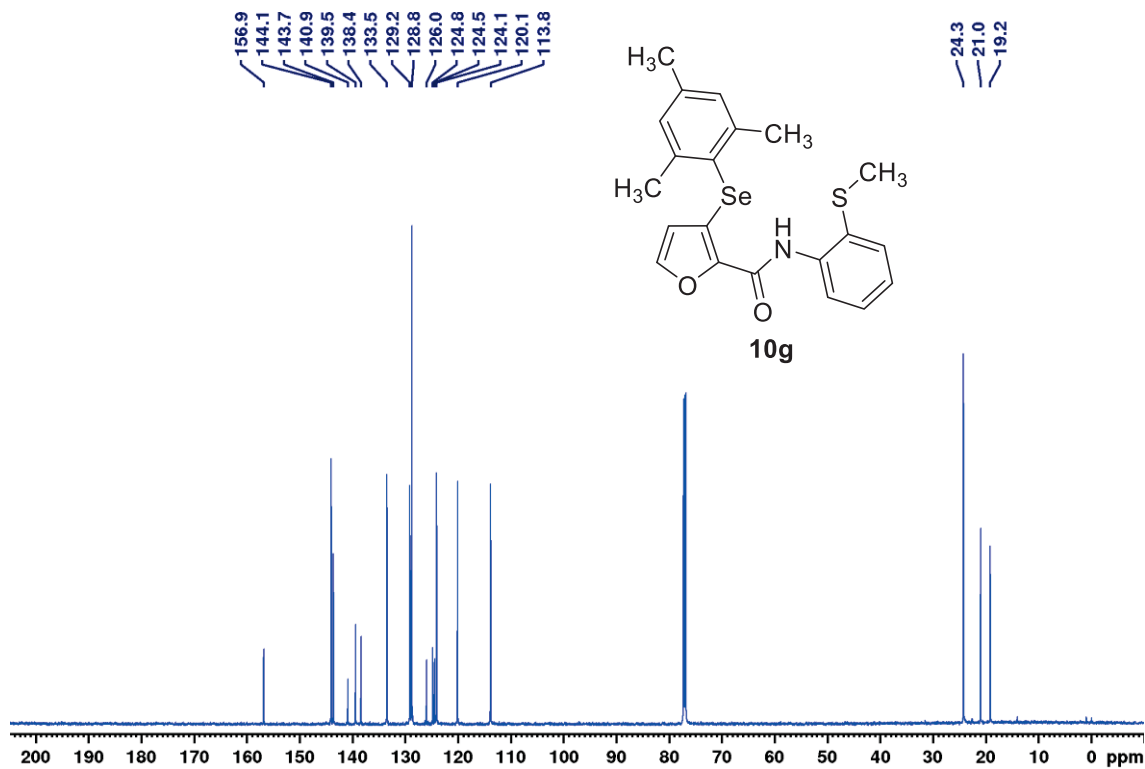


Figure 80: $^{13}\text{C NMR}$ spectrum (100 MHz, CDCl_3) of 3-(mesitylselanyl)-*N*-(2-(methylthio)phenyl)furan-2-carboxamide (**10g**).

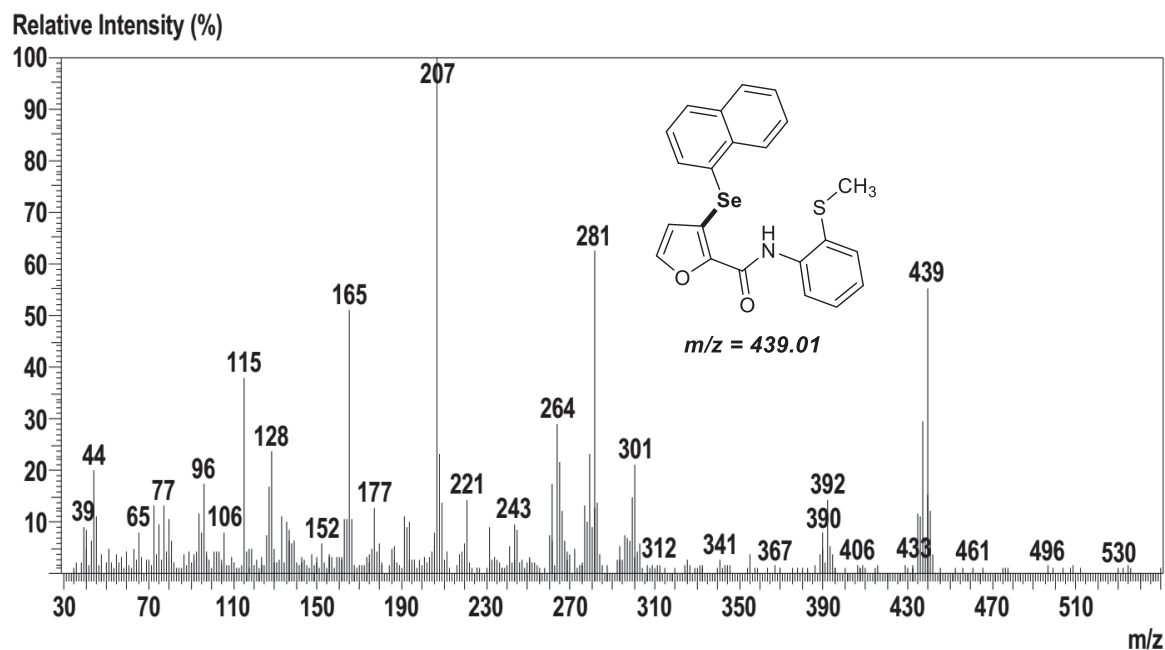


Figure 81: Mass spectrum (EI, 70 eV) of *N*-(2-(methylthio)phenyl)-3-(naphthalen-1-ylselanyl)furan-2-carboxamide (**10h**).

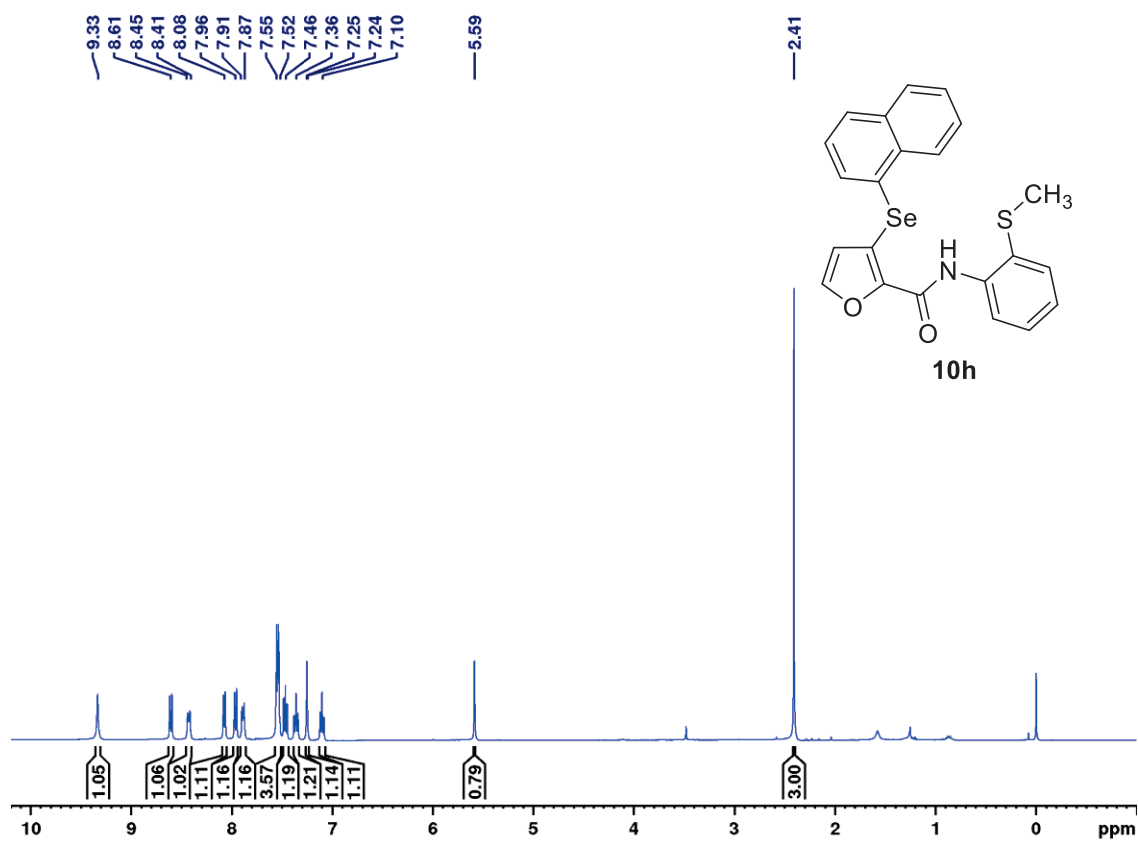


Figure 82: ^1H NMR spectrum (400 MHz, CDCl_3) of *N*-(2-(methylthio)phenyl)-3-(naphthalen-1-ylselanyl)furan-2-carboxamide (**10h**).

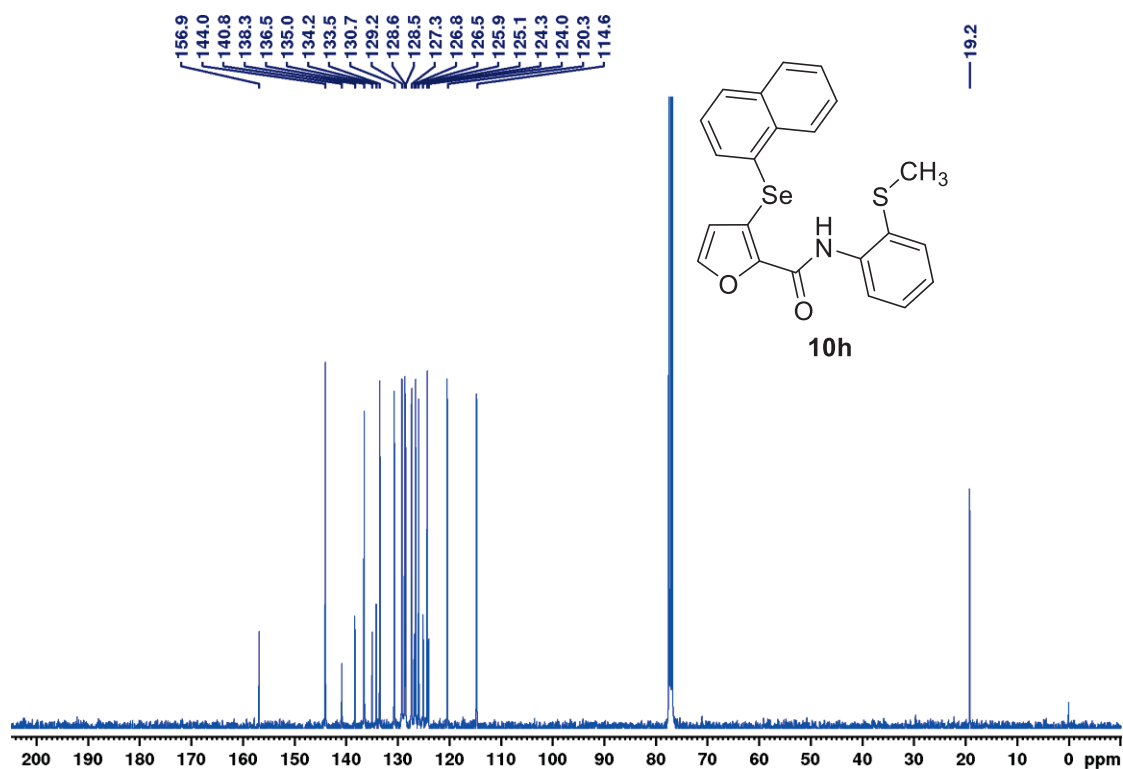


Figure 83: ¹³C NMR spectrum (100 MHz; CDCl₃) of *N*-(2-(methylthio)phenyl)-3-(naphthalen-1-ylselanyl)furan-2-carboxamide (**10h**).

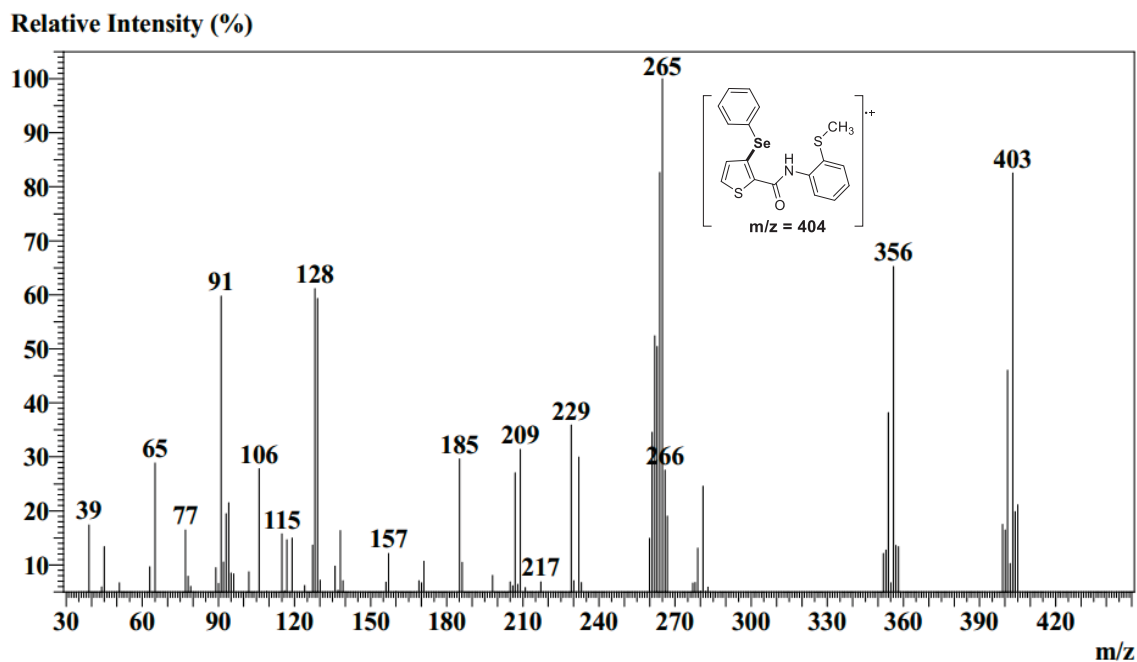


Figure 84: Mass spectrum (EI, 70 eV) of *N*-(2-(methylthio)phenyl)-3-(phenylselanyl)thiophene-2-carboxamide (**10i**).

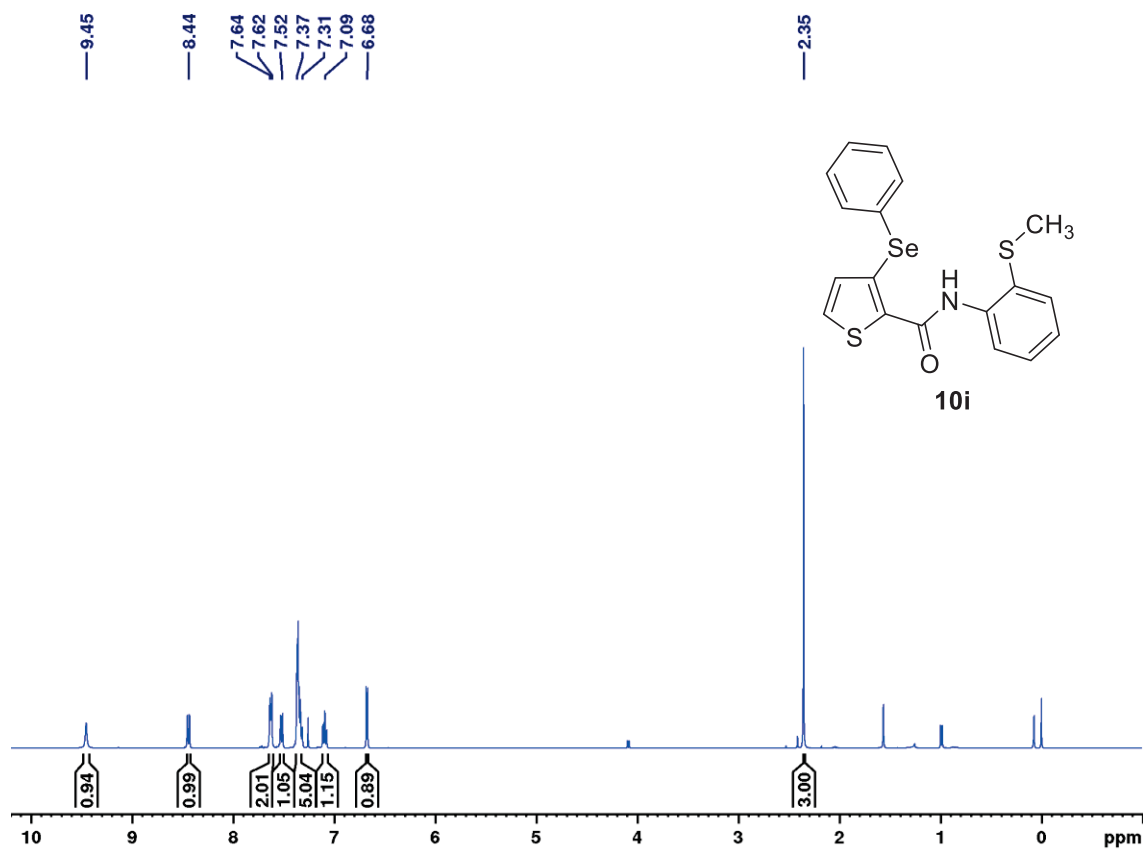


Figure 85: ¹H NMR spectrum (400 MHz, CDCl₃) of *N*-(2-(methylthio)phenyl)-3-(phenylselanyl)thiophene-2-carboxamide (**10i**).

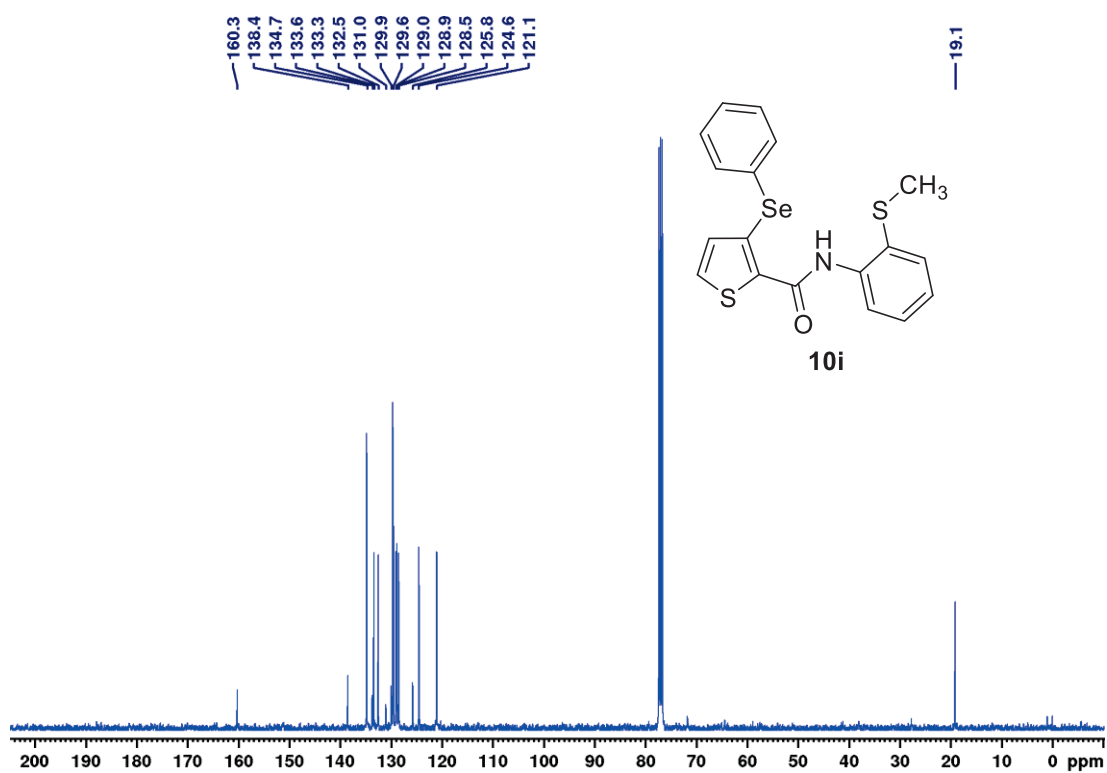


Figure 86: ¹³C NMR spectrum (100 MHz, CDCl₃) of *N*-(2-(methylthio)phenyl)-3-(phenylselanyl)thiophene-2-carboxamide (**10i**).

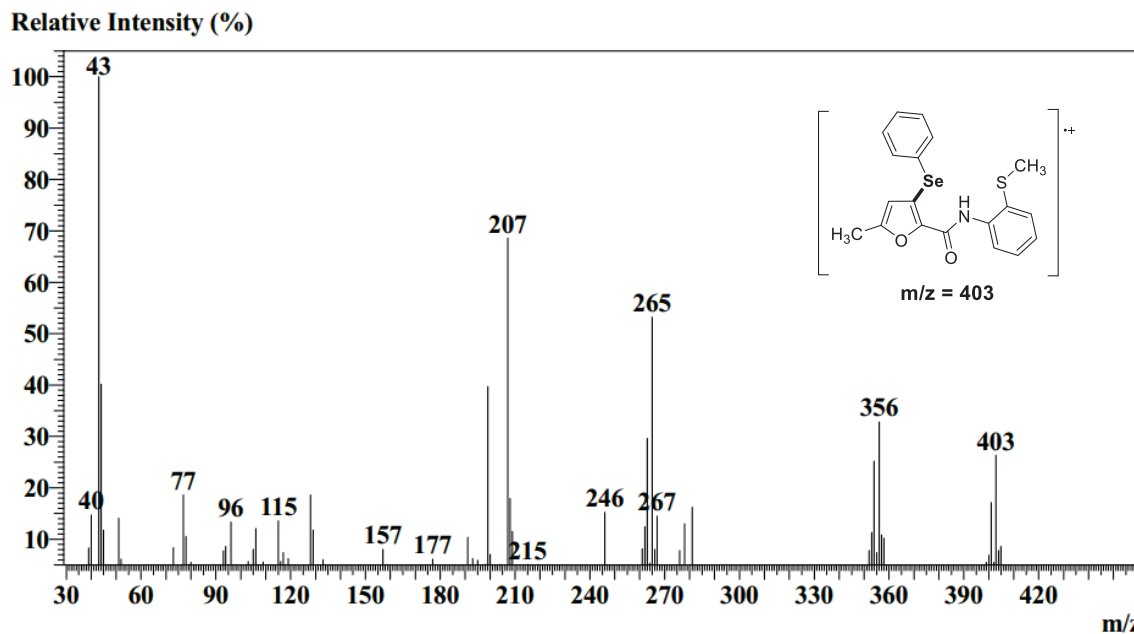


Figure 87: Mass spectrum (EI, 70 eV) of 5-methyl-*N*-(2-(methylthio)phenyl)-3-(phenylselanyl)furan-2-carboxamide (**10j**).

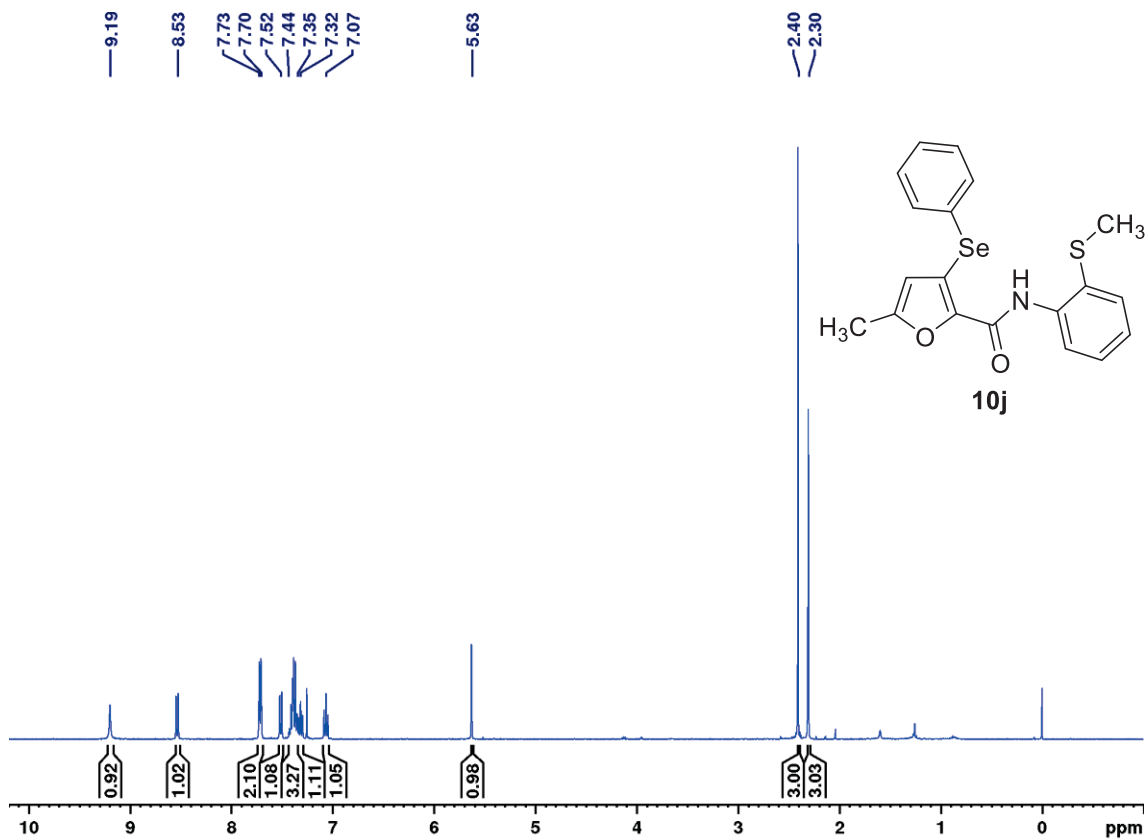


Figure 88: ^1H NMR Spectrum (400 MHz, CDCl_3) of 5-methyl-*N*-(2-(methylthio)phenyl)-3-(phenylselanyl)furan-2-carboxamide (**10j**).

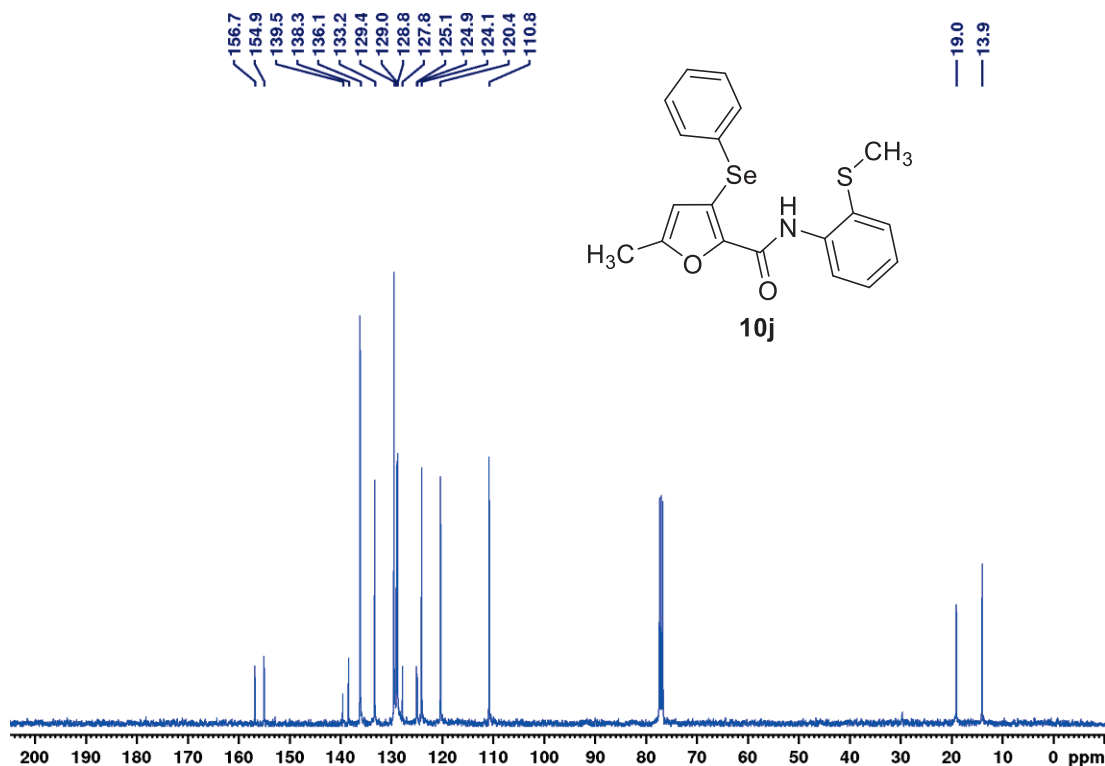


Figure 89: ^{13}C NMR Spectrum (100 MHz, CDCl_3) of 5-methyl-*N*-(2-(methylthio)phenyl)-3-(phenylselanyl)furan-2-carboxamide (**10j**).

Relative Intensity (%)

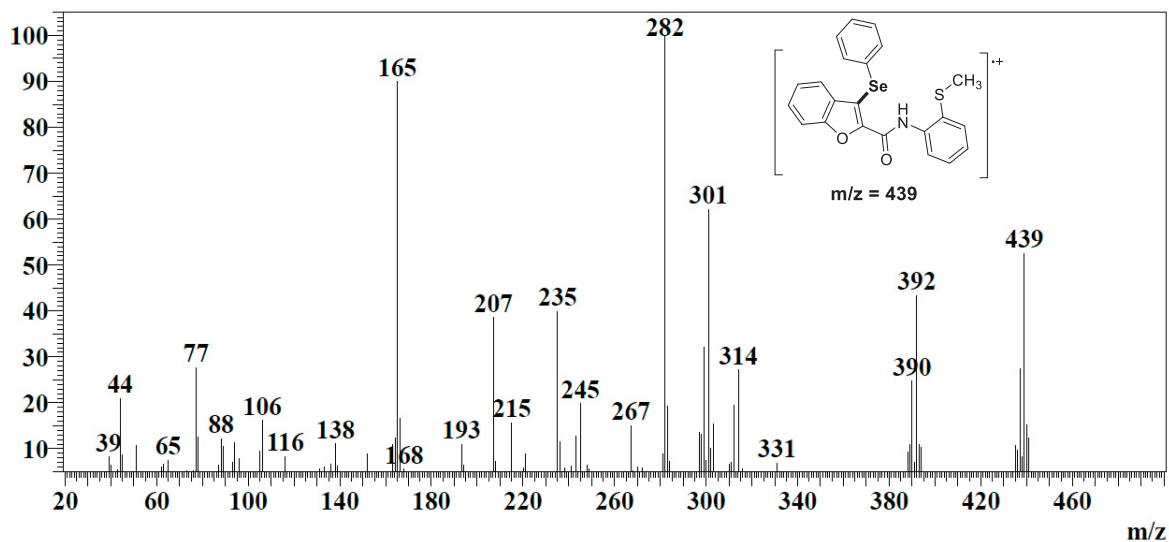


Figure 90: Mass spectrum (EI, 70 eV) of *N*-(2-(methylthio)phenyl)-3-(phenylselanyl)benzofuran-2-carboxamide (**10k**).

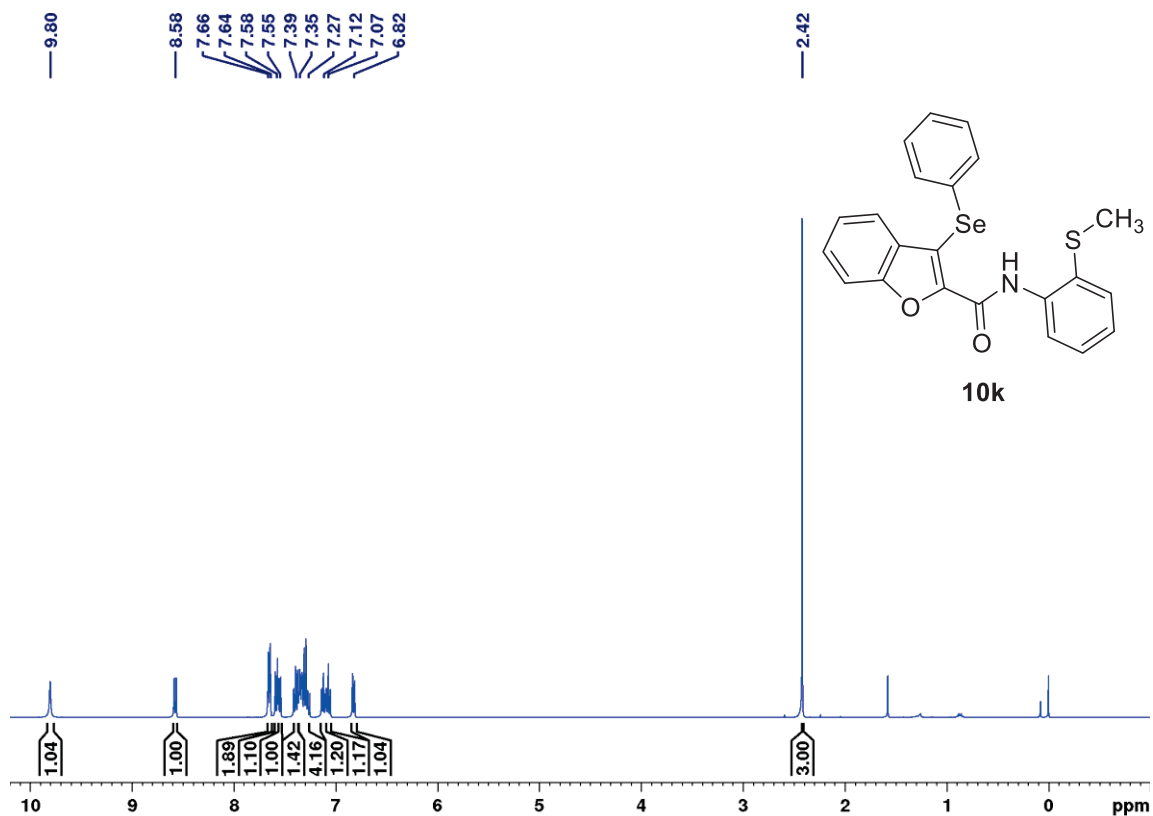


Figure 91: ^1H NMR Spectrum (400 MHz, CDCl_3) of *N*-(2-(methylthio)phenyl)-3-(phenylselanyl)benzofuran-2-carboxamide (**10k**).

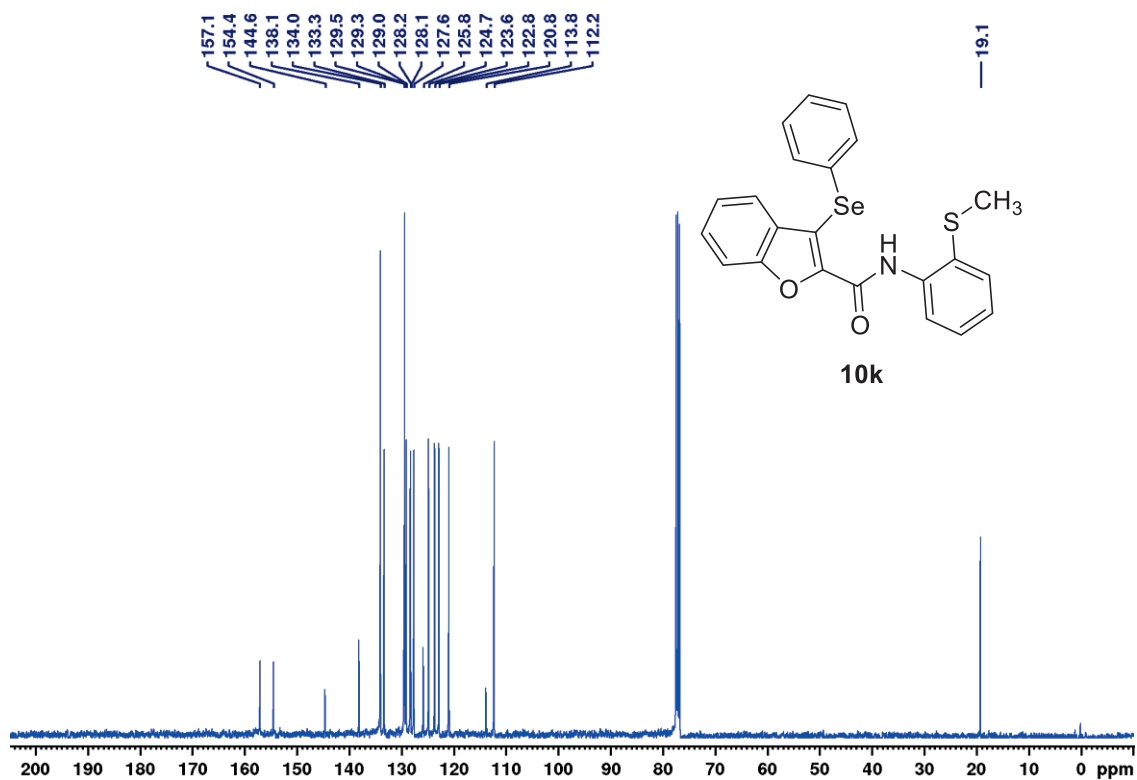


Figure 92: ^{13}C NMR Spectrum (100 MHz, CDCl_3) of *N*-(2-(methylthio)phenyl)-3-(phenylselanyl)benzofuran-2-carboxamide (**10k**).

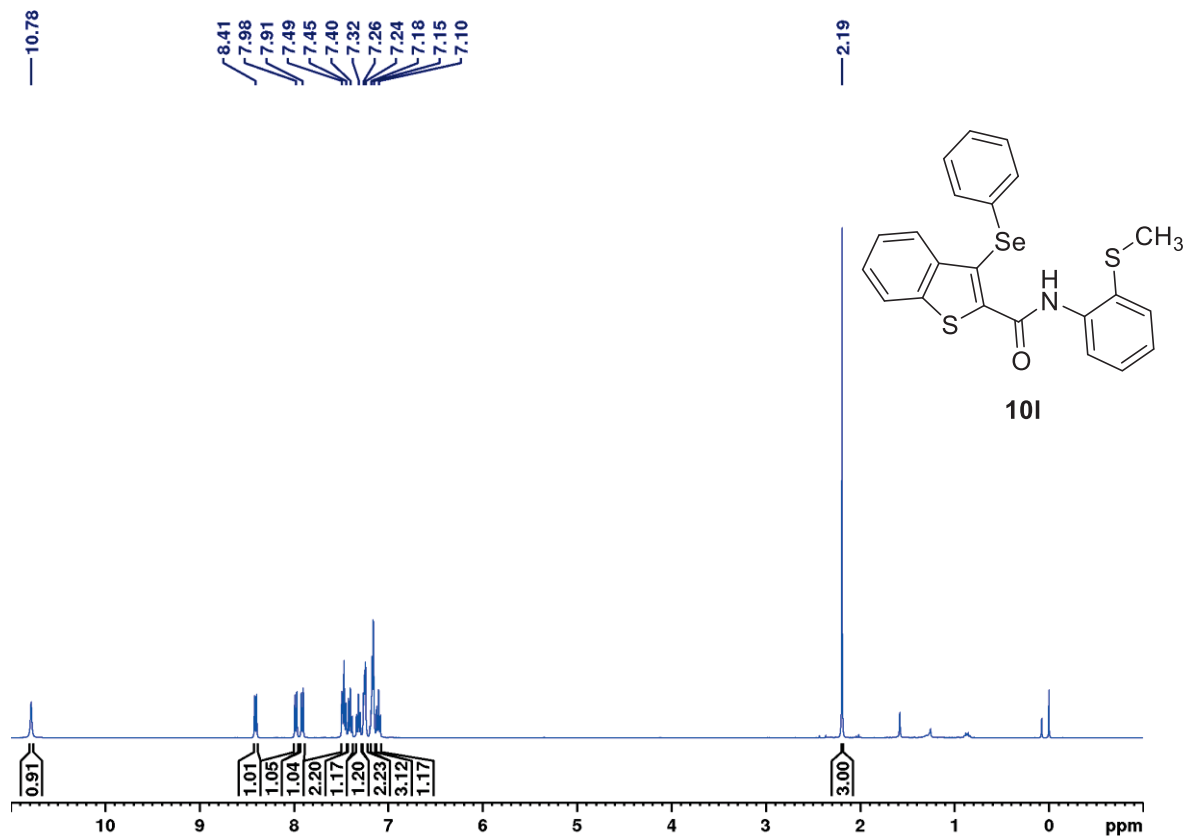


Figure 93: ¹H NMR Spectrum (400 MHz, CDCl₃) of *N*-(2-(methylthio)phenyl)-3-(phenylselanyl)benzo[*b*]thiophene-2-carboxamide (**10I**).

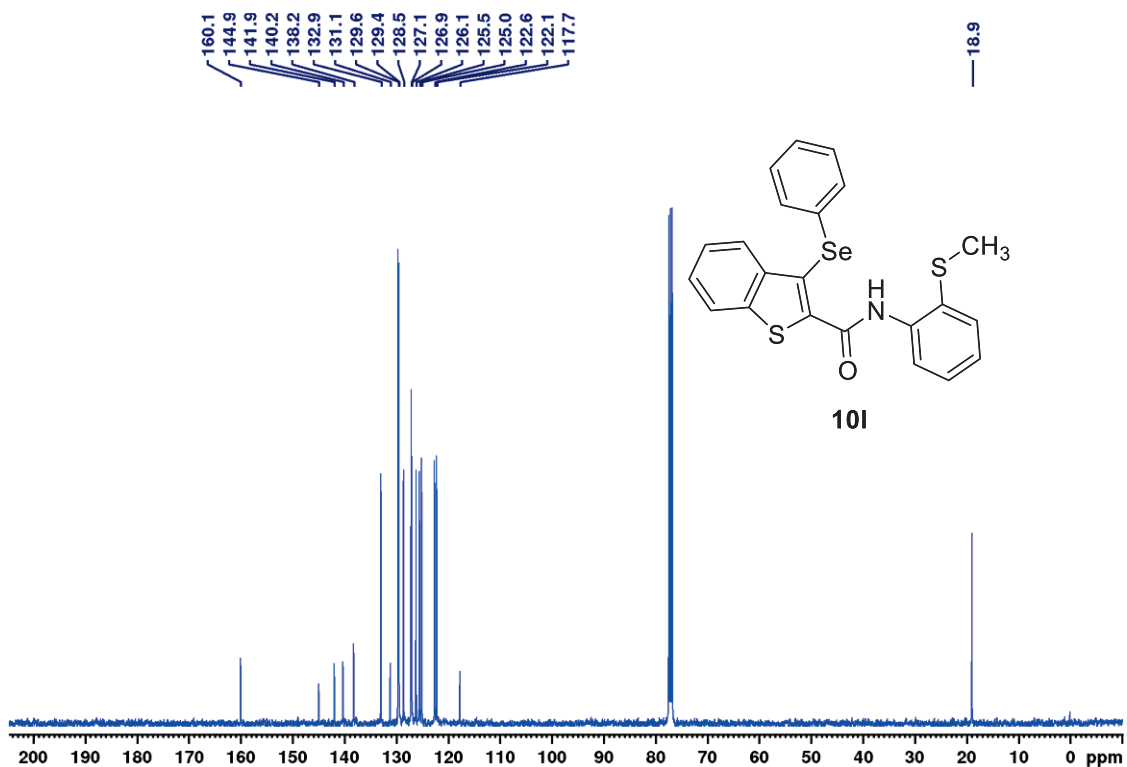
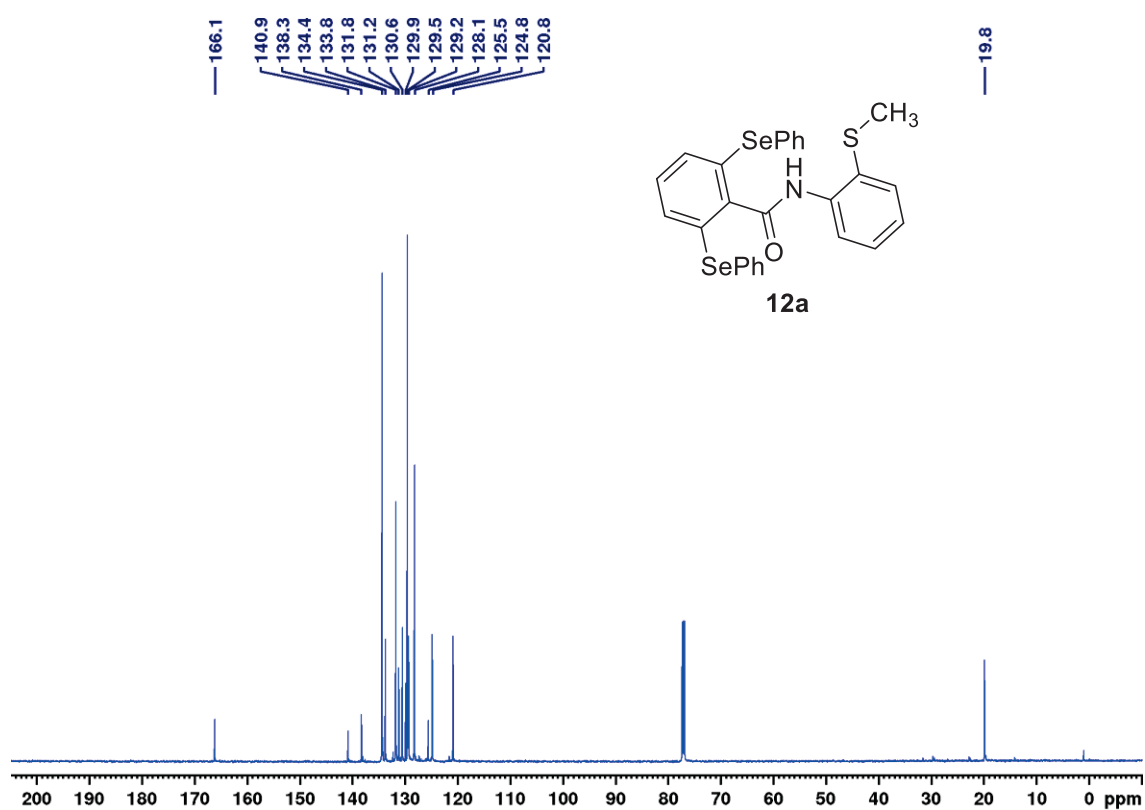
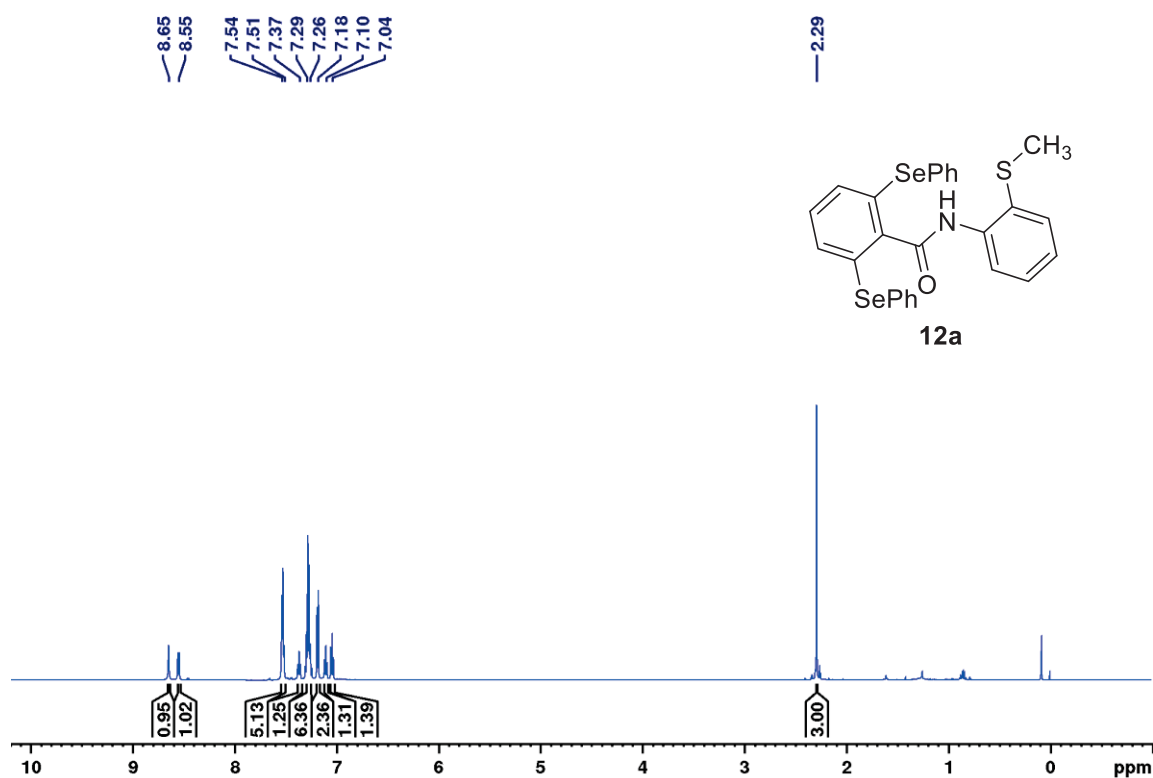


Figure 94: ¹³C NMR Spectrum (100 MHz, CDCl₃) of *N*-(2-(methylthio)phenyl)-3-(phenylselanyl)benzo[*b*]thiophene-2-carboxamide (**10I**).



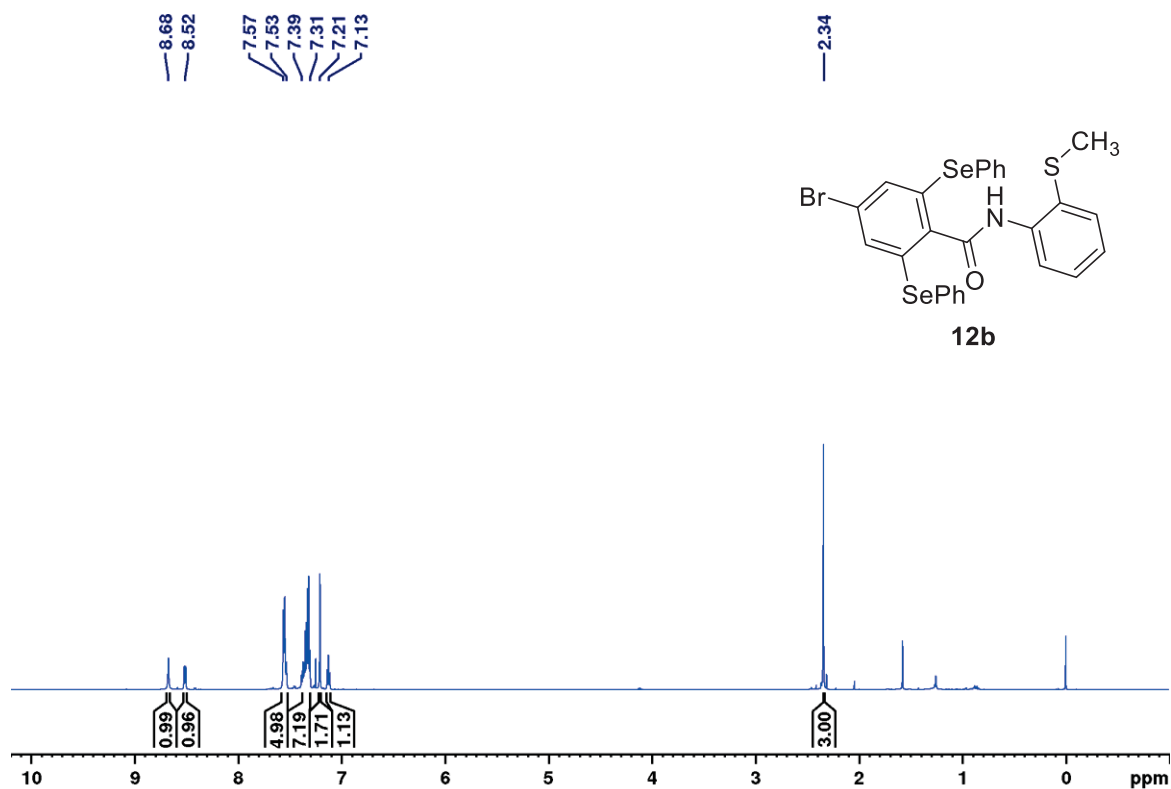


Figure 97: ¹H NMR spectrum (400 MHz, CDCl₃) of 4-bromo-*N*-(2-(methylthio)phenyl)-2,6-bis(phenylselanyl)benzamide (**12b**).

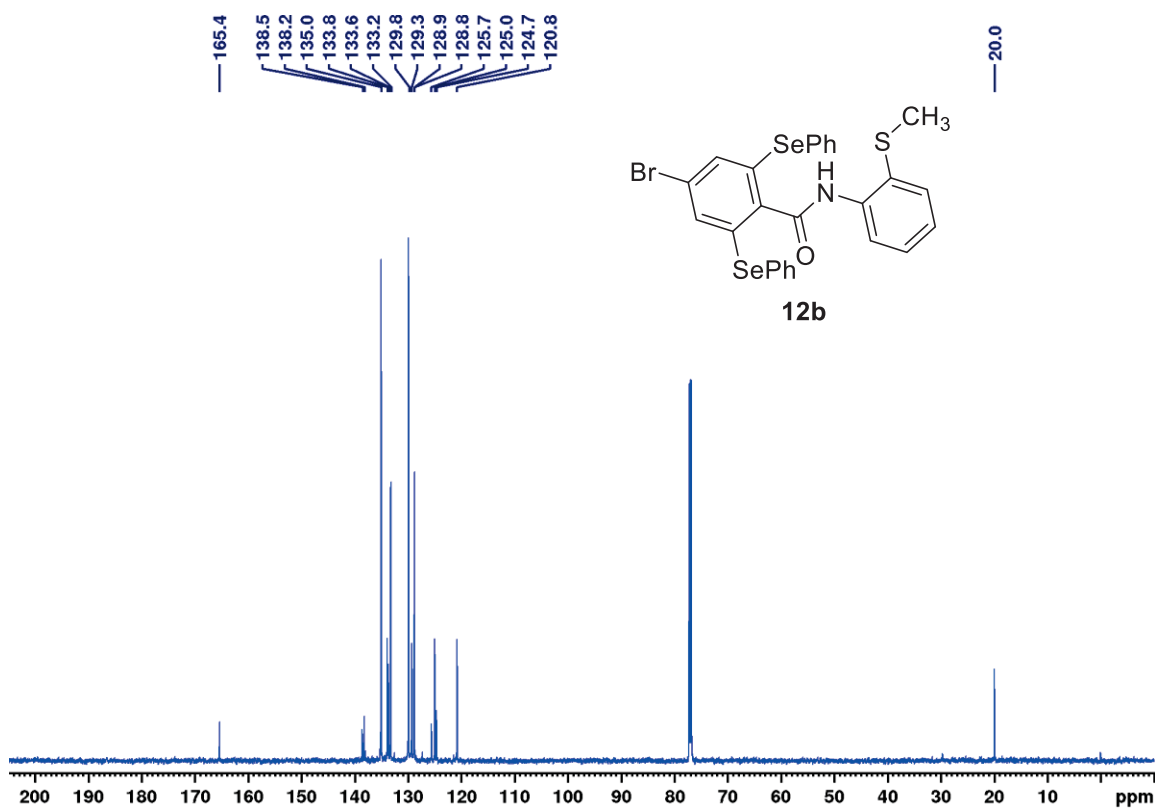
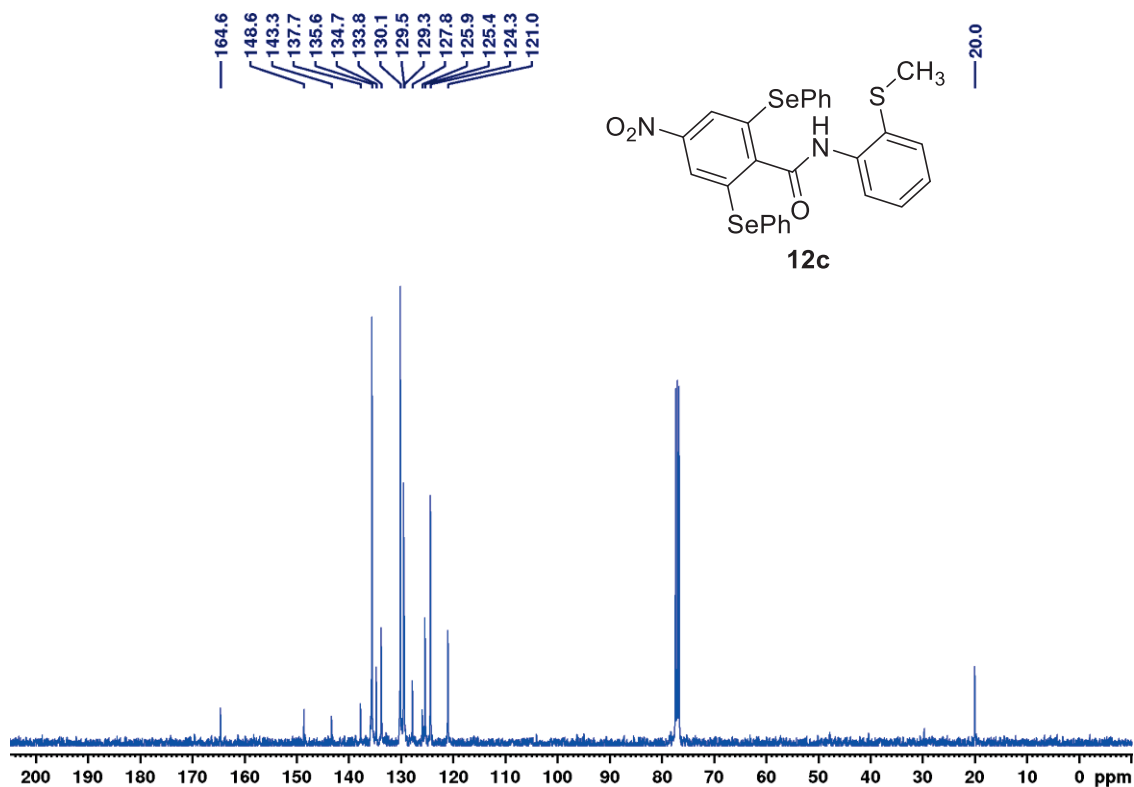
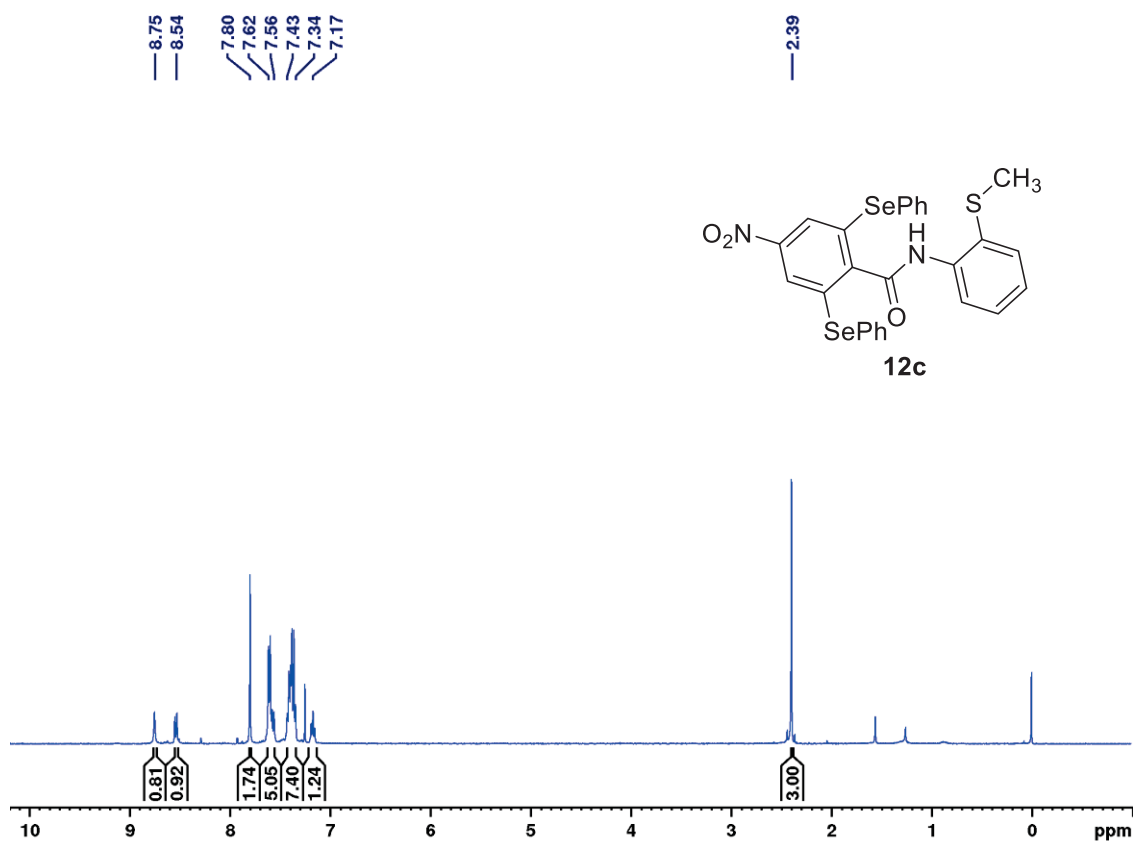


Figure 98: ¹³C NMR spectrum (100 MHz, CDCl₃) of 4-bromo-*N*-(2-(methylthio)phenyl)-2,6-bis(phenylselanyl)benzamide (**12b**).



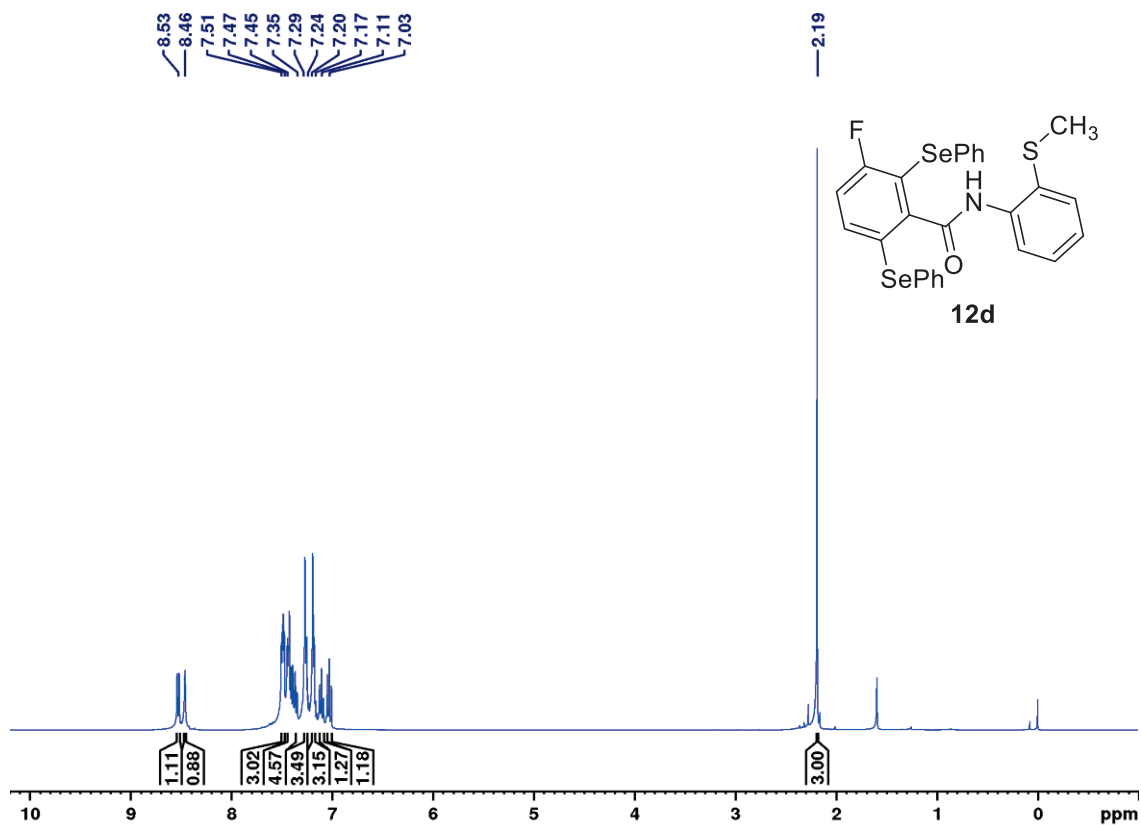


Figure 101: ¹H NMR spectrum (400 MHz, CDCl₃) 3-fluoro-*N*-(2-(methylthio)phenyl)-2,6-bis(phenylselanyl)benzamide (12d).

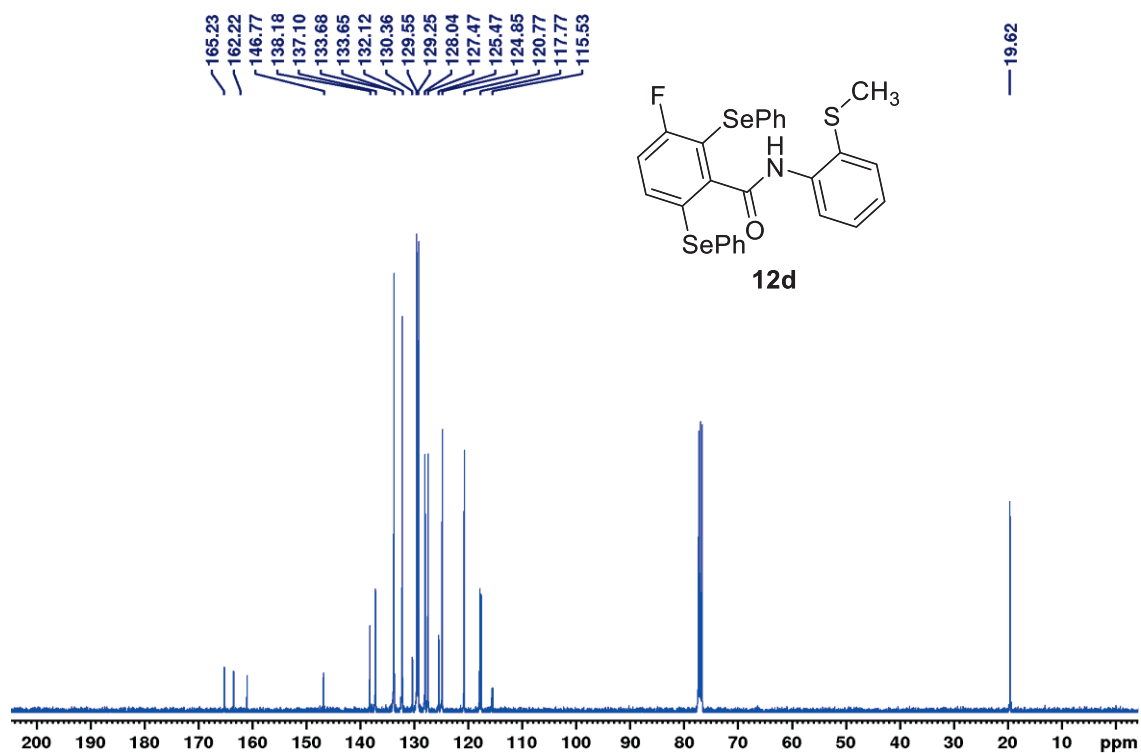


Figure 102: ¹³C NMR spectrum (100 MHz, CDCl₃) 3-fluoro-*N*-(2-(methylthio)phenyl)-2,6-bis(phenylselanyl)benzamide (12d).

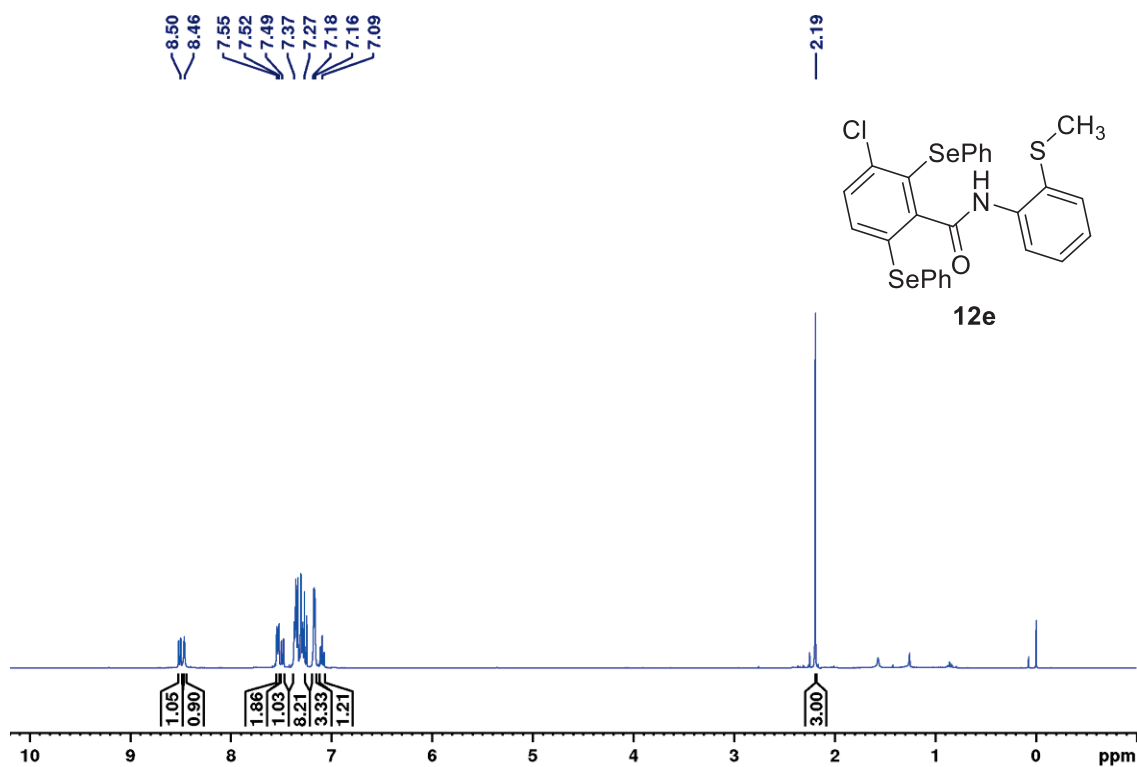


Figure 103: ¹H NMR spectrum (400 MHz, CDCl₃) 3-chloro-*N*-(2-(methylthio)phenyl)-2,6-bis(phenylselanyl)benzamide (12e).

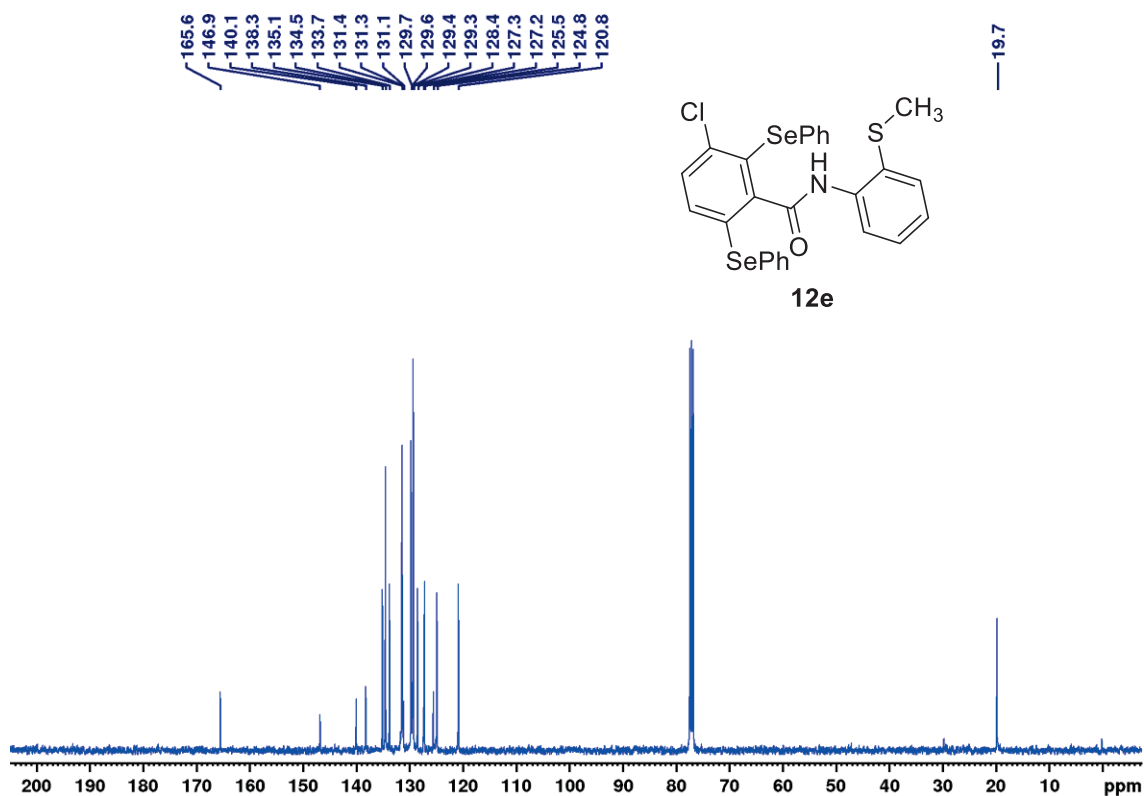


Figure 104: ¹³C NMR spectrum (100 MHz, CDCl₃) 3-chloro-*N*-(2-(methylthio)phenyl)-2,6-bis(phenylselanyl)benzamide (12e).

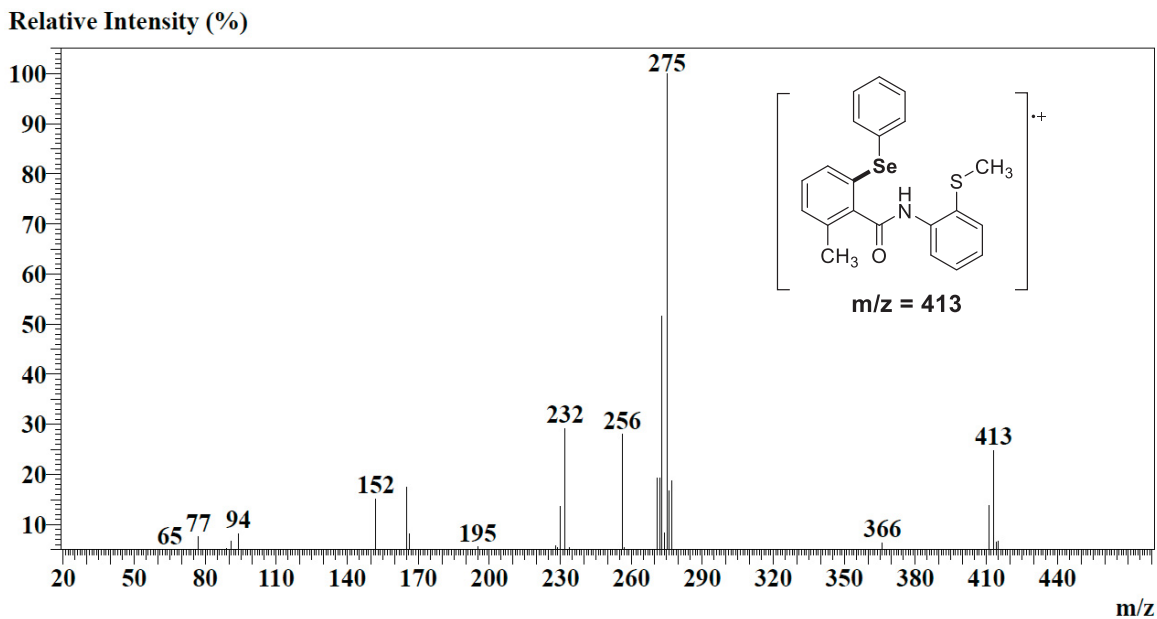


Figure 105: Mass spectrum (EI, 70 eV) of 2-methyl-*N*-(2-(methylthio)phenyl)-6-(phenylselanyl)benzamide (**12f**).

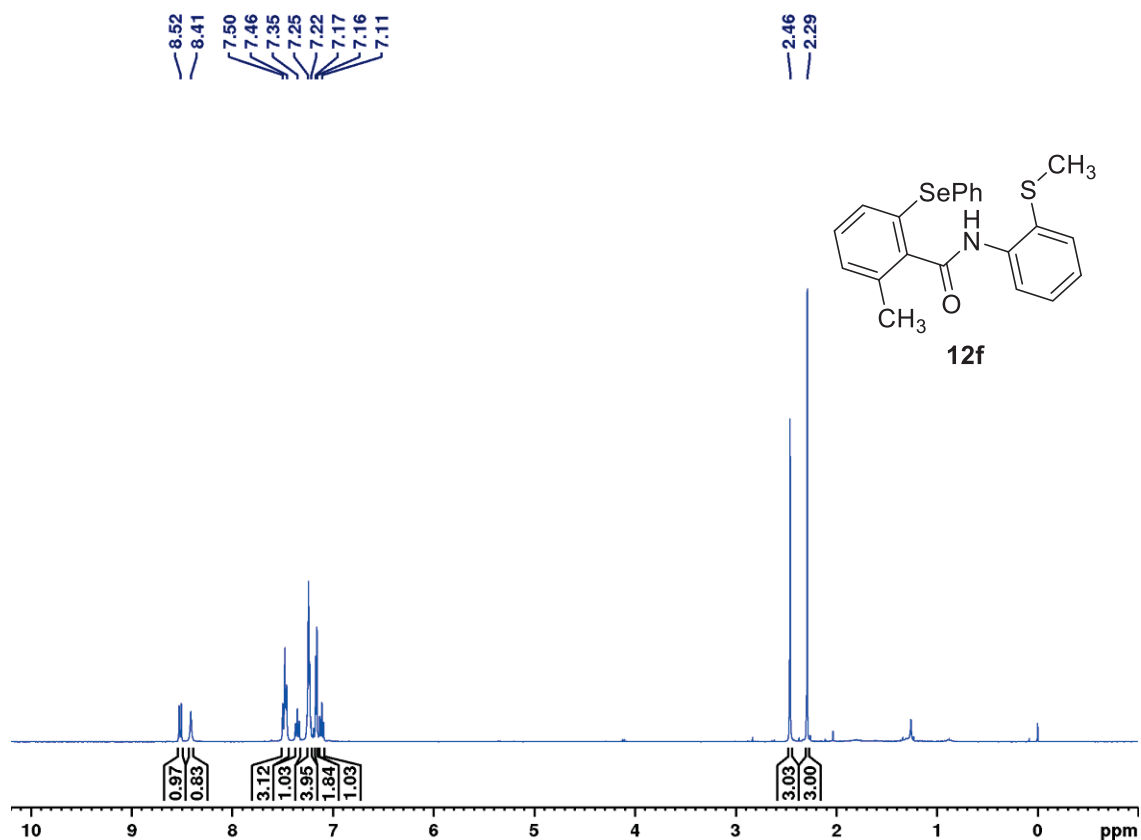


Figure 106: ^1H NMR (400 MHz, CDCl_3) of 2-methyl-*N*-(2-(methylthio)phenyl)-6-(phenylselanyl)benzamide (**12f**).

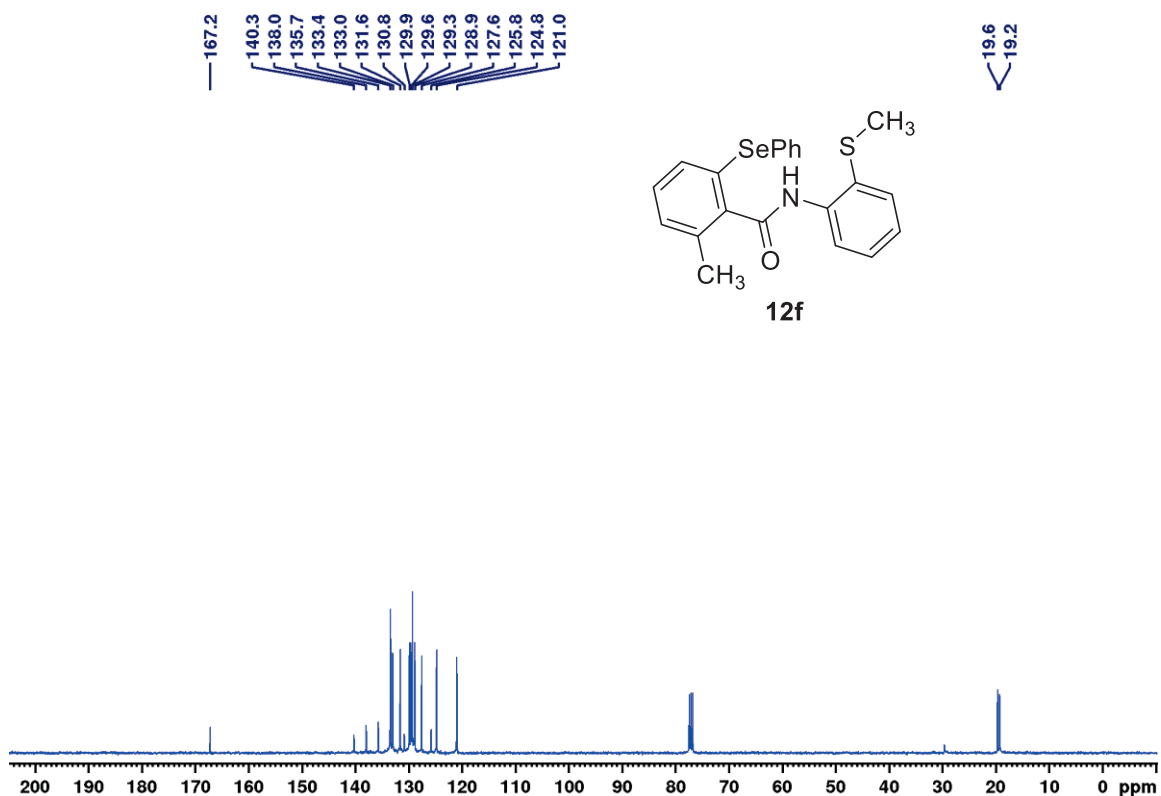


Figure 107: ^{13}C NMR (100 MHz, CDCl_3) of 2-methyl-*N*-(2-(methylthio)phenyl)-6-(phenylselanyl)benzamide (**12f**).

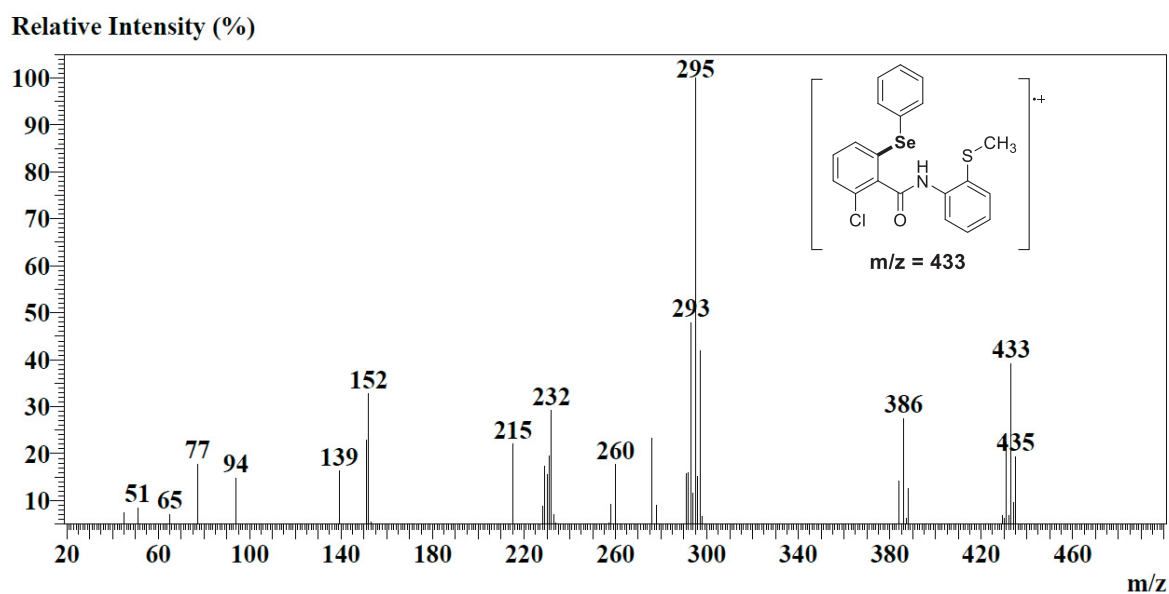


Figure 108: Mass spectrum (EI, 70 eV) of 2-chloro-*N*-(2-(methylthio)phenyl)-6-(phenylselanyl)benzamide (**12g**).

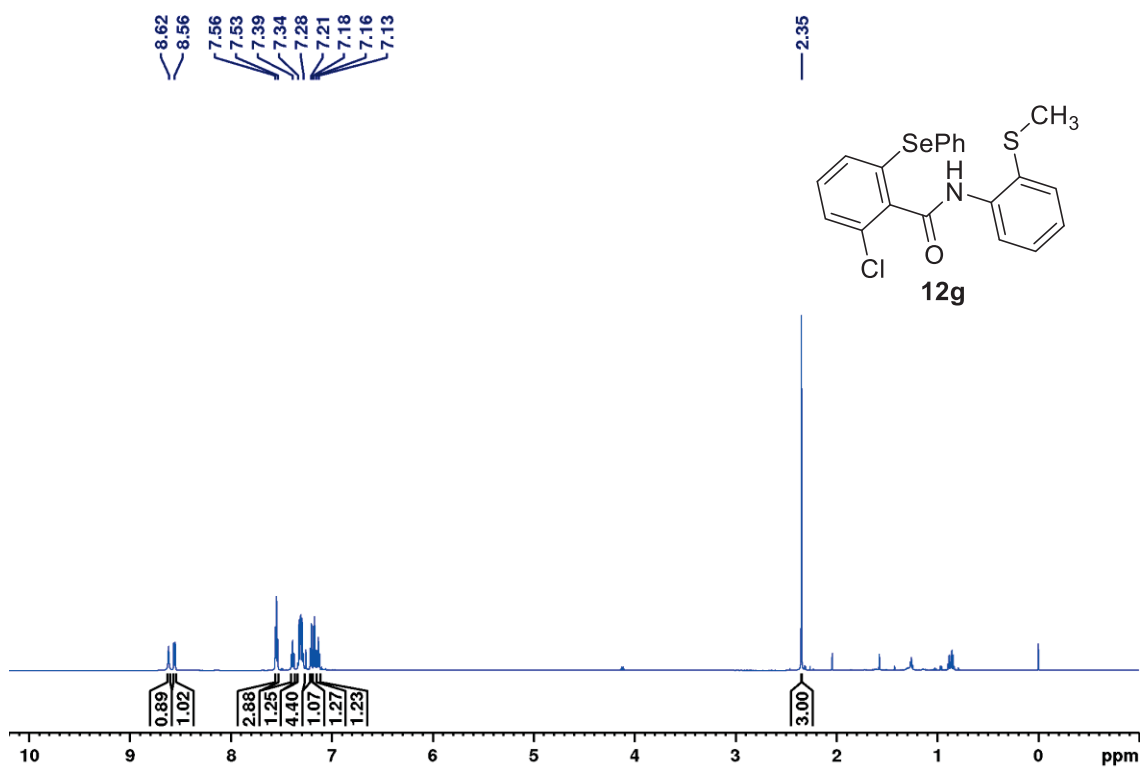


Figure 109: ¹H NMR (400 MHz, CDCl₃) of 2-chloro-N-(2-(methylthio)phenyl)-6-(phenylselanyl)benzamide (**12g**).

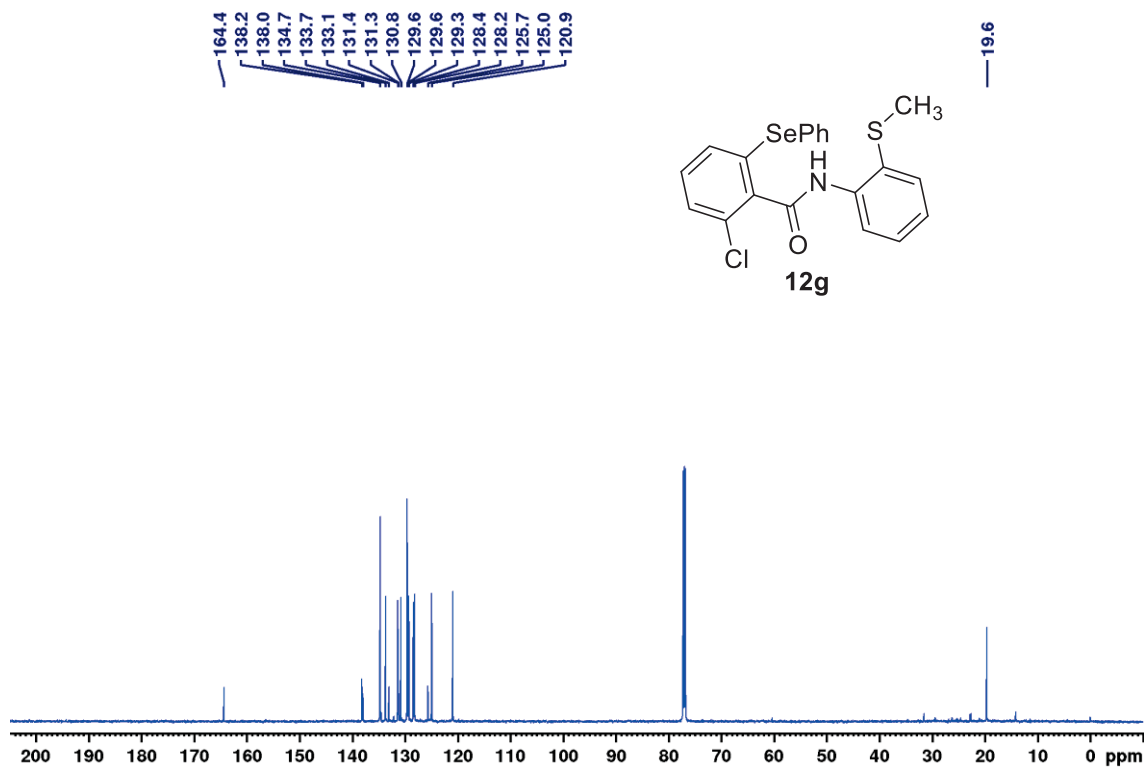


Figure 110: ¹³C NMR (100 MHz, CDCl₃) of 2-chloro-N-(2-(methylthio)phenyl)-6-(phenylselanyl)benzamide (**12g**).

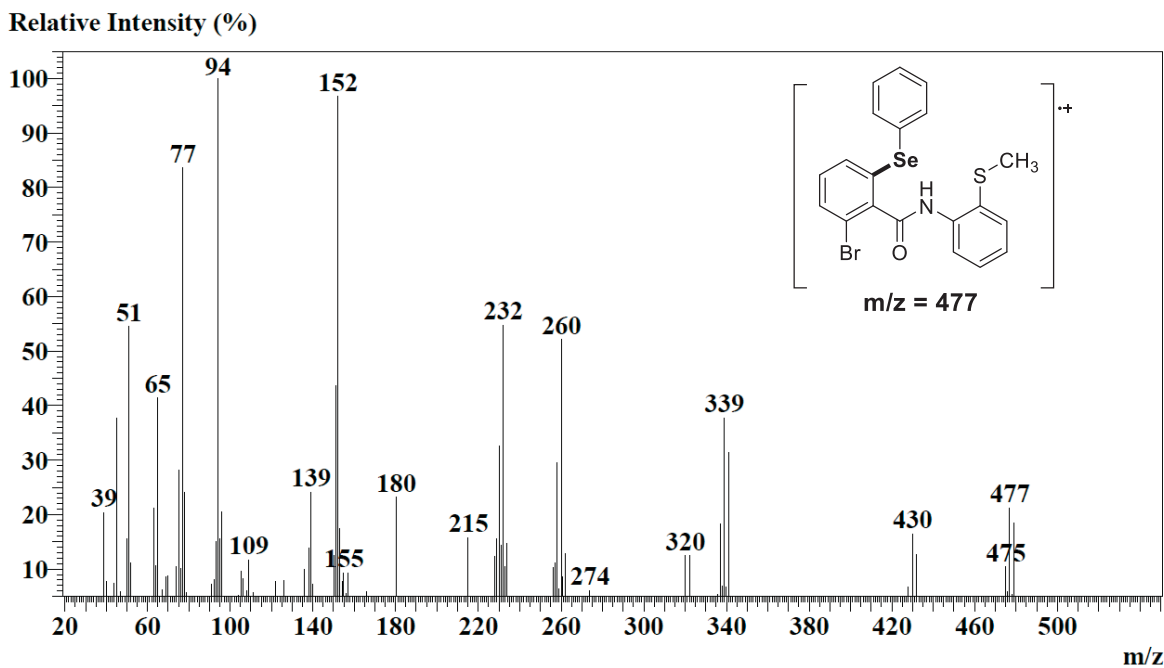


Figure 111: Mass spectrum (EI, 70 eV) of 2-bromo-*N*-(2-(methylthio)phenyl)-6-(phenylselanyl)benzamide (**12h**).

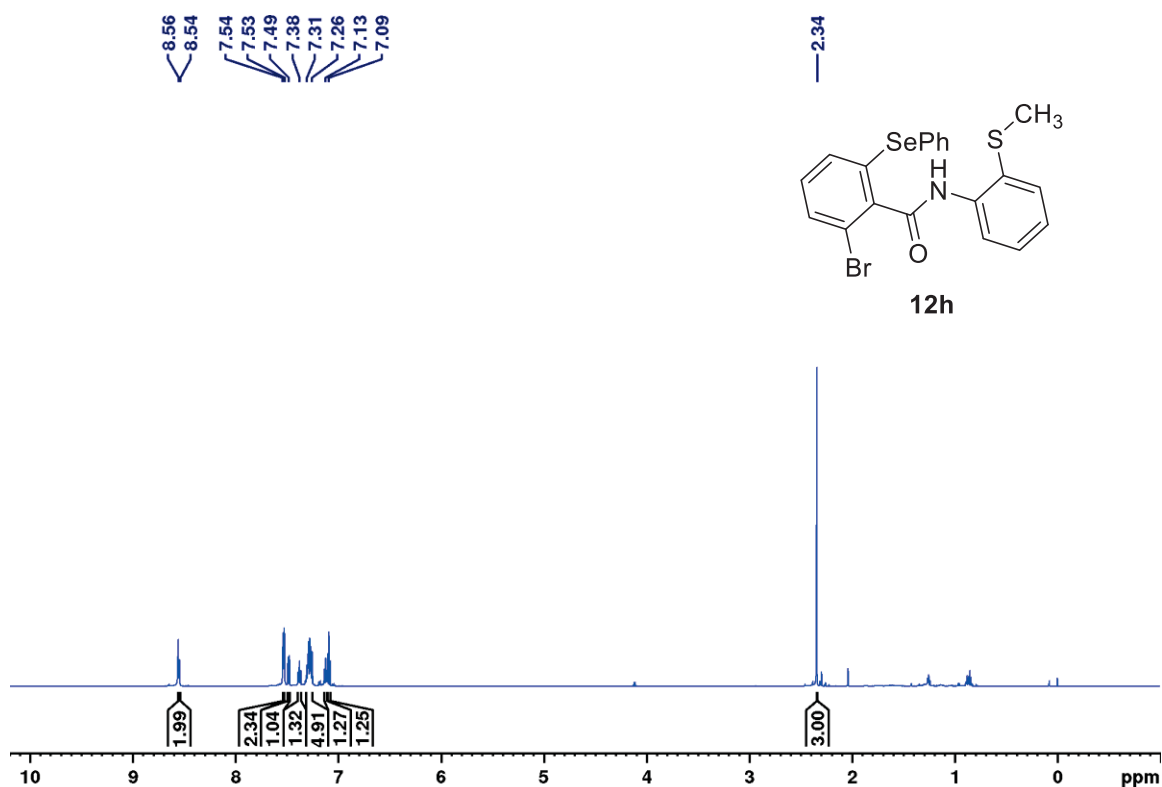


Figure 112: ^1H NMR (400 MHz, CDCl_3) of 2-bromo-*N*-(2-(methylthio)phenyl)-6-(phenylselanyl)benzamide (**12h**).

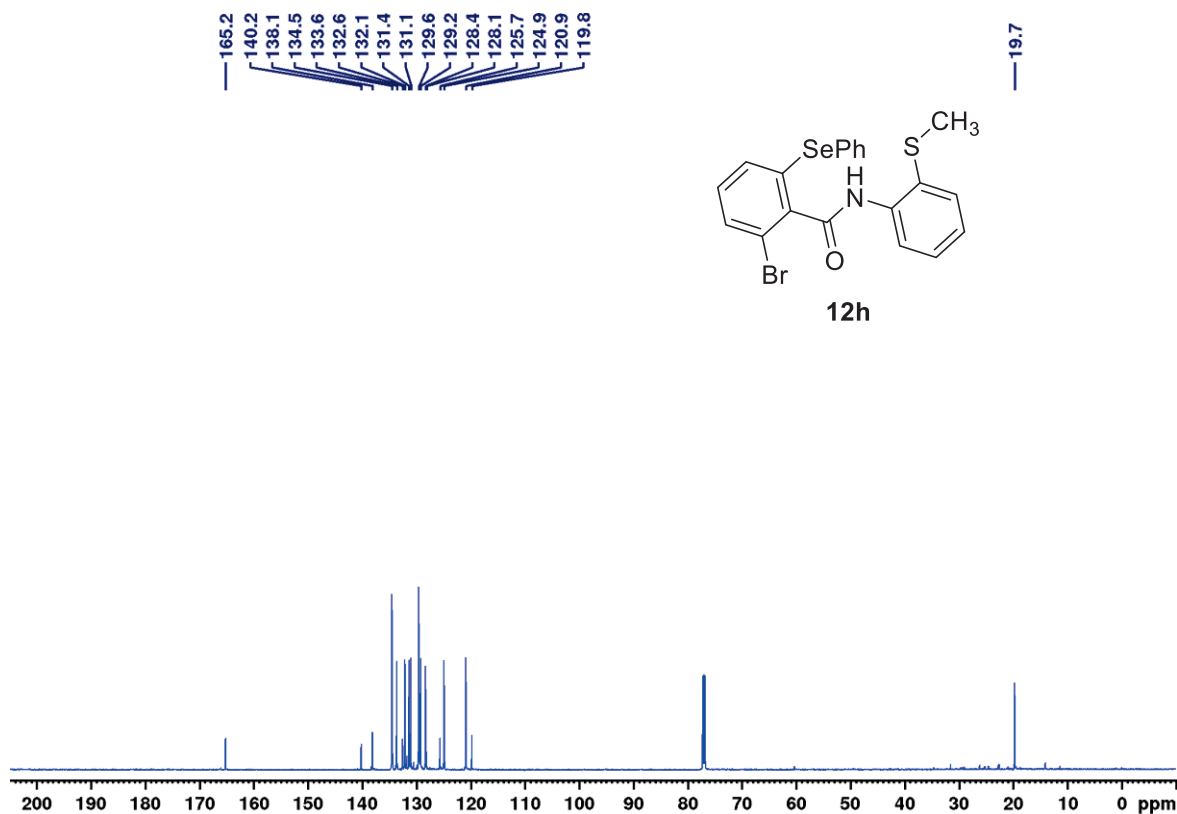


Figure 113: ¹³C NMR (100 MHz, CDCl₃) of 2-bromo-N-(2-(methylthio)phenyl)-6-(phenylselanyl)benzamide (**12h**).

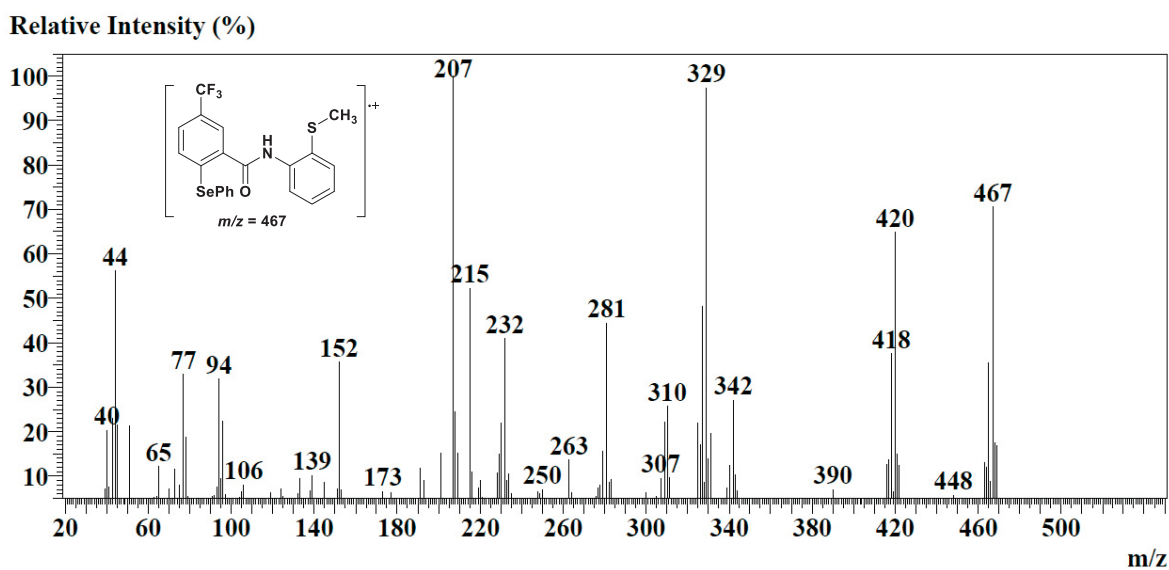


Figure 114: Mass spectrum (EI, 70 eV) of N-(2-(methylthio)phenyl)-2-(phenylselanyl)-3-(trifluoromethyl)benzamide (**12i**).

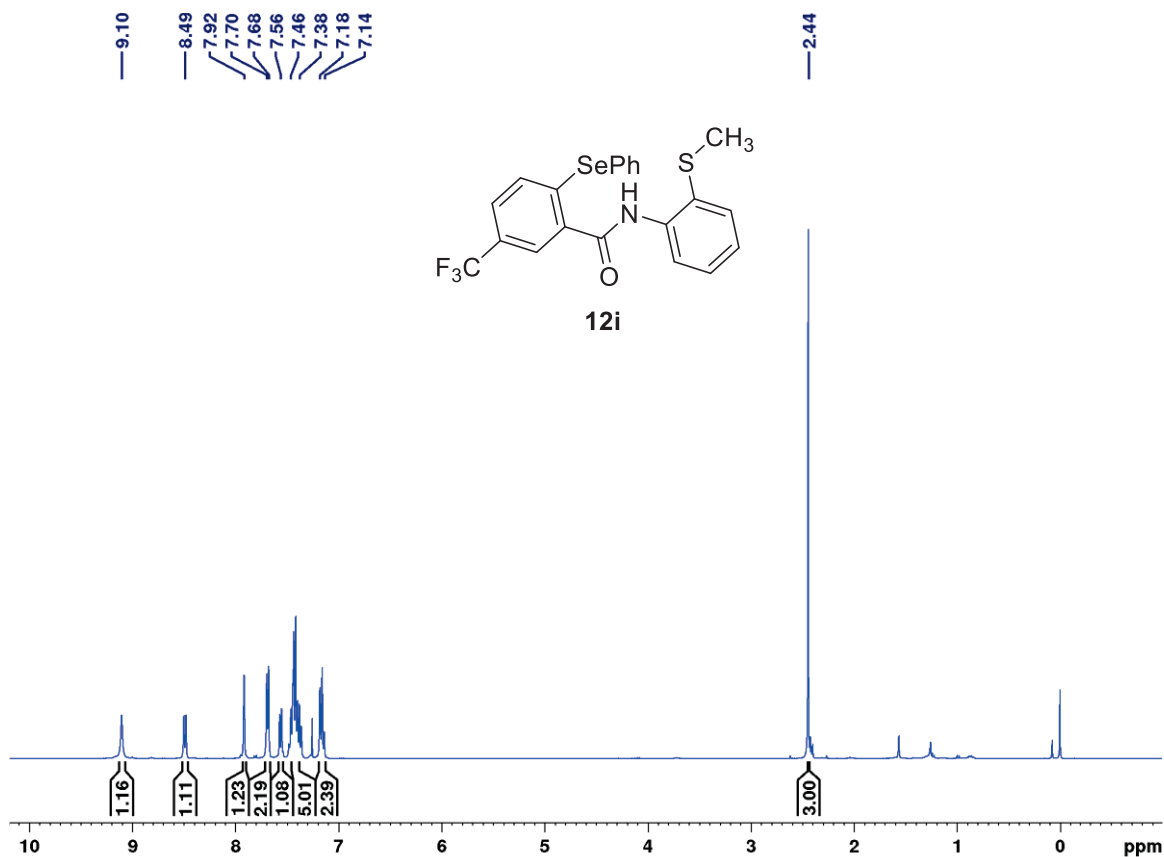


Figure 115: ^1H NMR spectrum (400 MHz, CDCl_3) *N*-(2-(methylthio)phenyl)-2-(phenylselanyl)-3-(trifluoromethyl)benzamide (**12i**).

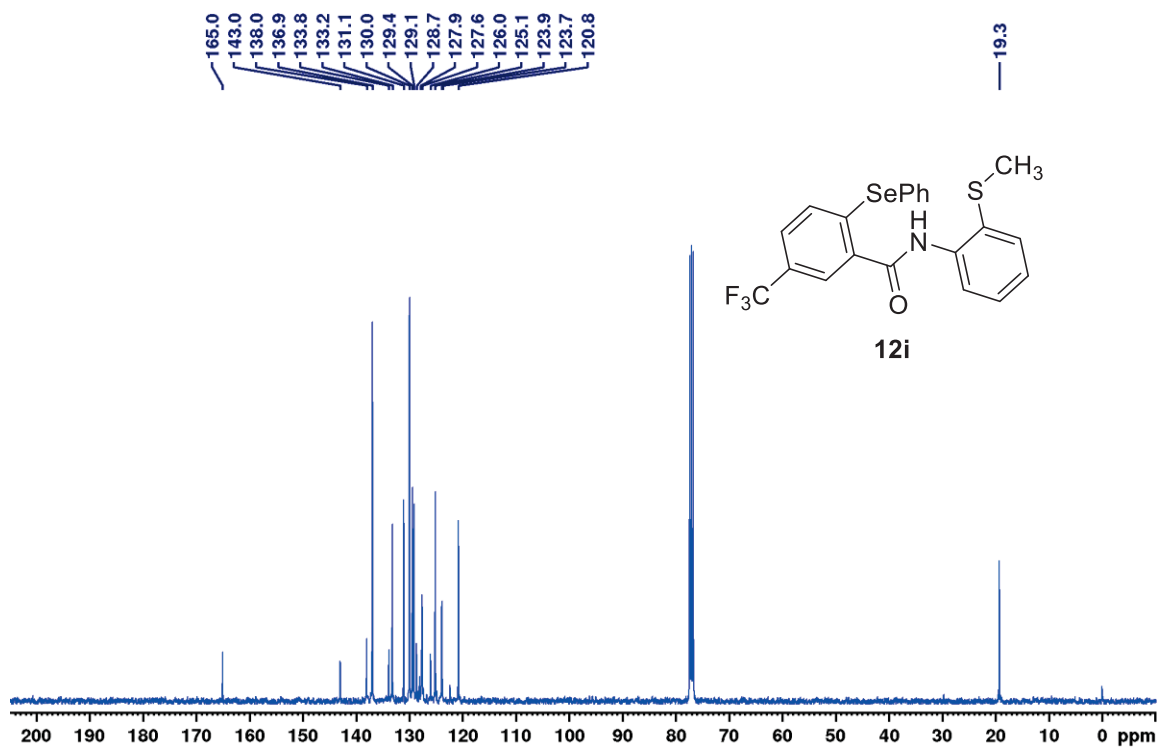


Figure 116: ^{13}C NMR spectrum (100 MHz, CDCl_3) *N*-(2-(methylthio)phenyl)-2-(phenylselanyl)-3-(trifluoromethyl)benzamide (**12i**).

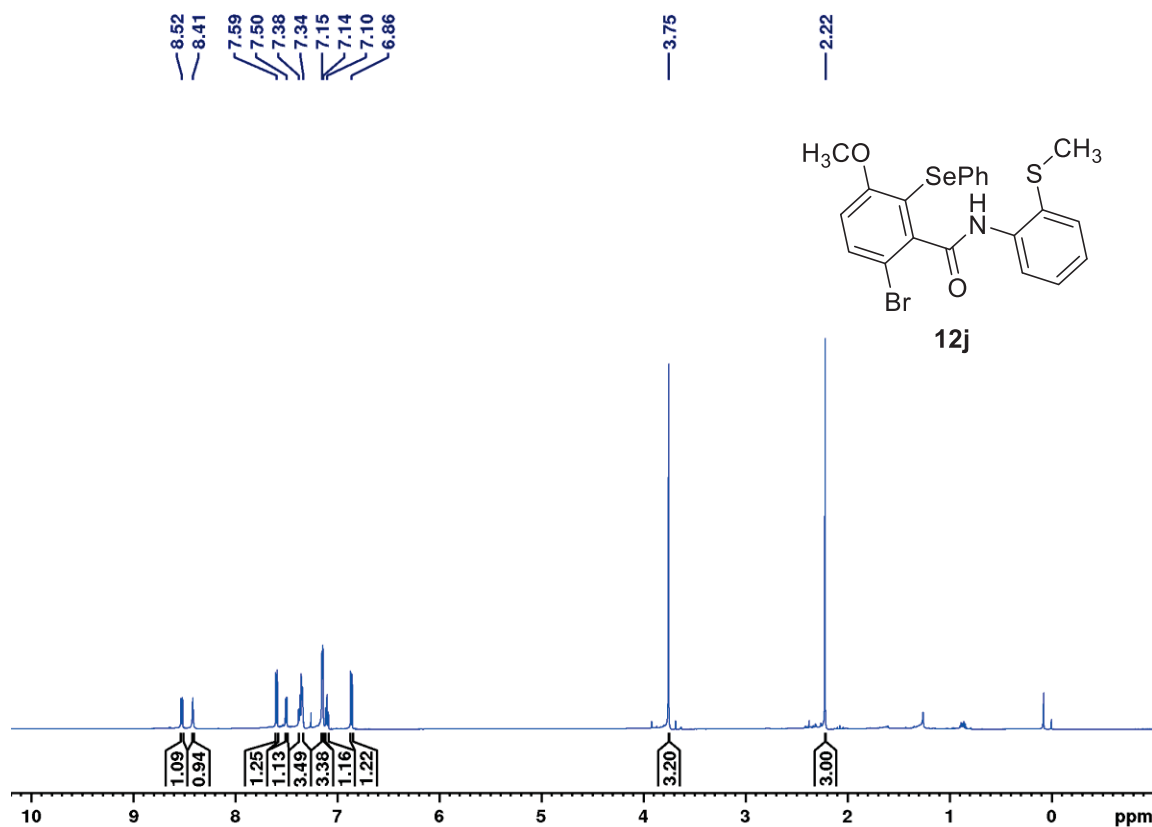


Figure 117: ¹H NMR spectrum (400 MHz, CDCl₃) 6-bromo-3-methoxy-N-(2-(methylthio)phenyl)-2-(phenylselanyl)benzamide (**12j**).

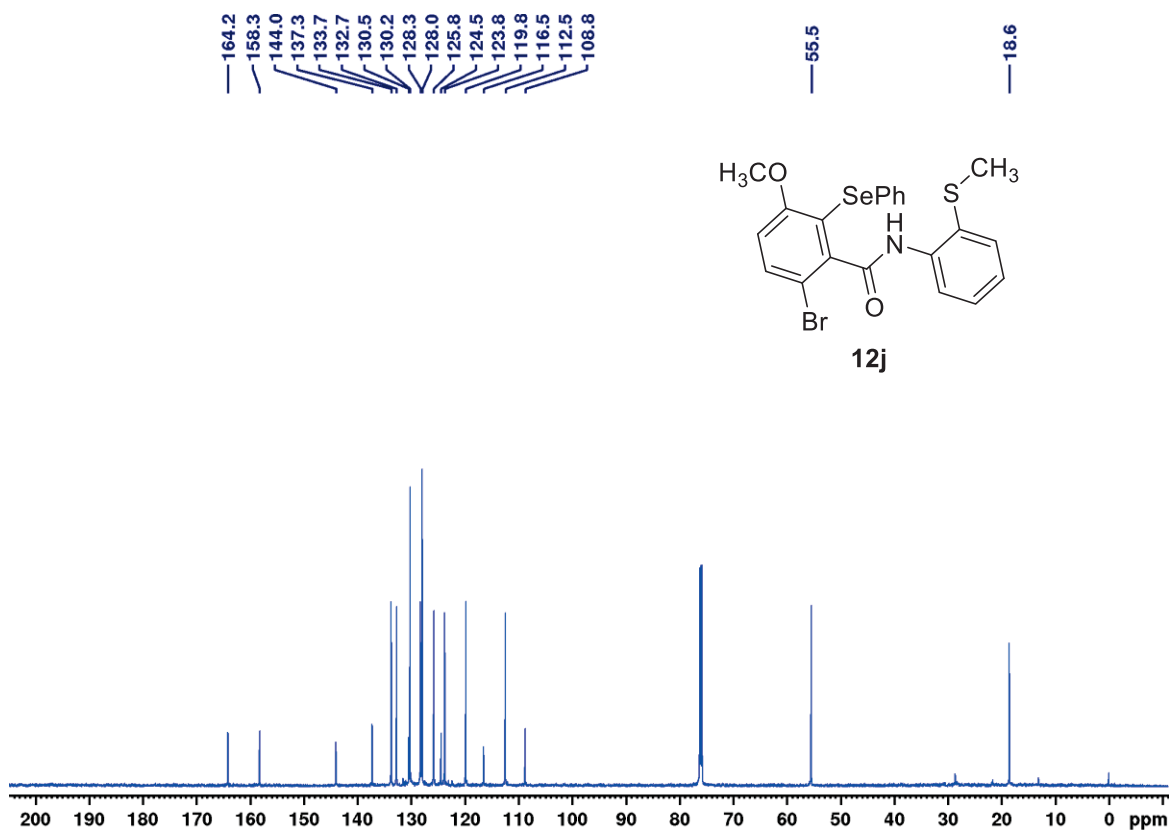


Figure 118: ¹³C NMR spectrum (100 MHz, CDCl₃) 6-bromo-3-methoxy-N-(2-(methylthio)phenyl)-2-(phenylselanyl)benzamide (**12j**).

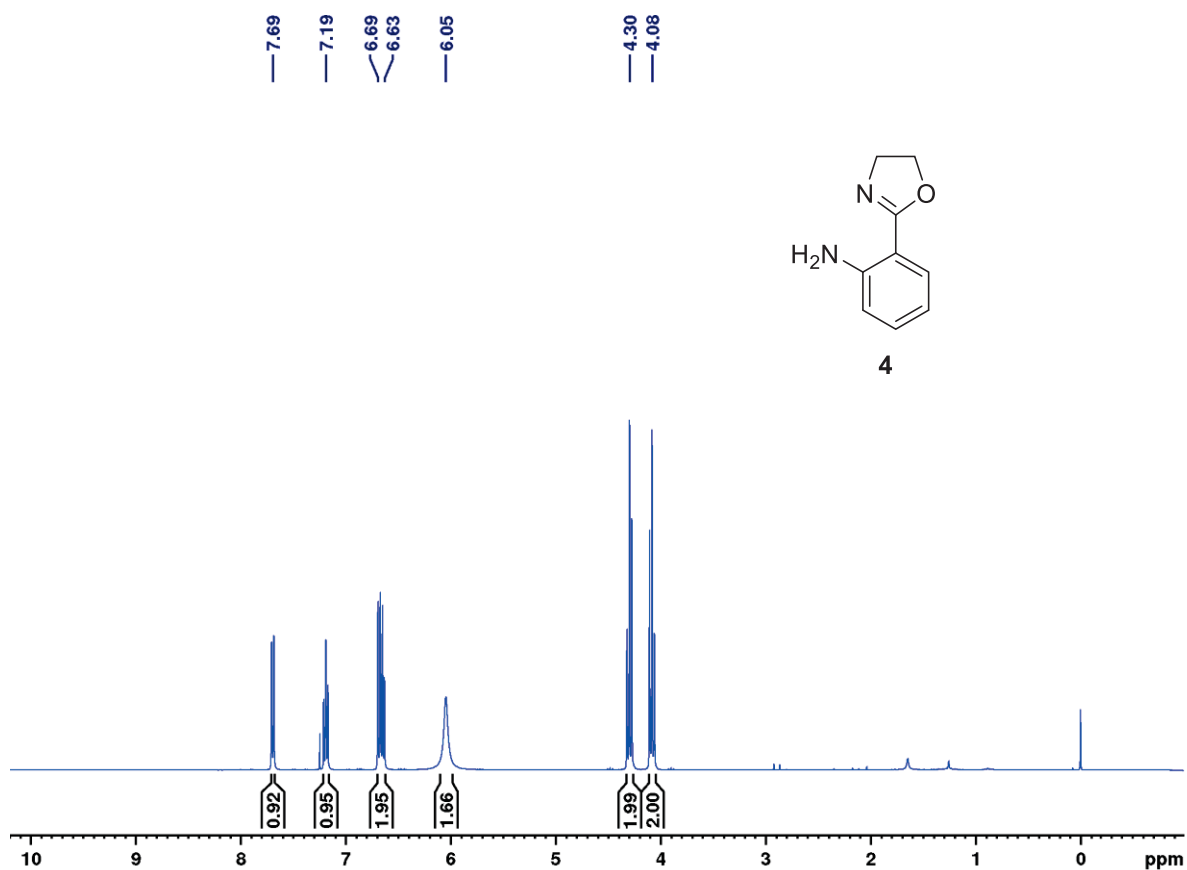


Figure 119: ¹H NMR spectrum (400 MHz, CDCl₃) of 2-(4,5-dihydrooxazol-2-yl)aniline (4).

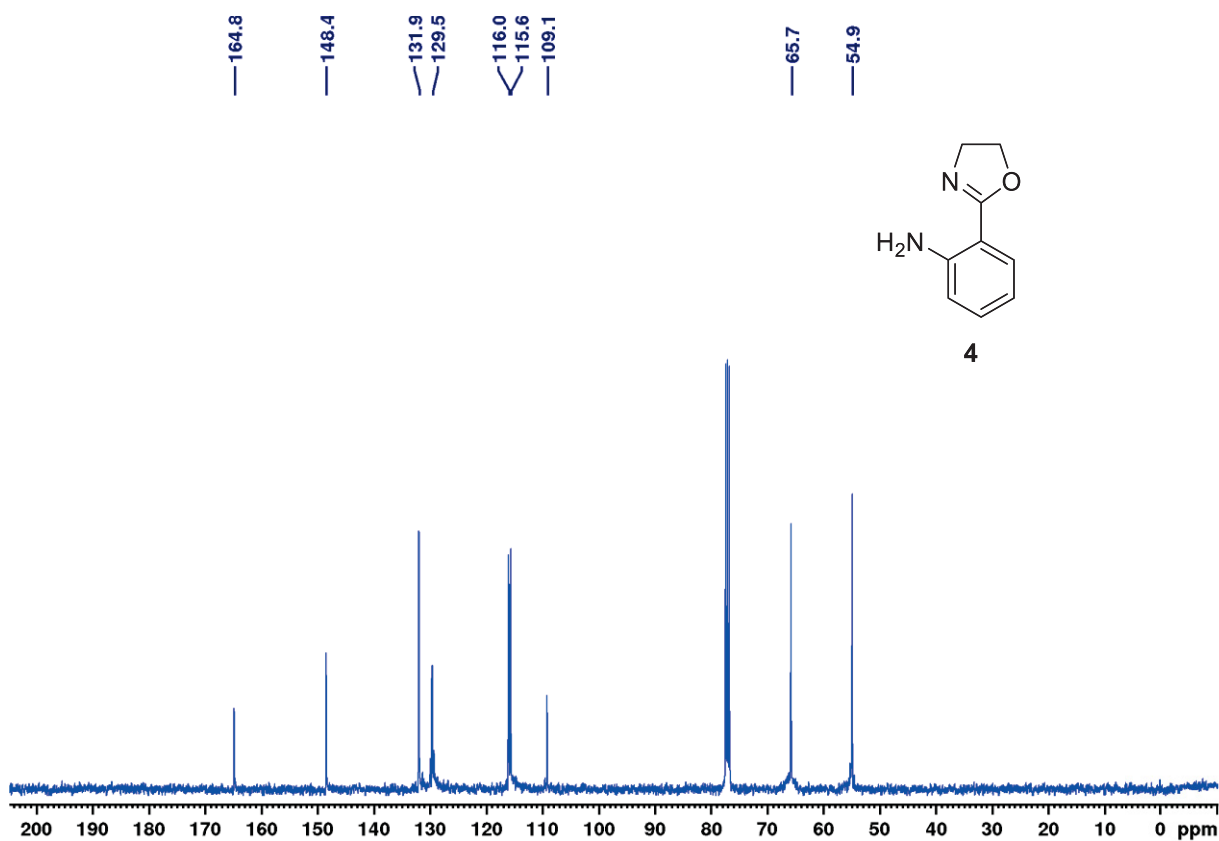


Figure 120: ¹³C NMR spectrum (100 MHz, CDCl₃) of 2-(4,5-dihydrooxazol-2-yl)aniline (4).

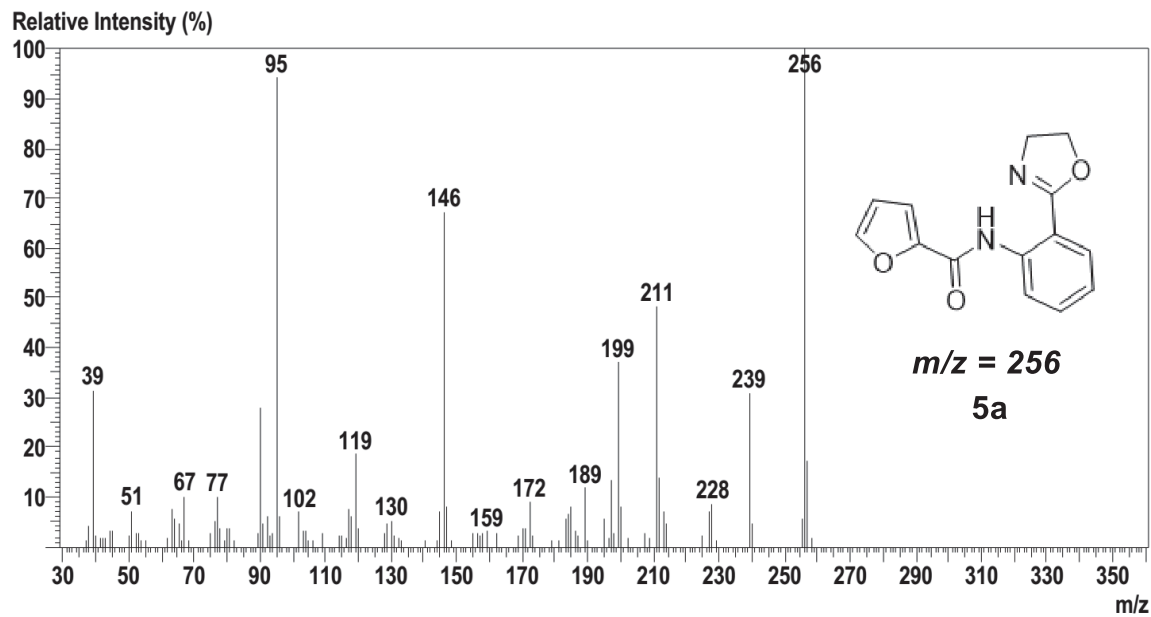


Figure 121: Mass spectrum (EI, 70 eV) of *N*-(2-(4,5-dihydrooxazol-2-yl)phenyl)furan-2-carboxamide (**5a**).

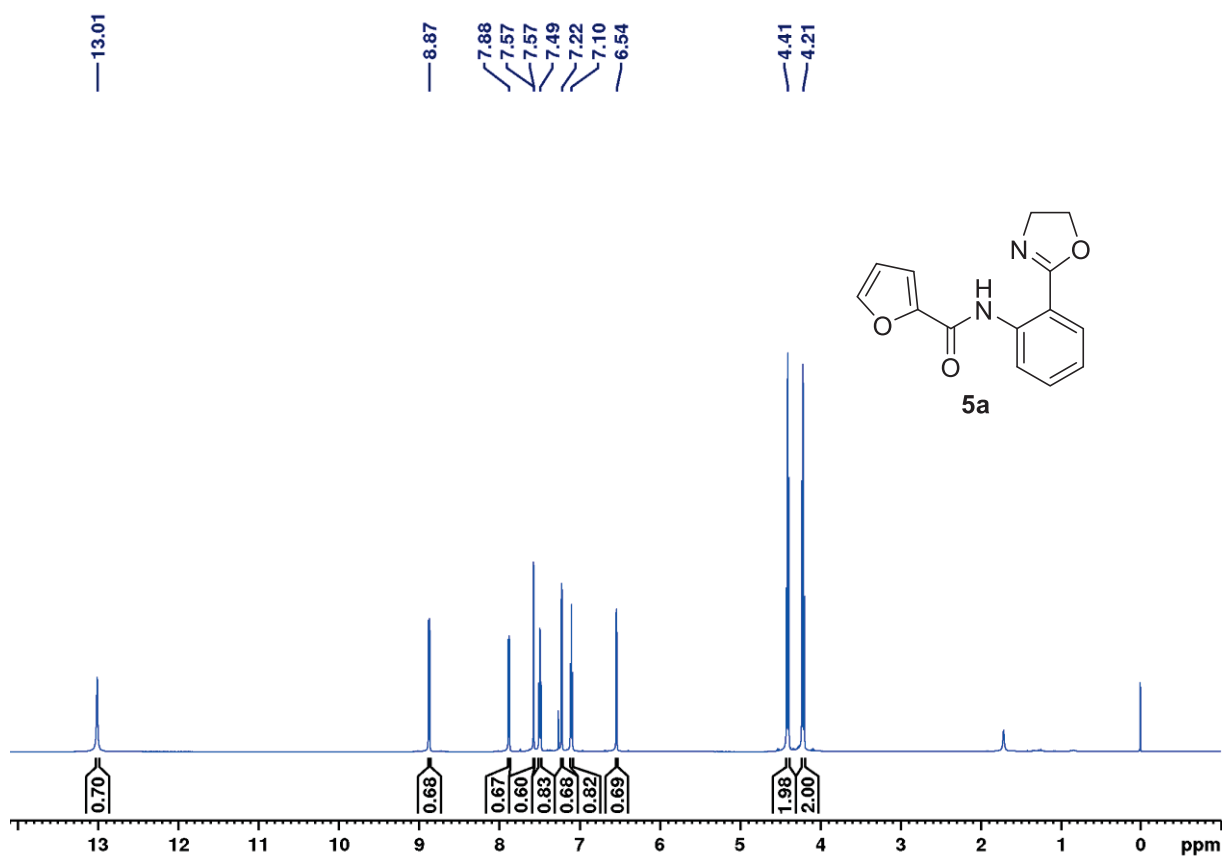


Figure 122: ¹H NMR spectrum (400 MHz, CDCl₃) of *N*-(2-(4,5-dihydrooxazol-2-yl)phenyl)furan-2-carboxamide (**5a**).

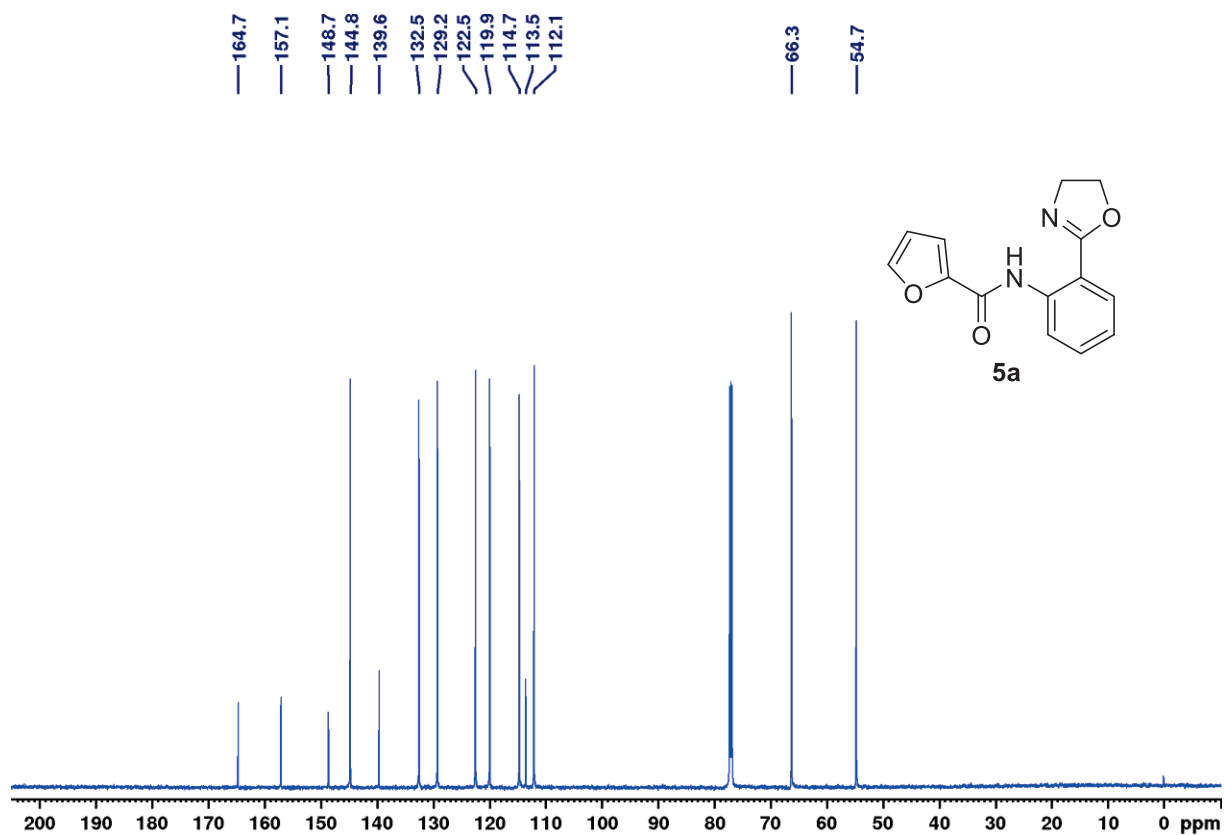


Figure 123: ¹³C NMR spectrum (100 MHz; CDCl₃) of *N*-(2-(4,5-dihydrooxazol-2-yl)phenyl)furan-2-carboxamide (**5a**).

REFERENCES

- 1 (a) Davies, H. M.; Morton, D. *J. Org. Chem.*, **2016**, 81,343-350; (b) Wei, Y.; Hu, P.; Zhang, M.; Su, W. *Chem. Rev.*, **2017**, 117, 8864-8907; (c) Davies, H. M. L.; Morton, D.; *Angew. Chem. Int. Ed.*, **2017**, 3, 936–943; (d) Chen, D. Y. K.; Youn, S. W. *A. Chem. Eur. J.*, **2012**, 18, 9452-9474; (e) Doyle, M. P.; Goldberg, K. I. *Chem. Res*, **2012**,777-777; (f) Abrams, D. J.; Provencher, P. A.; Sorensen, E. J. *Chem. Soc. Rev.*, **2018**, 47, 8925-8967; (g) Gutekunst, W. R.; Baran, P. S. *Chem. Soc. Rev.*, **2011**, 40, 1976; (h) Eisenstein, O.; Milani, J.; Perutz, R. N. *Chem. Rev.*, **2017**, 117, 8710; (i) He, J.; Wasa, M.; Chan, K. S.; Shao, Q.; Yu, J. Q. *Chem. Rev.*, **2016**, 117, 8754; (j) Hummel, J. R.; Boerth, J. A.; Ellman, J. A. *Chem. Rev.*, **2016**, 117, 9163; (k) Fumagalli, G.; Stanton, S.; Bower, J. F. *Chem. Rev.*, **2017**, 117, 9404; (l) Li, J. J. (ed). *C-H Bond Activation in Organic Synthesis*. CRC Press: Boca Raton, **2015**; (m) Yu, J.Q. *Science of Synthesis: Catalytic Transformations via C-H Activation*. vol. 1 e 2. Georg Thieme Verlag: Stuttgart.
- 2 (a) Dixneuf, P. H. Douet, *C-H Bond Activation and Catalytic Functionalization*. vol. 1 and 2. Springer: Heidelberg, **2016**; (b) Lei, A.; Shi, W.; Liu, C.; Zhang, H.; He, C. *Oxidative Cross-Coupling Reactions*. Wiley-VCH: Weinheim, **2016**; (c) Guo, X.X.; Gu, D.W.; Zhang, W. *Chem. Rev.*, **2015**, 115, 1622; (d) Alberico, D.; Scott, M. E.; Lautens, M. *Chem. Rev.*, **2007**, 107, 174;(e) Ackermann, L.; *Chem. Rev.*, **2011**, 111,1315; (f) Twilton, J.; Zhang, P.; Shaw, M. H.; Evans, R. W.; MacMillan, D. W. *Nature Reviews*, **2017**, 1, 0052; (g) Gandeepan, P.; Cheng, C.H. *Chem. Asian J.*, **2015**, 10, 824; (h) Mo, J.; Wang, L.; Liu, Y.; Cui, X. *Synthesis*, **2015**, 47, 439;(i) Gensch, T.; Hopkinson, M.N.; Glorius, F.; Wencel-Delord, J. *Chem. Soc. Rev.*, **2016**, 45, 2900; (j) Chu, J. C.; Rovis, T. *Angew. Chem. Int. Ed.*, **2018**, 57, 62; (k) Zhang, Y. F.; Shi, Z. J. *Acc. Chem* **2018**, 52, 161; (l) Li, C. J. *Acc. Chem. Res.*, **2008**, 42, 335; (m) Varun, B. V.; Dhineshkumar, J.; Bettadapur, K. R.; Siddaraju, Y.; Alagiri, K.; Prabhu, K. R. *Tetrahedron Lett.*, **2017**, 58, 803; (n) Girard, S. A.; Knauber, T.; Li, C. J. *Angew. Chem. Int. Ed.*, **2014**, 53, 74; (o) Shang, R.; Ilies, L.; Nakamura, E. *Chem. Rev.*, **2017**, 117, 9086; (p) Santoro, S.; Kozhushkov, S. I.; Ackermann, L.; Vaccaro, L. *Green Chem.*, **2016**, 18, 3471; (r) Hartwig, J. F.; Larsen, M. A. *ACS Cent. Sci.*, **2016**, 2, 281.
- 3 (a) Giri, R.; Shi, B. F.; Engle, K. M.; Maugel, N.; Yu, J. Q. *Chem. Soc. Rev.*, **2009**, 38, 3242; (b) Huang, Z.; Lumb, J. P, *ACS Catal.*, **2018**, 9, 521; (c) Kuninobu, Y.; Ida,

H.; Nishi, M.; Kanai, M. *Nature Chem.*, **2015**, *7*, 712; (d) Newton, C.G.; Wang, S. G.; Oliveira, C. C.; Cramer, N. *Chem. Rev.*, **2017**, *117*, 8908; (e) Davies, H. M. L.; Morton, D. *Chem. Soc. Rev.*, **2011**, *40*, 1857; (f) Qiu, G.; Wu, J. *Org. Chem. Front.*, **2015**, *2*, 169; (g) Xu, Y.; Dong, G.; *Chem. Sci.*, **2018**, *9*, 1424; (h) Sambriago, C.; Schönbauer, D.; Blicke, R.; Dao-Huy, T.; Pototschnig, G.; Schaaf, P.; Wiesinger, T.; Wencel-Delord, J.; Besset, T.; Maes, B. U. W.; Schnürch, M. *Chem. Soc. Rev.*, **2018**, *47*, 6603; (i) Kainz, Q. M.; Matier, C. D.; Bartoszewicz, A.; Zultanski, S. L.; Peters, J. C.; Fu, G. C. *Res., Science*, **2016**, *351*, 681.

4 (a) Hartwing, J. F.; *Nature*, **2008**, *455*, 314; (b) Louillat, M.L.; Patureau, F. W. *Chem. Soc. Rev.*, **2014**, *43*, 901; (c) Liu, Y.; Kim, J.; Chae, J. *Curr. Org. Chem.*, **2014**, *18*, 2049; (d) Wu, X. F. (ed). *Transition Metal-Catalyzed Heterocycle Synthesis via C-H Activation*. Wiley-VCH: Weinheim, **2016**; (e) Ribas, X. (ed). *C-H and C-X Bond Functionalization: Transition Metal Mediation*. RSC Publishing: Cambridge, **2013**; (f) Song, G.; Wang, F.; Li, X. *Chem. Soc. Rev.*, **2012**, *41*, 3651; (g) Park, Y.; Kim, Y.; Chang, S. *Chem. Rev.*, **2017**, *117*, 9247; (h) Ruiz-Castillo, P.; Buchwald, S. L.; *Chem. Rev.*, **2016**, *116*, 12564; (i) Henry, M. C.; Mostafa, M. A. B.; Sutherland, A. *Synthesis*, **2017**, *49*, 4586; (j) Ros, A.; Fernández R.; Lassaletta, J. M. *Chem. Soc. Rev.*, **2014**, *43*, 3229; (k) Xu, L.; Wang, G.; Zhang, S.; Wang, H.; Wang, L.; Liu, L.; Jiao, J.; Li, P. *Tetrahedron*, **2017**, *73*, 7123; (l) Hartwig, J. F.; Cheng, C.; *Science*, **2014**, *343*, 853; (m) Cheng, C.; Hartwig, J. F.; *Chem. Rev.*, **2015**, *115*, 8946; (n) Min, M.; Kang, D.; Jung, S.; Hong, S. *Adv. Synth. Catal.*, **2016**, *358*, 1296; (o) Lyons, T. W.; Sanford, M. S. *Chem. Rev.*, **2010**, *110*, 1147; (p) Das, R.; Kapur, M. *Asian J. Org. Chem.*, **2018**, *7*, 1524; (q) Hao, W.; Liu, Y. *Beilstein J. Org. Chem.*, **2015**, *11*, 2132.

5 (a) Fischer, C.; Koenig, B. *Beilstein J. Org. Chem.*, **2011**, *7*, 59; (b) Sperotto, E.; van Klink, G. P. M.; van Koten, G.; Vries, J. G. *Dalton Trans.*, **2010**, *39*, 10338. (c) Sambriago, C.; Marsden, S. P.; Blacker, A. J.; McGowan, P. C. *Chem. Soc. Rev.*, **2014**, *43*, 3525; (d) Ruiz-Catillo, P.; Buchwald, S. L.; *Chem. Rev.*, **2016**, *116*, 12564; (e) Foubelo, F.; Nájera, C.; Yus, M. *Chem. Rev.*, **2016**, *16*, 2521; (f) Chinchilla, R.; Nájera, C. *Chem. Soc. Rev.*, **2011**, *40*, 5084.; (g) Roy, D.; Uozumi, Y. *Adv. Synth. Catal.*, **2018**, *360*, 602; (h) Suzuki, A. *Angew. Chem. Int. Ed.*, **2011**, *50*, 6722; (i) Beletskaya, I. P.; Cheprakov, A. V. *Chem. Rev.*, **2000**, *100*, 3009.

6 (a) Lenardão, E. (ed) *New Frontiers in Organoselenium Compounds*; Springer: Cham, **2018**; (b) Nogueira, C. W.; Zeni, G.; Rocha, J. B. T. *Chem. Rev.*, **2004**, *104*,

6255; (c) Wirth, T. (ed). *Organoselenium Chemistry: Synthesis and Reactions*; Wiley-VCH: Weinheim, **2011**; (d) Mahmudov, K. T.; Kopylovich, M. N.; da Silva, M. F. C. G.; Pombeiro, A. J. L. *Dalton Trans.*, **2017**, 46, 10121; (e) Reich, H. J.; Hondal, R. J. *ACS Chem. Biol.*, **2016**, 11, 821; (f) Mukherjee, A. J.; Zade, S. S.; Sunoj, R. B. *Chem. Rev.*, **2010**, 110, 4357; (g) Carrera, E. I.; Seferos, D. S. *Macromolecules*, **2015**, 48, 297; (h) Manion, J. G.; Ye, S.; Proppe, A. H.; Laramée, A. W.; McKeown, G. R.; Kynaston, E. L.; Kelley, E. H.; Seferos, D. S. *ACS Appl. Energy Mater.*, **2018**, 1, 5033; (i) Xu, Z.; Fan, Q.; Meng, X. Guo, X.; Su, W.; Ma, W.; Zhang, M.; Li, Y. *Chem. Mater.*, **2017**, 29, 4811; (j) *Handbook of Thiophene-based Materials*; Perepichka, I. F.; Perepichka, D. F.; Eds.; WileyVCH: Weinheim, **2009**.

7 Rampon, D.; Lima, D. B.; Luz, E. Q.; Balaguez, R.; Schneider, P. H.; Alves, D. *Dalton Trans.*, **2019**, 48, 9851.

8 (a) Beletskaya, I. P.; Ananikov, V. P. *Chem. Rev.*, **2011**, 111, 1596; (b) Wang, L.; He, W.; Yu, Z. *Chem. Soc. Rev.*, **2013**, 42, 599; (c) Rampon, D. S.; Wessjohann, L. A.; Schneider, P. H. *J. Org. Chem.*, **2014**, 79, 5987. (d) Beletskaya, I. P.; Ananikov, V. P. *Chem. Rev.* **2022**, 122, 21, 16110–16293.

9 (a) Tang, C. W.; VanSlyke, S. A.; Chen, C. H. *J. Appl. Phys.* **1989**, 65, 3610; (b) Grimdsdale, A. C.; Chan, K. L.; Martin, R. E.; Jokisz, P. G.; Holmes, A. B. *Chem. Rev.* **2009**, 109, 897; (c) Mullen, K.; Scherf, U. *Organic Light-Emitting Devices: Synthesis, Properties and Applications*; Wiley-VCH Verlag GmbH & Co. KGaA: Weinheim, Germany, **2006**; (d) Wang, C.; Dong, H.; Hu, W.; Liu, Y.; Zhu, D. *Chem. Rev.* **2012**, 112, 2208.

10 (a) Coropceanu, V.; Cornil, J.; da Silva Filho, D. A.; Olivier, Y.; Silbey, R.; Bredas, J. L. *Chem. Rev.* **2007**, 107, 926; (b) Mas-Torrent, M.; Rovira, C. *Chem. Soc. Rev.* **2008**, 37, 827; (c) Allard, S.; Forster, M.; Souharce, B.; Thiem, H.; Scherf, U. *Angew. Chem., Int. Ed.* **2008**, 47, 4070; (d) Wu, W.; Liu, Y.; Zhu, D. *Chem. Soc. Rev.* **2010**, 39, 1489.

11 (a) Ooyama, Y.; Harima, Y. *Eur. J. Org. Chem.* **2009**, 2903; (b) Mishra, A.; Fischer, M. K. R.; Bauerle, P. *Angew. Chem., Int. Ed.* **2009**, 48, 2474; (c) Ning, Z.; Tian, H. *Chem. Commun.* **2009**, 5483.

12 Katritzky, A. R.; Ramsden, C. A.; Joule, J. A.; Zhdankin, V. V. *Handbook of heterocyclic chemistry*. Elsevier, **2010**.

13 (a) Scott, S. A.; Spencer, C. T.; O'Reilly, M. C.; Brown, A. K.; Lavieri, R. R.; Cho, C.; Jung, D.; Larock, R. C.; Brown, H. A.; Lindsley, C. W. *ACS. Chem. Biol.* **2015**, 10,

421. (b) Arsenyan, P.; Peagle, E.; Domracheva, I.; Gulbe, A.; Kanepe-Lapsa, I.; Shestakova, I. *Eur. J. Med. Chem.* **2014**, *87*, 471; (c) Paegle, E.; Domracheva, I.; Turovska, B.; Petrova, M.; Kanepe-Lapsa, I.; Gulbe, A.; Liepinsh, E.; Arsenyan, P. *Chem. Asian J.* **2016**, *11*, 1929; (d) Arsenyan, P.; Paegle, E.; Belyakov, S.; Shestakova, I.; Jaschenko, E.; Domracheva, I.; Popelis, J. *Eur. J. Med. Chem.* **2011**, *46*, 3434; (e) Wilhelm, E. A.; Gai, B. M.; Souza, A. C. G.; Bortolatto, C. F.; Roehrs, J. A.; Nogueira, C. W. *Mol. Cell. Biochem.* **2012**, *365*, 175; (f) Wilhelm, E. A.; Jesse, C. R.; Bortolatto, C. F.; Nogueira, C. W.; Savegnago, L. *Brain Res. Bull.* **2009**, *79*, 281; (g) Wilhelm, E. A.; Jesse, C. R.; Prigol, M.; Alves, D.; Schumacher, R. F.; Nogueira, C. W. *Cell Biol. Toxicol.* **2010**, *26*, 569; (h) Gai, B. M.; Stein, A. L.; Roehrs, J. A.; Bilheri, F. N.; Nogueira, C. W.; Zeni, G. *Org. Biomol. Chem.* **2012**, *10*, 798.

14 (a) Takimiya, K.; Osaka, I.; Mori, T.; Nakano, M. *Acc. Chem. Res.* **2014**, *47*, 1493-1502; (b) Cheng, Y. J.; Yang, S. H.; Hsu, C. S. *Chem. Rev.*, **2009**, *109*, 5868-5923; (c) Guo, X.; Facchetti, A.; Marks, T. J. *Chem. Rev.*, **2014**, *114*, 8943-9021; (d) Planells, M.; Schroeder, B. C.; McCulloch, I. *Macromolecules*, **2014**, *47*, 17, 5889-5894.

15 (a) Juang, S. H.; Lung, C. C.; Hsu, P. C.; Hsu, K. S.; Li, Y. C.; Hong, P. C.; Shiah, H. S.; Kuo, C. C.; Huang, C. W.; Wang, Y. C.; Huang, L.; Chen, T. S.; Chen, S. F.; Fu, K. C.; Hsu, C. L.; Lin, M. J.; Chang, C. J.; Ashendel, C. L.; Chan, T. C. K.; Chou, K. M.; Chang, J. Y. *Mol. Cancer Ther.* **2007**, *6*, 193; (b) Shiah, H. S.; Lee, W. S.; Juang, S. H.; Hong, P. C.; Lung, C. C.; Chang, C. J.; Chang, J. Y. *Biochem. Pharmacol.* **2007**, *73*, 610; (c) Wilhelm, E. A.; Jesse, C. R.; Bortolatto, C. F.; Nogueira, C. W.; Savegnago, L. *Brain Res. Bull.* **2009**, *79*, 281; (d) Wilhelm, E. A.; Jesse, C. R.; Roman, S. S.; Nogueira, C. W.; Savegnago, L. *Exp. Mol. Pathol.* **2009**, *87*, 20; (e) May, S. W.; Wang, L.; Gill-Woznichak, M. M.; Browner, R. F.; Ogonowski, A. A.; Smith, J. B.; Pollock, S. H. *J. Pharm. Exp. Ther.* **1997**, *283*, 470; (f) a) May, S. W. *Expert Opin. Invest. Drugs* **2002**, *11*, 1261; b) Wilhelm, E. A.; Jesse, C. R.; Bortolatto, C. F.; Nogueira, C. W.; Savegnago, L. *Pharmacol. Biochem. Behav.* **2009**, *93*, 419; g) Göbel, T.; Gsell, L.; Hüter, O. F.; Maienfisch, P.; Naef, R.; O'Sullivan, A. C.; Pitterna, T.; Rapold, T.; Seifert, G.; Sern, M.; Szczepanski, H.; Wadsworth, D. J. *Pestic. Sci.* **1999**, *55*, 355.

16 (a) Patai, S. in *Chemistry of Organic Selenium and Tellurium Compounds*, ed. Z. Rappoport, Wiley, Chichester, **2012**, vol. 3, 523-583; (b) Rhoden, C. R.; Zeni, G. *Org. Biomol. Chem.*, **2011**, *9*, 1301.

17 (a) Dalvie, D. K.; Kalgutkar, A. S.; Khojasteh-Bakht, S. C.; Obach, R. S.; O'Donnell, J. P. *Chem. Res. Toxicol.*, **2002**, 15, 269–299; (b) Gramec, D.; Peterlin Mašič, L.; Sollner Dolenc, M. *Chem. Res. Toxicol.*, **2014**, 27, 1344–1358. (c) Shah, R.; Verma, P. K. *Chem. Cent. J.* **2018**, 12, 1–22. (d) Gramec, D.; Peterlin Mašič, L.; Sollner Dolenc, M. *Chem. Res. Toxicol.* **2014**, 27, 1344–1358. (e) Jaladanki, C. K.; Taxak, N.; Varikoti, R. A.; Bharatam, P. V. *Chem. Res. Toxicol.*, **2015**, 28, 2364–2376. (f) Keri, R. S.; Chand, K.; Budagumpi, S.; Somappa, S. B.; Patil, S. A.; Nagaraja, B. M. *Eur. J. Med. Chem.* **2017**, 138, 1002–1033.

18 Chan, C. Y.; New, L. S.; Ho, H. K.; Chan, E. C. *Toxicol. Lett.*, **2011**, 206, 314–324.

19 Callaghan, J. T.; Bergstrom, R. F.; Ptak, L. R.; Beasley, C. M. *Clin. Pharmacokinet.* **1999**, 37, 177–193.

20 Grayson, M. L.; Crowe, S. M.; McCarthy, J. S.; Mills, J.; Mouton, J. W.; Norrby, S. R.; Pfaller, M. A. *Kucers' The Use of Antibiotics: A Clinical Review of Antibacterial Sixth Edition.* **2010**.

21 (a) Saito, M.; Osaka, I.; Suzuki, Y.; Takimiya, K.; Okabe, T.; Ikeda, S.; Asano, T. *Sci. Rep.* **2015**, 5, 14202; (b) Abe, M.; Mori, T.; Osaka, I.; Sugimoto, K.; Takimiya, K. *Chem. Mater.* **2015**, 27, 5049; (c) Takimiya, K.; Osaka I.; Mori, T.; Nakano, M. *Acc. Chem. Res.* **2014**, 47, 1493; (d) Takimiya, K.; Kunugi, Y.; Konda, Y.; Ebata, H.; Toyoshima, Y.; Otsubo, T. *J. Am. Chem. Soc.* **2006**, 128, 3044; (e) Takimiya, K.; Kunugi, Y.; Konda, Y.; Niihara, N.; Otsubo, T. *J. Am. Chem. Soc.* **2004**, 126, 5084; (f) Zeis, R.; Kloc, C.; Takimiya, K.; Kunugi, Y.; Konda, Y.; Niihara, N.; Otsubo, T. *Jpn. J. Appl. Phys. Part 1* **2005**, 44, 3712; (g) Shinamura, S.; Osaka, I.; Miyazaki, E.; Takimiya, K. *Heterocycles* **2011**, 83, 1187; (h) Maliakal, A.; Raghavachari, K.; Katz, H.; Chandross, E.; Siegrist, T. *Chem. Mater.* **2004**, 16, 4980; (i) Mondal, R.; Adhikari, R. M.; Shah, B. K.; Neckers D. C. *Org. Lett.* **2007**, 9, 2505; (j) Minemawari, H.; Yamada, T.; Matsui, H.; Tsutsumi, J.; Haas, S.; Chiba, R.; Kumai R.; Hasegawa, T. *Nature* **2011**, 475, 364; (k) Mei, J.; Diao, Y.; Appleton, A. L.; Fang, L.; Bao, Z. *J. Am. Chem. Soc.* **2013**, 135, 6724; (l) Patra, A.; Wijsboom, Y. H.; Leitus, G.; Bendikov, M. *Chem. Mater.* **2011**, 23, 896; (m) Perepichka, I. F.; Perepichka, D. F. *Handbook of Thiophene-based Materials.* Wiley VCH: Weinheim, **2009**; (n) Mori, T.; Nishimura, T.; Doi, I.; Miyazaki, E.; Osaka, I.; Takimiya, K.; *J. Am. Chem. Soc.* **2013**, 135, 13900.

22 Meng, H.; Bao, Z.; Lovinger, A. J.; Wang, B. C.; Mujisce, A. M. *J. Am. Chem. Soc.* **2001**, 123, 9214–9215.

23 Balaban, A. T.; Oniciu, D. C.; Katritzky, A. R. *Chem. Rev.*, **2004**, 104, 2777.

- 24 Yadav, V. K. Steric and stereoelectronic effects in organic chemistry. *Springer*. **2016**.
- 25 Garito, A. F.; Heeger, A. J. *Acc. Chem. Res.*, **1974**, 7, 232.
- 26 (a) Horner, K. E.; Karadakov, P. B. *J. Org. Chem.* **2013**, 78, 8037; (b) Ghomri, A.; Makelleche, S. M. *Tetrahedron*. **2010**, 941, 36; (c) Bird, C. W. *Tetrahedron*, **1992**, 48, 335-340.
- 27 Katritzky, A. R.; Ley, S. V.; Meth-Cohn, O.; Rees, C. W. *Comprehensive Organic Functional Group Transformations: Synthesis: Carbon with one Heteroatom attached by a Multiple Bond*, volume 3, **1995**.
- 28 (a) Wang, T.; Shi, S.; Hansmann, M. M.; Rettenmeier, E.; Rudolph, M.; Hashmi, A. S. K. *Angew. Chem. Int. Ed.* **2014**, 53, 3715-3719. (b) Nikbin, N.; Caratzoulas, S.; Vlachos, D. G. *APPL CATAL A-GEN.* **2014**, 485, 118-122.
- 29 Corma, A.; de la Torre, O.; Renz, M.; Vollandier, N. *Angew. Chem. Int. Ed.* **2011**, 50, 2375 –2378. (b) Nikbin, N.; Caratzoulas, S.; Vlachos, D. G. *APPL CATAL A-GEN.* **2014**, 485, 118-122.
- 30 Clayden, J. *Organolithiums: Selectivity for Synthesis*, **2002**.
- 31 Marshall, J. A.; Bartley, G. S.; Wallace, E. M. *J. Org. Chem.* **1996**, 61, 5729-5735.
- 32 Roethle, P. A.; Trauner, D. *Org. Lett.* **2006**, 8, 345-347.
- 33 (a) Reutov, O. A.; Beletskaya, I. P.; Butin, K. P. CH—Acids: A Guide to All Existing Problems of CH-Acidity with New Experimental Methods and Data, Including Indirect Electrochemical, Kinetic and Thermodynamic Studies. *Elsevier*. **1976**. (b) Shen, K.; Fu, Y.; Li, J. N.; Liu, L.; Guo, Q. X. *Tetrahedron*, **2007**, 63, 1568-1576. (c) Bordwell, F. G. *Acc. Chem. Res.* **1988**, 21, 456-463.
- 34 Lenardão, E. J.; Santi, C.; Sancineto, L. *New Frontiers in Organoselenium Compounds*. New York: Springer. **2018**.
- 35 Reich, H. J.; Hondal, R. J. *ACS Chem. Biol.* **2016**, 11, 821-841.
- 36 ((a) Christiaens, L.; Luxen, A.; Evers, M.; Thibaut, P.; Mbuyi, M. *Chemica Scripta*, **1984**, 24, 178; (b) Kumar, S.; Helt, J. C. P.; Autschbach, J.; Detty, M. R. *Organometallics*, **2009**, 28, 3426; (c) Fukuzawa, S. I.; Shimizu, E.; Atsumi, Y.; Haga, M.; Ogata, K., *Tetrahedron Lett.*, **2009**, 50, 2374; (d) Popov, I.; Do, H. Q.; Daugulis, O. *J. Org. Chem.*, **2009**, 74, 8309; (e) Yu, C.; Zhang, C.; Shi, X. *Eur. J. Org. Chem.*, **2012**, 1953; (f) Zou, L. H.; Reball, J.; Mottweiler, J.; Bolm, C. *Chem. Commun.*, **2012**, 48, 11307; (g) Yu, Y.; Zhou, Y.; Song, Z.; Liang, G. *Org. Biomol. Chem.*, **2018**, 16, 4958.

- 37 (a) Zhao, X.; Yu, Z.; Xu, T.; Wu, P.; Yu, H. *Org. Lett.*, **2007**, *9*, 5263; (b) Silveira, C. C.; Mendes, S. R.; Wolf, L.; Martins, G. M.; von Mühlen, L. *Tetrahedron*, **2012**, *68*, 10464; (c) Prasad, C. D.; Balkrishna, S. J.; Kumar, A.; Bhakuni, B. S.; Shrimali, K.; Biswas, S.; Kumar, S. *J. Org. Chem.*, **2013**, *78*, 1434; (d) Rafique, J.; Saba, S.; Rosario, A. R.; Zeni, G.; Braga, A. L. *RSC Adv.*, **2014**, *4*, 51648; (e) Gao, Z.; Zhu, X.; Zhang, R., *RSC Adv.*, **2014**, *4*, 19891. (f) Martins, G. M.; Meirinho, A. G.; Ahmed, N.; Braga, A. L.; & Mendes, S. R. *ChemElectroChem*. **2019**, *6*, 5928-5940. (g) Rafique, J.; Rampon, D. S.; Azeredo, J. B.; Coelho, F. L.; Schneider, P. H.; Braga, A. L. *Chem. Rec.* **2021**, *21*, 1–24. (h) Beletskaya, I. P.; Ananikov, V. P. *Chem. Rev.* **2011**, *111*, 1596–1636. (i) Perin, G.; Alves, D.; Jacob, R. G.; Barcellos, A. M.; Soares, L. K.; Lenardao, E. J. *ChemistrySelect*. **2016**, *2*, 205 – 258.
- 38 Ananikov, V. P.; Zaleskiy, S. S.; Beletskaya, I. P. *Curr. Org. Synth.*, **2011**, *8*, 2.
- 39 (a) Ivanova, A.; Arsenyan, P. *Coord. Chem. Rev.* **2018**, *370*, 55-68. (b) Iwasaki, M.; Nishihara, Y. *Dalton Trans.*, **2016**, *45*, 15278-15284. (c) Ma, W.; Kaplaneris, N.; Fang, X.; Gu, L.; Mei, R.; Ackermann, L. *Org. Chem. Front.*, **2020**, *7*, 1022-1060. (d) Qiu, G.; Zhou, K.; Wu, J. *Chem. Commun.*, **2018**, *54*, 12561. (e) Sundaravelu, N.; Sangeetha, S.; Sekar, G. *Org. Biomol. Chem.*, **2021**, *19*, 1459-1482.
- 40 (a) Stuhr-Hansen, N.; Sølling, T. I.; Henriksen, L. *Tetrahedron*, **2011**, *67*, 2633–2643. (b) Tiecco, M.; Testaferri, L.; Tingoli, M.; Marini, F.; *Tetrahedron*, **1994**, *50*, 10549–10554. (c) Press, J. B.; Gronowitz, S. *The Chemistry of Heterocyclic Compounds Thiophene and Its Derivatives. John Wiley and Sons, New York, Part*, **1985**, *1*, 353-456. (d) Engman, L.; Eriksson, P. *Heterocycles*, **1996**, *4*, 861-871. (e) Jen, K. Y.; Cava, M. P. *J. Org. Chem.* **1983**, *48*, 1449–1451. (f) Kibriya, G.; Samanta, S.; Singsardar, M.; Jana, S.; Hajra, A. *Eur. J. Org. Chem.* **2017**, *21*, 3055–3058.
- 41 (a) Kumar, S.; Helt, J. C. P.; Autschbach, J.; Detty, M. R. *ACS Publ.* **2009**, *28*, 3426–3436. (b) Popov, I.; Do, H. Q.; Daugulis, O. *J. Org. Chem.* **2009**, *74*, 8309–8313. (c) Jen, K. Y.; Benfaremo, N.; Cava, M. P.; Huang, W. S.; MacDiarmid, A. G. *J. Chem. Soc. Chem. Commun.* **1983**, 633–634. (d) Watthey, J. W.; Desai, M. *J. Org. Chem.* **1982**, *47*, 1755–1759. (e) Oda, M.; Enomoto, T.; Kawase, T.; Kurata, H. *Phosphorus, Sulfur Silicon Relat. Elem.* **1997**, *120*, 401–402. (f) Comins, D. L.; Killpack, M. O. *J. Org. Chem.* **1987**, *52*, 104–109. (g) Watanabe, M.; Snieckus, V. *J. Am. Chem. Soc.* **1980**, *102*, 1457–1460. (h) Zeni, G.; Nogueira, C. W.; Silva, D. O.; Menezes, P. H.; Braga, A. L.; Stefani, H. A.; Rocha, J. B. T. *Tetrahedron Lett.* **2003**,

44, 1387–1390. (i) Schwartz, P. O.; Förtsch, S.; Vogt, A.; Mena-Osteritz, E.; Bäuerle, P. *Beilstein J. Org. Chem.* **2019**, 15, 1379–1393. (j) Reich, H. J.; Willis, W. W. *J. Org. Chem.* **1980**, 45, 5227–5229. (k) Nolan, S. M.; Cohen, T. *J. Org. Chem.* **1981**, 46, 2473–2476. (l) Montaña, Á. M.; Grima, P. M.; Batalla, C.; Kociok-Köhn, G.; *Tetrahedron: Asymmetry* **2014**, 25, 677–689. (m) Marshall, J. A.; Bartley, G. S.; Wallace, E. M. *J. Org. Chem.* **1996**, 61, 5729–5735.

42 (a) Beletskaya, I. P.; Ananikov, V. P. *Chem. Rev.* **2011**, 111, 1596–1636. (b) Goldani, B.; Ricordi, V. G.; Seus, N.; Lenardão, E. J.; Schumacher, R. F.; Alves, D. *J. Org. Chem.* **2016**, 81, 11472–11476. (c) Mo, F.; Dong, G.; Zhang, Y.; Wang, J. *Org. Biomol. Chem.* **2013**, 11, 1582. (d) Zhao, H.; Jiang, Y.; Chen, Q.; Cai, M. *New J. Chem.* **2015**, 39, 2106–2115. (e) Fang, Y.; Rogge, T.; Ackermann, L.; Wang, S.-Y.; Ji, S.-J. *Nat. Commun.* **2018**, 9, 2240. (f) Reddy, K.; Reddy, V.; Madhav, B.; Shankar, J.; Nageswar, Y. *Synlett* **2011**, 1268–1272. (g) Reddy, V. P.; Kumar, A. V.; Rao, K. R. *J. Org. Chem.* **2010**, 75, 8720–8723. (h) Mohan, B.; Yoon, C.; Jang, S. Park, K. H. *ChemCatChem.* **2015**, 7, 405–412. (i) Wang, J.; Li, H.; Leng, T.; Liu, M.; Ding, J.; Huang, X.; Wu, H.; Gao, W.; Wu, G. *Org. Biomol. Chem.* **2017**, 15, 9718–9726. (j) Chatterjee, T.; Ranu, B. C. *J. Org. Chem.* **2013**, 78, 7145–7153. (k) Zheng, B.; Gong, Y.; Xu, H. *J. Tetrahedron* **2013**, 69, 5342–5347.

43 (a) Mandal, A.; Dana, S.; Sahoo, H.; Grandhi, G. S.; Baidya, M. *Org. Lett.* **2017**, 19, 2430–2433. (b) Jin, W.; Zheng, P.; Wong, W.; Law, G. L. *Asian J. Org. Chem.* **2015**, 4, 875–878. (c) Singh, B. K.; Bairy, G.; Jana, R. *ChemistrySelect.* **2017**, 2, 9227–9232.

44 Zhang, S.; Qian, P.; Zhang, M.; Hu, M.; Cheng, J. *J. Org. Chem.*, **2010**, 75, 6732.

45 Ricordi, V.; Thurow, S.; Penteadó, F.; Shumacher, R. F.; Perin, G.; Lenardão, E. J.; Alves, D. *Adv. Synth. Catal.*, **2015**, 357, 933.

46 Mandal, A.; Sahoo, H.; Baidya, M. *Org. Lett.*, **2016**, 18, 3202.

47 Iwasaki, M.; Tsuchiya, Y.; Nakajima, K.; Nishihara, Y. *Org. Lett.*, **2014**, 16, 4920.

48 (a) Qiu, R.; Reddy, V. P.; Iwasaki, T.; Kambe, N. *J. Org. Chem.*, **2015**, 80, 367. (b) Nishino, K.; Tsukahara, S.; Ogiwara, Y.; Sakai, N. *Eur. J. Org. Chem.* **2019**, 1588–1593.

49 Jin, W.; Zheng, P.; Wong, W. T.; Law, G. L. *Asian J. Org. Chem.* **2015**, 4, 875–878.

50 (a) Montalbetti, C. A.; Falque, V. *Tetrahedron.* **2005**, 61, 10827. (b) Valeur, E.; Bradley, M. *Chem. Soc. Rev.*, **2009**, 38, 606–631. (c) de Figueiredo, R. M.; Suppo, J.

- S.; Campagne, J. M. *Chem. Rev.* **2016**, 116, 12029–12122 (d) Massolo, E.; Pirola, M.; Benaglia, M. *Eur. J. Org. Chem.* **2020**, 4641–4651.
- 51 El-Faham, A.; Albericio, F. *Chem. Rev.* **2011**, 111, 6557.
- 52 Neises, B.; Steglich, W. *Angew. Chem., Int. Ed. Engl.*, **1978**, 17, 522.
- 53 Ghosh, A.K.; Shahabi, D. *Tetrahedron Lett.*, **2021**, 63, 152719.
- 54 (a) Joullié, M. M.; Lassen, K. M. *Arkivoc*, **2010**, 8, 189–250, (b) Dunetz, J. R.; Magano, J.; Weisenburger, G. A. *Org. Process Res. Dev.* **2016**, 20, 140–177.
- 55 Gao, J.; Yang, F.; Che, J.; Han, Y.; Wang, Y.; Chen, N.; Bak, D.W.; Lai, S.; Xie, X.; Weerapana, E.; Wang, C. *ACS Cent. Sci.* **2018**, 4, 960–970.
- 56 (a) Iwasaki, M.; Iyanaga, M.; Tsuchiya, Y.; Nishimura, Y.; Li, W.; Li, Z.; Nishihara, Y. *Chem. Eur. J.* **2014**, 20, 2459 – 2462. (b) Iwasaki, M.; Tsuchiya, Y.; Nakajima, K.; Nishihara, Y. *Org. Lett.* **2014**, 16, 4920–4923. (c) Canty, A. J.; Jin, H.; Skelton, B. W.; White, A. H. *Inorg. Chem.* **1998**, 37, 3975–3981.
- 57 Vásquez-Céspedes, S.; Ferry, A.; Candish, L.; Glorius, F. *Angew. Chem. Int. Ed.* **2015**, 54, 5772 –5776.
- 58 Gu, L.; Fang, X.; Weng, Z.; Song, Y.; Ma, W. *Eur. J. Org. Chem.* **2019**, 1825–1829.
- 59 (a) Lyons, T. W.; Sanford, M. S. *Chem. Rev.* **2010**, 110, 1147–1169. (b) Zhou, L.; Lu, W. *Chem. Eur. J.* **2014**, 20, 634 – 642. (c) Yeung, C. S.; *Chem. Rev.* **2011**, 111, 1215–1292. (d) McCann, S. D.; Stahl, S. S. *Acc. Chem. Res.* **2015**, 48, 1756–1766. (e) Alkaim, A. F.; Aljeboree, A. M.; Alrazaq, N. A.; Baqir, S. J.; Hussein, F. H.; Lilo, A. J. *Asian J. Chem*, **2014**, 9, 26, 8445. (f) Wu, Y.; Wang, J.; Mao, F.; Kwong, F. Y. *Chem. Asian J.* **2014**, 9, 26 – 47.
- 60 Kreitman, G. Y.; Danilewicz, J. C.; Jeffery, D. W.; Elias, R. J. *J. Agric. Food Chem.* **2017**, 65, 2564–2571.
- 61 (a) Ni, Y.; Zuo, H.; Li, Y.; Wu, Y.; Zhong, F. *Org. Lett.* **2018**, 20, 4350–4353. (b) Higashi, L. S.; Lundeen, M.; Hilti, E.; Seff, K. *Inorg. Chem.* **1977**, 16, 310. (c) Zhang, C.; McClure, J.; Chou, C. J. *J. Org. Chem.*, **2015**, 80, 4919. (d) Gogoi, P.; Gogoi, S. R.; Kalita, M.; Barman, P. *Synlett.* **2013**, 24, 873–877. (e) Arsenyan, P.; Lapcinska, S.; Ivanova, A.; Vasiljeva, J. *Eur. J. Org. Chem.* **2019**, 2019, 4951. (f) Taniguchi, N. *J. Org. Chem.*, **2006**, 71, 7874.
- 62 Guin, S.; Deb, A.; Dolui, P.; Chakraborty, S.; Singh, V. K.; Maiti, D. *ACS Catal.* **2018**, 8, 2664–2669

- 63 Shang, M., Sun, S. Z., Dai, H. X., & Yu, J. Q. *J. Am. Chem. Soc.* **2014**, 136, 3354–3357.
- 64 Armarengo, W. L. F.; Chal, L. L. C. *Purification of Laboratory Chemicals*, 5. Ed. Elsevier: Bostan, **2003**
- 65 Program APEX3, Bruker AXS Inc., Madison, WI (2015).
- 66 G. M. Sheldrick, SHELX – Programs for crystal structure determination (SHELXS-2013) and refinement (SHELXL-2014), *Acta Cryst.* (2008) **A64**, 112-122, (2015) **A71**, 3-8, and (2015) **C71**, 3-8s.
- 67 'International Tables for X-ray Crystallography', Kluwer Academic Publishers, Dordrecht (1992). Vol. C, pp. 500, 219 and 193.
- 68 L. J. Farrugia, (2012) *J. Appl. Cryst.* **45**, 849–854.
- 69 L. J. Farrugia, *J. Appl. Crystallogr.* 2012, 45, 849–854.
- 70 Padmavathi, R.; Sankar, R.; Gopalakrishnan, B.; Parella, R.; Babu, S. A. *Eur. J. Org. Chem.* **2015**, 3727–3742.
- 71 Yu, Z.; Zhang, S.; Shen, Z. *Chin. J. Chem.* **2018**, 36, 1139–1142.
- 72 Chen, S. Q.; Jiao, J. Y.; Zhang, X. G.; Zhang, X. H. *Tetrahedron*, **2019**, 246-252.
- 73 Tran, K. M.; Ho, N. T.; Le, T. T.; Nguyen, T. T.; Phan, N. T. *Asian J. Org. Chem.* **2021**, 10, 1-5.
- 74 Kim, H.; Heo, J.; Kim, J.; Baik, M. H.; Chang, S. *Am. Chem. Soc.* **2018**, 140, 14350–14356.
- 75 Chen, W.; Liu, M.; Li, H. J.; Wu, Y. C. *Org. Chem. Front.* **2021**, 8, 584-590.